11-29-2017 4:00 PM

# Hybrid Attitude Control and Estimation On SO(3)

Soulaimane Berkane, *The University of Western Ontario*

Supervisor: Tayebi, Abdelhamid, *The University of Western Ontario*

A thesis submitted in partial fulfillment of the requirements for the Doctor of Philosophy degree in Electrical and Computer Engineering

# Abstract

This thesis presents a general framework for hybrid attitude control and estimation design on the Special Orthogonal group $\mathbb{SO}(3)$. First, the attitude stabilization problem on $\mathbb{SO}(3)$ is considered. It is shown that, using a min-switch hybrid control strategy designed from a family of potential functions on $\mathbb{SO}(3)$, global exponential stabilization on $\mathbb{SO}(3)$ can be achieved when this family of potential functions satisfies certain properties. Then, a systematic methodology to construct these potential functions is developed. The proposed hybrid control technique is applied to the attitude tracking problem for rigid body systems. A smoothing mechanism is proposed to filter out the discrete behaviour of the hybrid switching mechanism leading to control torques that are continuous.

Next, the problem of attitude estimation from continuous body-frame vector measurements of known inertial directions is considered. Two hybrid attitude and gyro bias observers designed directly on $\mathbb{SO}(3) \times \mathbb{R}^3$ are proposed. The first observer uses a set of innovation terms and a switching mechanism that selects the appropriate innovation term. The second observer uses a fixed innovation term and allows the attitude state to be reset (experience discrete transition or jump) to an adequately chosen value on $\mathbb{SO}(3)$. Both hybrid observers guarantee global exponential stability of the zero estimation errors.

Finally, in the case where the body-frame vector measurements are intermittent, an event-triggered attitude estimation scheme on $\mathbb{SO}(3)$ is proposed. The observer consists in integrating the continuous angular velocity during the interval of time where the vector measurements are not available, and updating the attitude state upon the arrival of the vector measurements. Both cases of synchronous and asynchronous vector measurements with possible irregular sampling periods are considered. Moreover, some modifications to the intermittent observer are developed to handle different practical issues such as discrete-time implementation, noise filtering and gyro bias compensation.

*To all those whom I love...*

# Acknowledgement

I would like to express my deepest gratitude to my advisor, Professor Abdelhamid Tayebi, for his support, motivation and guidance throughout the four years I have spent at Western University. He taught me what it meant to be a high quality researcher who carries fundamental values such as honesty, vision, passion and rigorousness. His timely feedback and suggestions helped me to smoothly conduct my research and write my thesis.

I am grateful to my friend, colleague and collaborator, Dr. Abdelkader Abdessameud, with whom I have completed several parts of this research and shared countless discussions in the research field. I am also thankful to my alternate supervisor at Western, Dr. Ilia Polushin, who have helped me in several occasions.

I would also like to sincerely thank Prof. Jin Jiang and Dr. Lyndon Brown for taking the time to serve as my PhD thesis examiners and for their constructive comments and feedback.

I would especially like to thank Prof. Andrew R. Teel from the University of California Santa Barbara for agreeing to review and examine my thesis. I have had several fruitful discussions with him during our meetings at CDC and ACC conferences.

Lastly, I would like to extend my sincere appreciation to my family. To my mother, Chahrazed, my sisters and my friends for their support and prayers in all my pursuits. And of course, to my wife, Intissar, for her love, support and understanding.

# List of Symbols

- $\mathbb{N}$ and $\mathbb{N}_{>0}$ denote the natural and strictly positive natural numbers, respectively.
- $\mathbb{R}$, $\mathbb{R}_{\geq 0}$ and $\mathbb{R}_{>0}$ denote the real, nonnegative and positive real numbers, respectively.
- $\mathbb{R}^n$ is the $n$-dimensional Euclidean space .
- $\mathbb{R}^{n\times m}$ is the set of real-valued $n \times m$ matrices.
- Given $A \in \mathbb{R}^{n\times m}$, $A^\top$ denotes its transpose.
- Given $A \in \mathbb{R}^{n\times n}$, $\mathbf{det}(A)$ denotes its determinant.
- Given $A \in \mathbb{R}^{n\times n}$, $\mathbf{tr}(A)$ denotes the sum of its diagonal entries (trace).
- Given $A, B \in \mathbb{R}^{n\times m}$, their Euclidean inner product is defined as $\langle\langle A, B\rangle\rangle = \mathbf{tr}(A^\top B)$.
- Given $A \in \mathbb{R}^{n\times m}$, its Frobenius norm is $\|A\|_F = \sqrt{\langle\langle A, A\rangle\rangle}$.
- Given $x \in \mathbb{R}^n$, its Euclidean norm (2-norm) is given by $\|x\| = \sqrt{x^\top x}$.
- $\mathbb{S}^n = \{x \in \mathbb{R}^{n+1} : \|x\| = 1\}$ is the unit $n$-sphere embedded in $\mathbb{R}^{n+1}$.
- $\mathbb{B} = \{x \in \mathbb{R}^n : \|x\| \leq 1\}$ is the closed unit ball in Euclidean space.
- $\mathbb{SO}(3) = \{R \in \mathbb{R}^{3\times 3} : \mathbf{det}(R) = 1,\ RR^\top = R^\top R = I\}$ is the Special Orthogonal group of order 3 where $I$ denotes the three-dimensional identity matrix.
- $\mathfrak{so}(3) = \{\Omega \in \mathbb{R}^{3\times 3} : \Omega^\top = -\Omega\}$ is the set of all skew-symmetric $3 \times 3$ matrices and defines also the Lie algebra of $\mathbb{SO}(3)$.
- $\mathbb{Q} = \{(\eta, \epsilon) \in \mathbb{R} \times \mathbb{R}^3 : \eta^2 + \epsilon^\top \epsilon = 1\}$ is the set of unit quaternions.
- Given a rotation matrix $R \in \mathbb{SO}(3)$, let us define $|R|_I = \|I - R\|/\sqrt{8}$.
- The map $\mathbf{E} : \mathbb{R}^{3\times 3} \to \mathbb{R}^{3\times 3}$ is defined as $\mathbf{E}(M) = \frac{1}{2}(\mathbf{tr}(M)I - M^\top)$.
- The map $\mathbf{R}_a : \mathbb{R} \times \mathbb{S}^2 \to \mathbb{SO}(3)$ is defined as $\mathbf{R}_a(\theta, u) = I + \sin(\theta)[u]_\times + (1 - \cos(\theta))[u]_\times^2$.
- The map $\mathbf{R}_u : \mathbb{Q} \to \mathbb{SO}(3)$ is defined as $\mathbf{R}_u(\eta, \epsilon) = I + 2[\epsilon]_\times^2 + 2\eta[\epsilon]_\times$.

- The map $\mathbf{R}_r : \mathbb{R}^3 \to \mathbb{SO}(3)$ is defined as $\mathbf{R}_r(z) = \frac{1}{1+\|z\|^2}\left((1-\|z\|^2)I + 2zz^\top + 2[z]_\times\right)$.
- The map $\mathbf{P}_{\mathbb{SO}(3)} : \mathbb{R}^{3\times 3} \to \mathbb{SO}(3)$ is defined as the projection of $X \in \mathbb{R}^{3\times 3}$ on $\mathbb{SO}(3)$ (*i.e.* closest rotation matrix to $X$).
- The map $\mathbf{P}_{\mathfrak{so}(3)} : \mathbb{R}^{3\times 3} \to \mathfrak{so}(3)$ is defined as $\mathbf{P}_{\mathfrak{so}(3)}(M) = (M - M^\top)/2$.
- The map $[\cdot]_\times : \mathbb{R}^3 \to \mathfrak{so}(3)$ is defined as $[x]_\times y = x \times y$ for all $x, y \in \mathbb{R}^3$ where $\times$ denotes the cross product on $\mathbb{R}^3$.
- The map $\mathbf{vex} : \mathfrak{so}(3) \to \mathbb{R}^3$ is the inverse map of $[\cdot]_\times$.
- The map $\psi : \mathbb{R}^{3\times 3} \to \mathbb{R}^3$ is defined as $\psi = \mathbf{vex} \circ \mathbf{P}_{\mathfrak{so}(3)}$ where the symbol $\circ$ is used to denote function composition.
- The set $\Pi_{\mathbb{SO}(3)} = \{R \in \mathbb{SO}(3) : \mathbf{tr}(R) \neq -1\}$ is the set of all rotations with an angle different than 180°. In other words, $\Pi_{\mathbb{SO}(3)} = \mathbb{SO}(3) \setminus \mathbf{R}_a(\pi, \mathbb{S}^2)$.
- The set $\Pi_{\mathbb{Q}} = \{(\eta, \epsilon) \in \mathbb{Q} : \eta \neq 0\}$ is the double cover of $\Pi_{\mathbb{SO}(3)}$ in $\mathbb{Q}$.
- The map $\mathbf{P}_c : \mathbb{R}^3 \times \mathbb{R}^3 \to \mathbb{R}^3$, for a given $c \in \mathbb{R}_{\geq 0}$, defines the parameter projection function which is given in (2.3).
- Given a set $\mathcal{S}$, $\mathbf{cl}(\mathcal{S})$ denotes its closure ($\mathcal{S}$ together with all of its limit points).
- A set-valued map $\mathbf{F} : \mathcal{M} \rightrightarrows \mathcal{N}$ assigns to every $x \in \mathcal{M}$ a set of values $\mathbf{F}(x) \subseteq \mathcal{N}$.
- Let $\mathbf{F} : \mathcal{M} \rightrightarrows \mathcal{N}$ be a set-valued function. The domain of $\mathbf{F}$ is defined as the set $\mathrm{dom}\mathbf{F} = \{x \in \mathcal{M} : \mathbf{F}(x) \neq \emptyset\}$ where $\emptyset$ denotes the empty set.
- $\mathsf{C}^n(\mathcal{M}, \mathcal{N})$ is the set of all functions $f : \mathcal{M} \to \mathcal{N}$ such that the first $n \in \mathbb{N}$ derivatives of each function $f \in \mathsf{C}^n(\mathcal{M}, \mathcal{N})$ exist and are continuous.

# Contents

# List of Figures

# Chapter 1

# Introduction

## 1.1 General Introduction

Many mechanical systems can be modelled as a rigid body or an interconnection of multiple rigid bodies. For instance, most aerospace and marine vehicles such as Unmanned Aerial Vehicles (UAVs), Spacecraft, Satellite and Autonomous Underwater Vehicles (AUVs) can be considered as rigid body systems. Robotic arms composed of multiple rigid links and joints, also known as robot manipulators, are an example of rigid multi-body systems which are used in various applications including welding automation, manufacturing, robotically-assisted surgery and space stations robotic arms. The assumption of *rigidity*, which means non-deformation under the action of applied forces, for these class of mechanical systems is very important to simplify the analysis and controller design. In fact, the configuration of a rigid body can be fully described by translation and rotation of a reference frame attached to the body. This is in contrast to bodies that display fluid, elastic, and plastic behavior which require more parameters to describe their configuration [Terzopoulos *et al.*, 1987, Davatzikos, 1997, Elger and Roberson, 2013].

The design of efficient attitude control algorithms is of great importance for successful applications involving accurate positioning of rigid body systems such as satellites and spacecraft. These control schemes are (roughly speaking) of proportional-derivative type, where the proportional action is in terms of the orientation (attitude) and the derivative action (generating the necessary damping) is in terms of the angular velocity. In contrast to the angular velocity which can be directly measured using gyroscopes, there are no sensors that directly measure the orientation. This fact calls for the development of suitable attitude estimation algorithms that reconstruct the attitude using appropriate sensors such as inertial measurement units (IMUs) that provide measure-

ments in the body-attached frame of some known inertial vectors. Consequently, the attitude estimation and control problems have been the focus of many researchers from the aerospace and control communities, which led to a large body of work since 1960's. These fundamental problems come with many theoretical and practical challenges related to the topology of the motion space $\mathbb{SO}(3)$. Among, these challenges, the non-existence of global continuous time-invariant attitude estimation and control schemes on compact manifolds [Koditschek, 1988, Sanjay P. Bhat, 2000], which motivated the development of new alternatives such as the hybrid techniques that will be the focus of this thesis.

This thesis proposes a general framework for the design of hybrid attitude control and estimation algorithms. Within this framework, the global (singularity-free) attitude representation as a rotation matrix on $\mathbb{SO}(3)$ is used. Using this coordinate-free representation of the attitude, all the pitfalls of other attitude representations such as the Euler angles, Rodrigues parameters and the unit quaternions are avoided.

## 1.2 Attitude Control

The rigid body attitude control problem has received a growing interest during the last decades, with various applications in aerospace, marine engineering, and robotics see, for instance, [Kreutz and Wen, 1988, Joshi *et al.*, 1995, Pettersen and Egeland, 1999, Hughes, 1986, Tayebi and McGilvray, 2006]. Attitude control schemes can be categorized by the choice of the attitude parametrization, such as Euler-angles, unit quaternion, Rodrigues parameters and rotation matrices. The natural (intrinsic) representation of the attitude is done using rotation matrices on $\mathbb{SO}(3)$ (9 parameters). Early works on attitude control have focused on the use of less number of parameters to represent the attitude. This is motivated mainly by the need to save computational power and reduce the analysis complexity. The minimum number of parameters to represent the attitude is three. Examples of these 3-dimensional parametrizations are the Euler angles, the exponential coordinates and the Rodrigues parameters. However, as shown in [Stuelpnagel, 1964], it is topologically impossible to represent the attitude globally without singular points using only 3 parameters. For instance, the angular velocity cannot be extracted (globally) from the Euler angles rates due to the singularity of transformation matrix relating the time derivatives of the Euler angles to the angular velocity. This is a mathematical kinematic singularity which is often referred to as the *gimbal lock* [Hoag, 1963]. The Rodrigues parameters representation is also a three-parameters attitude representation, which allows to represent all attitudes except those of 180°. This geometric singularity implies that continuous control laws which use this representation are not

globally defined. The unit-quaternion representation is a four-parameters attitude representation which describes the attitude globally (singularity-free) compared to other three-parameters representations. This has motivated their wide use in many practical applications to represent the rigid-body attitude. For example, quaternion feedback has been used in spacecraft control [Wie *et al.*, 1989, Wie and Barba, 1985], manipulators control [Yuan, 1988], robot writs [Salcudean, 1988] and aerial vehicles [Tayebi and McGilvray, 2006]. A comprehensive study of unit quaternion feedback control appears in [Wen and Kreutz-Delgado, 1991] where different quaternion-based control laws have been investigated and compared. The controllers share the common structure of a proportional-derivative feedback plus some feedforward Coriolis torque compensation and/or adaptive compensation. Different robust [Joshi *et al.*, 1995], adaptive [Egeland and Godhavn, 1994], velocity-free [Lizarralde and Wen, 1996, Tayebi, 2008] quaternion feedbacks have been also developed in the past decades. The main drawback of using the unit-quaternion representation is the fact that every attitude can be represented, equivalently, by two different quaternions. This nonuniqueness in representing the attitude, if not taken carefully, might result in quaternion-based controllers with undesirable phenomena such as the so-called unwinding phenomenon [1] [Sanjay P. Bhat, 2000]. There have been some attempts to design quaternion-based attitude control systems that do not suffer from the unwinding phenomena by introducing discontinuities, see for instance [Thienel and Sanner, 2003]. However, these discontinuous attitude control systems suffer from non-robustness to arbitrary small measurement disturbances as discussed in [Mayhew and Teel, 2011a]. In [Mayhew, 2010, Mayhew *et al.*, 2011], hybrid controllers have been proposed to ensure robust global asymptotic stabilization via quaternion feedback. Also, other hybrid techniques where used in [Mayhew, 2010] to remove the ambiguity in *selecting* the best quaternion to represent an attitude measurement on $\mathbb{SO}(3)$.

With the advance of computational ressources and the fact that all existing parameterizations fail to represent the attitude of a rigid body both globally and uniquely, which results in control schemes that are either singular or exhibit some undesirable behavior, recent trends in attitude control have focused on the use of rotation matrices on $\mathbb{SO}(3)$ [Koditschek, 1988, Sanyal *et al.*, 2009, Chaturvedi *et al.*, 2011, Lee, 2012, Bayadi and Banavar, 2014]. The group $\mathbb{SO}(3)$ has the distinct feature of being a boundaryless compact manifold with a Lie group structure that allows the design and analysis of attitude control systems within the well established framework of geometric control [Bullo, 2005]. The group $\mathbb{SO}(3)$ is not diffeomorphic to any Euclidean space and hence there does not

[1] The unwinding phenomenon refer to the situation where the rigid body may start arbitrary close to the desired orientation yet rotates through large angles before converging to the desired attitude.

exist any continuous time-invariant feedback on $\mathbb{SO}(3)$ that achieves global asymptotic stability [Sanjay P. Bhat, 2000]. In [Koditschek, 1988], for instance, a continuous time-invariant control scheme has been shown to asymptotically track any smooth reference attitude trajectory starting from arbitrary initial conditions except from a set of Lebesgue measure zero. This is referred to as *almost* global asymptotic stability, and is mainly due to the appearance of undesired critical points (equilibria) when using the gradient of a smooth potential function in the feedback. In fact, any smooth potential function on $\mathbb{SO}(3)$ is guaranteed to have at least four critical points where its gradient vanishes [Morse, 1934].

In [Mayhew and Teel, 2011b], a hybrid feedback scheme has been proposed to overcome the topological obstruction to global asymptotic stability on $\mathbb{SO}(3)$ and, at the same time, ensure some robustness to measurement noise. The main idea in the latter paper is to design a hybrid algorithm based on a family of *smooth* potential functions and a hysteresis-based switching mechanism that selects the appropriate control action corresponding to the minimal potential function. It was shown that a sufficient condition to avoid the undesired critical points, and ensure global asymptotic stability, is the "synergism" property of the smooth potential functions. A family of potential functions on $\mathbb{SO}(3)$ is said to be synergistic if at each critical point (other than the desired one) of a potential function in the family, there exists another potential function in the family that has a lower value. Moreover, if all the potential functions in the family share the identity element $I_{3\times 3}$ as a critical point then it is called a *centrally* synergistic family. Thanks to the hysteresis gap, this type of hybrid controllers guarantee robustness to small measurement noise. Despite the originality of the proposed hybrid control framework, unfortunately, the search for families of potential functions on $\mathbb{SO}(3)$ enjoying the synergism property is not a straightforward task.

The angular warping technique has been used in [Mayhew and Teel, 2011d] to construct a central synergistic family of potential functions on $\mathbb{SO}(3)$ where the synergistic property is verified by computation only. Although in [Casau *et al.*, 2015b], necessary and sufficient conditions for this family of potential functions to be synergistic were derived, the major drawback of the angular warping approach is related to the difficulty of determining the synergistic gap which is required for the implementation of the hybrid controller. In an attempt to solve this problem the authors in [Mayhew and Teel, 2013a] tried to relax the centrality assumption by considering scaled, biased and translated modified trace functions. However, the sufficient synergism conditions provided therein were conservative, difficult to satisfy and only hand tuning of the parameters was proposed. Another form of non-central synergistic potential functions appeared in [Lee,

2015], by comparing the actual and desired directions, leading to a simple expression of the synergistic gap. It is important to mention here that, in contrast to the non-central approach, the control algorithm derived from each potential function in the central synergistic family guarantees (independently) almost global asymptotic stability results. It is also worth pointing out that non-central and central synergistic potential functions have been considered in [Mayhew and Teel, 2013b] and [Casau *et al.*, 2015a] to ensure, respectively, global asymptotic and global exponential stabilization on the $n$-dimensional sphere. However, the extension of these approaches to the *full* attitude control problem on $\mathbb{SO}(3)$ is not straightforward.

## 1.3 Attitude Estimation

It is unfortunate that there is no sensor that can provide direct measurements of a rigid body's attitude. Nevertheless, there exist many sensors (depending on the application at hand) that provide *partial* information about the rigid body' orientation. For instance the attitude of a rigid body can be recovered (reconstructed) using available body-frame measurements of known inertial directions. Small size UAVs are usually equipped with IMUs that typically include accelerometers and magnetometers, which provide body-referenced coordinates of the gravity vector and the Earth's magnetic field, respectively. For satellites, sun sensors and star trackers are usually used to provide body-frame measurements of known inertial directions. The problem of determining the attitude of a rigid body from vector measurements has been addressed, initially, as an optimization problem, also known as *Wahba's problem* [Wahba, 1965]. A great deal of research work has been devoted to solving Wahba's problem, see for instance [Shuster and Oh, 1981, Markley, 1988]. However, these static attitude reconstruction techniques are hampered by their inability to handle measurement noise. To overcome this problem, researchers looked for dynamic estimators where other measurements (such as angular velocity measurements) are used along with body-frame vector measurements to recover the attitude while filtering measurement noise. The gist of the idea is that the angular velocity can be integrated to estimate the attitude in the short-term, and then make long-term corrections using vector measurements. This leads to an attitude estimate that is less vulnerable to vibrations (because gyroscopes are accurate at high frequencies) and immune to long-term drift (because vector measurements are more reliable at low frequencies). Dynamic estimators can be, roughly speaking, classified into two categories: stochastic estimators (based on Kalman filtering techniques) and nonlinear estimators (based on nonlinear observer design techniques).

Stochastic estimators are usually variants of the Extended Kalman Filter and can be found in many references such as [Markley, 2003, Crassidis *et al.*, 2007, Choukroun, 2009]) for quaternion-based filtering and [Markley, 2006, Barrau and Bonnabel, 2015, Mueller *et al.*, 2016, Barrau and Bonnabel, 2017] for rotation matrix-based filtering. Unfortunately, the available stochastic attitude estimators have only locally proven stability and performance properties (see for instance [Barrau and Bonnabel, 2017]). Recently, a new class of dynamic nonlinear attitude estimators (observers) has emerged [Mahony *et al.*, 2008], and proved its ability in handling large rotational motions and measurement noise. This approach, coined nonlinear complementary filtering, was inspired from the linear attitude complementary filters, *e.g.,* [Tayebi and McGilvray, 2006], used to recover (locally) the attitude using gyro measurements and body-frame measurements of known inertial vectors. The smooth nonlinear complementary filters, such as those proposed in [Mahony *et al.*, 2008], are directly designed on $\mathbb{SO}(3)$ and are proved to guarantee *almost* global asymptotic stability (AGAS), which is as strong as the $\mathbb{SO}(3)$ space topology could permit. These smooth nonlinear observers ensure the convergence of the estimated attitude to the actual one from almost all initial conditions except from a set of critical points of zero Lebesgue measure. It has been noted, for instance in [Lee, 2012, Tse-Huai Wu and Lee, 2015, Zlotnik and Forbes, 2017], that starting from a configuration close to the undesired critical points, results in a slow convergence to the actual attitude. This observation has been formally proven in our recent work [Berkane and Tayebi, 2017a]. Further performance and robustness improvements for the complementary filtering approach have also been proposed recently in [Zlotnik and Forbes, 2016, Zlotnik and Forbes, 2017] and in [Berkane and Tayebi, 2017a]. On the other hand, a class of ($\mathbb{SO}(3)$ non-preserving) attitude observers has been proposed in [Batista *et al.*, 2012a, Batista *et al.*, 2012b] leading to global stability results. Theses observers provide an attitude estimate that is not confined to live in $\mathbb{SO}(3)$ but tends to it as time goes to infinity. A *non-central* hybrid attitude observer on $\mathbb{SO}(3)$ has been proposed in [Tse-Huai Wu and Lee, 2015] with global asymptotic stability. The term *non-central* means that individual observers (from the family of observers used in the hybrid scheme) do not, in general, guarantee (on their own) any estimation stability results (even locally). The design of globally exponentially stable observers on $\mathbb{SO}(3)$ is an open problem that has been solved in this thesis using hybrid techniques.

In the field of attitude estimation, most existing research developments consider either continuous measurements or regular synchronous discrete measurements. The attitude is not directly measurable, it is obtained from the fusion of different measurements from sensors with (possibly) different bandwidths and subject to packet dropouts. For in-

stance, landmark measurements using vision systems are obtained at much lower rates than the vector measurements obtained from an IMU. Also, GPS readings are often used in attitude estimation algorithms when linear accelerations are not negligible, such as in [Hua, 2010, Roberts and Tayebi, 2011, Martin and Salaün, 2008]. These readings are obtained at much lower rates compared to onboard IMU measurements. Therefore, it is interesting to design attitude estimation algorithms that take into account these practical constraints. State estimation using intermittent observations dates back to the early work that appeared in [Nahi, 1969, Hadidi and Schwartz, 1979]. Different versions of the Kalman filter for linear systems with intermittent measurements have been discussed in recent papers, see for instance [Smith and Seiler, 2003, Sinopoli *et al.*, 2004, Plarre and Bullo, 2009]. This problem is relevant when fusing sensors with multiple bandwidths and/or observing a system over a sensor network in which the sensor and controller are communicating over an unreliable link or a network subject to packets loss. In a deterministic setting, observer design for state estimation of linear time-invariant systems and some special classes of nonlinear systems with Lipschitz nonlinearities in the presence of sporadically available measurements have been recently proposed in [Raff and Allgöwer, 2007, Andrieu *et al.*, 2013, Ferrante *et al.*, 2016]. In the context of attitude estimation, the authors in [Barrau and Bonnabel, 2015] proposed an intrinsic attitude filter on $\mathbb{SO}(3)$ with (synchronous) discrete-time measurements of two vector observations. The proposed discrete invariant observer is shown to be almost globally convergent. In [Khosravian *et al.*, 2015], by exploiting the symmetry of the group $\mathbb{SO}(3)$, a predictor has been proposed to continuously predict the intermittent vector measurements using forward integration on $\mathbb{SO}(3)$ of the continuous angular velocity measurements. The measurements are allowed to be asynchronous (multirate) and subject to known constant delays. The proposed predictor can be, independently, combined with any asymptotically stable attitude/filter such as the explicit complementary filter [Mahony *et al.*, 2008].

## 1.4 Thesis Contributions

For general hybrid systems such as those modelled in the framework of [Goebel *et al.*, 2009, Goebel *et al.*, 2012], new Lyapunov-based sufficient conditions for exponential stability are proposed. The derived conditions relax the conditions presented in [Teel *et al.*, 2013, Theorem 1] in the sense that the Lyapunov function is allowed to increase during either the flow or the jump. This relaxation comes at the cost of imposing some conditions on the hybrid time domain where solutions exist. The newly proposed sufficient conditions are later used to prove some of the results presented in this thesis.

A new framework for global exponential stabilization on $\mathbb{SO}(3)$ is proposed. Our framework can be seen as an extension to the work of [Mayhew, 2010, Mayhew and Teel, 2011b, Mayhew and Teel, 2011d] on synergistic feedback on $\mathbb{SO}(3)$. In the former work, synergistic potential functions are shown to be sufficient for the design of hybrid controllers guaranteeing global asymptotic stability. In this work, a new class of potential functions, coined *exp-synergistic*, is proposed and shown to be sufficient for global exponential stabilization on $\mathbb{SO}(3)$. Moreover, a systematic methodology for the construction of these exp-synergistic potential functions is provided [Berkane and Tayebi, 2017e]. Note that in [Mayhew and Teel, 2011d] only existence results are reported for synergistic potential functions. Moreover, exp-synergism allows for *non-everywhere differentiable* potential functions to be used which presents an andvantage over the synergism concept. In fact, controllers derived from non-smooth potential functions have been shown to ensure better performance compared to those derived from traditional smooth potential functions, see for instance [Lee, 2012, Zlotnik and Forbes, 2017] where nonsmooth potential functions on $\mathbb{SO}(3)$ have been used to improve the performance of existing attitude control and estimation schemes. Using these hybrid tools, a hybrid control algorithm that ensures global exponential tracking of any attitude trajectory is derived [Berkane *et al.*, 2017b]. To the best of our knowledge, global exponential tracking on $\mathbb{SO}(3)$ has never been achieved before. Moreover, since discontinuities in the control might be undesirable in practical applications, a smoothing mechanism that moves the discontinuity in the control one integrator behind is proposed. In other words, the jumps in the hybrid controller are filtered and do not appear in the control torque. This smoothing approach is simpler than the one proposed in [Mayhew and Teel, 2013a] and can be implemented using only a first order low pass filter.

In the field of attitude estimation from continuous measurements, two hybrid estimation schemes guaranteeing both global exponential stability of the attitude and gyro-bias estimation errors are proposed [Berkane *et al.*, 2017a, Berkane and Tayebi, 2017b]. Both observers have a general structure of a nonlinear complementary filter on $\mathbb{SO}(3) \times \mathbb{R}^3$ where the attitude estimate evolves on $\mathbb{SO}(3)$ and the gyro-bias vector evolves on $\mathbb{R}^3$. The first observer approach uses a synergistic-based technique to generate a family of observer innovation terms among which the appropriate term is selected according to the evolution of the estimates. Each innovation (correction) term is nothing but a gradient of some cost function. A switching mechanism allows to jump to the innovation term that generates the minimum cost function while avoiding the undesired critical and singular points. An adequate choice of the cost function allows to express this hybrid observer using directly body-frame vector measurements of known *constant* inertial di-

rections without the need for attitude reconstruction. The second observer approach uses a fixed innovation term but allows for the attitude state to jump (reset) to an adequately selected value whenever the difference between the current cost function and the *post* cost function (value of the cost function after a possible reset) exceeds certain threshold. This threshold is selected in a way such that all undesired critical and singular points of the cost function lie in the set where the observer states are reset. The proposed reset-based hybrid observer can be directly expressed using body-frame measurements of know, possibly *time-varying*, inertial vectors.

The problem of attitude estimation from *intermittent* measurements have been formulated and tackled using measurement-triggered observers [Berkane and Tayebi, 2017d, Berkane and Tayebi, 2017c]. First, in the case where the body-frame measurements are collected synchronously at the same instants of time, an attitude observer on $\mathbb{SO}(3)$ is proposed which consists of a forward integration of the continuous angular velocity (propagation), and a jump equation (update) that uses the collected measurements to reset the rotation estimate to a value guaranteeing a smaller estimation error. This estimation scheme has a similar structure as the one proposed in [Barrau and Bonnabel, 2015] but with the use of the Rodrigues map instead of the exponential map to simplify the design. In the case where the measurements are collected asynchronously (not arriving at the same time) the update equation is executed at each instant of time where a new measurement arrives. Although this problem can also be tackled using the predictor based approach of [Khosravian *et al.*, 2015], our approach is a predictor-free solution that uses only a single vector measurement at a time to correct the attitude estimate, thus saving memory and computation. To analyze the behaviour of the proposed attitude estimation schemes, the closed-loop systems are extended with *virtual timers* which are reset to zero at the arrival time of a new measurement. Each timer is allowed to flow linearly when the corresponding measurement is not available. The extended closed-loop system is modelled as an autonomous hybrid system and almost global exponential, respectively asymptotic, stability is proved for the synchronous, respectively asynchronous, measurement-triggered observers. Some practical issues related to the implementation of the proposed estimation schemes are discussed which resulted in different extensions and modifications to the original algorithms. The first tackled issue is the discrete time implementation of the proposed estimation schemes. The observers are discretized using first order Euler-Lie method [Celledoni *et al.*, 2014]. Interestingly, the interconnection of the discrete version of the observer with a discrete approximation of the kinematic attitude equation yields an almost globally convergent estimator. This property is strong and does not hold, in general, for most existing continuous attitude estimators on $\mathbb{SO}(3)$ such

as [Mahony *et al.*, 2008]. Secondly, for both observers (synchronous and asychronous) the attitude estimate is further refined (filtered) through an averaging procedure on $\mathbb{SO}(3)$ using a shift register (containing the previous attitude estimates). A similar averaging idea was proposed in [Brodtkorb *et al.*, 2015] for a system evolving on the Euclidean space $\mathbb{R}^6$ where recursive states were introduced to filter out the noise in the intermittent position and velocity measurements used as input to an observer for marine vessels. In the case where the measurements are updated at very low frequencies, the discrete transitions in the attitude state might become undesirable. In this case, the estimation scheme can be smooth out by combing the intermittent observer with a smoother on $\mathbb{SO}(3)$ without affecting the stability properties. Finally, the practical problem of biased angular velocity measurements is considered. In this case the intermittent attitude observer is extended with a measurement-triggered bias estimation scheme. In the case where the measurements are synchronously available with a regular sampling, local exponential stability of the overall closed-loop system is shown.

## 1.5 List of Publications

The material presented in this work is based on the following publications, including submitted and under review papers:

### Journal Articles

1. **S. Berkane**, A. Abdessameud and A. Tayebi, "*Hybrid Global Exponential Stabilization on $SO(3)$*", Automatica, Vol. 81, pp. 279–285, 2017.

2. **S. Berkane** and A. Tayebi, *"Construction of Synergistic Potential Functions on $SO(3)$ with Application to Velocity-Free Hybrid Attitude Stabilization"*, IEEE Transactions on Automatic Control, Vol. 62, No. 1, pp. 495–501, 2017.

3. **S. Berkane**, A. Abdessameud and A. Tayebi, "*Hybrid Attitude and Gyro-bias Observer on $SO(3)$*", IEEE Transactions on Automatic Control, (to appear), 2017.

4. **S. Berkane** and A. Tayebi, "*Attitude Estimation with Intermittent Measurements*", Automatica (Submission No. 17-0878), 2017.

### Peer-Reviewed Conference Proceedings

1. **S. Berkane** and A. Tayebi, *"Attitude Observer Using Synchronous Intermittent*

*Vector Measurements"*, In Proceedings of the 56th IEEE Conference on Decision and Control (CDC), Melbourne, Australia, 2017.

2. **S. Berkane** and A. Tayebi, *"A Globally Exponentially Stable Hybrid Attitude and Gyro-bias Observer"*, In Proceedings of the 55th IEEE Conference on Decision and Control (CDC), Las Vegas, USA, 2016, pp. 308-313.

3. **S. Berkane**, A. Abdessameud and A. Tayebi, *"Global Hybrid Attitude Estimation on the Special Orthogonal Group SO(3)"*, In Proceedings of the 2016 American Control Conference, Boston, USA, 2016, pp. 113-118.

4. **S. Berkane** and A. Tayebi, *"On the Design of Synergistic Potential Functions on SO(3)"*, In Proceedings of the 54th IEEE Conference on Decision and Control, December 15-18, 2015. Osaka, Japan, pp. 270-275.

In addition, the work in the following papers has been carried out during the same period of time and is not included in this thesis:

## Journal Articles

1. **S. Berkane** and A. Tayebi, "*On the Design of Attitude Complementary Filters on* $SO(3)$", IEEE Transactions on Automatic Control, 2017, (to appear).

2. **S. Berkane**, A. Abdessameud and A. Tayebi, "*Hybrid Output Feedback For Attitude Tracking on* $SO(3)$", IEEE Transactions on Automatic Control (Submission No. 16-1824), 2016.

## Peer-Reviewed Conference Proceedings

1. **S. Berkane** and A. Tayebi, *"Attitude and Gyro Bias Estimation Using GPS and IMU Measurements"*, In Proceedings of the 56th IEEE Conference on Decision and Control (CDC), Melbourne, Australia, 2017.

2. **S. Berkane**, A. Abdessameud and A. Tayebi, *"Global Exponential Angular Velocity Observer for Rigid Body Systems"*, In Proceedings of the 55th IEEE Conference on Decision and Control (CDC), Las Vegas, USA, 2016, pp. 4154-4159.

3. **S. Berkane**, A. Abdessameud and A. Tayebi, *"On Deterministic Attitude Observers on the Special Orthogonal Group SO(3)"*, In Proceedings of the 55th IEEE Conference on Decision and Control (CDC), Las Vegas, USA, 2016, pp. 1165-1170.

4. **S. Berkane** and A. Tayebi, *"Velocity-Free Hybrid Attitude Stabilization Using Inertial Vector Measurements"*, In Proceedings of the 2016 American Control Conference, Boston, USA, 2016, pp. 6048-6053.

5. **S. Berkane** and A. Tayebi, *"Some Optimization Aspects on the Lie Group $SO(3)$"*, In Proceedings of the 15th IFAC Symposium on Information Control Problems in Manufacturing, May 11-13, 2015, Ottawa, Canada, pp. 1173-1177.

## 1.6 Thesis Outline

This thesis is organized as follows:

**Chapter 2** introduces the mathematical background and preliminary results that are used throughout the thesis. Section 2.1 provides the general notations used in this thesis. Section 2.2 describes the rigid body attitude, attitude parametrizations, attitude metrics, attitude visualization and useful identities and lemmas, some of which are newly derived in this work. Section 2.3 presents the hybrid systems framework used in this work and gives new relaxed conditions for exponential stability in hybrid systems. Finally, Section 2.4 presents some tools for numerical integration and simulation both on the Euclidean and the rotation group and for hybrid systems as well.

**Chapter 3** presents a framework for global exponential stabilization on the rotation group $\mathbb{SO}(3)$ via hybrid feedback. After an introduction, Section 3.2 explains the topological obstruction for global asymptotic stabilization on compact manifolds by considering the simple example of the unit circle $\mathbb{S}^1$. This example also motivates the hybrid feedback tools used in this work. Section 3.3 discusses the drawbacks of smooth stabilization on $\mathbb{SO}(3)$ and introduces the concept of exp-synergism as well as the main structure of a hybrid synergistic feedback that achieves global exponential stability on $\mathbb{SO}(3)$. Systematic methodologies for the construction of exp-synergistic potential functions from existing smooth and nonsmooth potential functions on $\mathbb{SO}(3)$ are presented. Section 3.4 applies the concept of hybrid synergistic feedback to the attitude tracking problem and simulation results are provided to illustrate the effectiveness of the proposed control algorithms.

**Chapter 4** is devoted to the attitude estimation problem on $\mathbb{SO}(3)$ using continuous/intermittent measurements. Section 4.2 presents two techniques for the design of globally exponentially stable attitude and gyro-bias observers on $\mathbb{SO}(3)$. The first tech-

nique uses exp-synergistic potential functions to derive different innovation terms for the observer while the second technique is based on resetting the attitude matrix to an adequate value if the current estimation error provides a "large" enough cost. Section 4.3 deals with the problem of attitude estimation from intermittent (sporadic) vector observations. Both cases of synchronous and asynchronous measurements are treated. Simulation results are provided in both sections to illustrate the effectiveness of the proposed estimation algorithms.

**Chapter 5** summarizes the findings of this thesis and presents some possible future directions.

**Appendices A, B and C** give the detailed proofs for all the lemmas, propositions and theorems, respectively, stated throughout the thesis.

# Chapter 2

# Background and Preliminaries

## 2.1 General Notations

For a general orthonormal basis $\mathcal{V} = \{v_1, \cdots, v_n\}$ of $\mathbb{R}^n$ we use the notation $x = [x_1, \cdots, x_n]^\top_\mathcal{V}$ if $x = \sum_{i=1}^n x_i v_i$. In particular, the notation $x = [x_1, \cdots, x_n]^\top$ is used when $x$ is represented with respect to the canonical (standard) basis of $\mathbb{R}^n$ denoted by $\{e_i\}_{1 \leq i \leq n}$. The ordered standard basis $\{e_1, \cdots, e_n\}$, along with the *origin* point $x = [0, \cdots, 0]^\top \in \mathbb{R}^n$ defines the Cartesian coordinate system on $\mathbb{R}^n$. For a given square matrix $A \in \mathbb{R}^{n \times n}$, the set $\mathcal{E}_\lambda(A)$ denotes the set of all eigenvalues of $A$. Note that if $A$ is symmetric, all the eigenvalues of $A$ are real and thus $\mathcal{E}_\lambda(A) \subset \mathbb{R}$. The set $\mathcal{E}_v(A)$ denotes the set of unit eigenvectors of $A$ and $\mathcal{E}_v^\mathbb{R}(A)$ corresponds to the set of real unit eigenvectors of $A$. For simplicity, when $\mathcal{E}_\lambda(A) \subset \mathbb{R}$, the set of eigenvalues of $A$ is ordered such that $\lambda_1^A \leq \lambda_2^A \cdots \leq \lambda_n^A$ where $\lambda_i^A$ is the $i$-th eigenvalue of $A$. In this case, $\lambda_{\min}^A$ and $\lambda_{\max}^A$ will denote the smallest and largest eigenvalues of $A$, respectively. Moreover, for $v \in \mathcal{E}_v(A)$, $\lambda_v^A$ denotes the eigenvalue of $A$ associated to the eigenvector $v$. If $a = [a_1, a_2, a_3]^\top_\mathcal{V}$ and $b = [b_1, b_2, b_3]^\top_\mathcal{V}$ are vectors in $\mathbb{R}^3$ expressed in the orthonormal basis $\mathcal{V} = \{v_1, \cdots, v_n\}$, then their cross product can be written as [Arfken *et al.*, 1999]

$$a \times b = \sum_{m,n,l} \varepsilon_{mnl} a_m b_n v_l, \tag{2.1}$$

where $\varepsilon_{mnl}$ is the Levi-Cevita symbol defined by

$$\varepsilon_{mnl} = \begin{cases} 0 & \text{for } m = n, m = l \text{ or } n = l \\ +1 & \text{for } (m,n,l) \in \{(1,2,3),(2,3,1),(3,1,2)\} \\ -1 & \text{for } (m,n,l) \in \{(1,3,2),(3,2,1),(2,1,3)\} \end{cases}. \tag{2.2}$$

Let $\phi \in \mathbb{R}^n$ be a given unknown constant parameter such that $\|\phi\| \leq c_\phi$ for some known constant scalar $c_\phi > 0$. The projection function $\mathbf{P}_{c_\phi} : \mathbb{R}^3 \times \mathbb{R}^3 \to \mathbb{R}^3$, obtained from [Krstic *et al.*, 1995], is defined as follows:

$$\mathbf{P}_{c_\phi}(\hat{\phi}, \mu) = \begin{cases} \mu & \text{if } \|\hat{\phi}\| < c_\phi \text{ or } \hat{\phi}^\top \mu \leq 0 \\ \left(I - \theta(\hat{\phi}) \frac{\hat{\phi}\hat{\phi}^\top}{\|\hat{\phi}\|^2}\right) \mu & \text{otherwise} \end{cases} . \tag{2.3}$$

where $\theta(\hat{\phi}) = \min(1, (\|\hat{\phi}\| - c_\phi)/\varepsilon)$ for some $\varepsilon > 0$ used to obtain a smooth projection function. Note that although the projection function depends on $\varepsilon$, this argument is removed for compactness. The projection operator is locally Lipschitz in its arguments and satisfies, along the trajectories of $\dot{\hat{\phi}} = \mathbf{P}_{c_\phi}(\hat{\phi}, \mu), \|\hat{\phi}(0)\| \leq c_\phi + \varepsilon$, the following important properties

$$\|\hat{\phi}(t)\| \leq c_\phi + \varepsilon, \ \forall t \geq 0, \tag{2.4}$$

$$(\hat{\phi} - \phi)^\top \mathbf{P}_{c_\phi}(\hat{\phi}, \mu) \leq (\hat{\phi} - \phi)^\top \mu, \tag{2.5}$$

$$\|\mathbf{P}_{c_\phi}(\hat{\phi}, \mu)\| \leq \|\mu\|. \tag{2.6}$$

Given a manifold $\mathcal{M}$, a tangent vector at $x \in \mathcal{M}$ is defined by $\gamma'(0) := d\gamma(\tau)/d\tau|_{\tau=0}$ for some smooth path $\gamma : \mathbb{R}_{\geq 0} \to \mathcal{M}$ such that $\gamma(0) = x$. The *tangent space* to $\mathcal{M}$ at $x$ is the set of all tangent vectors at $x$, denoted $\mathsf{T}_x\mathcal{M}$. The disjoint union of all tangent spaces forms the *tangent bundle* $\mathsf{T}\mathcal{M}$. Let $\mathcal{M}$ and $\mathcal{N}$ be two smooth manifolds and let $f : \mathcal{M} \to \mathcal{N}$ be a differentiable map. The *tangent map (differential)* of $f$ at a point $x \in \mathcal{M}$ is the map [Darryl D. Holm and Stoica, 2009]

$$\begin{aligned} df_x : \mathsf{T}_x\mathcal{M} &\to \mathsf{T}_{f(x)}\mathcal{N} \\ \xi &\mapsto df_x(\xi) := (f \circ \gamma)'(0), \end{aligned}$$

where $\gamma(t)$ is a path in $\mathcal{M}$ such that $\gamma(0) = x$ and $\gamma'(0) = \xi$. The inverse image of a subset $\mathcal{S}_\mathcal{N} \subseteq \mathcal{N}$ under the map $f$ is the subset of $\mathcal{M}$ defined by $f^{-1}(\mathcal{S}_\mathcal{N}) = \{x \in \mathcal{M} \mid f(x) \in \mathcal{S}_\mathcal{N}\}$. Let $f : \mathcal{M} \to \mathbb{R}$ be a differentiable real-valued function. A point $x \in \mathcal{M}$ is called a *critical point*[1] of $f$ if the differential map $df_x(\xi)$ is zero at $x$ for all $\xi \in \mathsf{T}_x\mathcal{M}$. The set $\mathcal{C}_f \subseteq \mathcal{M}$ denotes the set of all critical points of $f$ on $\mathcal{M}$. Let $\langle\ ,\ \rangle_x : \mathsf{T}_x\mathcal{M} \times \mathsf{T}_x\mathcal{M} \to \mathbb{R}$ be a *Riemannian metric* on $\mathcal{M}$. The *gradient* of $f$, denoted $\nabla f(x) \in \mathsf{T}_x\mathcal{M}$, relative to the Riemannian metric $\langle\ ,\ \rangle_x$ is uniquely defined by

$$df_x(\xi) = \langle \nabla f(x), \xi \rangle_x \quad \text{for all } \xi \in \mathsf{T}_x\mathcal{M}. \tag{2.7}$$

[1] For a reference, see Morse Theory 279 (VII.16), page 1049 of [Itô, 1993].

## 2.2 Rigid Body Attitude

Consider an inertial reference frame, denoted $\mathcal{I}$, attached to the origin on $\mathbb{R}^3$ and associated to the Cartesian coordinate system. The pose of a rigid body in 3D space is fully described by the position of its center of mass and the orientation of a body-attached frame, denoted $\mathcal{B}$, with respect to the inertial frame of reference, see Figure 2.1.

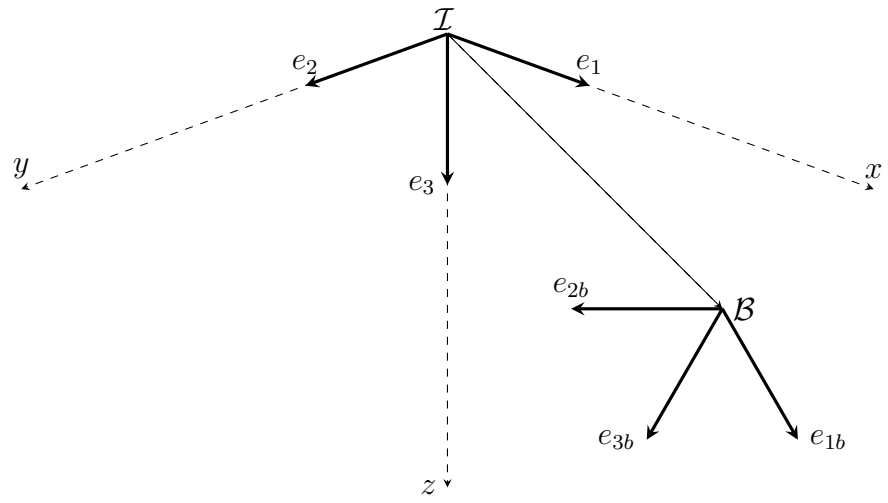


Figure 2.1: Coordinate systems: $\mathcal{I}$ (inertial reference frame) and $\mathcal{B}$ (body-attached frame).

The orientation of a rigid body is described by a *rotation matrix*, denoted $R$, that describes the orientation of the inertial frame $\mathcal{I}$ with respect to the body-attached frame $\mathcal{B}$ such that the body coordinate axes are defined by the unit vectors $e_{ib}$ which are defined as

$$e_{ib} = Re_i, \quad i \in \{1, 2, 3\}. \tag{2.8}$$

It turns out that the rotation matrix $R$ is an element of the *Special Orthogonal group* of order three defined by

$$\mathbb{SO}(3) := \{R \in \mathbb{R}^{3\times 3} : \mathbf{det}(R) = 1,\ RR^\top = R^\top R = I\}, \tag{2.9}$$

where $I$ denotes the three-dimensional identity matrix. $\mathbb{SO}(3)$ is a matrix Lie group under the matrix multiplication operator. The Lie algebra of $\mathbb{SO}(3)$ is denoted by $\mathfrak{so}(3)$ and consists of all skew-symmetric 3 by 3 matrices

$$\mathfrak{so}(3) := \left\{\Omega \in \mathbb{R}^{3\times 3} : \Omega^\top = -\Omega\right\}. \tag{2.10}$$

The Lie algebra $\mathfrak{so}(3)$ is isomorphic to $\mathbb{R}^3$ through the map $[\cdot]_\times : \mathbb{R}^3 \to \mathfrak{so}(3)$ defined by

$$\omega \mapsto [\omega]_\times = \begin{bmatrix} 0 & -\omega_3 & \omega_2 \\ \omega_3 & 0 & -\omega_1 \\ -\omega_2 & \omega_1 & 0 \end{bmatrix},$$

where $\omega = [\omega_1, \omega_2, \omega_3]^\top \in \mathbb{R}^3$. The inverse isomorphism of the map $[\cdot]_\times$ is defined by $\mathbf{vex} : \mathfrak{so}(3) \to \mathbb{R}^3$, such that $\mathbf{vex}([\omega]_\times) = \omega$, for all $\omega \in \mathbb{R}^3$ and $[\mathbf{vex}(\Omega)]_\times = \Omega$, for all $\Omega \in \mathfrak{so}(3)$. The composition map $\psi := \mathbf{vex} \circ \mathbf{P}_{\mathfrak{so}(3)}$ extends the definition of $\mathbf{vex}$ to $\mathbb{R}^{3\times3}$, where $\mathbf{P}_{\mathfrak{so}(3)} : \mathbb{R}^{3\times3} \to \mathfrak{so}(3)$ is the projection map on the Lie algebra $\mathfrak{so}(3)$ such that $\mathbf{P}_{\mathfrak{so}(3)}(A) := (A - A^\top)/2$. Accordingly, for a 3-by-3 matrix $A := [a_{ij}]_{i,j=1,2,3}$, one has

$$\psi(A) := \mathbf{vex}\left(\mathbf{P}_{\mathfrak{so}(3)}(A)\right) = \frac{1}{2}\begin{bmatrix} a_{32} - a_{23} \\ a_{13} - a_{31} \\ a_{21} - a_{12} \end{bmatrix}. \tag{2.11}$$

Also, the map $\mathbf{P}_{\mathbb{SO}(3)} : \mathbb{R}^{3\times3} \to \mathbb{SO}(3)$ is defined as the projection of $X \in \mathbb{R}^{3\times3}$ on $\mathbb{SO}(3)$ (*i.e.* closest rotation matrix to $X$). This rotation matrix can be obtained using the Singular Value Decomposition [Hartley *et al.*, 2013]. Let $X = UDV^\top$ be the SVD decomposition of $X$ such that the diagonal elements of $D$ are arranged in descending order. The closest orthogonal matrix to $X$ is given by

$$\mathbf{P}_{\mathbb{SO}(3)}(X) = U\mathrm{diag}(1, 1, d)V^\top \tag{2.12}$$

where $d = \mathrm{sign}(\mathbf{det}(UV^\top))$ ($+1$ or $-1$). The group $\mathbb{SO}(3)$ has a compact manifold structure where its *tangent spaces* are identified by $\mathsf{T}_R\mathbb{SO}(3) := \{R\Omega \mid \Omega \in \mathfrak{so}(3)\}$ for any $R \in \mathbb{SO}(3)$. Note that the Lie algebra can be also identified as the tangent space at the identity rotation $I$, *i.e.* $\mathsf{T}_I\mathbb{SO}(3) \equiv \mathfrak{so}(3)$. The Euclidean inner product on $\mathbb{R}^{3\times3}$, when restricted to the Lie-algebra of skew symmetric matrices, defines the following *left-invariant* Riemannian metric on $\mathbb{SO}(3)$

$$\langle R\Omega_1, R\Omega_2\rangle_R := \langle\langle \Omega_1, \Omega_2 \rangle\rangle, \tag{2.13}$$

for all $R \in \mathbb{SO}(3)$ and $\Omega_1, \Omega_2 \in \mathfrak{so}(3)$. The kinematic relation between an attitude trajectory $R(t) \in \mathbb{SO}(3)$ and the angular velocity vector can be obtained by differentiating

the orthogonality condition $RR^\top = I$ which gives

$$\frac{d}{dt}(R^\top R) = R^\top \dot{R} + (\dot{R})^\top R = 0. \tag{2.14}$$

It follows that $R(t)^\top \dot{R}(t) \in \mathfrak{so}(3)$ for all times $t \geq 0$ or, equivalently, there exists $\omega(t) \in \mathbb{R}^3$ such that $R(t)^\top \dot{R}(t) = [\omega(t)]_\times$. This leads to write

$$\dot{R}(t) = R(t)[\omega(t)]_\times, \tag{2.15}$$

which represents the attitude kinematics where $\omega(t)$ is referred to as the angular velocity vector. If $R$ is a rotation matrix describing the orientation of a body frame with respect to an inertial frame then $\omega(t)$ is the body-referenced (expressed in body frame coordinates) angular velocity of the body frame with respect to the inertial frame.

### 2.2.1 Attitude Parametrizations

The natural nine parameters representation of the attitude as an element of $\mathbb{SO}(3)$ is unique and nonsingular. However, due to the presence of the constraints $R^\top R = RR^\top = I$ and $\mathbf{det}(R) = 1$, it is possible to represent an attitude $R \in \mathbb{SO}(3)$ with fewer parameters. In this subsection, low order attitude parametrizations such as the exponential coordinates, the angle-axis, the unit quaternions and the Rodrigues vector representations are described. Although not covered here, some other attitude representations are used in the litterature such as the Euler angles, the modified Rodrigues parameters amongst others. For more details on attitude representations the reader is referred to [Shuster, 1993], [Murray *et al.*, 1994], and [Hughes, 1986].

#### 2.2.1.1 Exponential Coordinates Representation

Since the vector space $\mathfrak{so}(3)$ corresponds to the Lie algebra of $\mathbb{SO}(3)$, it allows to represent elements of $\mathbb{SO}(3)$ via the exponential map. Given a *rotation vector* $x \in \mathbb{R}^3$, the corresponding rotation matrix is given by the exponential map $\exp([x]_\times) \in \mathbb{SO}(3)$ which is defined by the following compact formula on $\mathbb{SO}(3)$

$$\exp([x]_\times) = \begin{cases} I & x = 0 \\ I + \frac{\sin(||x||)}{||x||}[x]_\times + \frac{1-\cos(||x||)}{||x||^2}[x]_\times^2 & x \neq 0 \end{cases}. \tag{2.16}$$

Equation (2.16) is referred to as Rodrigues formula. For a given rotation matrix $R \in \mathbb{SO}(3)$ such that $R = \exp([x]_\times)$, the three-parameters vector $x \in \mathbb{R}^3$ is often referred to

as the exponential coordinates of $R$. The exponential map is a diffeomorphism between $\Pi_{\mathfrak{so}(3)} = \{[x]_\times \in \mathfrak{so}(3) \mid x \in \mathbb{R}^3, ||x|| < \pi\}$ and $\Pi_{\mathbb{SO}(3)} = \{R \in \mathbb{SO}(3) \mid \mathbf{tr}(R) \neq -1\}$. The inverse map $\log : \Pi_{\mathbb{SO}(3)} \to \Pi_{\mathfrak{so}(3)}$ is given by

$$\log(R) = \begin{cases} 0_{3\times 3} & R = I, \\ \frac{\theta(R)}{2\sin(\theta(R))}(R - R^T) & R \neq I, \end{cases} \tag{2.17}$$

where $\theta : \Pi_{\mathbb{SO}(3)} \to [0, \pi)$ is the angle of rotation and is defined by

$$\theta(R) = \arccos\left(\frac{\mathbf{tr}(R) - 1}{2}\right). \tag{2.18}$$

Let $R(t)$ be a smooth curve on $\mathbb{SO}(3)$ evolving according to the kinematic equation (2.15) such that $\mathbf{tr}(R(t)) \neq -1$ for all $t \geq 0$. Let $x(t) = \mathbf{vex}(\log(R(t)))$ be the exponential coordinates of $R(t)$ then one has (see [Bullo and Murray, 1995])

$$\dot{x}(t) = \left(I + \frac{1}{2}[x(t)]_\times + \alpha(\|x(t)\|)[x(t)]_\times^2\right)\omega(t) \tag{2.19}$$

where $\alpha(y) := (1 - (y/2)\cot(y/2))/y^2$.

#### 2.2.1.2 Angle-Axis Representation

Given a unit vector $u \in \mathbb{S}^2$ and an angle $\theta \in \mathbb{R}$, we define the following map

$$\mathbf{R}_a(\theta, u) := \exp([\theta u]_\times) = I + \sin(\theta)[u]_\times + (1 - \cos(\theta))[u]_\times^2. \tag{2.20}$$

The above parametrization of $\mathbb{SO}(3)$ is often known as the angle-axis parametrization. For a given matrix $R \in \mathbb{SO}(3)$, this parametrization is not unique. In fact, for attitudes of angle $\pi$, it is not difficult to show that $\mathbf{R}_a(\pi, u) = \mathbf{R}_a(-\pi, u)$ for all $u \in \mathbb{S}^2$. The following composition rule is recalled

$$\mathbf{R}_a(\theta_1, u)\mathbf{R}_a(\theta_2, u) = \mathbf{R}_a(\theta_1 + \theta_2, u), \quad \forall \theta_1, \theta_2 \in \mathbb{R}, \forall u \in \mathbb{S}^2. \tag{2.21}$$

Consider an attitude trajectory $R(t) = \mathbf{R}_a(\theta(t), u(t))$ satisfying the attitude kinematics equation (2.15), then one has

$$\dot{\theta}(t) = u(t)^\top \omega(t), \tag{2.22}$$

$$\dot{u}(t) = \frac{1}{2}\left([u(t)]_\times - \cot(\theta(t)/2)[u(t)]_\times^2\right)\omega(t). \tag{2.23}$$

#### 2.2.1.3 Unit Quaternions Representation

A unit quaternion $Q = (\eta, \epsilon) \in \mathbb{Q}$, consists of a scalar part $\eta$ and three-dimensional vector $\epsilon$, such that $\mathbb{Q} := \{(\eta, \epsilon) \in \mathbb{R} \times \mathbb{R}^3 : \eta^2 + \epsilon^\top \epsilon = 1\}$. The relation between the quaternion representation and the angle-axis representation is given by

$$\eta = \cos(\theta/2), \tag{2.24}$$

$$\epsilon = \sin(\theta/2)\, u. \tag{2.25}$$

Therefore, in view of (2.20), a unit quaternion represents a rotation matrix through the map $\mathbf{R}_u : \mathbb{Q} \to \mathbb{SO}(3)$ defined as

$$\mathbf{R}_u(\eta, \epsilon) = I + 2[\epsilon]_\times^2 + 2\eta[\epsilon]_\times. \tag{2.26}$$

The set $\mathbb{Q}$ forms a group with the quaternion product, denoted by $\odot$, being the group operation and quaternion inverse defined by $Q^{-1} = (\eta, -\epsilon)$ as well as the identity-quaternion $Q = (1, 0_{3\times1})$, where $0_{3\times1} \in \mathbb{R}^3$ is a column vector of zeros. Given $Q_1, Q_2 \in \mathbb{Q}$ where $Q_1 = (\eta_1, \epsilon_1)$ and $Q_2 = (\eta_2, \epsilon_2)$ the quaternion product is defined by

$$Q_1 \odot Q_2 = \left(\eta_1\eta_2 - \epsilon_1^\top \epsilon_2, \eta_1\epsilon_2 + \eta_2\epsilon_1 + [\epsilon_1]_\times \epsilon_2\right), \tag{2.27}$$

and satisfying

$$\mathbf{R}_u(Q_1)\mathbf{R}_u(Q_2) = \mathbf{R}_u(Q_1 \odot Q_2). \tag{2.28}$$

Unit quaternions, also known as *versors*, are simpler to compose compared to the exponential coordinates and more compact compared to rotation matrices. The quaternion map $\mathbf{R}_u$ represents a two-to-one map in the sense that the two quaternions $(\eta, \epsilon)$ and $(-\eta, -\epsilon)$ corresponds to the same rotation matrix on $\mathbb{SO}(3)$ (same attitude). Let $R(t) = \mathbf{R}_u(\eta(t), \epsilon(t))$ satisfying the attitude kinematic equation (2.15), then the corresponding quaternion kinematics are given by

$$\dot{\eta}(t) = -\frac{1}{2}\epsilon(t)^\top \omega(t), \tag{2.29}$$

$$\dot{\epsilon}(t) = \frac{1}{2}\left(\eta(t) I + [\epsilon(t)]_\times\right)\omega(t). \tag{2.30}$$

#### 2.2.1.4 Rodrigues Vector Representation

Another useful attitude representation is the well known *Rodrigues vector* on $\mathbb{R}^3$ which is also associated to the Cayley transform. Consider the map $\mathbf{R}_r : \mathbb{R}^3 \to \mathbb{SO}(3)$ such that

$$\mathbf{R}_r(z) = (I - [z]_\times)(I + [z]_\times)^{-1} = \frac{1}{1 + \|z\|^2}\left((1 - \|z\|^2)I + 2zz^\top + 2[z]_\times\right). \tag{2.31}$$

Note that since $[z]_\times$ is skew-symmetric all its eigenvalues are pure imaginary. Thus, all the eigenvalues of the matrix $I + [z]_\times$ are non zero and therefore its inverse exists. The map $\mathbf{R}_r$ is a diffeomorphism between $\mathbb{R}^3$ and $\Pi_{\mathbb{SO}(3)}$. The inverse map $\mathbf{Z} : \Pi_{\mathbb{SO}(3)} \to \mathbb{R}^3$ is given by

$$\mathbf{Z}(R) = \mathbf{vex}\big((I - R)(I + R)^{-1}\big) = \frac{2\psi(R)}{1 + \mathbf{tr}(R)}. \tag{2.32}$$

It is not difficult to show that the following relations hold for all quaternions $(\eta, \epsilon) \in \Pi_{\mathbb{Q}}$ and all angle-axes $(\theta, u) \in \mathbb{R} \times \mathbb{S}^2$, such that $\theta \neq k\pi, k \in \mathbb{Z}$,

$$\mathbf{Z}(\mathbf{R}_u(\eta, \epsilon)) = \frac{\epsilon}{\eta}, \tag{2.33}$$

$$\mathbf{Z}(\mathbf{R}_a(\theta, u)) = \tan(\theta/2)u. \tag{2.34}$$

The vector $\mathbf{Z}(R) \in \mathbb{R}^3$ defines the vector of Rodrigues parameters. Note that the Rodrigues vector is sometimes defined using the unit quaternion or the angle-axis representation [Shuster, 1993]. It can be verified that the time derivative of the Rodrigues vector $\mathbf{Z}(R)$ along the trajectories of (2.15) is given by

$$\frac{d}{dt}\mathbf{Z}(R) = \frac{1}{2}\big(I + [\mathbf{Z}(R)]_\times + \mathbf{Z}(R)\mathbf{Z}(R)^\top\big)\omega. \tag{2.35}$$

### 2.2.2 Metrics on $\mathbb{SO}(3)$

Roughly speaking, a metric (or distance) tells us how two elements of a given manifold are close to each other. More rigorously, a metric on $\mathbb{SO}(3)$ is a function $\mathbf{d} : \mathbb{SO}(3) \times \mathbb{SO}(3) \to \mathbb{R}_{\geq 0}$ that satisfies the following properties for all $R_1, R_2, R_3 \in \mathbb{SO}(3)$:

- Non-negativity: $\mathbf{d}(R_1, R_2) \geq 0$.
- Identity of indiscernibles: $\mathbf{d}(R_1, R_2) = 0$ if and only if $R_1 = R_2$.
- Symmetry: $\mathbf{d}(R_1, R_2) = \mathbf{d}(R_2, R_1)$.
- Triangle inequality: $\mathbf{d}(R_1, R_3) \leq \mathbf{d}(R_1, R_2) + \mathbf{d}(R_2, R_3)$.

One possible way to measure the distance between two rotation matrices on $\mathbb{SO}(3)$ is to use the Frobenious norm on the embedding Euclidean space $\mathbb{R}^{3\times 3}$ as follows:

$$\mathbf{d}_E(R_1, R_2) = \|R_1 - R_2\|_F, \tag{2.36}$$

which defines the Euclidean (or Chordal) distance on $\mathbb{SO}(3)$. It can be verified that $\mathbf{d}_E(\cdot,\cdot)$ satisfies the following property

$$\mathbf{d}_E(R_1, R_2) = \mathbf{d}_E(I, R_1R_2^\top) = \sqrt{2\mathbf{tr}(I - R_1R_2^\top)} \leq \sqrt{8}, \tag{2.37}$$

where the fact that $R_1R_2^\top \in \mathbb{SO}(3)$, and hence $\mathbf{tr}(R_1R_2) \geq -1$, has been used to obtain the upper bound of $\mathbf{d}_E(\cdot,\cdot)$. Throughout this work, the following *normalized* attitude norm on $\mathbb{SO}(3)$ is used

$$|R|_I = \frac{\mathbf{d}_E(I, R)}{\sqrt{8}} = \frac{\|I - R\|_F}{\sqrt{8}} = \frac{\sqrt{\mathbf{tr}(I - R)}}{\sqrt{4}}. \tag{2.38}$$

Another interesting attitude distance on $\mathbb{SO}(3)$ is what is known as the *Geodesic* or

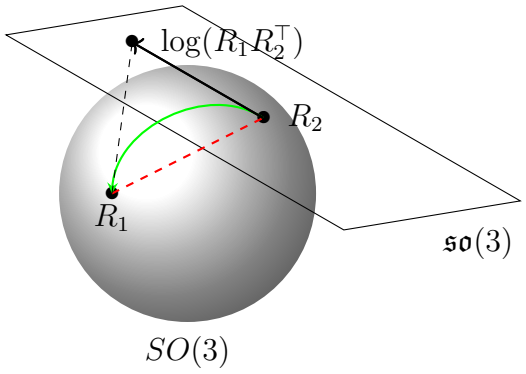


Figure 2.2: Euclidean distance (red dashed) and Geodesic distance (green solid).

Riemannian metric (also known as the angular distance). It is defined as the length of the shortest path on $\mathbb{SO}(3)$ between two rotation matrices. Formally, the geodesic distance on $\mathbb{SO}(3)$ is defined as

$$\mathbf{d}_G(R_1, R_2) = \frac{1}{\sqrt{2}}\|\log(R_1R_2^\top)\|_F. \tag{2.39}$$

Note that $\mathbf{d}_G(R_1, R_2)$ measures the rotation angle between the two matrices $R_1$ and $R_2$ or, equivalently, the angle of the rotation error $R_1R_2^\top$ which lies in the interval $[0, \pi]$.

### 2.2.3 Attitude Visualization

Visualizing the orientation information of a rigid body in 3D space can be done in different ways depending on the application at hand. One possible way consists in using the frame-based description of the orientation as in Figure 2.1. In fact, assume a given trajectory $R(t) : \mathbb{R}_{\geq 0} \to \mathbb{SO}(3)$ then three base vectors trajectories can be obtained as follows

$$e_{ib}(t) = R(t)e_i, \quad i \in \{1, 2, 3\}, \tag{2.40}$$

where each vector $e_{ib}$ describes a trajectory on the unit sphere $\mathbb{S}^2$. Therefore, the rotation path $R(t)$ is visualized by plotting three trajectories on $\mathbb{S}^2$ as demonstrated in Figure 2.3. Alternatively, if plotting three trajectories on the same sphere is cumbersome, one can draw three spheres (instead on one sphere) and plot each trajectory $R(t)e_1, R(t)e_2$ and $R(t)e_3$ on each of these spheres.

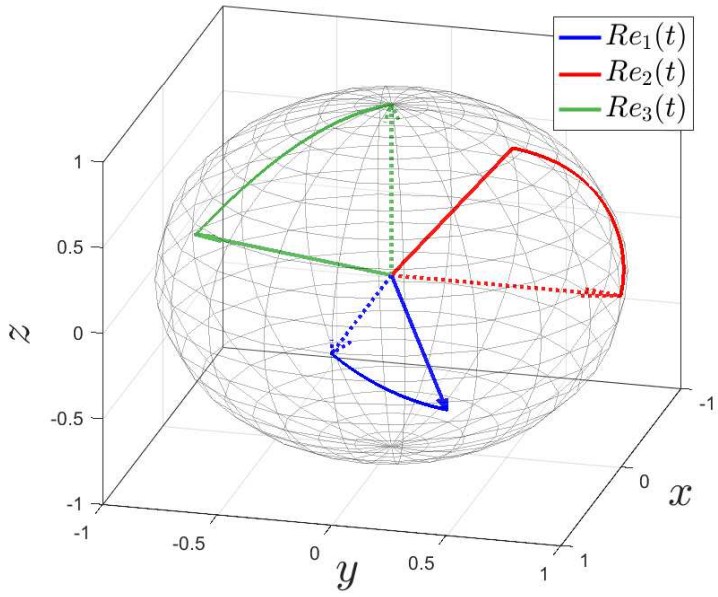


Figure 2.3: Visualization of 3D rotations using the body-frame unit axes $R(t)e_1$, $R(t)e_2$ and $R(t)e_3$. The initial body frame is plotted in dashed and the final body frame is plotted in bold. The trajectory is generated using the angular velocity $\omega(t) = [e^{-t}, e^{-2t}, e^{-3t}]^\top$ with $R(0) = I$ and $t \in [0, 20]$ seconds.

Another way to visualize rotations is to consider the exponential coordinates. The rotation vector $\theta u$ is plotted in x-y-z coordinates where the angle $\theta$ is between 0 and $\pi$ and $u$ dictating the orientation (direction) of the vector in 3D space, see Figure 2.4. Alternatively, the two quantities $\theta$ (angle of rotation) and $u$ (axis of rotation) can be plotted separately to allow clearer reading in applications where the variations of both

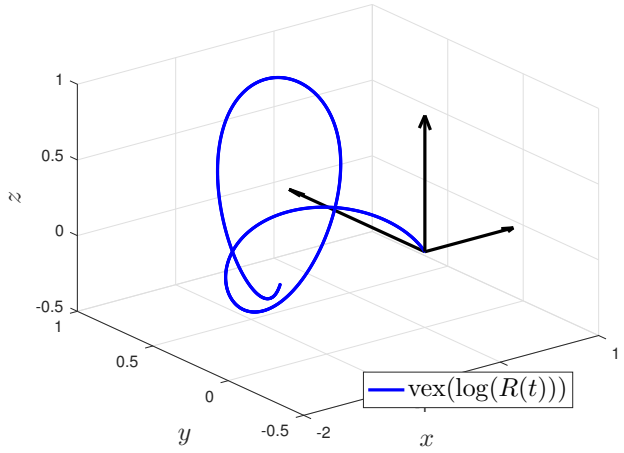


Figure 2.4: Visualization of 3D rotations using the exponential coordinates. The trajectory is generated using the angular velocity $\omega(t) = [-\sin(t), 0, 0.3\cos(t)]^\top$ with $R(0) = I$ and $t \in [0, 10]$ seconds.

quantities are needed to be analyzed separately, see Figure 2.5.

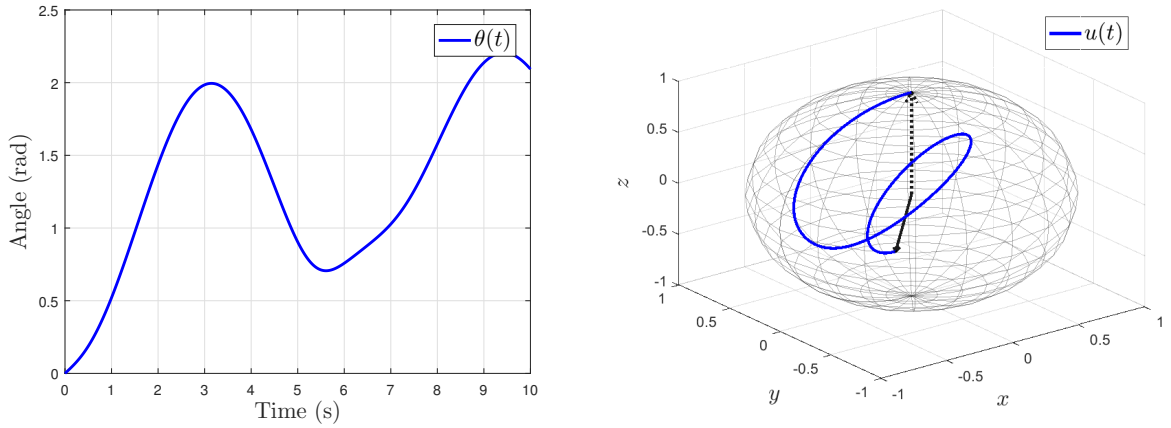


Figure 2.5: Visualization of 3D rotations using the angle-axis representation. The trajectory is generated using the angular velocity $\omega(t) = [-\sin(t), 0, 0.3\cos(t)]^\top$ with $R(0) = I$ and $t \in [0, 10]$ seconds.

### 2.2.4 Useful Identities and Lemmas

In this subsection, useful relations and lemmas, which will be used throughout the dissertation, are provided. Some of these relations are well known and need not to be proved. Other relations, however, are newly derived in this work.

The matrix trace $\mathbf{tr}(\cdot)$ and $\mathbf{det}(\cdot)$ functions have many properties which can be found

in linear algebra textbooks [Lang, 1987]. Here, some of these useful properties are recalled. For any $M, N \in \mathbb{R}^{3\times 3}, x, y \in \mathbb{R}^3$ and $\alpha \in \mathbb{R}$ one has

$$\mathbf{tr}(M^\top) = \mathbf{tr}(M), \tag{2.41}$$
$$\mathbf{tr}(M+N) = \mathbf{tr}(M) + \mathbf{tr}(N), \tag{2.42}$$
$$\mathbf{tr}(\alpha M) = \alpha \mathbf{tr}(M), \tag{2.43}$$
$$\mathbf{tr}(MN) = \mathbf{tr}(NM), \tag{2.44}$$
$$\mathbf{tr}(MN) = 0 \quad (\text{if } M = M^\top \text{ and } N = -N^\top) \tag{2.45}$$
$$\mathbf{det}(MN) = \mathbf{det}(M)\mathbf{det}(N) \tag{2.46}$$
$$\mathbf{det}(I + xy^\top) = 1 + x^\top y. \tag{2.47}$$

Using these properties of the trace function, the following identities are easily derived in a straightforward manner. For all $x, y \in \mathbb{R}^3$ and $R, P \in \mathbb{SO}(3)$ one has

$$\mathbf{tr}(xy^\top) = x^\top y, \tag{2.48}$$
$$\mathbf{tr}(yx^\top(I - RP^\top)) = \frac{1}{2}\|R^\top x - P^\top y\|^2 - \frac{1}{2}\|x - y\|^2. \tag{2.49}$$

The cross product map $[\cdot]_\times$ has many interesting properties and appeared in many references dealing with rigid body attitude applications [Shuster, 1993]. For any $x, y \in \mathbb{R}^3$ one has

$$[x]_\times y = x \times y, \tag{2.50}$$
$$[x]_\times y = -[y]_\times x, \tag{2.51}$$
$$[x]_\times^3 = -\|x\|^2 [x]_\times, \tag{2.52}$$
$$[x]_\times [y]_\times = -(x^\top y)I + yx^\top, \tag{2.53}$$
$$x \times y = 2\psi(yx^\top), \tag{2.54}$$
$$[x \times y]_\times = yx^\top - xy^\top, \tag{2.55}$$
$$\langle\langle [x]_\times, [y]_\times \rangle\rangle = 2x^\top y, \tag{2.56}$$

Moreover, for any $x, y \in \mathbb{R}^3$, $M \in \mathbb{R}^{3\times3}$ and $R \in \mathbb{SO}(3)$ the following relations hold

$$\langle\langle M, [x]_\times\rangle\rangle = \langle\langle \mathbf{P}_{\mathfrak{so}(3)}(M), [x]_\times\rangle\rangle, \tag{2.57}$$
$$[(Mx)\times(My)]_\times = M[x\times y]_\times M^\top, \tag{2.58}$$
$$M[x]_\times + [x]_\times M^\top = [(\mathbf{tr}(M)I - M^\top)x]_\times, \tag{2.59}$$
$$\psi(MR) = R^\top\psi(RM), \tag{2.60}$$
$$R[x]_\times R^\top = [Rx]_\times. \tag{2.61}$$

The matrix square of a rotation $R \in \mathbb{SO}(3)$ is also a rotation around the same axis and with double angle. The rotation $R^2$ can be obtained from $R$ using the following relation [Shuster, 1993]

$$R^2 = R^\top + \mathbf{tr}(R)R - \mathbf{tr}(R)I. \tag{2.62}$$

Using this relation, one obtains the following lemma whose proof is provided in Appendix A.1.

**Lemma 2.2.1** *For any symmetric matrix $M = M^\top \in \mathbb{R}^{3\times3}$ and $R \in \mathbb{SO}(3)$ one has*

$$\mathbf{tr}(M(I - R^2)) = (1 + \mathbf{tr}(R))\mathbf{tr}(M(I - R)), \tag{2.63}$$
$$\mathbf{P}_{\mathfrak{so}(3)}(MR^2) = \mathbf{tr}(R)\mathbf{P}_{\mathfrak{so}(3)}(MR) + \mathbf{P}_{\mathfrak{so}(3)}(MR^\top) \tag{2.64}$$
$$\langle\langle \mathbf{P}_{\mathfrak{so}(3)}(R), \mathbf{P}_{\mathfrak{so}(3)}(MR)\rangle\rangle = \frac{1}{2}\mathbf{tr}(M(I - R^2)). \tag{2.65}$$

It turns out that, in the field of attitude control and estimation, the following mapping $\mathbf{E} : \mathbb{R}^{3\times3} \to \mathbb{R}^{3\times3}$ defined by

$$\mathbf{E}(M) = \frac{1}{2}\big(\mathbf{tr}(M)I - M^\top\big) \tag{2.66}$$

is important and its properties are very handy when deriving the control laws and the proofs of stability. The following lemmas are needed throughout the thesis and are proved in Appendix A.

**Lemma 2.2.2** *Consider the map $\mathbf{E} : \mathbb{R}^{3\times3} \to \mathbb{R}^{3\times3}$ defined in (2.66). Let $M \in \mathbb{R}^{3\times3}$ and let $v$ be an eigenvector of $M^\top$ associated to the eigenvalue $\lambda_v^{M^\top}$. Then, the following hold*

*i)* $\mathbf{E}^{-1}(M) = \mathbf{tr}(M)I - 2M^\top$.

*ii) $v$ is an eigenvector of $\mathbf{E}(M)$, respectively $\mathbf{E}^{-1}(M)$, associated to the eigenvalue $\lambda_v^{\mathbf{E}(M)} = \frac{1}{2}\big(\mathbf{tr}(M) - \lambda_v^{M^\top}\big)$, respectively $\lambda_v^{\mathbf{E}^{-1}(M)} = \mathbf{tr}(M) - 2\lambda_v^{M^\top}$.*

**Lemma 2.2.3** *Consider the map* $\mathbf{E} : \mathbb{R}^{3\times 3} \to \mathbb{R}^{3\times 3}$ *defined in* (2.66). *Then, for any symmetric matrix* $M \in \mathbb{R}^{3\times 3}$, *any rotation matrix* $R \in \mathbb{SO}(3)$ *and any vector* $x \in \mathbb{R}^3$ *one has*

$$x^\top[\lambda_{\min}^{\mathbf{E}(M)} - \mathbf{E}(MR)]x \leq \frac{1}{2}\mathbf{tr}(M(I-R))\|x\|^2, \tag{2.67}$$

$$x^\top[\mathbf{E}(M) - \mathbf{E}(MR)]y \leq \frac{1}{2}\mathbf{tr}(M(I-R))x^\top y + \frac{1}{2}\|M(I-R)\|_F\|x\|\|y\|, \tag{2.68}$$

$$2\lambda_{\min}^{M} - \mathbf{tr}(M) \leq \mathbf{tr}(MR) \leq \max\big(\mathbf{tr}(M), 2\lambda_{\max}^{M} - \mathbf{tr}(M)\big), \tag{2.69}$$

$$\mathbf{E}(M) \geq 0 \Rightarrow \|\mathbf{E}(MR)\|_F \leq \|\mathbf{E}(M)\|_F. \tag{2.70}$$

**Lemma 2.2.4** *Consider the trajectories of* $\dot{R}(t) = R(t)[\omega(t)]_\times$ *with* $R(0) \in \mathbb{SO}(3)$ *and* $\omega(t) \in \mathbb{R}^3$ *for all* $t \geq 0$. *Then, for all* $M \in \mathbb{R}^{3\times 3}$

$$\nabla\mathbf{tr}(M(I-R)) = R\mathbf{P}_{\mathfrak{so}(3)}(MR), \tag{2.71}$$

$$\frac{d}{dt}\mathbf{tr}(M(I-R(t))) = 2\psi(MR(t))^\top\omega(t), \tag{2.72}$$

$$\frac{d}{dt}\psi(MR(t)) = \mathbf{E}(MR(t))\omega(t). \tag{2.73}$$

**Lemma 2.2.5** *Let* $M \in \mathbb{R}^{3\times 3}$ *be a symmetric matrix. Then, for all* $\theta \in \mathbb{R}, u \in \mathbb{S}^1, (\eta, \epsilon) \in \mathbb{Q}$ *and* $z \in \mathbb{R}^3$, *one has*

$$\mathbf{tr}(M(I - \mathbf{R}_a(\theta, u))) = 2(1-\cos(\theta))u^\top\mathbf{E}(M)u, \tag{2.74}$$

$$\mathbf{tr}(M(I - \mathbf{R}_u(\eta, \epsilon))) = 4\epsilon^\top\mathbf{E}(M)\epsilon, \tag{2.75}$$

$$\mathbf{tr}(M(I - \mathbf{R}_r(z))) = 4[1+\|z\|^2]^{-1}z^\top\mathbf{E}(M)z. \tag{2.76}$$

*Moreover, one has*

$$\psi(M\mathbf{R}_a(\theta, u)) = (\sin(\theta)I - (1-\cos(\theta))[u]_\times)\mathbf{E}(M)u, \tag{2.77}$$

$$\psi(M\mathbf{R}_u(\eta, \epsilon)) = 2(\eta I - [\epsilon]_\times)\mathbf{E}(M)\epsilon, \tag{2.78}$$

$$\psi(M\mathbf{R}_r(z)) = 2[1+\|z\|^2]^{-1}(I - [z]_\times)\mathbf{E}(M)z. \tag{2.79}$$

**Lemma 2.2.6** *Let* $M \in \mathbb{R}^{3\times 3}$ *be a symmetric matrix and* $R \in \mathbb{SO}(3)$ *be a rotation*

*matrix. Then the following relations hold:*

$$4\lambda_{\min}^{\mathbf{E}(M)}|R|_I^2 \leq \mathbf{tr}(M(I-R)) \leq 4\lambda_{\max}^{\mathbf{E}(M)}|R|_I^2, \tag{2.80}$$

$$\|\psi(MR)\|^2 = \alpha(M,R)\mathbf{tr}(\mathbf{E}^{-1}(\mathbf{E}(M)^2)(I-R)), \tag{2.81}$$

$$(1-|R|_I^2) \leq \alpha(M,R) \leq (1-\xi^2|R|_I^2) \quad \textit{if } \mathbf{E}(M) \geq 0, \tag{2.82}$$

$$\psi(R)^\top\psi(MR) = \psi(R)^\top\mathbf{E}(M)\psi(R), \tag{2.83}$$

*where* $\alpha(M,R) = (1-|R|_I^2\cos^2(u,\mathbf{E}(M)u))$, $\xi = \lambda_{\min}^{\mathbf{E}(M)}/\lambda_{\max}^{\mathbf{E}(M)}$ *and* $u \in \mathbb{S}^2$ *is the axis of rotation* $R$*. Moreover, the following upper bound holds*

$$\|\psi(MR)\|^2 \leq (\lambda_{\max}^{\mathbf{E}(M)})^2\bar{\psi}(\xi^2), \quad \textit{if } \mathbf{E}(M) \geq 0, \tag{2.84}$$

*where* $\bar{\psi}(\cdot)$ *is defined as* $\bar{\psi}(\xi^2) = 1/\xi^2$ *if* $\xi^2 \geq 1/2$ *and* $\bar{\psi}(\xi^2) = 4(1-\xi^2)$ *otherwise.*

**Lemma 2.2.7** *Let* $M = \sum_{i=1}^n \rho_i x_i x_i^\top$ *with* $n \geq 1$, $\rho_i \in \mathbb{R}$ *and* $x_i \in \mathbb{R}^3$, $i = 1,\ldots,n$*. Then, the following holds for any rotation matrices* $R, P \in \mathbb{SO}(3)$*:*

$$\mathbf{tr}(M(I-RP^\top)) = \frac{1}{2}\sum_{i=1}^n \rho_i\|R^\top x_i - P^\top x_i\|^2, \tag{2.85}$$

$$\psi(MRP^\top) = \frac{1}{2}P\sum_{i=1}^n \rho_i(R^\top x_i \times P^\top x_i) \tag{2.86}$$

**Lemma 2.2.8** *Let* $M$ *be a symmetric matrix. For all* $(\theta,u) \in \mathbb{R}\times\mathbb{S}^2$ *and* $v \in \mathcal{E}_v^{\mathbb{R}}(M)$*, the following holds*

$$\mathbf{tr}(M(I-\mathbf{R}_a(\pi,v)\mathbf{R}_a(\theta,u))) = 4\lambda_v^{\mathbf{E}(M)} - 4\sin^2(\theta/2)\Delta(v,u), \tag{2.87}$$

*where* $\Delta(v,u)$ *is given by*

$$\Delta(v,u) = v^\top\left(\mathbf{E}(M) + [u]_\times\mathbf{E}(M)[u]_\times\right)v. \tag{2.88}$$

## 2.3 Hybrid Systems Framework

A hybrid system is a dynamical system that allows both continuous flows and discrete jumps (transitions) of the state. In this thesis, the framework of hybrid systems developed in [Goebel and Teel, 2006, Goebel *et al.*, 2009, Goebel *et al.*, 2012] is considered. Let $\mathcal{M}$ be a given manifold embedded in $\mathbb{R}^n$. A general model of a hybrid system takes the

form:

$$\begin{cases} \dot{x} & \in \mathbf{F}(x), & x \in \mathcal{F}, \\ x^+ & \in \mathbf{J}(x), & x \in \mathcal{J}, \end{cases} \tag{2.89}$$

where the *flow map*, $\mathbf{F} : \mathcal{M} \rightrightarrows \mathsf{T}\mathcal{M}$ ($\rightrightarrows$ denotes a set-valued mapping) governs the continuous flow of $x$ on the manifold $\mathcal{M}$, the *flow set* $\mathcal{F} \subseteq \mathcal{M}$ dictates where the continuous flow could occur. The *jump map*, $\mathbf{J} : \mathcal{M} \rightrightarrows \mathcal{M}$, governs discrete jumps of the state $x$, and the *jump set* $\mathcal{J} \subseteq \mathcal{M}$ defines where the discrete jumps are permitted.

Solutions to hybrid systems are parametrized by the amount of time spent in the flow set $t \in \mathbb{R}_{\geq 0}$ and by the number of jumps of the state $j \in \mathbb{N}$. Solutions to hybrid systems are therefore defined on a *hybrid time domain*. A subset $\mathbb{H} \subset \mathbb{R}_{\geq 0} \times \mathbb{N}$ is a *hybrid time domain*, if it is a union of finitely or infinitely many intervals of the form $[t_j, t_{j+1}] \times \{j\}$ where $0 = t_0 \leq t_1 \leq t_2 \leq ...$, with the last interval, if existent, being possibly of the form $[t_j, T) \times \{j\}$ with $T$ finite or $T = +\infty$. The ordering of points on each hybrid time domain is such that $(t, j) \preceq (t', j')$ if $t \leq t'$ and $j \leq j'$. A *hybrid arc* is a function $x : \text{dom } x \to \mathcal{M}$, where the domain of the function $x$ (*i.e.* dom $x$) is a hybrid time domain and, for each fixed $j$, $t \mapsto x(t, j)$ is a locally absolutely continuous function on the interval $\mathbb{T}_j = \{t : (t, j) \in \text{dom } x\}$. A hybrid arc $x$ is called complete if dom $x$ is unbounded and Zeno if it is complete and the projection of dom $x$ on $\mathbb{R}_{\geq 0}$ is bounded.

The hybrid arc $x$ is a solution to the hybrid system (2.89) if $x(0, 0) \in \mathcal{F} \cup \mathcal{J}$ and the following conditions are satisfied:

- **Flow condition**: for each $j \in \mathbb{N}$ such that $\mathbb{T}_j$ has a nonempty interior,

$$\dot{x}(t, j) \in \mathbf{F}(x(t, j)), \qquad \text{for almost all } t \in \mathbb{T}_j, \tag{2.90}$$

$$x(t, j) \in \mathcal{F}, \qquad \text{for all } t \in [\min \mathbb{T}_j, \sup \mathbb{T}_j). \tag{2.91}$$

- **Jump condition**: for each $(t, j) \in \text{dom } x$ such that $(t, j + 1) \in \text{dom } x$,

$$x(t, j + 1) \in \mathbf{J}(x(t, j)), \tag{2.92}$$

$$x(t, j) \in \mathcal{J}. \tag{2.93}$$

Consider a hybrid arc $x$ that is not eventually discrete. Let $\bar{j}(t) = \max\{j : (t, j) \in \text{dom } x\}$ and let $T = \sup\{t : (t, j) \in \text{dom } x, j \in \mathbb{N}\}$. Then, the time projection of $x$ is defined as

the function $x_{\downarrow t} : [0, T) \to \mathcal{M}$ such that

$$x_{\downarrow t} = x(t, \bar{j}(t)). \tag{2.94}$$

In the framework [Goebel *et al.*, 2012], three *Basic Conditions* (or Assumptions) have been introduced to guarantee the existence of solutions, the robustness of stability to small perturbations and other useful properties. The hybrid system (2.89) is said to satisfy the basic conditions if:

C1) $\mathcal{F}$ and $\mathcal{J}$ are closed sets in $\mathbb{R}^n$.

C2) The set-valued function $\mathbf{F}$ is outer semicontinuous[2] and locally bounded[3] on $\mathcal{F}$ and, for all $x \in \mathcal{F}$, the set $\mathbf{F}(x)$ is nonempty and convex[4]

C3) The set-valued function $\mathbf{J}$ is outer semicontinuous and locally bounded on $\mathcal{J}$ and, for all $x \in \mathcal{J}$, the set $\mathbf{J}(x)$ is nonempty.

### 2.3.1 Exponential Stability for Hybrid Systems

Since most of the stability results, derived in this thesis, are exponential, only the definition of exponential stability for hybrid systems of the form (2.89) is recalled here. The reader is referred to [Goebel *et al.*, 2012] for other definitions of stability and asymptotic stability for hybrid systems.

**Definition 2.3.1 (Exponential stability [Teel *et al.*, 2013])** *A closed set $\mathcal{A} \subset \mathcal{M}$ is said to be (locally) exponentially stable for the hybrid system* (2.89) *if there exist strictly positive real numbers $k, \lambda, \mu$ such that each solution $x$ satisfying $|x(0,0)|_{\mathcal{A}} < \mu$ also satisfies, for all $(t, j) \in \operatorname{dom} x$,*

$$|x(t, j)|_{\mathcal{A}} \leq k \exp(-\lambda(t + j))|x(0, 0)|_{\mathcal{A}} \tag{2.95}$$

*where $|x|_{\mathcal{A}}$ denotes a distance function from $x \in \mathcal{M}$ to $\mathcal{A}$. It is said to be globally exponentially stable if one allows $\mu \to +\infty$.*

Note that in the above definition of exponential stability, the exponential convergence is indeed *uniform* since the scalars $\lambda$ and $k$ are independent from the initial conditions.

[2]The set-valued function $\mathbf{F}$ is outer semicontinuous if its graph $\{(x, y) : x \in \mathcal{M}, y \in \mathbf{F}(x)\} \subset \mathbb{R}^{2n}$ is closed. Equivalently, for all $x_0 \in \mathcal{F}$ one has $\limsup_{x \to x_0} \mathbf{F}(x) \subseteq \mathbf{F}(x_0)$.

[3]A set-valued function $\mathbf{F}$ is locally bounded on $\mathcal{F}$ if for every compact set $K \subset \mathcal{F}$, $F(K)$ is bounded.

[4]A convex set is a subset of an affine space that is closed under convex combinations. Roughly speaking, given any two points in a convex set, each point on the line joining these two points is in the set as well.

Throughout the text, the adjective "uniform" is omitted for simplicity. Given $\mu > 0$, define the set $\mathcal{A} + \mu\mathbb{B} := \{x \in \mathcal{M} : |x|_{\mathcal{A}} < \mu\}$. The following theorem [Teel *et al.*, 2013] provides sufficient conditions for exponential stability.

**Theorem 2.3.2** *For system* (2.89)*, the closed set $\mathcal{A} \subset \mathcal{M}$ is locally exponentially stable if there exist positive real numbers $\underline{\alpha}, \bar{\alpha}, \lambda_1, \lambda_2, \mu, p$ and a function $\mathbf{V} : \mathrm{dom}\mathbf{V} \to \mathbb{R}$ where $\mathcal{F} \cup \mathcal{J} \cup \mathbf{J}(\mathcal{J}) \subset \mathrm{dom}\mathbf{V}$, that is continuously differentiable on an open set containing $\mathbf{cl}(\mathcal{F})$ and satisfies*

$$\underline{\alpha}|x|^p_{\mathcal{A}} \leq \mathbf{V}(x) \leq \bar{\alpha}|x|^p_{\mathcal{A}}, \qquad \forall x \in (\mathcal{F} \cup \mathcal{J} \cup \mathbf{J}(\mathcal{J})) \cap (\mathcal{A} + \mu\mathbb{B}), \tag{2.96}$$

$$\langle \nabla \mathbf{V}(x), f \rangle \leq -\lambda_1 \mathbf{V}(x), \qquad \forall x \in \mathcal{F} \cap (\mathcal{A} + \mu\mathbb{B}), f \in \mathbf{F}(x), \tag{2.97}$$

$$\mathbf{V}(g) \leq \exp(-\lambda_2)\mathbf{V}(x), \qquad \forall x \in \mathcal{J} \cap (\mathcal{A} + \mu\mathbb{B}), g \in \mathbf{J}(x). \tag{2.98}$$

*If these bounds hold with $\mu = \infty$ then the set $\mathcal{A}$ is globally exponentially stable.*

The sufficient conditions for exponential stability provided in Theorem 2.3.2 require that all solutions guarantee exponential decrease of the function $\mathbf{V}$ during *both* the flows and the jumps. It turns out that for hybrid systems of the form (2.89) this condition is quite restrictive. In other words, under some mild conditions on the solutions, exponential stability can still hold even in the case where some solutions do not ensure a decrease in $\mathbf{V}$ during either the flow or the jump.

**Theorem 2.3.3** *For system* (2.89)*, the closed set $\mathcal{A} \subset \mathcal{M}$ is locally exponentially stable if there exist positive real numbers $\underline{\alpha}, \bar{\alpha}, \mu, p$, real numbers $\lambda_1, \lambda_2$ and a function $\mathbf{V} : \mathrm{dom}\mathbf{V} \to \mathbb{R}$ where $\mathcal{F} \cup \mathcal{J} \cup \mathbf{J}(\mathcal{J}) \subset \mathrm{dom}\mathbf{V}$, that is continuously differentiable on an open set containing $\mathbf{cl}(\mathcal{F})$ and satisfies*

$$\underline{\alpha}|x|^p_{\mathcal{A}} \leq \mathbf{V}(x) \leq \bar{\alpha}|x|^p_{\mathcal{A}}, \qquad \forall x \in (\mathcal{F} \cup \mathcal{J} \cup \mathbf{J}(\mathcal{J})) \cap (\mathcal{A} + \mu\mathbb{B}), \tag{2.99}$$

$$\langle \nabla \mathbf{V}(x), f \rangle \leq -\lambda_1 \mathbf{V}(x), \qquad \forall x \in \mathcal{F} \cap (\mathcal{A} + \mu\mathbb{B}), f \in \mathbf{F}(x), \tag{2.100}$$

$$\mathbf{V}(g) \leq \exp(-\lambda_2)\mathbf{V}(x), \qquad \forall x \in \mathcal{J} \cap (\mathcal{A} + \mu\mathbb{B}), g \in \mathbf{J}(x), \tag{2.101}$$

*such that one of these conditions hold:*

*i)* $\lambda_1$ *and* $\lambda_2$ *are strictly positive scalars.*

*ii)* $\lambda_2 \leq 0$*,* $\lambda_1 > -\lambda_2\gamma$ *and, for all* $(t, j) \in \mathrm{dom}\ x$*,* $j \leq \gamma t + J$ *where* $\gamma \geq 0$ *and* $J \in \mathbb{N}$*.*

*iii)* $\lambda_1 \leq 0$*,* $\lambda_2 > -\lambda_1\gamma$ *and, for all* $(t, j) \in \mathrm{dom}\ x$*,* $t \leq \gamma j + T$ *where* $\gamma, T \geq 0$*.*

*If these conditions hold with $\mu = \infty$ then the set $\mathcal{A}$ is globally exponentially stable.*

**Proof** See Appendix C.1.

Compared to Theorem 2.3.2, the conditions of Theorem 2.3.3 do not require that *both* $\lambda_1$ and $\lambda_2$ are positive. Instead, only one of the two scalars $\lambda_1, \lambda_2$ is required to be positive and the other one can take arbitrary values in $\mathbb{R}$. This allows for scenarios where we have either an increase during the flows or an increase during the jumps. The price to pay is that some conditions on the hybrid time domain are imposed. These conditions are often referred to as persistent flow (respectively persistent jump) conditions and have been exploited in [Goebel *et al.*, 2012, Section 3.3] and [Prieur *et al.*, 2014] to derive sufficient conditions for global uniform asymptotic stability in the case where there is no *strict* decrease across the jumps (respectively flows). Many classes of hybrid systems satisfy these persistent flow/jump conditions. For instance, hybrid systems that exhibit dwell-time solutions[5] can be shown to satisfy the persistent flow condition in item *ii)* of Theorem 2.3.3. Moreover, in a state estimation problem using intermittent measurements (such as the one discussed in Chapter 4) there exists a maximum time $T$ such that the observer state is updated every $T$ period of time. Therefore the flow time $t$ is naturally bounded by $t \leq T(j+1)$ which allows to use item *iii)* of Theorem 2.3.3.

**Remark 2.3.4** *In Theorem 2.3.3, global exponential stability of the set $\mathcal{A}$ is stated when the scalar $\mu = +\infty$. When the set $\mathcal{A}$ is locally exponentially stable and the set $\mathcal{M} \setminus \mathcal{R}$, where $\mathcal{R} \subseteq \mathcal{M}$ is contained in the region of attraction, has Lebesgue measure zero, the exponential stability is stated as almost global exponential stability.*

## 2.4 Numerical Integration Tools

In this section, the numerical integration schemes used in this work are discussed. Most mechanical systems are governed by differential equations whose solutions are known to evolve on a given manifold embedded in $\mathbb{R}^n$. There are two main techniques to numerically solve differential equations on general manifolds: embedded and intrinsic. In the first method, one embeds the given manifold in $\mathbb{R}^n$ and then employs classical integration methods on the Euclidean manifold $\mathbb{R}^n$ such as the Runge-Kutta methods. The drawback of these methods when applied to manifolds is that, in general, it is not possible to guarantee that the solution will stay on the given manifold. On the other hand, intrinsic methods are developed to guarantee that the update rule for the integration scheme keeps

[5] A solution to a hybrid system is called a "dwell-time solution" if there is a minimum elapsed time between each two consecutive jumps. In other words, there is a dwell time $\tau_D > 0$ such that jumps are separated by at least $\tau_D$ amount of time.

the state of the system on this manifold. The price to pay is that these methods might be computationally expensive compared to the classical methods on $\mathbb{R}^n$.

### 2.4.1 Numerical Integration on $\mathbb{R}^n$

Consider the ordinary differential equation (ODE) on $\mathbb{R}^n$

$$\dot{x} = f(t, x), \quad x(0) = x_0. \tag{2.102}$$

The objective of numerical integration methods is to approximate the time solution for the above ODE given knowledge of the function $f$ and the initial data $(0, x_0)$. The most basic and simplest method is to use the well known explicit Euler method which is named after Leonhard Euler, who treated it in his book *Institutionum calculi integralis* (published 1768-70). Choose a value $h$ for the size of every step and set $t_n = nh$. Then, it is possible to iteratively compute the approximate of $x$ at time $t_n$, denoted $x_n \approx x(t_n)$, using the first order update rule

$$x_{n+1} = x_n + hf(t_n, x_n), \quad n \in \mathbb{N}_0. \tag{2.103}$$

Higher order integration schemes can be used to obtain better accuracy. The Runge-Kutta methods provide a family of implicit and explicit integration schemes to approximate the solutions of an ODE. These methods were developed around 1900 by the German mathematicians C. Runge and M. W. Kutta. Here, some of the commonly used Runge-Kutta methods are recalled. Euler method mentioned above is the first order Runge-Kutta method. The following are some common Runge-Kutta methods:

- Heun's method (explicit trapezoidal rule) is given by the formula

$$x_{n+1} = x_n + \frac{h}{2}\left(f_1 + f_2\right), \tag{2.104}$$

  where $f_1 = f(t_n, x_n)$, and $f_2 = f(t_n + h, x_n + hf_1)$.

- A Runge-Kutta method (3rd order, 3 stages) is given by the formula

$$x_{n+1} = x_n + \frac{h}{6}\left(f_1 + 4f_2 + f_3\right), \tag{2.105}$$

  where $f_1 = f(t_n, x_n)$, $f_2 = f(t_n + \frac{h}{2}, x_n + \frac{h}{2}f_1)$, and $f_3 = f(t_n + h, x_n - hf_1 + 2hf_2)$.

- Classical Runge-Kutta method (4-th order, 4 stages) is given by the formula

$$x_{n+1} = x_n + \frac{h}{6}\left(f_1 + 2f_2 + 2f_3 + f_4\right), \tag{2.106}$$

where $f_1 = f(t_n, x_n)$, $f_2 = f(t_n + \frac{h}{2}, x_n + \frac{h}{2}f_1)$, $f_3 = f(t_n + \frac{h}{2}, x_n + \frac{h}{2}f_2)$, and $f_4 = f(t_n + h, x_n + hf_3)$.

### 2.4.2 Numerical Integration on $\mathbb{SO}(3)$

During the last decades, numerical integration methods that preserve certain nice properties on differential manifolds have been widely discussed [Crouch and Grossman, 1993, Munthe-Kaas, 1995]. Amongst these methods, Lie group integrators played an important role in numerical methods for Hamiltonian problems. In a series of papers, Munthe-Kaas [Munthe-Kaas, 1995, Munthe-Kaas, 1998, Munthe-Kaas, 1999] presented what are now known as the Runge-Kutta-Munthe-Kaas (RK-MK) methods. Consider the following initial value problem on $\mathbb{SO}(3)$

$$\dot{R} = R[\omega(t, R)]_\times, \quad R(0) \in \mathbb{SO}(3). \tag{2.107}$$

Using adapted results from [Munthe-Kaas, 1998] to the Lie group $\mathbb{SO}(3)$, it is possible to iteratively approximate the solution $R(t)$ of (2.107) at time $t_n$, denoted $R(t_n) \approx R_n$, using one of the following RK-MK methods on $\mathbb{SO}(3)$

- RK-MK1 method (also known as Lie-Euler method) is given by the formula

$$R_{n+1} = R_n \exp(h[\omega(t_n, R_n)]_\times). \tag{2.108}$$

The above formula can be easily derived by assuming that the angular velocity $\omega(t, R)$ between $t_n$ and $t_{n+1}$ and (exact) integrating the kinematic equation (2.107) between $t_n$ and $t_{n+1}$.

- RK-MK2 method is given by the formula

$$R_{n+1} = R_n \exp(h[\omega_1 + \omega_2]_\times/2), \tag{2.109}$$

where $\omega_1 = \omega(t_n, R_n)$ and $\omega_2 = \omega(t_n + h, R_n \exp(h\omega_1))$.

- RK-MK3 method is given by the formula

$$R_{n+1} = R_n \exp([\tilde{\omega}]_\times), \tag{2.110}$$

$$\tilde{\omega} = \frac{h}{6}(\omega_1 + 4\omega_2 + \omega_3) + \frac{h^2}{36}(4\omega_1 \times \omega_2 + \omega_1 \times \omega_3), \tag{2.111}$$

where $\omega_1 = \omega(t_n, R_n)$, $\omega_2 = \omega(t_n + h/2, R_n \exp(h[\omega_1]_\times/2))$ and $\omega_3 = \omega(t_n + h, R_n \exp(h[-\omega_1 + 2\omega_2]_\times))$.

- RK-MK4 method is given by the formula

$$R_{n+1} = R_n \exp([\tilde{\omega}]_\times), \tag{2.112}$$

$$\tilde{\omega} = \frac{h}{6}(\omega_1 + 2\omega_2 + 2\omega_3 + \omega_4) + \frac{h^2}{36}\sum_{i<j} \omega_i \times \omega_j, \tag{2.113}$$

where $\omega_1 = \omega(t_n, R_n)$, $\omega_2 = \omega(t_n + h/2, R_n \exp(h[\omega_1]_\times/2))$, $\omega_3 = \omega(t_n + h/2, R_n \exp(h[\omega_2]_\times/2))$, and $\omega_4 = \omega(t_n + h, R_n \exp(h[\omega_3]_\times))$.

### 2.4.3 Numerical Integration of Hybrid Systems

The main objective when developing a numerical integration scheme is to approximate with arbitrary precision, by adjusting the step size, the solutions of the mathematical model under consideration. Moreover, when dealing with control systems it is desirable that the simulated model preserves, for example, asymptotic stability even in a practical sense. The theory of numerical simulation and integration for continuous time differential equations is well understood and developed and can be found in several textbooks. However there is a little that has been done when the system under consideration is a hybrid system; combining continuous and discrete dynamics. Under the framework [Goebel *et al.*, 2012], a hybrid simulator model for hybrid systems written in the form (2.89) is introduced. The authors in [Sanfelice and Teel, 2006] established conditions on the data of the hybrid simulator model such that the following properties hold:

- On compact hybrid time domains, every simulation to a hybrid system is arbitrarily close to a solution of the hybrid system;
- Asymptotically stable compact sets for a hybrid system are semiglobally practically asymptotically stable compact sets for the hybrid simulator;
- Asymptotically stable compact sets for the hybrid simulator are continuous in the step size $h$.

Given a step size $h$, a hybrid simulator for (2.89) is defined as follows

$$\begin{cases} x^+ \in \mathbf{F}_h(x), & x \in \mathcal{F}_h, \\ x^+ \in \mathbf{J}_h(x), & x \in \mathcal{J}_h, \end{cases} \tag{2.114}$$

where $\mathbf{F}_h : \mathcal{M} \rightrightarrows \mathcal{M}$ is the integration scheme for the flows of (2.89), $\mathcal{F}_h \subset \mathcal{M}$ dictates where the integration update rule is allowed, $\mathbf{J}_h : \mathcal{M} \rightrightarrows \mathcal{M}$ is the jump mapping that approximates the jump map $\mathbf{J}$ of the hybrid system (2.89), and $\mathcal{J}_h \subset \mathcal{M}$ defines where the jump mapping $\mathbf{J}_h$ is enabled. The map $\mathbf{F}_h$ is constructed from the flow map $\mathbf{F}$ using a particular integration scheme (explicit Euler method, Runge-Kutta methods, *etc*). Note that the flow and jump maps $\mathcal{F}$ and $\mathcal{J}$ are not necessarily the same as the maps $\mathcal{F}_h$ and $\mathcal{J}_h$ (they consist in general of perturbations of $\mathcal{F}$ and $\mathcal{J}$). In some situations, however, it can be reasonable to choose $\mathbf{J}_h \equiv \mathbf{J}$, $\mathcal{F}_h \equiv \mathcal{F}$ and $\mathcal{J}_h \equiv \mathcal{J}$. Sufficient conditions for these data to guarantee the above mentioned desirable properties as well as the existence of solutions for arbitrary large simulation horizon are roughly summarized as follows:

- Closeness of the solutions of the integration scheme $\mathbf{F}_h$ to the true solutions of $\dot{x} \in \mathbf{F}(x)$;
- The sets $\mathcal{F}_h$ and $\mathcal{J}_h$ converge to $\mathcal{F}$ and $\mathcal{J}$ when the step size $h$ tends to zero;
- $\mathbf{F}_h$ is such that for each compact set $\mathcal{K} \subset \mathcal{M}$ and for each $x \in \mathcal{F}_h \cap \mathcal{K}$ one has $\mathbf{F}_h(x) \subset \mathcal{F}_h \cup \mathcal{J}_h$;
- $\mathbf{J}_h$ is such that $\mathbf{J}_h(\mathcal{J}_h) \subset \mathcal{F}_h \cup \mathcal{J}_h$.

The first condition is verified by most well known methods such as Runge-Kutta methods discussed earlier. Moreover, in situations where $\mathcal{F}_h \cup \mathcal{J}_h \equiv \mathcal{M}$, the last two conditions above are naturally met and, in this case, it is sufficient to pick $\mathbf{J}_h \equiv \mathbf{J}$. Note that the hybrid simulation model (2.114) is purely discrete and therefore it is resonable to parametrize its solutions by two discrete variables $j$ (number of jumps in $\mathcal{J}_h$) and $n$ (number of integration steps) which define a discrete time domain [Sanfelice and Teel, 2006]. Note that in the work [Sanfelice and Teel, 2006], the trajectories of the hybrid system are allowed to "enter" the jump set (referred to as *enabling semantics*) compared to some other integration schemes where the jumps are forced when the trajectories hit the boundary of the jump set (referred to as *forcing or trigerring semantics*), see [Sprinkle *et al.*, 2005].

# Chapter 3

# Hybrid Attitude Control on $\mathbb{SO}(3)$

## 3.1 Introduction

This chapter presents a framework for global exponential stabilization on the rotation group $\mathbb{SO}(3)$ by means of hybrid feedback. First, the concept of synergism proposed in [Mayhew and Teel, 2011b, Mayhew and Teel, 2011d, Mayhew and Teel, 2013a], which is shown to be sufficient for global asymptotic stability, is extended to a new concept that is coined "exp-synergism" which is shown to be sufficient for global exponential stability on $\mathbb{SO}(3)$. Exp-synergism imposes more restrictive conditions on the potential functions used in the attitude control design but allows for a broader class of potential functions which are not necessarily differentiable everywhere on $\mathbb{SO}(3)$. In fact, exp-synergistic families of "smooth" potential functions on $\mathbb{SO}(3)$ is synergistic but the opposite does not hold in general. A min-switch hybrid control strategy along with an exp-synergistic family of potential functions on $\mathbb{SO}(3)$ can be employed to guarantee robust global exponential stabilization for the kinematic system on $\mathbb{SO}(3)$.

Next, we proceed to the construction of such families of potential functions on $\mathbb{SO}(3)$ satisfying the exp-synergism property. It is shown that some existing and well known smooth and nonsmooth potential functions on $\mathbb{SO}(3)$ (such as the trace function and the geodesic distance) can be used along with a newly proposed angular warping map on $\mathbb{SO}(3)$ to generate exp-synergistic families of potential functions. In contrast to other existing central synergistic families of potential functions on $\mathbb{SO}(3)$, our proposed approach for the construction of exp-synergistic potential functions on $\mathbb{SO}(3)$ allows for the explicit determination of the synergistic gap and therefore facilitate the real-time implementation of the proposed hybrid control schemes.

Finally, using the proposed hybrid control approach, the attitude tracking problem for rigid body systems (Spacecraft, Unmanned Aerial Vehicles (UAVs), Autonomous

Underwater Vehicles (AUVs),...,etc) is tackeled. This results in a control algorithm guaranteeing robust and global exponential tracking, which are shown to exceed most existing and commercial attitude control algorithms. To the best of our knowledge, there is no similar solution to the full attitude tracking control problem in the literature. Moreover, an alternative design ensuring a continuous control input torque without sacrificing the global exponential stability result is derived. The proposed *smoothing* procedure is much simpler than the backstepping procedure proposed in [Mayhew and Teel, 2013a]. The results presented in this chapter are based on our work in [Berkane and Tayebi, 2017e, Berkane *et al.*, 2017b, Berkane and Tayebi, 2015a]

## 3.2 Motivation Using Planar Rotations on $\mathbb{S}^1$

In this section, the example of planar rotations is considered to motivate some of the results of this chapter. Working with the simple example of the unit circle $\mathbb{S}^1$, which is a submanifold of $\mathbb{SO}(3)$, helps the reader to better understand the problem addressed in this chapter and the rational behind some of the introduced techniques. Nevertheless, the control of planar rotations is in fact an interesting control problem in its own right. It arises in many engineering applications in robotics (autonomous planar vehicles, pendulum systems, gimbal pointing mechanism...etc ), see for instance [Rue, 1969, Repoulias and Papadopoulos, 2007, Masten, 2008, Mayhew *et al.*, 2008, Osborne *et al.*, 2008].

Consider a point mass with coordinates $x = (x_1, x_2) \in \mathbb{R}^2$ restricted to evolve on the unit circle $\mathbb{S}^1$ with angular velocity $\omega \in \mathbb{R}$. The task is to design a control law for the control input $\omega$ in order to globally stabilize the point mass to the coordinate point $e_1 = [1, 0]^\top$ as demonstrated in Figure 3.1. Although it looks simple, this problem is far from being trivial. In fact, the unit circle $\mathbb{S}^1$ is a compact manifold and hence it is not diffeomorphic to any Euclidean space which prevents the existence of continuous time-invariant state feedback which globally asymptotically stablizes any equilibrium point. This is a well known topological obstruction on compact manifolds [Sanjay P. Bhat, 2000]. To better understand this issue, consider the kinematic equation of $x$

$$\dot{x} = \begin{bmatrix} -\omega x_2 \\ \omega x_1 \end{bmatrix} = \omega \begin{bmatrix} 0 & -1 \\ 1 & 0 \end{bmatrix} x := \omega S x. \tag{3.1}$$

A routine for the design of controllers is to pick a suitable Lyapunov function (energy function or potential function) and then design a controller such that the energy is de-

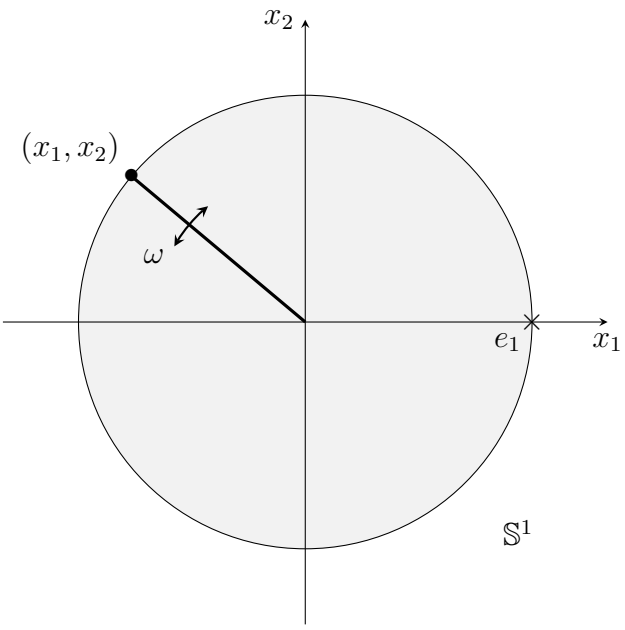


Figure 3.1: Control problem of planar rotations on $\mathbb{S}^1$.

caying to zero. A natural potential function on $\mathbb{S}^1$ is the following "height" function

$$\Phi_E(x) = 1 - e_1^\top x = \frac{1}{2}\|x - e_1\|^2. \tag{3.2}$$

Note that $2\Phi_E(x)$ represents the square of the *chord* connecting the point $x$ and the point $e_1$, see Figure 3.2. Therefore $\Phi_E(x)$ is related to the natural Euclidean distance on the plan $\mathbb{R}^2$. The time derivative of $\Phi_E$ along the trajectories of (3.1) satisfies

$$\dot{\Phi}_E(x) = \nabla\Phi_E(x)^\top \dot{x} = -e_1^\top \omega S x = \omega x_2. \tag{3.3}$$

A natural choice for the control input $\omega$ is the following

$$\omega = -x_2, \tag{3.4}$$

which yields $\dot{\Phi}_E(x) = -x_2^2 \leq 0$. Therefore, the closed-loop system has two equilibria (critical points) at $\pm e_1$. Moreover the *desired* equilibrium $e_1$ is stable and attractive whereas the *undesired* equilibrium $-e_1$ is unstable and repeller, see Figure 3.3. As stated previously, due to the topological obstruction on $\mathbb{S}^1$ the appearance of the undesired equilibrium is unavoidable when using continuous time-invariant feedback. Although the undesired critical point $-e_1$ is unstable and repeller, it introduces several other issues. First, the vector field, as seen in Figure 3.3, is vanishing near the undesired critical

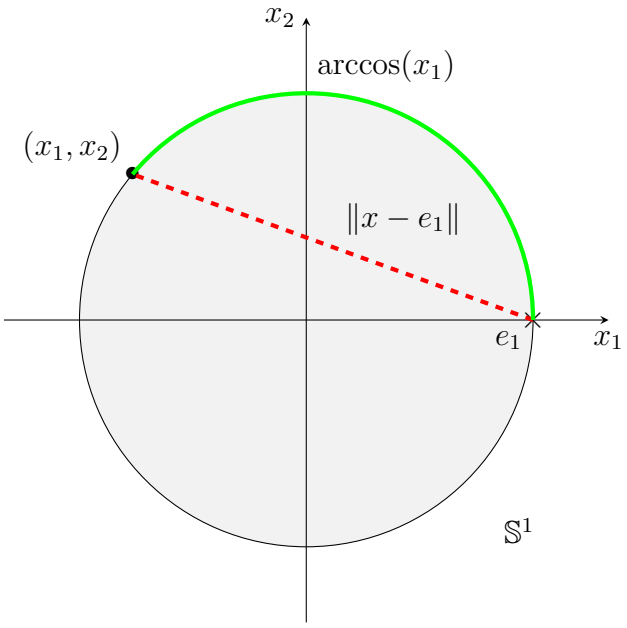


Figure 3.2: The Euclidean (Geodesic) distance between $x$ and $e_1$ plotted in dashed red (solid green).

point $-e_1$ which causes trajectories starting arbitrarily close to $-e_1$ to converge arbitrary *slow* to the desired equilibrium point $e_1$. Moreover, since $-e_1$ is a repeller and due to the nature of manifold $\mathbb{S}^1$, the vector fields near $-e_1$ have opposite directions. That is to say, trajectories starting above $-e_1$ will take the opposite path to $e_1$ compared to trajectories below $-e_1$. Consequently, in the presence of measurement noise, a chattering phenomenon may occur causing the point mass to get stuck around the undesired equilibrium.

A possible remedy for the problem of slow convergence near the undesired critical point is to employ *nonsmooth* potential functions on $\mathbb{S}^1$. Consider the following potential function on $\mathbb{S}^1$

$$\Phi_G(x) = \frac{1}{2}\arccos(x_1)^2. \tag{3.5}$$

Note also that $2\Phi_G(x)$ represents the square of the *arc* connecting the point $x$ and the point $e_1$ (geodesic distance on $\mathbb{S}^1$), see Figure 3.2. The time derivative of $\Phi_G$ along the trajectories of (3.1) is given, for all $x \neq \pm e_1$, by

$$\dot{\Phi}_G(x) = -\frac{\arccos(x_1)\dot{x}_1}{\sqrt{1-x_1^2}} = \omega\frac{\arccos(x_1)x_2}{\sqrt{1-x_1^2}}. \tag{3.6}$$

Therefore, if one chooses the control law $\omega = -f(x_1)x_2$ where $f(x_1) = \arccos(x_1)/\sqrt{1-x_1^2}$

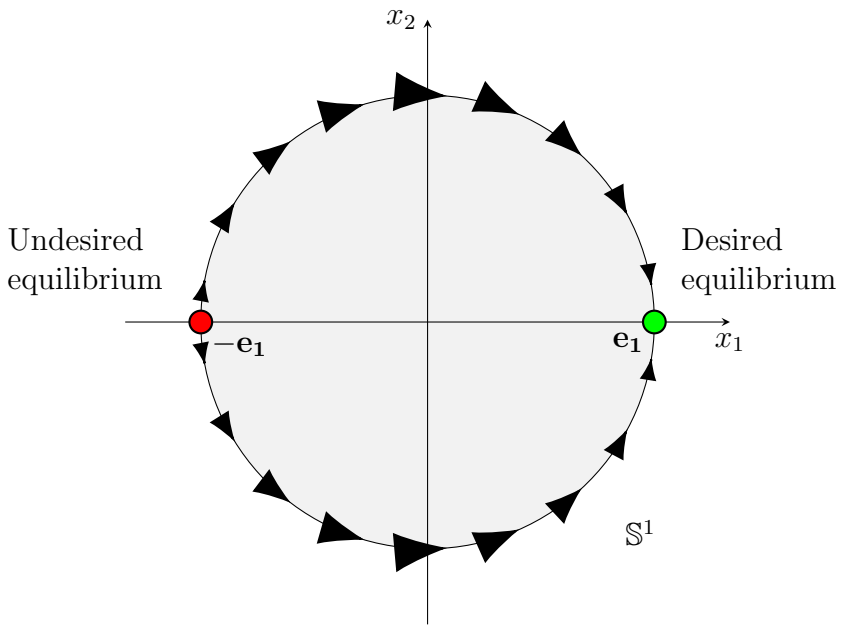


Figure 3.3: Vector fields on $\mathbb{S}^1$ with control input $\omega = -x_2$ (potential function $\Phi_E(x)$). The desired critical point $e_1$ is plotted in green and the undesired critical point $-e_1$ is plotted in red.

then $\dot{\Phi}_G(x) = -f(x_1)^2 x_2^2 \leq 0$. Note that the function $f$ has the following properties

$$\lim_{x_1 \to 1} f(x_1) = 1, \tag{3.7}$$

$$\lim_{x_1 \to -1} f(x_1) = +\infty, \tag{3.8}$$

Therefore, for $x$ close to $e_1$, the applied control $\omega = -f(x_1)x_2$ becomes equivalent to the control law based on $\Phi_E$ developed above. However, when $x$ gets closer to $-e_1$, the function $f(x_1)$ grows unbounded causing a *singularity* in the control. Note that although $f(x_1)$ is unbounded near 180°, the product $f(x_1)x_2$ is bounded and therefore the control input $\omega$ is bounded near 180°. As shown in Figure 3.4, the vector field near $-e_1$ is not vanishing compared to the previous control law. Hence, it is expected that convergence rates starting from large rotations will be improved. However, this control law, in addition to being singular at 180°, is vulnerable to noise which may cause chattering near 180°. Note that although the singularity at 180° can be removed by applying a memoryless discontinuous control law, the vulnerability to noise can not be avoided. In fact, the results in [Mayhew and Teel, 2011a] show that when a compact set cannot be globally asymptotically stabilized by continuous feedback due to topological obstructions, it cannot be robustly globally asymptotically stabilized by discontinuous feedback either.

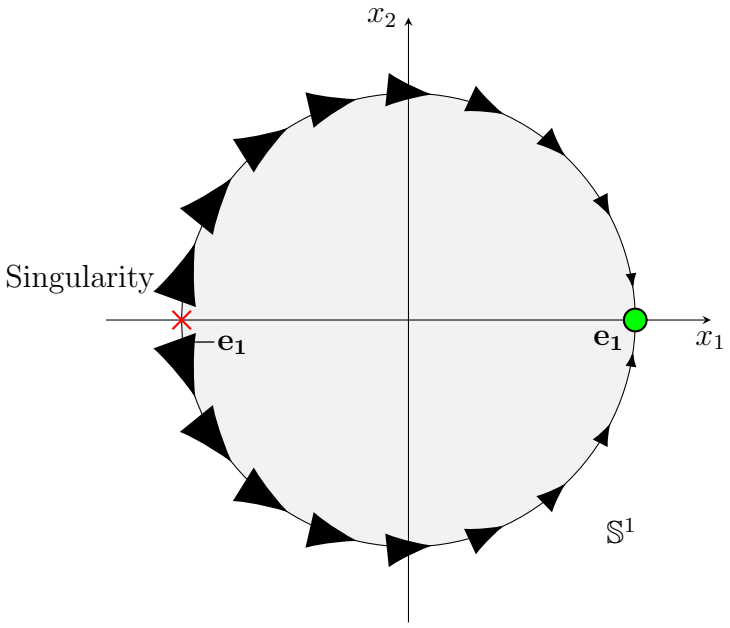


Figure 3.4: Vector fields on $\mathbb{S}^1$ with control input $\omega = -f(x_1)x_2$ (potential function $\Phi_G(x)$). The desired critical point $e_1$ is plotted in green and the singular point $-e_1$ is plotted in red.

One way to deal with the above mentioned topological obstruction to robust global asymptotic stabilization on compact manifolds is to consider hybrid control laws employing hysteresis as done in [Mayhew and Teel, 2013b, Mayhew and Teel, 2010]. The idea consists in designing two or more controllers which will be *allowed* to activate in different overlapping compact subregions of the manifold $\mathbb{S}^1$. Each subregion where a given controller is activated will not contain any singular and/or undesired critical points of the controller. A hybrid switching mechanism is employed to switch between the controller configurations allowing to avoid all the critical and singular points of each controller. To illustrate this concept, consider a hybrid controller with two configurations $\kappa_1(x)$ and $\kappa_2(x)$, see Figure 3.5. A *synergistic* hybrid controller combining both controllers takes the following form with $q \in \{1, 2\}$

$$\omega = \kappa_q(x), \qquad x \in \mathbf{cl}(\mathbb{S}^1 \setminus \mathcal{C}_q), \tag{3.9}$$

$$q^+ = 3 - q, \qquad x \in \mathcal{C}_q, \tag{3.10}$$

where $\mathcal{C}_q$ is the region of $\mathbb{S}^1$ where the controller $\kappa_q(x)$ is not allowed to operate (it may contain undesired critical and/or singular points). A necessary condition to implement this hybrid scheme is $\mathcal{C}_1 \cap \mathcal{C}_2 = \emptyset$, otherwise the hybrid controller remains jumping (without flowing) between the two controllers when $x \in \mathcal{C}_1 \cap \mathcal{C}_2$.

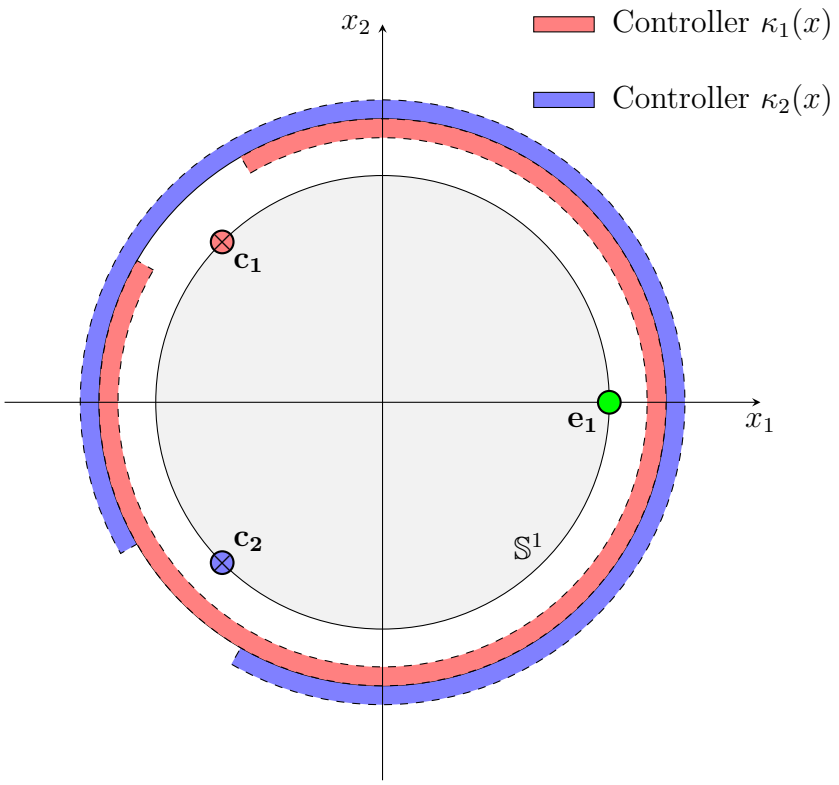


Figure 3.5: Hybrid control on the unit circle $\mathbb{S}^1$ with two modes of operation. The first (second) controller is allowed to activate on the red (blue) region. The point $c_1$ ($c_2$) represents an undesired critical or singular point of the first (second) controller.

In [Mayhew and Teel, 2010], the authors generate new potential functions by applying a diffeomorphism to the smooth potential function $\Phi_E(x)$ that stretches and compresses the unit circle while leaving the desired equilibrium $e_1$ unchanged. From each generated potential function, a feedback law will be derived. Under some sufficient conditions on the family of potential functions, using a min-switch mechanism, the critical points of each potential function are avoided guaranteeing, therefore, robust global asymptotic stability. The inconvenience of the technique in [Mayhew and Teel, 2010] is that the sufficient conditions were only verified by computation. In the following, a remedy to the drawbacks of [Mayhew and Teel, 2010] is explained by proposing a new diffeomorphism.

Let $\mathcal{Q} \subset \mathbb{N}$ be a subset of finite indices. Consider the following map $\Gamma : \mathbb{S}^1 \times \mathcal{Q} \to \mathbb{S}^1$

$$\Gamma(x, q) = \mathbf{R}(\theta(x, q))x, \tag{3.11}$$

where $\theta : \mathbb{S}^1 \times \mathcal{Q} \to \mathbb{R}$ is a real-valued function, $q \in \mathcal{Q}$ is a discrete variable and $\mathbf{R} : \mathbb{R} \to \mathbb{SO}(2)$ represents a rotation map to the group of planar rotations $\mathbb{SO}(2)$ which

is given by

$$\mathbf{R}(\theta) = \begin{bmatrix} \cos(\theta) & -\sin(\theta) \\ \sin(\theta) & \cos(\theta) \end{bmatrix}. \tag{3.12}$$

The idea is to design a suitable angle function $\theta$ such that the undesired critical points of the composite functions $\Phi_E(\Gamma(x,q)), q \in \mathcal{Q}$ have different locations while the desired critical point at $e_1$ remains unchanged; hence one needs $\Gamma(e_1,q) = e_1$ for all $q \in \mathcal{Q}$. Furthermore, the function $\theta(\cdot,\cdot)$ need not to be singular anywhere on $\mathbb{S}^1$ as this might introduce further complications when differentiating the map $\Gamma$. For simplicity of discussion let us consider a hybrid controller with two configurations such that $\mathcal{Q} = \{1,2\}$. Using the map $\Gamma$, one can design two potential functions on $\mathbb{S}^1$ as follows:

$$\Phi_1(x) = \Phi_E(\Gamma(x,1)), \tag{3.13}$$

$$\Phi_2(x) = \Phi_E(\Gamma(x,2)). \tag{3.14}$$

For a fixed $q \in \{1,2\}$ the time derivative of $\Phi_q$ along the trajectories of (3.1) can be shown to satisfy

$$\dot{\Phi}_q(x) = -e_1^\top \dot{\Gamma}(x,q) = -\omega \left(1 + \nabla\theta(x,q)^\top S x\right) e_1^\top S \Gamma(x,q) \tag{3.15}$$

where $\nabla\theta(x,q)$ is the gradient of $\theta$ with respect to the first argument $x$. Therefore, the following controller is derived:

$$\omega = \kappa(x,q) := \left(1 + \nabla\theta(x,q)^\top S x\right) e_1^\top S \Gamma(x,q). \tag{3.16}$$

Note that the above control input reduces to (3.4) when the map $\theta(x,q) \equiv 0$ which implies that $\Gamma(x,q) \equiv x$. The critical points can be obtained by vanishing the gradient of $\Phi_q$, which is equivalent of setting the above control input to zero. This leads to

$$\Gamma(x,q) = \pm e_1 \tag{3.17}$$

and/or

$$1 + \nabla\theta(x,q)^\top S x = 0. \tag{3.18}$$

Let us suppose for a moment that $\theta$ has been designed such that the condition (3.18) is not met for all $(x,q) \in \mathbb{S}^1 \times \mathcal{Q}$. In this case, the critical points of $\Phi_q$ will be uniquely

defined by condition (3.17). The following choice of the function $\theta(x, q)$ allows for explicit computation of the solutions of (3.17)

$$\theta(x, q) = 2 \arcsin(k_q \Phi_E(x)), \quad k_q \neq 0. \tag{3.19}$$

**Proposition 3.2.1** *Consider the map $\Gamma$ given in (3.11) such that $\theta$ is defined by (3.19). Assume that the scalar $k_q$ satisfies*

$$|k_q| < \frac{\sqrt{3}}{4}. \tag{3.20}$$

*Then $|\nabla\theta(x, q)^\top Sx| < 1$ for all $(x, q) \in \mathbb{S}^1 \times \mathcal{Q}$. Moreover, the critical points of the potential function $\Phi_E \circ \Gamma(x, q)$ are defined by $\mathcal{C} = \mathcal{C}_d \cup \mathcal{C}_u$ such that $\mathcal{C}_d = \{e_1\} \times \mathcal{Q}$ and $\mathcal{C}_u = \cup_{q\in\mathcal{Q}}(c_q, q)$ where $c_q \in \mathbb{S}^1$ is given explicitly by*

$$c_q = \frac{1}{4}\left[\frac{1 + 4k_q^2 - \sqrt{1 + 16k_q^2}}{k_q^2},\ \frac{(-1 + \sqrt{1 + 16k_q^2})^{\frac{3}{2}}}{\sqrt{2}k_q|k_q|}\right]^\top. \tag{3.21}$$

**Proof** See Appendix B.1.

Proposition 3.2.1 proposes a set of potential functions on $\mathbb{S}^1$, namely $\{\Phi_E \circ \Gamma(x, q)\}_{q\in\mathcal{Q}}$, which have a common desired critical point $e_1$ and different undesired critical points $\{c_q\}_{q\in\mathcal{Q}}$. These undesired critical points are function of the scalars $\{k_q\}_{q\in\mathcal{Q}}$. Now, it remains to design a hybrid controller of the form (3.9) guaranteeing global exponential stability of the equilibrium point $e_1$.

The idea of *synergism* consists in showing that at a given undesired critical point $c_q$ of a given potential function $\Phi_E \circ \Gamma(x, q)$ there exists another index $p \in \mathcal{Q}$ such that the potential function $\Phi_E \circ \Gamma(x, p)$ has a lower value. If this synergism property is satisfied, one can design a hybrid controller that switches to the minimum potential function's controller whenever the current potential function exceeds the minimum potential function by a certain threshold.

**Proposition 3.2.2** *Consider the map $\Gamma$ given in (3.11) such that $\theta$ is defined by (3.19) with $\mathcal{Q} = \{1, 2\}$. Assume that $k_2 = -k_1 = k$ such that $k$ satisfies condition 3.20. Then, for all $(x, q) \in \mathcal{C}_u$ one has*

$$\Phi_E \circ \Gamma(x, q) - \Phi_E \circ \Gamma(x, p) := \delta^* = \frac{\left(-1 + \sqrt{16\,k^2 + 1}\right)^3}{16k^4}, \qquad p \neq q. \tag{3.22}$$

**Proof** See Appendix B.2.

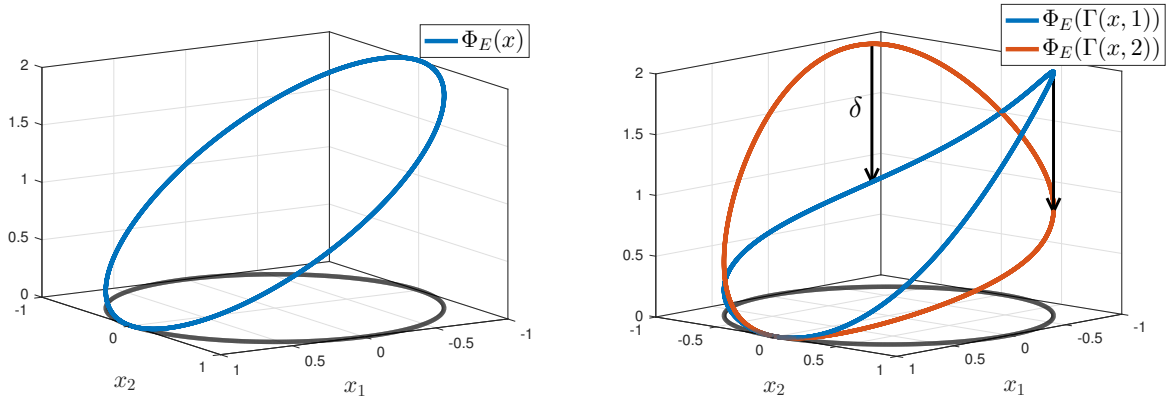


Figure 3.6: Plot of the original potential function $\Phi_E(x)$ (left) and the new composite potential functions $\Phi_E(\Gamma(x,1))$ and $\Phi_E(\Gamma(x,2))$ (right) with $k = 1/4$. The synergistic gap $\delta^*$ between the two potential functions is equal to 16/9.

Consequently, it is shown in Proposition 3.2.2 that at any given undesired critical point of $\Phi_E(\Gamma(x,q))$, the potential function $\Phi_E(\Gamma(x,p))$ with $p \neq q$ has a lower value with a gap $\delta^* > 0$ given explicitly function of the scalar $k$. Using this property, the following hybrid controller immediately follows

$$\omega = \kappa(x,q), \qquad (x,q) \in \mathcal{F}, \tag{3.23}$$

$$q^+ = \arg\min_{p\in\mathcal{Q}} \Phi_E(\Gamma(x,p)), \qquad (x,q) \in \mathcal{J}, \tag{3.24}$$

where the *flow* set $\mathcal{F}$ and *jump* set $\mathcal{J}$ are defined as follows

$$\mathcal{F} = \{(x,q) : \Phi_E \circ \Gamma(x,q) - \min_{p\in\mathcal{Q}} \Phi_E \circ \Gamma(x,p) \leq \delta\}, \tag{3.25}$$

$$\mathcal{J} = \{(x,q) : \Phi_E \circ \Gamma(x,q) - \min_{p\in\mathcal{Q}} \Phi_E \circ \Gamma(x,p) \geq \delta\}, \tag{3.26}$$

where $0 < \delta < \delta^*$ and the synergistic gap $\delta^*$ is given in Proposition 3.2.2. The idea of the proposed hybrid controller is to switch to the configuration with minimum potential function $\Phi_E \circ \Gamma(x,q)$ whenever the gap between the current potential function and the minimum one exceeds some threshold $\delta$. If the potential function $\Phi_E \circ \Gamma(x,q)$ is taken as a Lyapunov function candidate then the jump equation (3.24) allows to guarantee a decrease in the Lyapunov function between jumps. The above proposed control scheme can be shown to guarantee global exponential stability of the set $\{e_1\} \times \mathcal{Q}$. It should be mentioned also that it is possible to use the non-smooth (geodesic) potential function $\Phi_G(x)$, given in (3.5), to derive a hybrid controller that avoids the singular points of

$\Phi_G \circ \Gamma(x, q)$ using a similar min-switch strategy. Since the objective of this thesis is the control and estimation on $\mathbb{SO}(3)$, these discussions on the unit circle will not be pursued further. The reader is referred to [Mayhew and Teel, 2013b, Casau *et al.*, 2015a] for a detailed treatment of hybrid control on the general unit sphere $\mathbb{S}^n$. The ideas discussed in this section for the hybrid control of planar rotations will inspire our proposed control designs for the general group of $3D$ rotations, namely the Special Orthogonal group $\mathbb{SO}(3)$ which will be the goal of the next sections.

## 3.3 Attitude Stabilization on $\mathbb{SO}(3)$

In this section, an approach to design hybrid controllers for the attitude kinematics (first order system) that achieves robust global exponential stability on $\mathbb{SO}(3)$ is proposed. Discussions about stabilization and tracking for the full rigid body attitude dynamics (second order system) will be detailed in the next section. First, the new concept of exp-synergistic potential functions on $\mathbb{SO}(3)$ is introduced. Then, exp-synergistic potential functions are shown to be sufficient to design hybrid control algorithms guaranteeing global exponential stability on $\mathbb{SO}(3)$. Lastly, a systematic methodology for the construction of such potential functions on $\mathbb{SO}(3)$ is provided.

### 3.3.1 Problem Formulation

Consider the following kinematics system on $\mathbb{SO}(3)$

$$\dot{R} = R[\omega]_\times, \tag{3.27}$$

where $R \in \mathbb{SO}(3)$ represents the attitude state and $\omega \in \mathbb{R}^3$ is the control input. The stabilization control problem for system (3.27) consists in designing an appropriate input $\omega$ such that $(R = I)$ is globally exponentially stable. Note that there is no loss of generality in considering the stabilization problem of the identity rotation $I$. In fact, assume that our problem is the tracking of the desired time varying trajectory $\dot{R}_d(t) = R_d(t)[\omega_d(t)]_\times$ for some $\omega_d(t) \in \mathbb{R}^3$ and $R_d(0) \in \mathbb{SO}(3)$. Let $\tilde{R} = RR_d^\top$ be the attitude tracking error and let the control input $\omega = \omega_d + R_d\bar{\omega}$ for some virtual input $\bar{\omega} \in \mathbb{R}^3$. Therefore, it is not difficult to show that one has $\dot{\tilde{R}} = \tilde{R}[\bar{\omega}]_\times$ which implies that the original tracking problem is reduced to a stabilization problem for the attitude tracking error $\tilde{R}$.

### 3.3.2 Smooth Attitude Stabilization on $\mathbb{SO}(3)$

A natural solution to tackle this problem is to consider a gradient-based control approach. Consider for example the following weighted trace potential function used in many attitude control problems [Koditschek, 1988, Bullo and Murray, 1999, Sanyal *et al.*, 2009]

$$\Psi_{1,A}(R) = \frac{1}{2}\mathbf{tr}(A(I-R)), \tag{3.28}$$

where $A \in \mathbb{R}^{3\times 3}$ is a symmetric matrix. Note that the condition for $\Psi_{1,A}(R)$ to be a valid (positive definite with respect to $I$) potential function on $\mathbb{SO}(3)$ is that the matrix $\mathbf{E}(A)$, with the map $\mathbf{E}(\cdot)$ defined in (2.66), is symmetric positive definite. Intuitively, by looking at the expression of $\Psi_{1,A}(R)$ in terms of quaternions (see (2.75)) it can be seen that $\Psi_{1,A}(R)$ is positive definite with respect to the quaternion $(\pm 1, 0)$, which represents the identity rotation, if and only if $\mathbf{E}(A)$ is symmetric positive definite. Consider the following gradient-based controller

$$\omega = -2k\psi(R^\top \nabla\Psi_{1,A}(R)), \quad k > 0. \tag{3.29}$$

Then, by using $\Psi_{1,A}(R)$ as the Lyapunov function candidate one obtains the following time derivative of the Lyapunov function along the trajectories of (3.27)

$$\dot{\Psi}_{1,A}(R) = \langle \nabla\Psi_{1,A}(R), \dot{R}\rangle_R = \langle\langle \nabla\Psi_{1,A}(R), R[\omega]_\times\rangle\rangle = -2k\|\nabla\Psi_{1,A}(R)\|_F^2 \leq 0. \tag{3.30}$$

This shows that the equilibrium point $R = I$ is stable. Moreover, using LaSalle's invariance principle it can be concluded that all solutions must converge to the largest invariant set where the gradient of $\Psi_{1,A}(R)$ vanishes (critical points). In view of (2.71) the gradient of $\Psi_{1,A}(R)$ is given by $\nabla\Psi_{1,A}(R) = \frac{1}{2}R\mathbf{P}_{\mathfrak{so}(3)}(AR)$ which implies that the closed-loop system under the feedback (3.29) can be written as

$$\dot{R} = -kR[\psi(AR)]_\times = -\frac{k}{2}R(AR - R^\top A) = -\frac{k}{2}(RAR - A). \tag{3.31}$$

The equilibria of the above system which correspond to the critical points of $\Psi_{1,A}(R)$ satisfy $AR = R^\top A$. This set of critical points is given by (see [Mayhew and Teel, 2013a, Lemma 4])

$$\mathcal{C}_{\Psi_{1,A}} = \{I\} \cup \mathbf{R}_a(\pi, \mathcal{E}_v^{\mathbb{R}}(A)), \tag{3.32}$$

which contains the identity rotation and all the rotations of 180° around an eigenvector of $A$. An other interesting observation from (3.31) is that if $R$ is symmetric then $\dot{R}$ is

also symmetric and, therefore, the subset of $\mathbb{SO}(3)$ where $R$ is symmetric is invariant under the flows of (3.31). This set is identified by $R = R^\top$ which implies that $R^2 = I$. It can be shown that the solutions of $R^2 = I$ are identified by the set $\{I\} \cup \mathbf{R}_a(\pi, \mathbb{S}^2)$. Therefore starting inside the set $\mathbf{R}_a(\pi, \mathbb{S}^2)$ the trajectories of the system will eventually converge to $\mathbf{R}_a(\pi, \mathcal{E}_v^{\mathbb{R}}(A))$. Moreover during the flows of (3.31) one has

$$\frac{d}{dt}\mathbf{tr}(I - R) = -\mathbf{tr}(\dot{R}) = -\frac{k}{2}\mathbf{tr}(A - RAR) = -\frac{k}{2}\mathbf{tr}(A(I - R^2)) \leq 0. \tag{3.33}$$

This implies that all trajectories starting outside $\mathbf{R}_a(\pi, \mathbb{S}^2)$ will converge to the desired identity rotation $R = I$. In this case, the equilibrium $R = I$ is said to be *almost* globally asymptotically stable since from almost all initial conditions (specifically initial attitudes with angle less than 180°) the trajectories of the system converge to $R = I$. The set $\mathbf{R}_a(\pi, \mathbb{S}^2)$ has a Lebegue measure of zero with respect to $\mathbb{SO}(3)$. Although the obtained asymptotic stability result for the equilibrium $R = I$ is strong the existence of the undesired equilibria in $\mathbf{R}_a(\pi, \mathbb{S}^2)$ limits the performance of this control law as explained hereafter.

First, let us derive the time-explicit solution of the differential equation (3.31) which allows to study the trajectories of the system starting at different initial conditions outside the set $\mathbf{R}_a(\pi, \mathbb{S}^2)$.

**Theorem 3.3.1** *Consider the dynamic system* (3.31). *Let* $R(0) \in \Pi_{\mathbb{SO}(3)}$ *then*

$$R(t) = \mathbf{R}_r(\exp(-k\mathbf{E}(A)t)\mathbf{Z}(R(0))), \quad t \geq 0. \tag{3.34}$$

**Proof** See Appendix C.2.

Theorem 3.3.1 provides a closed form solution for the attitude kinematics system (3.27) under the gradient-based feedback (3.29) or, equivalently, the matrix differential equation (3.31) on $\mathbb{SO}(3)$. To the best of the author's knowledge, there is no available work providing such an explicit time solution. The obtained closed form solution is not only appealing from a theoretical stand point but it is also beneficial to understand the behaviour of the trajectories of (3.31) without requiring complex analysis tools. From (3.34) it can be noticed that the Rodrigues vector $\mathbf{Z}(R(t))$ is exponentially decaying to zero from all initial conditions. Note that this vector is only defined for rotations which have an angle different from 180°. It is worth pointing out that, although the Rodrigues vector is converging exponentially, the attitude does not necessary converge exponentially fast since there is a mapping $\mathbf{R}_r$ between the two quantities. The following Corollary

provides an explicit expression of the attitude norm, which will be very useful in studying the performance of the closed-loop system.

**Corollary 3.3.2** *Consider the dynamic system* (3.31). *Let* $R(0) \in \Pi_{\mathbb{SO}(3)}$. *Then, for all* $t \geq 0$, *one has*

$$|R(t)|_I^2 = \frac{\psi(R(0))^\top e^{-2k\mathbf{E}(A)t}\psi(R(0))}{4(1-|R(0)|_I^2)^2 + \psi(R(0))^\top e^{-2k\mathbf{E}(A)t}\psi(R(0))}. \tag{3.35}$$

**Proof** The result can be directly derived from Theorem 3.3.1 by noticing that

$$\|\mathbf{Z}(R(t))\|^2 = \|e^{-k\mathbf{E}(A)t}\mathbf{Z}(R(0))\|^2 = \frac{\psi(R(0))^\top e^{-2k\mathbf{E}(A)t}\psi(R(0))}{4(1-|R(0)|_I^2)^2}, \tag{3.36}$$

and from (2.76) $|R(t)|_I^2 = \mathbf{tr}(I-R)/4 = \|\mathbf{Z}(R)\|^2/(1+\|\mathbf{Z}(R)\|^2)$ which implies (3.35).

Corollary 3.3.2 provides an explicit expression showing the evolution of the Euclidean distance $|R(t)|_I$ with respect to time. Note that it is not difficult to show that $\psi(R) = \sin(\theta)u$ where $R = \mathbf{R}_a(\theta, u)$. Therefore, from (3.35), for the same initial attitude angle, initial attitudes with rotation axis $u(0)$ equals the eigenvector corresponding to the largest eigenvalue of $\mathbf{E}(A)$ generates a larger attitude norm $|R(t)|_I$ compared to an initial attitude with rotation axis $u(0)$ equals the eigenvector corresponding to the smallest eigenvalue of $\mathbf{E}(A)$. The following Corollary provides upper and lower bounds of $|R(t)|_I$.

**Corollary 3.3.3** *Consider the dynamic system* (3.31). *Let* $R(0) \in \Pi_{\mathbb{SO}(3)}$, *then the attitude norm is bounded as follows*

$$\beta(|R(0)|_I, t, k\lambda_{\max}^{\mathbf{E}(A)}) \leq |R(t)|_I \leq \beta(|R(0)|_I, t, k\lambda_{\min}^{\mathbf{E}(A)}), \tag{3.37}$$

*for all* $t \geq 0$, *such that* $\beta(s,t,\lambda) = se^{-\lambda t}/\big(1-s^2(1-e^{-2\lambda t})\big)^{\frac{1}{2}}$.

**Proof** Note that

$$\psi(R(0))^\top e^{-2k\mathbf{E}(A)t}\psi(R(0)) \leq e^{-2k\lambda_{\min}^{\mathbf{E}(A)}t}\|\psi(R(0))\|^2 = 4e^{-2k\lambda_{\min}^{\mathbf{E}(A)}t}|R(0)|_I^2(1-|R(0)|_I^2)$$

which, in view of (3.35) and the fact that the map $x \to x/(x+a)$ is non-decreasing for all $a \geq 0$, implies that

$$|R(t)|_I^2 \leq e^{-2k\lambda_{\min}^{\mathbf{E}(A)}t}|R(0)|_I^2/(1-|R(0)|_I^2 + e^{-2k\lambda_{\min}^{\mathbf{E}(A)}t}|R(0)|_I^2) = \big(\beta(|R(0)|_I, t, k\lambda_{\min}^{\mathbf{E}(A)})\big)^2.$$

Following similar steps as above, the lower bound can be derived.

According to the upper bound on the attitude distance given in Corollary 3.3.3, it is clear that for small initial conditions, *i.e.,* $|R(0)|_I \ll 1$, the attitude satisfies $|R(t)|_I \leq |R(0)|_I \exp(-k\lambda_{\min}^{\mathbf{E}(A)} t)$ which shows the local exponential stability of the equilibrium point $|R|_I = 0$. Moreover, the convergence rate of the attitude to $R = I$ is given in the following corollary

**Corollary 3.3.4** *Starting from any initial condition $R(0) \in \Pi_{\mathbb{SO}(3)}$, the time $t_B$ necessary to enter the ball of radius $|R(t_B)|_I = B$ satisfies*

$$t_B \geq \frac{1}{k\lambda_{\max}^{\mathbf{E}(A)}} \ln\left(\frac{|R(0)|_I(1-B^2)^{\frac{1}{2}}}{B(1-|R(0)|_I^2)^{\frac{1}{2}}}\right). \tag{3.38}$$

**Proof** Using the lower bound of (3.37), the time $t_B$ needs to satisfy the constraint $\beta(|R(0)|_I, t_B, k\lambda_{\max}^{\mathbf{E}(A)}) \leq |R(t_B)|_I = B$. Using straightforward algebraic manipulations, this inequality reads $e^{-k\lambda_{\max}^{\mathbf{E}(A)} t_B} \leq \frac{B^2(1-|R(0)|_I^2)}{|R(0)|_I^2(1-B^2)}$, which leads to the result of the corollary by taking the $\ln(\cdot)$ function on both sides of the last inequality.

According to Corollary 3.3.4, it is clear that large initial conditions, *i.e.,* $|R(0)|_I \to 1$, will result in low convergence rates. Whenever the initial attitude is closer to the manifold of all rotations of 180° the stabilization task will take longer time. This fact about the transient-response performance degradation of smooth attitude controllers on $\mathbb{SO}(3)$ has been numerically and experimentally observed in recent works such as [Lee, 2012, Tse-Huai Wu and Lee, 2015, Zlotnik and Forbes, 2017]. Moreover, it is possible to show that the above control scheme is not robust to a certain class of small bounded vanishing disturbances, see [Berkane and Tayebi, 2017a].

### 3.3.3 Synergistic and Exp-Synergistic Potential Functions

As discussed in the previous section, smooth controllers derived from smooth potential functions on $\mathbb{SO}(3)$ suffer from performance degradation (low convergence rates, reduced robustness) when the initial attitude is large. On the other hand, controllers derived from nonsmooth potential functions on $\mathbb{SO}(3)$ are susceptible to singularities thus not very desirable in practice. To cope with these shortcomings, one can design different controllers from a "family" of potential functions which will be then coordinated in a hybrid fashion to yield the desirable robust global exponential stabilization on $\mathbb{SO}(3)$. This collective behaviour that leads to an improvement in the performance of the control scheme is referred to as "synergism". In this subsection, the formal definition of synergism is recalled and the new notion of exp-synergism for a family of potential functions

on $\mathbb{SO}(3)$ is defined.

Given a finite index set $\mathcal{Q} \subset \mathbb{N}$, let $\mathsf{C}^0\left(\mathbb{SO}(3) \times \mathcal{Q}, \mathbb{R}_{\geq 0}\right)$ denote the set of positive-valued and continuous functions $\Phi : \mathbb{SO}(3) \times \mathcal{Q} \to \mathbb{R}_{\geq 0}$. If, for each $q \in \mathcal{Q}$, the map $R \mapsto \Phi(R, q)$ is differentiable on the set $\mathcal{D}_q \subseteq \mathbb{SO}(3)$ then the function $\Phi(R, q)$ is continuously differentiable on $\mathcal{D} \subseteq \mathbb{SO}(3) \times \mathcal{Q}$, where $\mathcal{D} = \cup_{q \in \mathcal{Q}} \mathcal{D}_q \times \{q\}$, in which case one denotes $\Phi \in \mathsf{C}^1\left(\mathcal{D}, \mathbb{R}_{\geq 0}\right)$. Additionally, for all $(R, q) \in \mathcal{D}$, $\nabla\Phi(R, q) \in \mathsf{T}_R\mathbb{SO}(3)$ denotes the gradient of $\Phi$, with respect to $R$, relative to the Riemannian metric (2.13).

**Definition 3.3.5 (Potential Function)** *A function $\Phi$ is said to be a potential function on $\mathcal{D} \subseteq \mathbb{SO}(3) \times \mathcal{Q}$ with respect to the set $\mathcal{I}_\mathcal{Q} = \{I\} \times \mathcal{Q} \subseteq \mathcal{D}$ if:*

*i) $\Phi$ is continuous, i.e. $\Phi \in \mathsf{C}^0\left(\mathbb{SO}(3) \times \mathcal{Q}, \mathbb{R}_{\geq 0}\right)$*

*ii) $\Phi$ is continuously differentiable on $\mathcal{D}$, i.e. $\Phi \in \mathsf{C}^1(\mathcal{D}, \mathbb{R}_{\geq 0})$*

*iii) $\Phi$ is positive definite with respect to $\mathcal{I}_\mathcal{Q}$, i.e. $\Phi(R, q) = 0$ if $(R, q) \in \mathcal{I}_\mathcal{Q}$ and $\Phi(R, q) > 0$ otherwise*

The set of all potential functions on $\mathcal{D}$ with respect to $\mathcal{I}_\mathcal{Q}$ is denoted as $\mathcal{P}_\mathcal{D}$, where a function $\Phi(R, q) \in \mathcal{P}_\mathcal{D}$ can be seen as a family of potential functions on $\mathbb{SO}(3)$ encoded into a single function indexed by $q$. When the finite index set $\mathcal{Q}$ reduces to a single element, for example $\mathcal{Q} = \{1\}$, then the argument $q$ is omitted and $\mathcal{D} \subseteq \mathbb{SO}(3)$. For a given potential function $\Phi(R, q) \in \mathcal{P}_\mathcal{D}$, the set of critical points of $\Phi$ is defined as follows

$$\mathcal{C}_\Phi = \left\{(R, q) \in \mathcal{D} : \nabla\Phi(R, q) = 0\right\}. \tag{3.39}$$

Note that if $\Phi(R, q) \in \mathcal{P}_\mathcal{D}$ then the map $R \mapsto \Phi(R, q)$ is positive definite on $\mathbb{SO}(3)$ with respect to $I$ for each $q \in \mathcal{Q}$. Thus, the identity rotation $I$ must be a critical point[1] for $R \mapsto \Phi(R, q)$, $\forall q \in \mathcal{Q}$ and therefore the set $\mathcal{I}_\mathcal{Q}$ is included in the set of critical points of $\Phi$ or, for short, $\mathcal{I}_\mathcal{Q} \subseteq \mathcal{C}_\Phi$.

**Definition 3.3.6 (Synergism [Mayhew and Teel, 2013a])** *For a given finite index set $\mathcal{Q} \subset \mathbb{N}$, let $\Phi \in \mathcal{P}_{\mathbb{SO}(3) \times \mathcal{Q}}$. The potential function $\Phi$ is said to be centrally synergistic, with gap exceeding $\delta > 0$, if and only if the following condition holds*

$$\Phi(R, q) - \min_{m \in \mathcal{Q}} \Phi(R, m) > \delta, \quad \forall (R, q) \in \mathcal{C}_\Phi \setminus \mathcal{I}_\mathcal{Q}. \tag{3.40}$$

[1] In fact, for any locally smooth function $f : \mathcal{M} \to \mathbb{R}$ such that $f$ is locally positive definite function about $x_0$, the point $x_0$ is a critical point of $f$ and the Hessian of $f$ is positive semidefinite at $x_0$.

Condition (3.40) implies that at any given undesired critical point $(R, q) \in \mathcal{C}_\Phi \setminus \mathcal{I}_\mathcal{Q}$, there exists another point $(R, m) \in \mathbb{SO}(3) \times \mathcal{Q}$ such that $\Phi(R, m)$ has a lower value than $\Phi(R, q)$. The term "central" refers to the fact that all the potential functions $R \mapsto \Phi(R, q)$ share the identity element $I$ as a critical point such that $\nabla\Phi(I, q) = 0$ for all $q \in \mathcal{Q}$.

**Definition 3.3.7 (Exp-Synergism)** *Consider a set of parameters $\mathcal{T} = (\Phi, \mathcal{Q}, \delta)$ containing a potential function $\Phi \in \mathcal{P}_\mathcal{D}$, $\mathcal{D} \subseteq \mathbb{SO}(3) \times \mathcal{Q}$, a finite index set $\mathcal{Q} \subset \mathbb{N}$ and a scalar $\delta > 0$. Let the subset $\mathcal{F}_\mathcal{T} \subseteq \mathbb{SO}(3) \times \mathcal{Q}$ be defined as:*

$$\mathcal{F}_\mathcal{T} = \{(R, q) : \Phi(R, q) - \min_{m \in \mathcal{Q}} \Phi(R, m) \leq \delta\}. \tag{3.41}$$

*The potential function $\Phi$ is said to be exp-synergistic, with gap exceeding $\delta > 0$, if and only if there exist constants $\alpha_i > 0$, $i = 1, \ldots, 4$, such that the following hold:*

$$\alpha_1 |R|_I^2 \leq \Phi(R, q) \leq \alpha_2 |R|_I^2, \qquad \forall (R, q) \in \mathbb{SO}(3) \times \mathcal{Q}, \tag{3.42}$$

$$\alpha_3 |R|_I^2 \leq \|\nabla\Phi(R, q)\|_F^2 \leq \alpha_4 |R|_I^2, \qquad \forall (R, q) \in \mathcal{F}_\mathcal{T}, \tag{3.43}$$

$$\mathcal{F}_\mathcal{T} \subseteq \mathcal{D}. \tag{3.44}$$

Definition 3.3.7 considers a wider class of potential functions, compared to Definition 3.3.6, by allowing each potential function $R \mapsto \Phi(R, q)$ to be nondifferentiable on some region of the manifold $\mathbb{SO}(3)$. However, the exp-synergism definition imposes more restrictive conditions as compared to Definition 3.3.6 in the sense that the potential function and its gradient are quadratically bounded by the attitude distance on $\mathbb{SO}(3)$. It can be verified that if $\Phi \in \mathcal{P}_\mathcal{D}$ with $\mathcal{D} = \mathbb{SO}(3) \times \mathcal{Q}$ is an exp-synergistic potential function then it is synergistic as well. In fact, condition (3.43) implies that the gradient $\nabla\Phi(R, q)$ does not vanish expect at $\mathcal{I}_\mathcal{Q}$ which is equivalent to condition (3.40). The opposite does not hold in general. The exp-synergism property, as will become clear in the next subsection, plays an important role to ensure desirable exponential decay when using a gradient-based feedback on $\mathbb{SO}(3)$.

### 3.3.4 Hybrid Attitude Stabilization on $\mathbb{SO}(3)$

In this subsection, exp-synergistic potential functions are shown to be instrumental for the global exponential stabilization on $\mathbb{SO}(3)$. Let $\mathcal{Q} \subset \mathbb{N}$ be a finite index set, $\Phi \in \mathcal{P}_\mathcal{D}$ be a potential function on $\mathcal{D} \subseteq \mathbb{SO}(3) \times \mathcal{Q}$ and $\delta > 0$. Define $\mathcal{T} = (\Phi, \mathcal{Q}, \delta)$ and consider the following switching mechanism of the discrete state variable $q$, which dictates the

current *mode* of operation of the hybrid control system,

$$\mathbf{H}_{\mathcal{T}} \begin{cases} \dot{q} = 0, & (R,q) \in \mathcal{F}_{\mathcal{T}}, \\ q^+ \in \mathbf{J}_{\mathcal{T}}(R), & (R,q) \in \mathcal{J}_{\mathcal{T}}, \end{cases} \tag{3.45}$$

where $\mathbf{J}_{\mathcal{T}}(R) = \arg\min_{m\in\mathcal{Q}} \Phi(R,m)$ is the jump map and the flow set $\mathcal{F}_{\mathcal{T}}$ and jump set $\mathcal{J}_{\mathcal{T}}$ are defined as follows:

$$\mathcal{F}_{\mathcal{T}} = \{(R,q) : \Phi(R,q) - \min_{m\in\mathcal{Q}} \Phi(R,m) \leq \delta\}, \tag{3.46}$$

$$\mathcal{J}_{\mathcal{T}} = \{(R,q) : \Phi(R,q) - \min_{m\in\mathcal{Q}} \Phi(R,m) \geq \delta\}. \tag{3.47}$$

In this case the attitude matrix $R \in \mathbb{SO}(3)$ is considered as an input to the hybrid system $\mathbf{H}_{\mathcal{T}}$ which is parametrized by the potential function $\Phi$, the index set $\mathcal{Q}$ and the hysteresis gap $\delta > 0$. The output of this hybrid dynamical system is the index $q \in \mathcal{Q}$ and one can write for short

$$q = \mathbf{H}_{\mathcal{T}}(R). \tag{3.48}$$

It is worthwhile mentioning that the above hybrid mechanism, inspired by [Mayhew

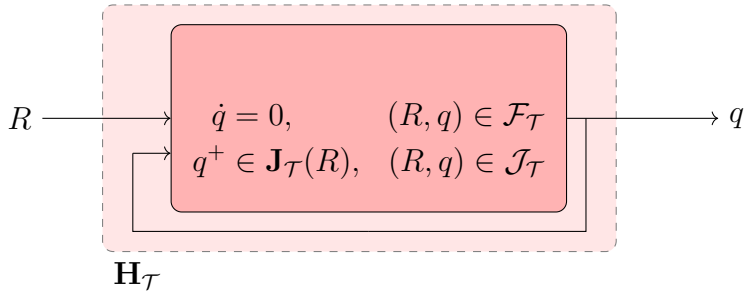


Figure 3.7: Synergistic hybrid switching mechanism.

and Teel, 2011b], uses a "min-switch" strategy to select a control law derived from the minimal potential function among some family of potential functions on $\mathbb{SO}(3)$. Such a control input for system (3.27) is given in the following theorem.

**Theorem 3.3.8** *Let $\mathcal{Q} \subset \mathbb{N}$ be a finite index set and $\Phi \in \mathcal{P}_{\mathcal{D}}$ be a potential function on $\mathcal{D} \subseteq \mathbb{SO}(3) \times \mathcal{Q}$. Consider system (3.27) with the control input*

$$\omega = -\psi\left(R^\top \nabla\Phi(R,q)\right), \tag{3.49}$$

*where $q = \mathbf{H}_{\mathcal{T}}(R)$ with $\mathcal{T} = (\Phi, \mathcal{Q}, \delta)$ for some $\delta > 0$. If the potential function $\Phi$ is*

*exp-synergistic with gap exceeding $\delta$, then the set $\mathcal{A}_1 = \{I\} \times \mathcal{Q}$ is globally exponentially stable.*

**Proof** See Appendix C.3.

The result in Theorem 3.3.8 provides a systematic method for the design of hybrid attitude control algorithms for system (3.27) guaranteeing global exponential stability. It is worth pointing out that, in addition to the structurally simple expression of the controller proposed so far, the result in this subsection reduces the stabilisation problem of systems (3.27) to the problem of finding appropriate exp-synergistic potential functions, in the sense of Definition 3.3.7, with some synergistic gap that can be specified using the control parameters. This will be the objective of the next subsection.

### 3.3.5 Construction of Exp-Synergistic Potential Functions

The focus of this subsection will be on the design of exp-synergistic potential functions on the rotation group $\mathbb{SO}(3)$ which are shown to be sufficient for the design of global hybrid attitude stabilization schemes. The first work dealing with the construction of synergistic potential functions on $\mathbb{SO}(3)$ appeared in [Mayhew and Teel, 2011d]. It consists of stretching and compressing $\mathbb{SO}(3)$ by applying diffeomorphic transformations, which allow to relocate the critical points while leaving the identity element unchanged leading to a synergistic family of potential functions. Despite the originality of this approach, it was abandoned mainly due to the difficulty in finding an explicit expression of the synergistic gap. In this section, we build up from the ideas in [Mayhew and Teel, 2011d] towards more generic constructions of exp-synergistic potential functions on $\mathbb{SO}(3)$ via "angular warping", while providing a thorough analysis of the synergism properties.

**Lemma 3.3.9** *Let $\mathcal{Q} \subset \mathbb{N}$ be a finite index set and $\{u_q\}_{q\in\mathcal{Q}} \subset \mathbb{S}^2$ be a set of unit vectors. Let us consider the map*[2] *$\Gamma : \mathbb{SO}(3) \times \mathcal{Q} \to \mathbb{SO}(3)$ such that*

$$\Gamma(R, q) := R\mathbf{R}_a(\theta_q(R), u_q), \tag{3.50}$$

*where $\theta_q : \mathbb{SO}(3) \to \mathbb{R}$ is a real-valued differentiable function. Then, the following hold:*

1. *The time derivative of $\Gamma(R, q)$, as defined in (3.50), along the trajectories of $\dot{R} = R[\omega]_\times$ is given by*

$$\frac{d}{dt}\Gamma(R, q) = \Gamma(R, q)[\Theta(R, q)\omega]_\times, \tag{3.51}$$

[2] The multiplication by the additional rotation $\mathbf{R}_a(\theta_q(R), u)$ is done on the *right* of the original rotation matrix $R$ for our convenience. It is left to the reader to explore the other option.

*where* $\Theta(R,q)^\top = \mathbf{R}_a(\theta_q(R), u_q) + 2\psi(R^\top \nabla\theta_q(R))u_q^\top$.

2. *If* $\det(\Theta(R,q)) \neq 0$ *for all* $(R,q) \in \mathbb{SO}(3) \times \mathcal{Q}$, *then for each* $q \in \mathcal{Q}$ *the map* $R \mapsto \Gamma(R,q)$ *is everywhere a local diffeomorphism.*

3. *If* $\det(\Theta(R,q)) \neq 0$ *for all* $(R,q) \in \mathbb{SO}(3) \times \mathcal{Q}$ *and* $\Gamma^{-1}(\{I\}) = \{I\} \times \mathcal{Q}$ *then for any* $\Psi \in \mathcal{P}_{\mathcal{D}_\Psi}$ *with* $\mathcal{D}_\Psi \subseteq \mathbb{SO}(3)$ *one has* $\Psi \circ \Gamma \in \mathcal{P}_{\Gamma^{-1}(\mathcal{D}_\Psi)}$ *and the set of critical points of* $\Psi \circ \Gamma$ *is given by* $\mathcal{C}_{\Psi\circ\Gamma} = \Gamma^{-1}(\mathcal{C}_\Psi)$.

**Proof** See Appendix A.8.

Lemma 3.3.9 shows that, under some conditions on the transformation $\Gamma$, one can construct a new family of potential functions on $\mathbb{SO}(3)$ by considering the composition of a *basic* potential function on $\mathbb{SO}(3)$ and the map $\Gamma$. What we will investigate next is the search for a suitable basic function $\Psi$, a suitable angle function $\theta_q(\cdot)$ and the set of unit vectors $\{u_q\}_{q\in\mathcal{Q}}$ such that the composite function $\Psi \circ \Gamma(R,q)$ is an exp-synergistic potential function.

### Non-Weighted Potential Functions

Consider the following potential functions on $\mathbb{SO}(3)$:

$$\Psi_1(R) = \frac{1}{2}\mathbf{tr}(I - R), \tag{3.52}$$

$$\Psi_2(R) = 2 - \sqrt{1 + \mathbf{tr}(R)}. \tag{3.53}$$

The smooth potential function $\Psi_1(R)$ has been widely used in the literature for attitude control problems [Koditschek, 1988, Bullo and Murray, 1999, Sanyal *et al.*, 2009]. The nonsmooth potential function $\Psi_2(R)$ is non differentiable at $\mathbf{tr}(R) = -1$ which corresponds to the set of all attitudes of angle $\pi$. The potential function $\Psi_2(R)$ has been used in [Lee, 2012] for attitude tracking to obtain faster convergence for large attitude manoeuvres and also appeared in [Saccon *et al.*, 2010] as a solution to the kinematic optimal control on $\mathbb{SO}(3)$. Note that there exists a similar nonsmooth potential function $\Psi_3(R) = \frac{2}{\pi^2}\|\log(R)\|_F^2$ which is related to the geodesic distance on $\mathbb{SO}(3)$ as defined in (2.39) between the rotation matrix $R$ and the identity rotation $I$. It has been used for instance in [Bullo and Murray, 1995] for attitude stabilization and in [Berkane and Tayebi, 2015b] for optimal kinematic attitude control on $\mathbb{SO}(3)$ and the results of this section can be extended or modified to use $\Psi_3(R)$. It is interesting to see the expressions

of $\Psi_i, i = 1, 2$ in terms of unit quaternions and angle axis representations. Let $(\eta, \epsilon) \in \mathbb{Q}$ and $(\theta, u) \in \mathbb{R} \times \mathbb{S}^2$. Then, using (2.74)-(2.75) one can verify that

$$\Psi_1(\mathbf{R}_u(\eta, \epsilon)) = 2(1 - \eta^2), \qquad \Psi_1(\mathbf{R}_a(\theta, u)) = 1 - \cos(\theta), \tag{3.54}$$

$$\Psi_2(\mathbf{R}_u(\eta, \epsilon)) = 2(1 - |\eta|), \qquad \Psi_2(\mathbf{R}_a(\theta, u)) = 2(1 - |\cos(\theta/2))|) \tag{3.55}$$

which corresponds to widely used potential functions [Fjellstad and Fossen, 1994, Thienel and Sanner, 2003]. In view of (2.71), the gradients of the two potential functions are given by

$$\nabla\Psi_1(R) = \frac{1}{2} R\mathbf{P}_{\mathfrak{so}(3)}(R), \tag{3.56}$$

$$\nabla\Psi_2(R) = \frac{R\mathbf{P}_{\mathfrak{so}(3)}(R)}{2\sqrt{1 + \mathbf{tr}(R)}}. \tag{3.57}$$

Note that the gradient of $\Psi_2$ is not defined on the set $\mathbf{R}_a(\pi, \mathbb{S}^2)$ which is the set of all rotations of angle 180°. Both gradients vanish at the desirable equilibrium $R = I$. However, $\nabla\Psi_1(R)$ vanishes as well at the undesired equilibria given by $\mathbf{R}_a(\pi, \mathbb{S}^2)$. Consequently, when choosing any of the potential functions $\Psi_1$ or $\Psi_2$ one is faced with either the problem of undesired critical points (for $\Psi_1$) or the problem of singular points (for $\Psi_2$). The following proposition provides a construction of two exp-synergistic potential

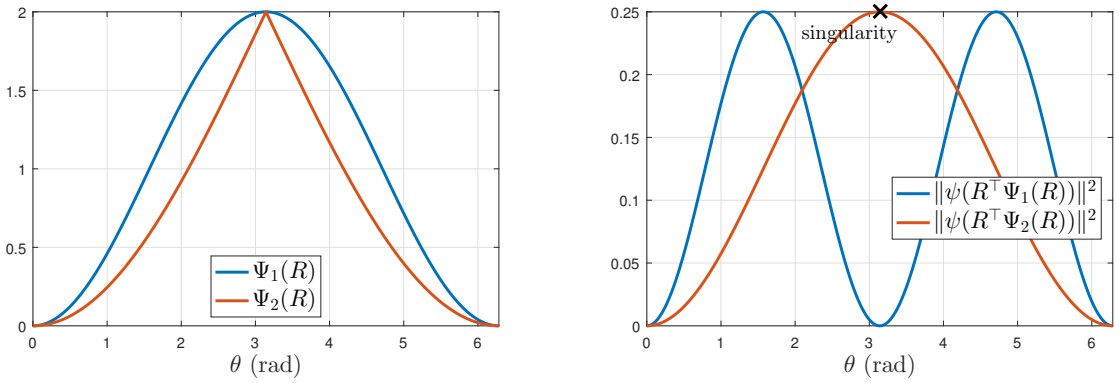


Figure 3.8: Plot of the attitude potential functions $\Psi_1$ and $\Psi_2$ with their corresponding gradients norm for different values of the attitude angle (attitude axis is fixed). The potential function $\Psi_1$ has an undesired critical point at $\theta = \pi$ while the attitude potential function $\Psi_2$ is singular at $\theta = \pi$.

functions from $\Psi_1$ and $\Psi_2$.

**Proposition 3.3.10** *Let $\mathcal{Q} = \{1, 2, ..., 6\}$ be a finite index set. Consider the transfor-*

*mation* $\Gamma : \mathbb{SO}(3) \times \mathcal{Q} \to \mathbb{SO}(3)$ *defined as*

$$\Gamma(R, q) = R\mathbf{R}_a(2 \arcsin\left(k|R|_I^2\right), u_q), \tag{3.58}$$

*where* $0 < k < 1/\sqrt{2}$, $u_{m+3} = -u_m$, $m \in \{1, 2, 3\}$, *and* $\{u_1, u_2, u_3\}$ *is an orthonormal set of vectors. Then, the following hold*

- $\Psi_1 \circ \Gamma \in \mathcal{P}_{\mathcal{D}}$, *with* $\mathcal{D} = \mathbb{SO}(3) \times \mathcal{Q}$, *is exp-synergistic with a gap exceeding* $\delta_1 < \bar{\delta}_1 = [-1 + \sqrt{1 + 4k^2}]^3/12k^4$.
- $\Psi_2 \circ \Gamma \in \mathcal{P}_{\mathcal{D}}$, *with* $\mathcal{D} = \Gamma^{-1}(\Pi_{\mathbb{SO}(3)})$, *is exp-synergistic with a gap exceeding* $\delta_2 < \bar{\delta}_2 = [-1 + \sqrt{1 + 4k^2}]^{\frac{3}{2}}/\sqrt{6}k^2$.

**Proof** See Appendix B.3.

In Proposition 3.3.10, the transformation $\Gamma(R, q)$ can be seen as a perturbation to $R$ about the unit vector $u_q$ by an angle $2 \arcsin\left(k|R|_I^2\right)$. This allows to *stretch/compress* the manifold $\mathbb{SO}(3)$ in order to move the critical/singular points of $\Psi_i(R)$ to different locations on $\mathbb{SO}(3)$. As per why the choice of 6 configurations, it can be intuitively motivated by the example of the unit circle discussed in the previous section. For a unit circle (single axis of rotation), one needs two configurations to avoid the undesired point at $\pi$ angle. Since any rotation axis in $\mathbf{R}_a(\pi, \mathbb{S}^2)$ can take arbitrary directions (3 degrees of freedom) this resulted in $2 \times 3 = 6$ configurations. Nevertheless, it is not claimed that this is the minimum number of configurations to construct an exp-synergistic family of potential functions from $\Psi_1$ or $\Psi_2$ by angular warping. It is left to the reader to explore more options.

**Remark 3.3.11** *The angular warping transformation defined in* (3.58) *can be written using the quaternion map as follows*

$$\Gamma(R, q) = R\mathbf{R}_u\big([1 - k^2|R|_I^4]^{\frac{1}{2}}, k|R|_I^2 u_q\big), \tag{3.59}$$

*which is computationally less consuming (suitable for implementation) compared to the map* $\mathbf{R}_a$ *which involves the use of* sin *and* cos *functions. Nevertheless, for illustrative purposes, the map* $\mathbf{R}_a$ *is often used.*

Figure 3.9 (respect. Figure 3.10) illustrates the value of each potential function $\Psi_1 \circ \Gamma(R, q)$ (respect. $\Psi_2 \circ \Gamma(R, q)$) at different angles of rotations. It can be seen from these figures that when the potential function $\Psi_1 \circ \Gamma(R, q)$ (respect. $\Psi_2 \circ \Gamma(R, q)$) is at a given critical (respect. singular) point it is guaranteed that the gap between the potential

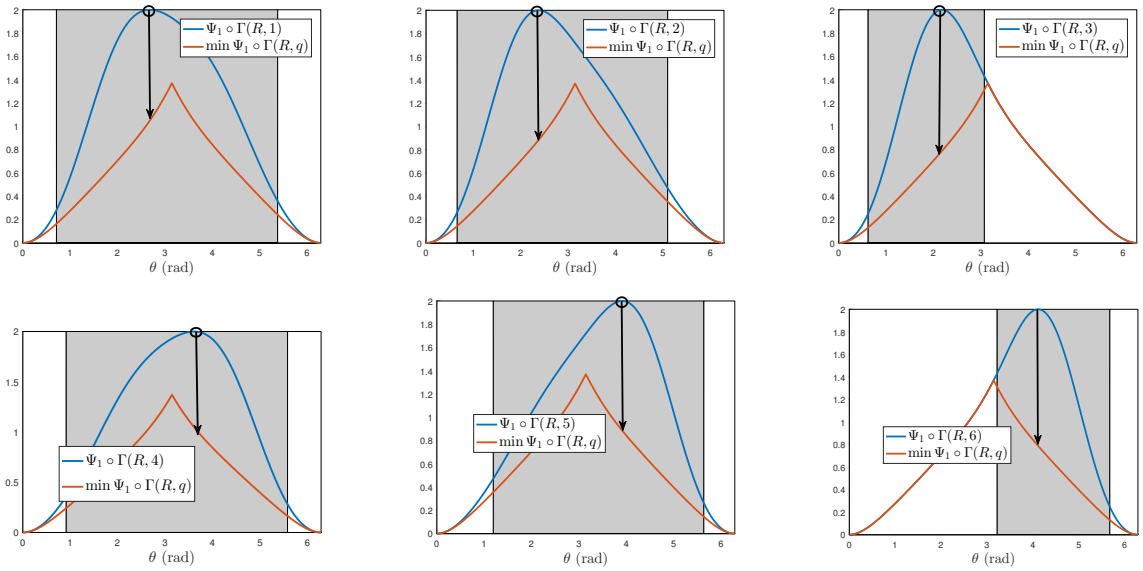


Figure 3.9: Plot of the function $\Psi_1 \circ \Gamma(R(\theta), q)$ (solid blue) for different values of $q$ along the path $R(\theta) = \mathbf{R}_a(\theta, [1,2,3]^\top/\sqrt{14})$ with $\theta \in [0, 2\pi]$, $k = 0.7$ and $u_m = e_m, m = 1,2,3$. The gray filled area indicates when $(R,q) \in \mathcal{J}_\mathcal{T}$ and the white area indicates when $(R,q) \in \mathcal{F}_\mathcal{T}$. The sets $\mathcal{F}_\mathcal{T}$ and $\mathcal{J}_\mathcal{T}$ are defined in (3.46)-(3.47) with $\Phi = \Psi_1 \circ \Gamma$ and $\delta = 0.12$. Note that all critical points, marked with a circle, are contained in the jump set $\mathcal{J}_\mathcal{T}$. The downward arrows indicate that at a given critical point, $q$ can be switched to decrease the value of potential function $\Psi_1 \circ \Gamma(R,q)$.

function and the minimum of the potential functions exceeds the threshold $\bar{\delta}_1$ (respect. $\bar{\delta}_2$). A switch to the minimum potential function will guarantee a decrease in the current potential function which is illustrated by the downwards arrows in the figures.

### Weighted Potential Functions

The weighted version of the trace potential function $\Psi_1(R)$ defined in (3.52) is the potential function $\Psi_{1,A}$ given in (3.28) for some symmetric matrix $A$ such that $\mathbf{E}(A)$ is positive definite. It is interesting to propose a weighted version for the nondifferentiable potential function $\Psi_2(R)$ defined in (3.53). Consider the following potential function

$$\Psi_{2,A}(R) := \sqrt{4\lambda_{\max}^{\mathbf{E}(A)}} - \sqrt{4\lambda_{\max}^{\mathbf{E}(A)} - \mathbf{tr}(A(I-R))}, \quad \mathbf{E}(A) > 0. \tag{3.60}$$

A similar function has also been used in [Zlotnik and Forbes, 2017] with $\lambda_{\min}^{\mathbf{E}(A)}$ instead of $\lambda_{\max}^{\mathbf{E}(A)}$ in (3.60). Here, $\lambda_{\max}^{\mathbf{E}(A)}$ is used to ensure that $\Psi_{2,A}(R)$ is well defined over the whole manifold $\mathbb{SO}(3)$. In fact, in view of (2.75), the maximum value of $\mathbf{tr}(A(I-R))$ on $\mathbb{SO}(3)$ does not exceed $4\lambda_{\max}^{\mathbf{E}(A)}$. The advantage of introducing this class of potential functions on

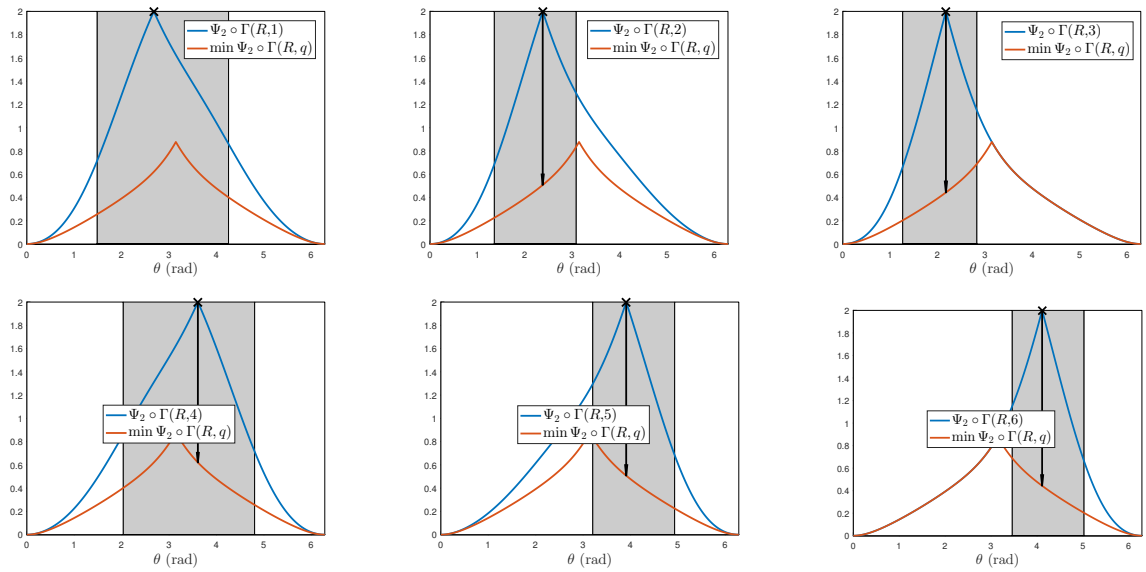


Figure 3.10: Plot of the function $\Psi_2 \circ \Gamma(R(\theta), q)$ (solid blue) for different values of $q$ along the path $R(\theta) = \mathbf{R}_a(\theta, [1,2,3]^\top/\sqrt{14})$ with $\theta \in [0, 2\pi]$, $k = 0.7$ and $u_m = e_m, m = 1,2,3$. The gray filled area indicates when $(R,q) \in \mathcal{J}_\mathcal{T}$ and the white area indicates when $(R,q) \in \mathcal{F}_\mathcal{T}$. The sets $\mathcal{F}_\mathcal{T}$ and $\mathcal{J}_\mathcal{T}$ are defined in (3.46)-(3.47) with $\Phi = \Psi_2 \circ \Gamma$ and $\delta = 0.46$. Note that all singular points, marked with a cross, are contained in the jump set $\mathcal{J}_\mathcal{T}$. The downward arrows indicate that at a given critical point, $q$ can be switched to decrease the value of potential function $\Psi_2 \circ \Gamma(R,q)$.

$\mathbb{SO}(3)$ is to enhance the convergence rates when starting from large attitude errors. This is a consequence of the additional *state-dependent* gain $[4\lambda^{\mathbf{E}}_{\max}(A) - \mathbf{tr}(A(I-R))]^{-\frac{1}{2}}$ in the gradient of $\Psi_{2,A}(R)$, compared to the gradient of $\Psi_{1,A}(R)$, introduced by the square root function. Note that $\Psi_{2,A}(R)$ has a mixture of critical and singular points. The sets of critical and singular points for $\Psi_{2,A}(R)$ are given by

$$\mathcal{C}_{\Psi_{2,A}} = \mathcal{C}_{\Psi_{1,A}} \setminus \mathcal{S}_{\Psi_{2,A}}, \tag{3.61}$$

$$\mathcal{S}_{\Psi_{2,A}} = \left\{ R \in \mathbb{SO}(3) : R = \mathbf{R}(\pi, v), v \in \mathcal{E}^{\mathbb{R}}_v(A), \mathbf{E}(A)v = \lambda^{\mathbf{E}(A)}_{\max} v \right\}. \tag{3.62}$$

Next, a construction, via angular warping, is given for two exp-synergistic potential functions designed from the two weighted potential functions $\Psi_{1,A}(R)$ and $\Psi_{2,A}(R)$. For this purpose, let us define the set of indices $\mathcal{Q} = \{1,2\}$ and consider the transformation $\Gamma : \mathbb{SO}(3) \times \mathcal{Q} \to \mathbb{SO}(3)$ defined as

$$\Gamma(R,q) = R\mathbf{R}_a(2 \arcsin\left(k\mathbf{tr}(A(I-R))\right), u_q), \tag{3.63}$$

where $u_1 = -u_2 = u \in \mathbb{S}^2$.

**Lemma 3.3.12** *Let $u \in \mathbb{S}^2$ be a unit vector and $A = A^\top > 0$ be a symmetric positive definite matrix. Consider the transformation $\Gamma$ defined in* (3.63)*. If the the scalar gain $k$ satisfies the bound*

$$0 < k < \frac{1}{4\lambda_{\max}^{\mathbf{E}(A)}\sqrt{1+\bar{\psi}(\xi^2)}}, \tag{3.64}$$

*with $\xi := \lambda_{\min}^{\mathbf{E}(A)}/\lambda_{\max}^{\mathbf{E}(A)}$ and $\bar{\psi}(\cdot)$ defined in Lemma 2.2.6 then $\Gamma^{-1}(\{I\}) = \{I\} \times \mathcal{Q}$ and $\mathbf{det}(\Theta(R,q)) \neq 0$ for all $(R,q) \in \mathbb{SO}(3) \times \mathcal{Q}$.*

**Proof** See Appendix A.9.

In view of Lemma 3.3.12 and the result of Lemma 3.3.9, the condition on $k$ in (3.64) guarantees that the map $\Gamma(R,q)$ in (3.63) is everywhere a local diffeomorphism and that the map $\Gamma(R,q)$ can be composed with existing potential functions on $\mathbb{SO}(3)$ to yield valid families of potential functions on $\mathbb{SO}(3) \times \mathcal{Q}$. Our next task is to use the transformation $\Gamma(R,q)$ defined in (3.63) to build exp-synergistic potential functions from $\Psi_{1,A}$ and $\Psi_{2,A}$. Since the set of critical points for $\Psi_{1,A}$ and the union set of the singular and critical points for $\Psi_{2,A}$ coincide (note that $\mathcal{C}_{\Psi_{1,A}} = \mathcal{C}_{\Psi_{2,A}} \cup \mathcal{S}_{\Psi_{2,A}}$), one needs to guarantee that there exists a certain gap between $\Psi_{1,A} \circ \Gamma(R,1)$ and $\Psi_{1,A} \circ \Gamma(R,2)$ and between $\Psi_{2,A} \circ \Gamma(R,1)$ and $\Psi_{2,A} \circ \Gamma(R,2)$ whenever $(R,q) \in \mathcal{C}_{\Psi_{1,A}\circ\Gamma}, q \in \mathcal{Q}$. To motivate the following construction, the focus next will be on the potential function $\Psi_{1,A} \circ \Gamma(R,q)$ and, later, the exp-synergism result is stated for $\Psi_{2,A} \circ \Gamma(R,q)$ as well.

**Lemma 3.3.13** *Let $u \in \mathbb{S}^2$ be a unit vector and $A$ be a symmetric positive definite matrix with distinct eigenvalues. Consider the potential function $\Psi_{1,A}$ in* (3.28) *and the transformation $\Gamma$ defined in* (3.63) *where $k$ satisfies* (3.64)*. Then, $\Psi_{1,A} \circ \Gamma$ is synergistic if and only if the following condition holds*

$$\min_{i\in\{1,2,3\}} \Delta(v_i, u) > 0, \tag{3.65}$$

*where $\{v_1, v_2, v_3\}$ is the set of unit orthonormal eigenvectors of $A$ and $\Delta(\cdot,\cdot)$ is defined in Lemma 2.2.8.*

**Proof** See Appendix A.10.

Lemma 3.3.13 provides the necessary and sufficient condition for the composite function $\Psi_{1,A} \circ \Gamma$ to be synergistic. Now, one needs to characterize the feasible set where the condition (3.65) is satisfied.

**Lemma 3.3.14** *The feasible region where condition* (3.65) *holds is characterized by the inequality*

$$-\varrho_{33}(u^\top v_1)^2 + \varrho_{23} < (u^\top v_2)^2 < -\varrho_{32}(u^\top v_1)^2 + \varrho_{22}, \tag{3.66}$$

*where* $\varrho_{ij} = (\lambda_i^A + (-1)^j \lambda_1^A)/(\lambda_3^A + \lambda_2^A)$. *This region is plotted in Figure 3.11.*

**Proof** See Appendix A.11.

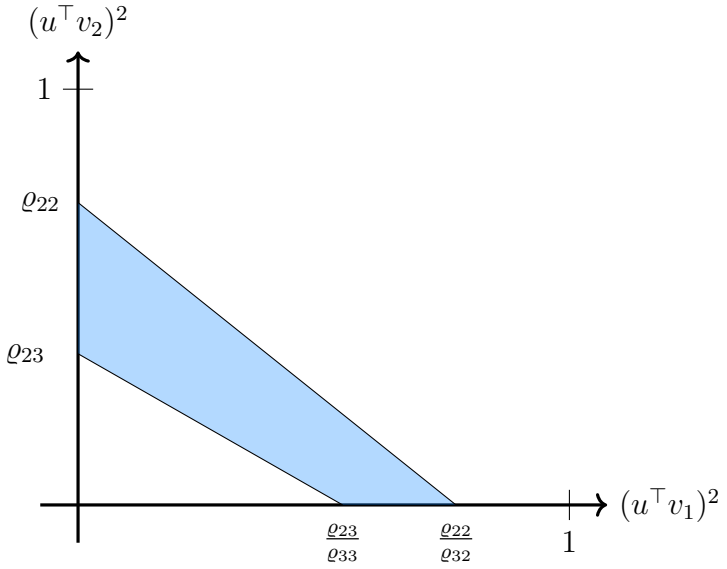


Figure 3.11: The feasible region of the synergy condition (3.65)

.

If one chooses the direction $u \in \mathbb{S}^2$ of the angular warping to lie inside the feasible region of Lemma 3.3.14 then there exists a synergy gap between the configurations of the composite function $\Psi_{1,A} \circ \Gamma$. An example of a choice for $u \in \mathbb{S}^2$ that satisfies the feasible region of Lemma 3.3.14 is the solution of the following max-min optimization

$$\max_{u \in \mathbb{S}^2} \min_{i \in \{1,2,3\}} \Delta(v_i, u). \tag{3.67}$$

**Proposition 3.3.15** *The unit vector* $u \in \mathbb{S}^2$ *solution to the optimization* (3.67) *is given by*

$$\begin{cases} u^\top v_1 = 0,\ (u^\top v_i)^2 = \frac{\lambda_i^A}{(\lambda_2^A + \lambda_3^A)}, i \in \{2,3\}, & \text{if } \lambda_2^A \geq \frac{\lambda_1^A \lambda_3^A}{\lambda_3^A - \lambda_1^A} \\ (u^\top v_i)^2 = 1 - \frac{4 \prod_{j \neq i} \lambda_j^A}{\sum_\ell \sum_{k \neq \ell} \lambda_\ell^A \lambda_k^A}, i \in \{1,2,3\}, & \text{otherwise.} \end{cases} \tag{3.68}$$

**Proof** See Appendix B.4.

Under the above derived conditions of synergism, it is shown in the next proposition that $\Psi_{1,A} \circ \Gamma$ and $\Psi_{2,A} \circ \Gamma$ are both exp-synergistic potential functions with guaranteed gaps.

**Proposition 3.3.16** *Let $A$ be symmetric positive definite. Consider the transformation $\Gamma$ defined in* (3.63) *with $k$ satisfying* (3.64) *and $u \in \mathbb{S}^2$ satisfying* (3.66)*. Then,*

- $\Psi_{1,A} \circ \Gamma \in \mathcal{P}_{\mathcal{D}}$*, with* $\mathcal{D} = \mathbb{SO}(3) \times \mathcal{Q}$*, is exp-synergistic with a gap exceeding* $0 < \delta_1 < \bar{\delta}_1$ *such that* $\bar{\delta}_1 = \sigma(k, \lambda_{\min}^{\mathbf{E}(A)}, \underline{\Delta}(u))$*,* $\underline{\Delta}(u) = \min_{i \in \{1,2,3\}} \Delta(v_i, u)$ *and* $\sigma(\cdot,\cdot,\cdot)$ *is defined in* (B.26)-(B.27)*.*
- $\Psi_{2,A} \circ \Gamma \in \mathcal{P}_{\mathcal{D}}$*, with* $\mathcal{D} = \{(R, q) : \Gamma(R, q) \notin \mathcal{S}_{\Psi_{2,A}}\}$*, is exp-synergistic with a gap exceeding* $0 < \delta_2 < \bar{\delta}_2$ *such* $\bar{\delta}_2 = -\sqrt{4\lambda_{\max}^{\mathbf{E}(A)} - 4\lambda_{\min}^{\mathbf{E}(A)}} + \sqrt{4\lambda_{\max}^{\mathbf{E}(A)} - 4\lambda_{\min}^{\mathbf{E}(A)} + 2\sigma(k, \lambda_{\min}^{\mathbf{E}(A)}, \underline{\Delta}(u))}$.

**Proof** See Appendix B.5.

In the construction of exp-synergistic potential functions given in Proposition 3.3.16, one assumes that the weighting matrix $A$ is symmetric positive definite with distinct eigenvalues. Note that $A > 0$ is more restrictive than the condition $\mathbf{E}(A) > 0$ which is sufficient for $\Psi_{1,A}$ to be a valid potential function on $\mathbb{SO}(3)$. It is an open problem to construct exp-synergistic potential functions via angular warping from $\Psi_{1,A}(R)$ or $\Psi_{2,A}(R)$ in the case where $A$ is only positive semidefinite and $\mathbf{E}(A)$ is positive definite. When using these exp-synergistic potential functions in a hybrid controller such as (3.49), it is required to compute their gradient with respect to the first argument $R$. It follows from (B.24) and (A.15) that the gradient of $\Psi_{1,A} \circ \Gamma$ is given by

$$\nabla(\Psi_{1,A} \circ \Gamma)(R, q) = \frac{1}{2} R[\Theta(R, q)^\top \psi(A\Gamma(R, q))]_\times, \tag{3.69}$$

$$\Theta(R, q) = \mathbf{R}_a(2 \arcsin(k\mathbf{tr}(A(I - R))), u_q)^\top + \frac{4k u_q \psi(AR)^\top}{\sqrt{1 - k^2 \mathbf{tr}^2(A(I - R))}}. \tag{3.70}$$

Moreover, in view of (3.28) and (3.60), the gradient of $\Psi_{2,A} \circ \Gamma$ can be written as

$$\nabla(\Psi_{2,A} \circ \Gamma)(R, q) = \frac{\nabla(\Psi_{1,A} \circ \Gamma)(R, q)}{\sqrt{4\lambda_{\max}^{\mathbf{E}(A)} - \mathbf{tr}(A(I - \Gamma(R, q)))}}. \tag{3.71}$$

### 3.3.6 Illustration of the Switching Mechanism

To shed some light on how the hybrid switching mechanism, introduced in (3.45)-(3.47), allows to achieve global results and improve the convergence rates compared to non-hybrid algorithms, the hybrid switching mechanism is implemented, separately, as follows. Consider the weighting matrix $A = \text{diag}(1, 2, 3)$, index set $\mathcal{Q} = \{1, 2\}$ and unit vectors $u_1 = -u_2 = u$ such that $u = [0, \sqrt{2/5}, \sqrt{3/5}]^\top$ which is chosen to satisfy (3.68). Let the parameter $k = 4.45 \times 10^{-2}$ which satisfies condition (3.64). The switching mechanism (3.45)-(3.47) is implemented with the potential function $\Phi = \Psi_{2,A} \circ \Gamma$ and the hysteresis gap $\delta = 0.95\bar{\delta}_2$ where $\bar{\delta}_2$ is defined in Proposition 3.3.16. According to Appendix A.10, for each $q \in \mathcal{Q}$, the potential function $\Phi(R, q)$ admits three undesired critical/singular points. In the case of $q = 1$, these undesired points, denoted $\{\bar{R}_1, \bar{R}_2, \bar{R}_3\}$, are explicitly given by

$$\bar{R}_i = \mathbf{R}_a(\pi, v_i)\mathbf{R}_a(2\arcsin(k\bar{\Psi}_i), u_1)^\top, \tag{3.72}$$

$$\bar{\Psi}_i = \frac{-1 + \sqrt{1 + 64k^2\Delta(v_i, u)\lambda_{v_i}^{\mathbf{E}(A)}}}{8k^2\Delta(v_i, u)}, \tag{3.73}$$

for $i \in \{1, 2, 3\}$ where $v_i$ is the eigenvector associated to the eigenvalue $\lambda_i^A$. Since $A$ is diagonal one has $v_i = e_i$ for $i = 1, 2, 3$. Using (A.34) it can be verified that $\Delta(v_1, u) = 0.7$ and $\Delta(v_2, u) = \Delta(v_3, u) = 0.5$ which allows to compute the values

$$\begin{aligned}
\bar{\Psi}_1 &\simeq 9.59,\\
\bar{\Psi}_2 &\simeq 7.81,\\
\bar{\Psi}_3 &\simeq 5.89.
\end{aligned}$$

Therefore, making use of the composition of rotations, one can calculate the critical/singular points of $\Phi(R, 1)$ according to (3.72). One obtains $\bar{R}_i = \mathbf{R}_a(\theta_i, w_i)$ for some angles $\theta_i \in \mathbb{R}$ and unit vectors $w_i \in \mathbb{S}^2$. More, precisely, the unit vectors are

$$\begin{aligned}
w_1 &= [0.9063, 0.3274, -0.2673]^\top,\\
w_2 &= [-0.2741, 0.9617, 0]^\top,\\
w_3 &= [0.1685, 0, 0.9857]^\top.
\end{aligned}$$

Now let us generate three attitude trajectories as follows: $R_i(\theta) = \mathbf{R}_a(\theta, w_i)$ where $\theta \in [0, 2\pi]$. This guarantees that each trajectory $R_i(\theta)$ will pass through the singular/critical point $\bar{R}_i$ for some value of $\theta$. For each trajectory $R_i(\theta)$, the values of the individual

potential functions $\Phi(R_i(\theta), 1)$ and $\Phi(R_i(\theta), 2)$ as well as $\Phi(R_i(\theta), q)$, where the index $q$ is initialized at $q = 1$ and evolves according to the hybrid dynamical system (3.45)-(3.47), are calculated. The norm of the gradient of these potential function is also calculated and the results are plotted in Figure (3.12). For instance, if one takes the second trajectory (2nd column), Figure (3.12) illustrates how the switching mechanism allows, starting from the initial configuration $q = 1$, to jump to the minimum potential function $\Phi(R, 2)$ when the difference between the two configurations exceeds the threshold $\delta$. Then, a second switch happens when the difference between the current potential function, now $\Phi(R, 2)$, and the minimum potential function, now $\Phi(R, 1)$, exceeds $\delta$. It can be seen also that the gradient of $\Phi(R, q)$ does not vanish, during the flows of the hybrid system, except at the identity rotation. Similar discussions can be conducted for the other two trajectories where one encounters a singular point (1st column) or a critical point (3rd column) for $\Phi(R, 1)$. The hybrid switching mechanism allows to avoid the singularity and/or the undesired critical point by switching between its two configurations. A similar discussion can be derived using trajectories that pass through the singular/critical points for $\Phi(R, 2)$ or when considering the potential function $\Phi = \Psi_{1,A} \circ \Gamma$ instead.

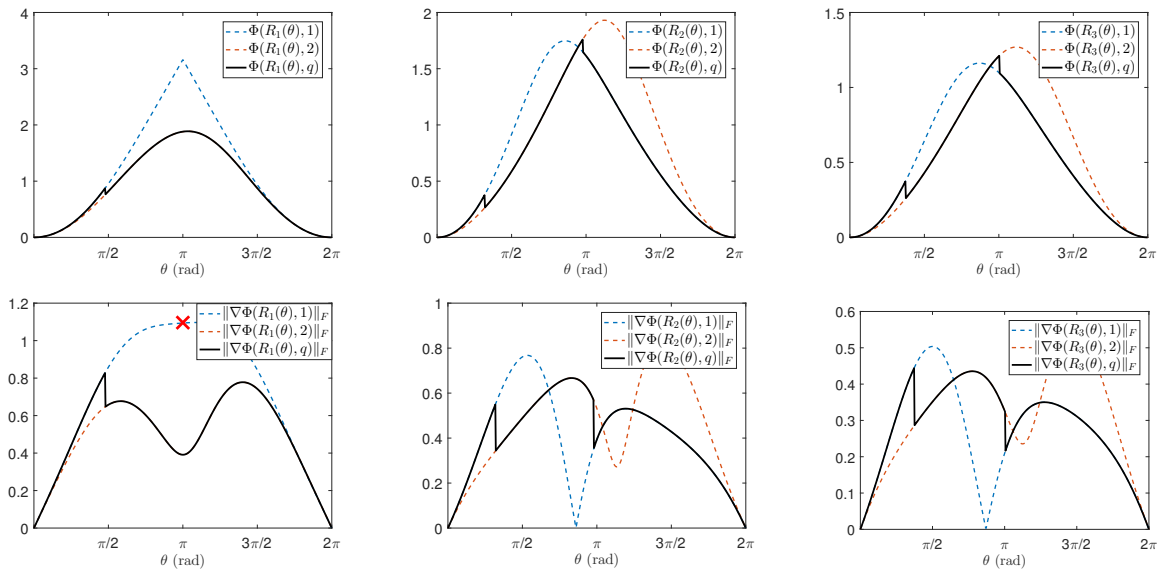


Figure 3.12: Plot of the potential function $\Phi(R, q)$ (first row) and its gradient's norm (second row) along the trajectories $R_i(\theta)$, $i = 1, 2, 3$, which passes through the singular/critical points of $\Phi(R, 1)$.

## 3.4 Attitude Tracking for Rigid Body Systems

### 3.4.1 Problem Formulation

The attitude dynamics of a rigid body are given by

$$\dot{R} = R[\omega]_\times, \tag{3.74}$$

$$I_B\dot{\omega} = [I_B\omega]_\times\omega + u_\tau, \tag{3.75}$$

where $R \in \mathbb{SO}(3)$ denotes a rotation matrix from the body-attached frame $\mathcal{B}$ to the inertial frame $\mathcal{I}$, $\omega \in \mathbb{R}^3$ is the angular velocity of the rigid body expressed in the body-attached frame $\mathcal{B}$, $I_B \in \mathbb{R}^{3\times3}$ is the constant symmetric positive-definite inertia matrix of the rigid body with respect to the body-fixed frame and $u_\tau \in \mathbb{R}^3$ is the input torque expressed in the body-fixed frame.

Assume that a good estimate of $R$ can be obtained from the available measurements. Although no available sensor can provide measurements of the full attitude matrix $R$, body-frame vector measurements of known inertial directions can be used to reconstruct or estimate the attitude. A detailed description and improved solutions for the attitude estimation problem will be addressed in Chapter 4. Also, assume that the angular velocity $\omega$, which can be measured using a gyroscope, is available for feedback. Consider a time-varying reference attitude trajectory $R_d(t) \in \mathbb{SO}(3)$, satisfying

$$\dot{R}_d(t) = R_d(t)[\omega_d(t)]_\times,\ R_d(0) \in \mathbb{SO}(3), \tag{3.76}$$

for some desired angular velocity vector $\omega_d(t) \in \mathbb{R}^3$.

**Assumption 3.4.1** *The desired angular acceleration $\dot{\omega}_d(t)$ is uniformly bounded such that there exists $c_{\dot{\omega}_d} > 0$ and $\|\dot{\omega}_d(t)\| \le c_{\dot{\omega}_d}$ for all $t \ge 0$.*

Note that, under the assumption of bounded $\dot{\omega}_d$, the desired trajectory (3.76) can be generated by the following autonomous differential inclusion

$$\left.\begin{aligned}\dot{R}_d &= R_d[\omega_d]_\times \\ \dot{\omega}_d &\in c_{\dot{\omega}_d}\mathbb{B}\end{aligned}\right\} \qquad (R_d, \omega_d) \in \mathbb{SO}(3) \times \mathbb{R}^3. \tag{3.77}$$

We may also need the following assumption on the boundedness of $\omega_d$.

**Assumption 3.4.2** *The desired angular velocity $\omega_d(t)$ is uniformly bounded such that there exists $c_{\omega_d} >$ and $\|\omega_d(t)\| \le c_{\omega_d}$ for all $t \ge 0$.*

Our objective is to design a control law for the input $u_\tau$ such that global tracking of the reference attitude $R_d(t)$ is achieved. To this end, the synergistic hybrid approach developed in this chapter is adopted. Before this, let us discuss some of the existing smooth attitude control schemes which our hybrid tracking controllers will be developed upon.

### 3.4.2 Smooth Attitude Tracking on $\mathbb{SO}(3)$

Using the $\mathbb{SO}(3)$ group operation, one defines the following "intrinsic" attitude tracking errors

$$\tilde{R} = RR_d^\top, \quad \bar{R} = R_d^\top R. \tag{3.78}$$

The attitude errors $\tilde{R}$ and $\bar{R}$ are often called the left and right attitude errors, respectively. In fact, the left (right) attitude error is invariant under left (right) matrix multiplication in the sense that it preserves the Lie group invariance properties with respect to constant rotations. Both attitude errors can be used as a measure of the error between the actual attitude $R$ and the desired attitude $R_d$. In fact it is easy to check that $\tilde{R} = I$ is equivalent to $\bar{R} = I$ thanks to the fact that $\tilde{R} = R_d\bar{R}R_d^\top$. However, physically speaking the right attitude error $\bar{R}$ is more meaningful than its counterpart $\tilde{R}$. The right attitude error corresponds to the relative orientation generated by the difference of the actual angular velocity and the desired angular velocity expressed in the body-attached frame. This fact has motivated its wide use in attitude control problems, see [Meyer, 1971, Koditschek, 1988, Wen and Kreutz-Delgado, 1991, Egeland and Godhavn, 1994, Sanyal *et al.*, 2009, Lee, 2012, Mayhew and Teel, 2013a]. The left attitude error has appeared less frequently, see for instance [Bullo and Murray, 1999, Forbes, 2013]. As will be discussed later, the use of the left attitude error has several advantages compared to the right attitude error.

The corresponding left and right angular velocity errors can be obtained by differentiating the left and right attitude errors which results in

$$\dot{\tilde{R}} = \tilde{R}[R_d\tilde{\omega}]_\times, \qquad \tilde{\omega} = \omega - \omega_d, \tag{3.79}$$

$$\dot{\bar{R}} = \bar{R}[\bar{\omega}]_\times, \qquad \bar{\omega} = \omega - \bar{R}^\top\omega_d. \tag{3.80}$$

The right angular velocity error $\bar{\omega}$ represents the error between the body-frame angular velocity $\omega$ and the body-frame representation, namely $\bar{R}^\top\omega_d$, of the desired angular velocity $\omega_d$. Therefore both quantities are compared in the same body frame. The

control laws discussed in this thesis have the following structure

$$u_\tau = \text{PD-like feedback} + \text{Feedforward compensation} \tag{3.81}$$

The proportional feedback is a function of the attitude error (left or right) and the derivative feedback is in terms of the corresponding angular velocity error (left or right). The PD action guarantees stability, error tracking and disturbance rejection while the feedforward term is used to enhance the tracking performance by compensating for the system dynamics.

The first smooth control law uses the left (attitude and angular velocity) tracking errors and is given by (see [Bullo and Murray, 1999])

$$u_\tau = -R_d^\top \psi(K_1 \tilde{R}) - K_2 \tilde{\omega} + [\omega_d]_\times I_B \omega + I_B \dot{\omega}_d, \tag{3.82}$$

where $K_2$ is a positive definite matrix and $K_1$ is a symmetric matrix such that $\mathbf{E}(K_1)$ is positive definite. The second control law uses the right tracking errors and is given by (see [Tayebi, 2008, Lee, 2012])

$$u_\tau = -\psi(K_1 \bar{R}) - K_2 \bar{\omega} + [\bar{R}^\top \omega_d]_\times I_B \bar{R}^\top \omega_d + I_B \bar{R}^\top \dot{\omega}_d. \tag{3.83}$$

Both controllers can be shown to guarantee almost global asymptotic tracking and local exponential tracking, see [Bullo and Murray, 1999, Lemma 9]. Interestingly, one can further simplify the feedforward term of the control law (3.82) as demonstrated in the following proposition.

**Proposition 3.4.3** *Consider the desired reference trajectory* (3.76) *under Assumption* (3.4.2)*. Consider the attitude dynamics* (3.74)-(3.75) *under the control law*

$$u_\tau = -R_d^\top \psi(K_1 \tilde{R}) - K_2 \tilde{\omega} + [\omega_d]_\times I_B \omega_d + I_B \dot{\omega}_d, \tag{3.84}$$

*where $K_1$ is a symmetric matrix such that $\mathbf{E}(K_1)$ is positive definite and $K_2$ is a positive definite matrix satisfying*

$$\lambda_{\min}^{K_2} > \lambda_{\max}^{I_B} c_{\omega_d}. \tag{3.85}$$

*Then the equilibrium point $(\tilde{R}, \tilde{\omega}) = (I, 0)$ is exponentially stable from all initial condi-*

*tions such that*

$$\mathbf{tr}(K_1(I - \tilde{R}(0))) + \tilde{\omega}(0) I_B \tilde{\omega}(0) < 4\lambda_{\min}^{\mathbf{E}(K_1)}.$$

**Proof** See Appendix B.6.

The control law (3.84) has a simpler feedforward term compared to the previously proposed control laws (3.82) and (3.82). In fact, the feedforward term $[\omega_d]_\times I_B \omega_d + I_B \dot{\omega}_d$ is state-independent and can be computed offline given the desired trajectory of the rigid body's attitude. This simplification in the control law comes at the cost of a gain condition in (3.85).

### 3.4.3 Hybrid Attitude Tracking on $\mathbb{SO}(3)$

As discussed in Section 3.3.2, smooth stabilization or tracking on $\mathbb{SO}(3)$ can not achieve global results which might lead to performance degradation when considering large manoeuvres. The proportional feedback for the attitude tracking control laws discussed above can be modified and enhanced by including a hybrid dynamical system in the spirit of the hybrid synergistic feedback approach discussed in subsection 3.3.4. In fact the proportional term $\psi(K_1 \tilde{R})$ is related to the gradient of the potential function $\Psi_{1,K_1}(\tilde{R})$ defined in (3.28). The idea of the hybrid tracking algorithm is to take, instead, a proportional term which corresponds to a gradient of an exp-synergistic potential function which changes configuration according to a min-switch strategy.

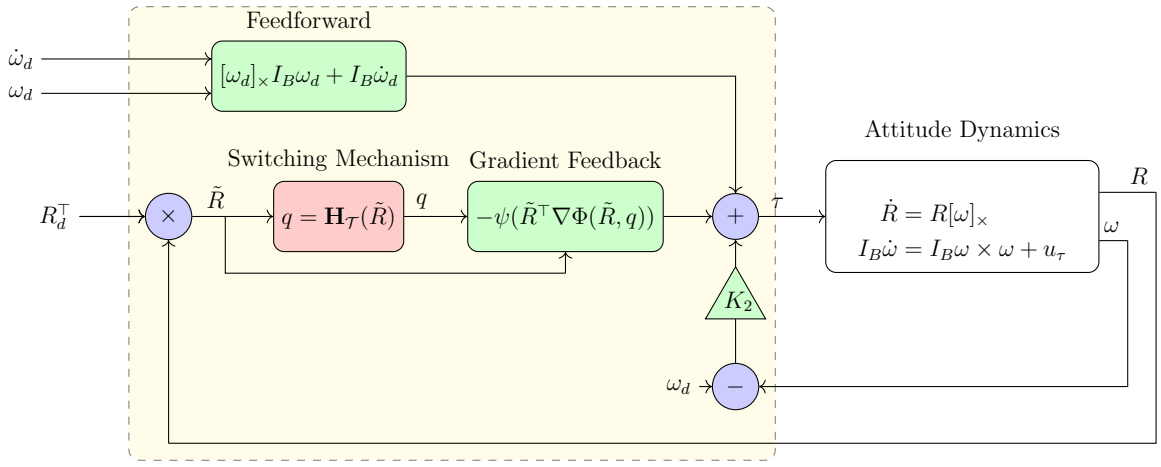


Figure 3.13: Hybrid attitude tracking algorithm using an exp-synergistic potential function $\Phi : \mathbb{SO}(3) \times \mathcal{Q} \to \mathbb{R}_{\geq 0}$.

**Theorem 3.4.4** *Consider a desired reference trajectory generated by* (3.77) *under Assumptions* (3.4.1)-(3.4.2). *Consider the attitude dynamics* (3.74)-(3.75) *under the control law*

$$u_\tau = -R_d^\top \psi(\tilde{R}^\top \nabla\Phi(\tilde{R}, q)) - K_2\tilde{\omega} + [\omega_d]_\times I_B\omega + I_B\dot{\omega}_d, \tag{3.86}$$

*where* $K_2$ *is a positive definite matrix,* $\Phi \in \mathcal{P}_\mathcal{D}$ *with* $\mathcal{D} \subseteq \mathbb{SO}(3) \times \mathcal{Q}$, $\mathcal{Q} \subset \mathbb{N}$, $\delta > 0$ *and* $q = \mathbf{H}_\mathcal{T}(\tilde{R})$ *with* $\mathcal{T} = (\Phi, \mathcal{Q}, \delta)$ *and* $\mathbf{H}_\mathcal{T}(\cdot)$ *defined in* (3.45)-(3.47). *If* $\Phi$ *is exp-synergistic with gap exceeding* $\delta$, *then the set* $\mathcal{A}_2 = \{(\tilde{R}, q, \tilde{\omega}, R_d, \omega_d) : \tilde{R} = I,\ \tilde{\omega} = 0\}$ *is globally exponentially stable.*

**Proof** See Appendix C.4.

In Theorem 3.4.4 a hybrid controller has been derived using the left attitude and angular velocity errors. It has the same structure as the smooth controller (3.84) with the proportional term $\psi(K_1\tilde{R})$ being replaced by $\psi(\tilde{R}^\top \nabla\Phi(\tilde{R}, q))$ $\Phi \in \mathcal{P}_\mathcal{D}$ with $\mathcal{D} \subseteq \mathbb{SO}(3) \times \mathcal{Q}$ is an exp-synergistic potential function with gap exceeding $\delta > 0$ and the index $q$ is the output of the hybrid dynamical system (3.45)-(3.47). Note that the feedforward term $[\omega_d]_\times I_B\omega$ can be replaced by $[\omega_d]_\times I_B\omega_d$ as in (3.84) under the gain condition (3.85) without affecting the nature of the stability result. Also, a similar hybrid controller obtained from the right attitude and angular velocity errors can be derived. It is left to the reader to verify the global exponential stability result.

Note that the proposed hybrid attitude tracking scheme is subject to discontinuous jumps due to the direct switching in the hybrid controller configuration. This might be undesirable from a practical point of view as discontinuities in the torque might excite unmoderated dynamics. To cope with this shortcoming, a dynamic extension is proposed for the originally derived hybrid controllers to smooth out the proportional term (which contains discontinuous jumps) and allows to obtain a continuous control input guaranteeing the same exponential tracking results.

**Theorem 3.4.5** *Consider a desired reference trajectory generated by* (3.77) *under Assumptions* (3.4.1)-(3.4.2). *Consider the attitude dynamics* (3.74)-(3.75) *under the control law*

$$u_\tau = -R_d^\top x - K_2\tilde{\omega} + [\omega_d]_\times I_B\omega + I_B\dot{\omega}_d, \tag{3.87}$$

$$\dot{x} = -K_3(x - \psi(\tilde{R}^\top \nabla\Phi(\tilde{R}, q))), \quad x(0) \in c_x\mathbb{B}, \tag{3.88}$$

*where* $K_2, K_3$ *are positive definite matrices,* $\Phi \in \mathcal{P}_\mathcal{D}$ *with* $\mathcal{D} \subseteq \mathbb{SO}(3) \times \mathcal{Q}$, $\mathcal{Q} \subset \mathbb{N}$, $c_x > 0$ *and* $q = \mathbf{H}_\mathcal{T}(\tilde{R})$ *with* $\mathcal{T} = (\Phi, \mathcal{Q}, \delta)$, $\delta > 0$ *and* $\mathbf{H}_\mathcal{T}(\cdot)$ *defined in* (3.45)-(3.47). *If* $\Phi$ *is*

*exp-synergistic with gap exceeding $\delta$, then there exists a positive constant $k_3$ such that for $K_3 > k_3 I > 0$, the set $\mathcal{A}_3 := \{(\tilde{R}, q, \tilde{\omega}, \tilde{x}, R_d, \omega_d) : \tilde{R} = I, \tilde{\omega} = 0, \tilde{x} = 0\}$ is globally exponentially stable, where $\tilde{x} = x - \psi(\tilde{R}^\top \nabla\Phi(\tilde{R}, q))$.*

**Proof** See Appendix C.5.

The integral action on the hybrid term $\psi(\tilde{R}^\top \nabla\Phi(\tilde{R}, q))$ in (3.88) moves the discontinuity (jump) one integrator away from the control input $u_\tau$. Therefore, the output of the hybrid controller (3.87)-(3.88) is made continuous without sacrificing the global exponential stability.

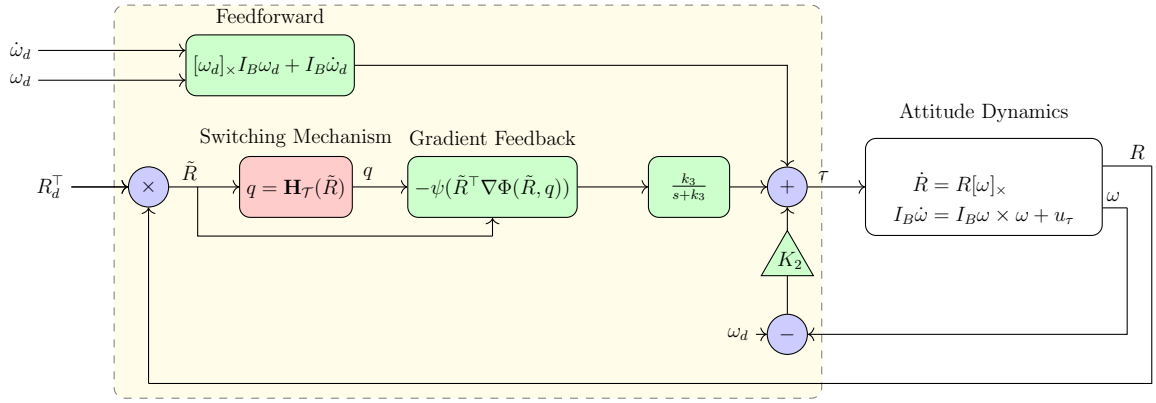


Figure 3.14: Smoothed hybrid attitude tracking algorithm using an exp-synergistic potential function $\Phi : \mathbb{SO}(3) \times \mathcal{Q} \to \mathbb{R}_{\geq 0}$.

### 3.4.4 Simulations

In this section, some simulation results are provided to show the performance of the proposed attitude tracking control schemes. The moment of inertia of the rigid body considered in this simulation around the roll, pitch and yaw axes is given by

$$I_B = \begin{bmatrix} 1.59 & 0 & 0 \\ 0 & 1.50 & 0 \\ 0 & 0 & 2.97 \end{bmatrix} \times 10^{-2} \ (\text{Kg.m}^2) \tag{3.89}$$

The desired attitude trajectory being set for the simulation tests is generated from (3.76). The desired angular acceleration is

$$\dot{\omega}_d(t) = \begin{bmatrix} 0.03\sin(0.1t + 7\pi/12) \\ 0.03\sin(0.3t + \pi/2) \\ 0.05\sin(0.1t + \pi/2) \end{bmatrix} \ (\text{rad/sec}^2), \tag{3.90}$$

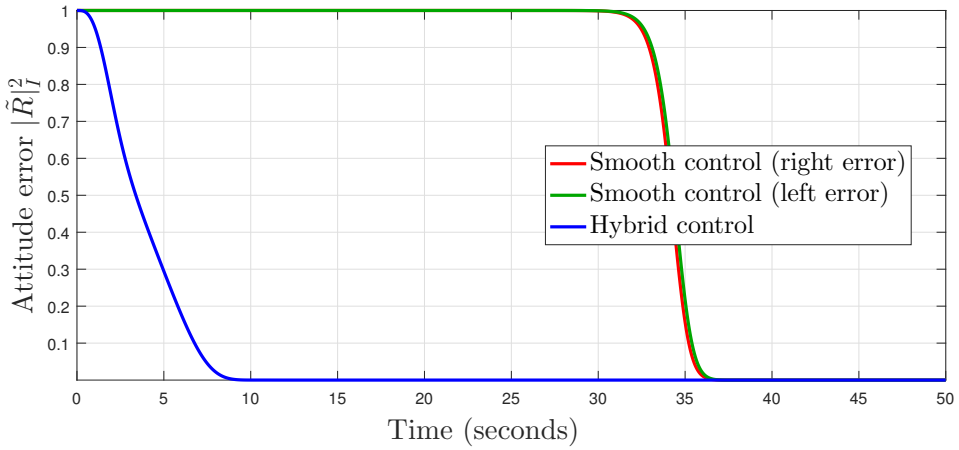


Figure 3.15: Total attitude tracking error (Euclidean distance) versus time.

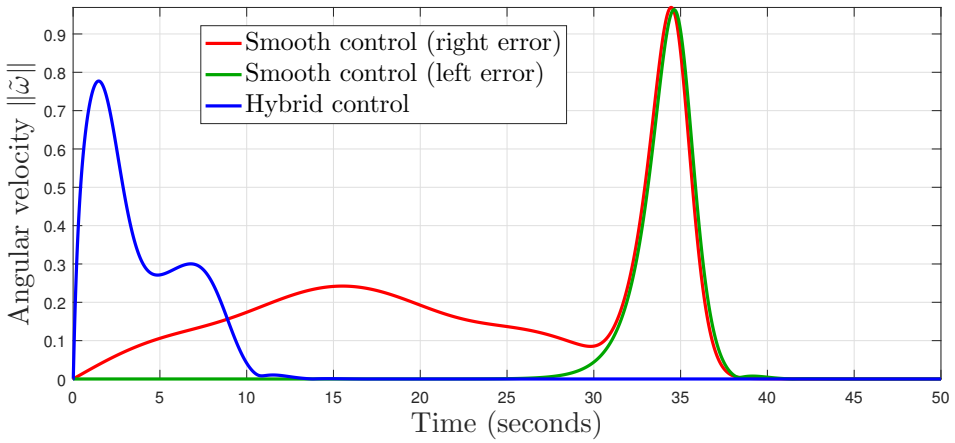


Figure 3.16: Norm of the angular velocity tracking error versus time.

and the initial desired angular rates and attitude matrix are $\omega_d(0) = [0,0,0]^\top$ (rad/sec) and $R_d(0) = I$, respectively. In the first simulation scenario, the initial conditions $\omega(0) = [0,0,0]^\top$ (rad/sec) and $R(0) = \mathbf{R}_a(\pi, [0.6, 0.8, 0]^\top)$ are considered. The gains are set as $K_1 = K_2 = 5 \times 10^{-2} I$ for all controllers. Note that locally, all controllers (smooth or hybrid, left or right error) are identical. Particularly, both the smooth control (right error) which corresponds to the controller (3.83) and the smooth control (left error) which corresponds to controller (3.84) are implemented. The hybrid control law (3.86) is implemented using the non-weighted exp-synergistic potential function $\Psi_1 \circ \Gamma$ with parameters $k = 0.64$ and $\delta = 0.064$ as in Proposition 3.3.10. In the second simulation

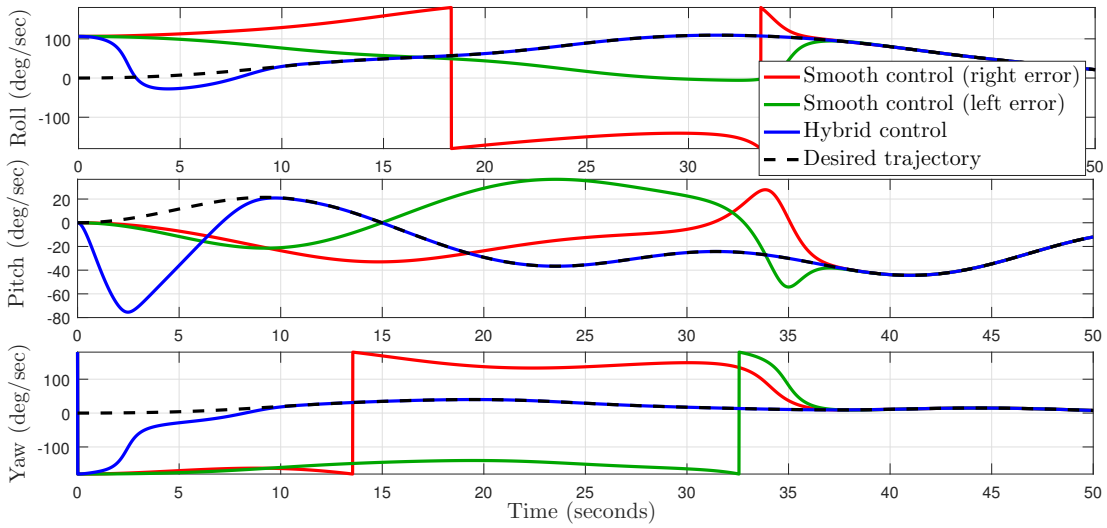


Figure 3.17: True Euler angles (colored) and desired Euler angles (dashed) versus time.

scenario, the performance of the smoothed hybrid controller (3.87)-(3.88) is compared to the raw hybrid controller (3.86). Consider the initial states as follows $\omega(0) = [-5, -2, 3]^\top$ (rad/sec) and $R(0) = \mathbf{R}_a(\pi, [0, 1, 0]^\top)$. The control gain $K_3$ in (3.87)-(3.88) is chosen as $K_3 = 10I$ while the remaining parameters of the hybrid switching mechanism $(\Phi, \mathcal{Q}, \delta)$ are chosen as in the previous scenario.

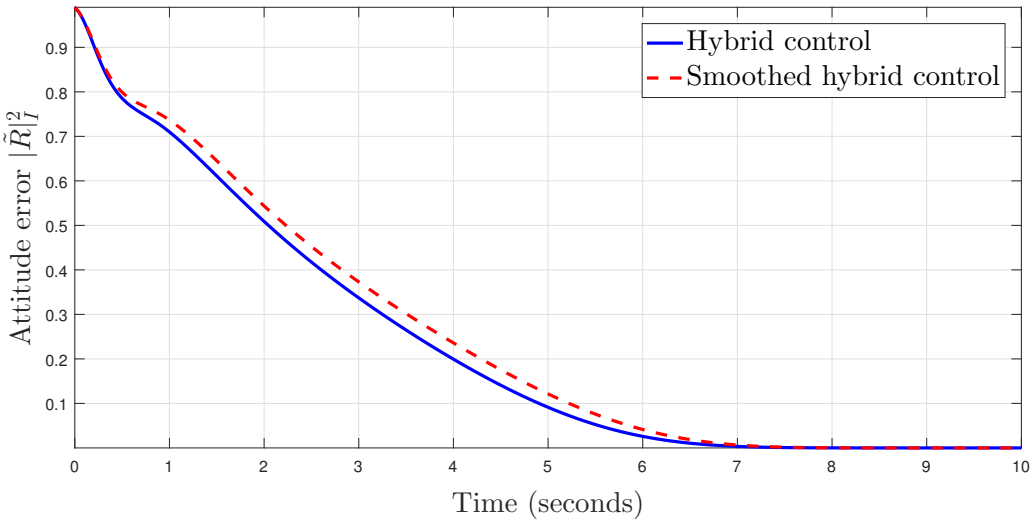


Figure 3.18: Total attitude tracking error (Euclidean distance) versus time.

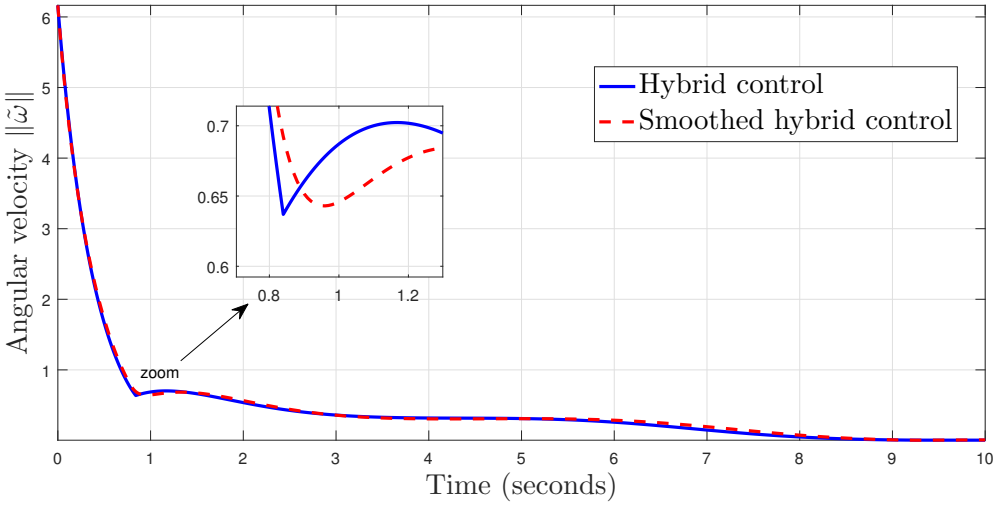


Figure 3.19: Norm of the angular velocity tracking error versus time.

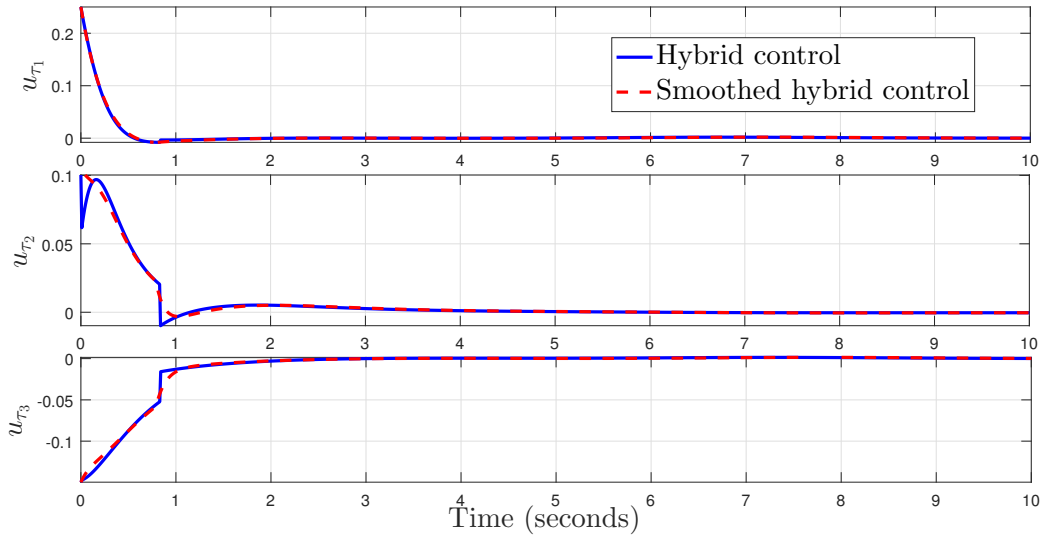


Figure 3.20: Torque components versus time.

## 3.5 Conclusion

In this chapter, the use of hybrid techniques has been investigated to solve the long standing problem of global exponential stabilization on the Special Orthogonal group of rotations $\mathbb{SO}(3)$. The notion of exp-synergism for a family of differentiable or non-differentiable potential functions on $\mathbb{SO}(3)$ has been introduced. When a given family of potential functions on $\mathbb{SO}(3)$ is exp-synergistic, one can employ a min-switch strategy that selects the controller designed from the minimal potential function. The exp-synergism property guarantees that all the undesired critical or singular points of the family of

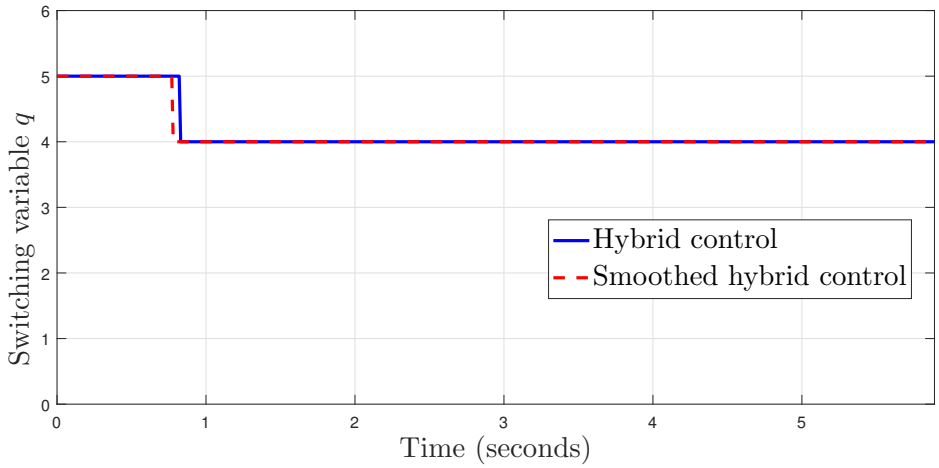


Figure 3.21: Switching variable versus time. Note that the initial value is $q(0,0) = 2$. The hybrid controller immediately switches to the configuration $q = 5$ at the start.

potential functions must lie in the jump set of the hybrid controller. A rigorous Lyapunov analysis for hybrid systems is used to show global exponential stability of the closed-loop systems under investigation. Moreover, an insightful construction of exp-synergistic potential functions, derived from already known individual weighted and non-weighted potential functions on $\mathbb{SO}(3)$, is proposed. The proposed hybrid stabilization approach has been applied to the attitude tracking problem for rigid body systems and yields improved tracking performance compared to non-hybrid attitude tracking algorithms.

# Chapter 4

# Hybrid Attitude Estimation on $\mathbb{SO}(3)$

## 4.1 Introduction

In this chapter, two different observer design problems related to the attitude estimation on $\mathbb{SO}(3)$ are formulated. The first problem, similar to [Mahony *et al.*, 2008], considers the attitude estimation using a set of $n \geq 2$ body-frame vector measurements of known constant inertial vectors alongside biased gyro measurements. Our objective is to incorporate hybrid switching mechanisms to enlarge the domain of exponential stability of the traditional nonlinear complementary filter on $\mathbb{SO}(3)$ [Mahony *et al.*, 2008, Grip *et al.*, 2012a]. Two approaches are proposed: a synergistic-based approach and a reset-based approach. In the synergistic-based approach, exp-synergistic potential functions from Chapter 3 are used to design a set of innovation terms for the passive nonlinear complementary filter [Mahony *et al.*, 2008]. A hysteresis switching between these innovation terms allows to keep the estimation error inside the region of exponential stability. The second approach relies on resetting the attitude state to a different value (selected from a set of adequately chosen rotation matrices) whenever the attitude error is close to leave the domain of exponential stability. This condition is detected by comparing the value of a cost function at the current rotation and at the rotation after a potential jump has occurred. Both estimation approaches are shown to guarantee global exponential stability, are expressed directly using vector measurements and provide improved performance compared to the state of the art attitude estimators on $\mathbb{SO}(3)$. These results appeared in our work [Berkane *et al.*, 2017a, Berkane and Tayebi, 2017b].

The second problem that is addressed in this chapter is the attitude estimation on $\mathbb{SO}(3)$ using intermittent vector measurements where the body frame vector measurements are considered arriving at possibly different instants of time with possible packets loss. This problem is mainly motivated by applications where multiple sensors (GPS,

landmarks, vision sensors, IMU) are centrally fused to estimate the attitude of a rigid body. Measurement-triggered state observers on $\mathbb{SO}(3)$ are proposed to solve the problem in the case where the measurements are synchronous and asynchronous. A hybrid systems framework is proposed to model and capture the dynamics of the event-triggered behaviour of the closed-loop systems. Almost global exponential stability and almost global asymptotic stability is shown for the synchronous observer and asynchronous observer, respectively. The results of this part have been published in [Berkane and Tayebi, 2017c, Berkane and Tayebi, 2017d].

## 4.2 Attitude Estimation Using Continuous Vector Measurements

In this section, the problem of attitude and gyro bias estimation from continuous body-frame vector measurements and biased angular velocity readings is considered. This problem has been tackled recently using nonlinear observer design on $\mathbb{SO}(3)$ see, for instance, [Mahony *et al.*, 2008, Grip *et al.*, 2012b, Izadi and Sanyal, 2014, Zlotnik and Forbes, 2017] . In this work, hybrid nonlinear observers on $\mathbb{SO}(3)$ are proposed to solve this problem with global exponential stability results; a result that has not been achieved in previous works.

### 4.2.1 Problem Formulation

Let $R \in \mathbb{SO}(3)$ denote a rotation matrix from the body-attached frame $\mathcal{B}$ to the inertial frame $\mathcal{I}$. The rotation matrix $R$ evolves according to the kinematics equation

$$\dot{R} = R[\omega]_\times, \tag{4.1}$$

where $\omega \in \mathbb{R}^3$ is the angular velocity of the body-attached frame $\mathcal{B}$ with respect to the inertial frame $\mathcal{I}$ expressed in the body-attached frame $\mathcal{B}$. Assume that the angular velocity $\omega(t)$ is uniformly bounded and a continuous biased measurement of $\omega(t)$, denoted by $\omega_y$, is available such that

$$\omega_y = \omega + b_\omega. \tag{4.2}$$

where $b_\omega \in \mathbb{R}^3$ represents a constant or slowly varying bias. Also, suppose that a set of $n \geq 2$ sensors measuring direction vectors, denoted by $b_i$, $i = 1, \ldots, n$ in the body-attached frame which are associated to a set of $n$ known (possibly time-varying) inertial

vectors, denoted by $a_i$, $i = 1, \ldots, n$, such that

$$b_i = R^\top a_i. \tag{4.3}$$

As in most attitude estimation problems, one needs to impose an observability condition which requires that, at each instant of time, at least two inertial vectors are non-collinear. This is formally stated as follows.

**Assumption 4.2.1** *For any $t \geq 0$, there exist $i, j \in \{1, \cdots, n\}$ such that the inertial vectors $a_i(t)$ and $a_j(t)$ are non-collinear.*

The body-frame vectors $b_i$ can be obtained, for example, from an IMU that typically includes an accelerometer and a magnetometer measuring, respectively, the gravitational field and Earth's magnetic field expressed in the body-attached frame. Moreover, the following realistic assumptions are needed.

**Assumption 4.2.2** *There exists constants $c_\omega, c_{\dot\omega}, c_b > 0$ such that $\|\omega(t)\| \leq c_\omega$, $\|\dot\omega(t)\| \leq c_{\dot\omega}$ for all $t \geq 0$ and $\|b_\omega\| \leq c_b$.*

Our objective consists in designing an algorithm that provides attitude estimates on $\mathbb{SO}(3)$ while estimating the gyro-bias vector, using the above described available measurements, leading to global exponential stability results.

The available state-of-the-art attitude observer that solves a similar problem is the *explicit complementary filter* (ECF) proposed in [Mahony *et al.*, 2008]. The ECF takes the following form:

$$\dot{\hat R} = \hat R \left[\omega_y - \hat b_\omega + k_1 \hat{\mathbf{w}}\right]_\times, \tag{4.4}$$

$$\dot{\hat b}_\omega = -k_2 \hat{\mathbf{w}}, \tag{4.5}$$

$$\hat{\mathbf{w}} = \frac{1}{4}\sum_{i=1}^{n} \rho_i (b_i \times \hat R^\top a_i), \tag{4.6}$$

where $\hat R(0) \in \mathbb{SO}(3)$ and $\hat b_\omega(0) \in \mathbb{R}^3$ are the initial conditions of the attitude estimate $\hat R$ and the gyro bias estimate $\hat b_\omega$, respectively. The gains $k_1, k_2, \rho_1, \cdots, \rho_n$ are chosen strictly positive. The structure of the ECF is very intuitive. The attitude estimate is propagated using a forward integration of the biased angular velocity plus and innovation term. The innovation term has a proportional-integral structure where the error vector $\hat{\mathbf{w}}$ is constructed by weighting and summing the "cross product vector errors" between the measured direction vectors $b_i = R^\top a_i$ and their corresponding estimates $\hat R^\top a_i$.

Note that the vector error is not taken as $b_i - \hat{R}^\top a_i$ which is the traditional error in an Euclidean space. Instead the cross product $b_i \times \hat{R}^\top a_i$ is used which is more intrinsic to the rotation group $\mathbb{SO}(3)$. The use of this type of correction allows to derive strong stability results (almost global asymptotic stability and local exponential stability) for this filter. The intuitive fact that the cross product error $b_i \times \hat{R}^\top a_i$ vanishes when $b_i$ and $\hat{R}^\top a_i$ are parallel (0° and 180°) leads to the appearance of undesired equilibria when the attitude estimation error has an angle of 180°.

### 4.2.2 Synergistic-Based Approach

In this subsection, a hybrid approach for the design of globally exponentially stable attitude observers on $\mathbb{SO}(3)$ is developed based on the synergistic approach proposed in Chapter 3. First, a hybrid attitude and gyro-bias observer relying on a generic indexed potential function on $\mathbb{SO}(3) \times \mathcal{Q}$, where $\mathcal{Q} \subset \mathbb{N}$ is a finite index set, satisfying the exp-synergism property is proposed. Global exponential stability of the estimation errors is shown. By picking some suitable exp-synergistic potential functions developed in the previous chapter, the resulting hybrid observer is explicitly formulated using the available vector measurements.

Let $\hat{R}$ and $\hat{b}_\omega$ denote, respectively, the estimate of the rigid body rotation matrix $R$ and the estimate of the constant bias vector $b_\omega$. Also, define $\tilde{R} = R\hat{R}^\top$ and $\tilde{b}_\omega = b_\omega - \hat{b}_\omega$ as the attitude and gyro bias estimation errors, respectively. Consider a potential function $\Phi \in \mathcal{P}_\mathcal{D}$, for some $\mathcal{D} \subseteq \mathbb{SO}(3) \times \mathcal{Q}$, such that $\mathcal{Q} \subset \mathbb{N}$ is a set of discrete indices and $\delta > 0$. Let $\mathcal{T} = (\Phi, \mathcal{Q}, \delta)$ and consider the following hybrid attitude and gyro-bias estimation scheme:

$$\dot{\hat{R}} = \hat{R}\left[\omega_y - \hat{b}_\omega + K_1 \hat{R}^\top \mathbf{w}(\tilde{R}, q)\right]_\times, \tag{4.7}$$

$$\dot{\hat{b}}_\omega = -k_2 \hat{R}^\top \mathbf{w}(\tilde{R}, q), \tag{4.8}$$

$$\mathbf{w}(\tilde{R}, q) = \psi\big(\tilde{R}^\top \nabla\Phi(\tilde{R}, q)\big) \tag{4.9}$$

where the *current* configuration of the observer is dictated by the switching variable $q \in \mathcal{Q}$ which is the output of the hybrid dynamical system

$$q = \mathbf{H}_\mathcal{T}(\tilde{R}) \tag{4.10}$$

where $\mathbf{H}_\mathcal{T}$ is as defined in (3.45). The matrix gain $K_1$ and the scalar gain $k_2$ are both positive definite. The above nonlinear observer is a copy of (4.1) plus an innovation

(correction) term. The constant bias is compensated by means of an integral feedback. The current configuration of the hybrid observer, dictated by the switching variable $q \in \mathcal{Q}$, remains constant during the flows of $\mathbf{H}_{\mathcal{T}}$. Only the variable $q \in \mathcal{Q}$ changes values during the jumps of the hybrid observer leading to a change in the observer correction term. The observer states $\hat{R}$ and $\hat{b}_\omega$ are kept unchanged which results in a hybrid estimation scheme with continuous estimation output. According to (3.46)-(3.47), the observer flows (evolves according to the continuous dynamics (4.7)-(4.9)) as long as the difference between the current value of the potential function $\Phi(\tilde{R}, q)$ and the minimum value across all values of $q \in \mathcal{Q}$ does not exceed certain threshold $\delta > 0$. The jump of the observer is triggered when the difference between the current value of the potential function $\Phi(\tilde{R}, q)$ and the minimum value across all values of $q \in \mathcal{Q}$ exceeds the threshold $\delta > 0$.

The initial state variables of the observer are selected as $\hat{R}(0,0) \in \mathbb{SO}(3)$, $\hat{b}_\omega(0,0) \in \mathbb{R}^3$. Consequently, one can verify from (4.7) that $\hat{R}$ is naturally confined to lie on $\mathbb{SO}(3)$ for all hybrid times $(t, j) \succeq (0, 0)$. It should be noted that the above proposed hybrid estimation scheme depends on the attitude estimation error $\tilde{R}$ which is not available. Later in this subsection, we will address the design of the potential function $\Phi(\tilde{R}, q)$ with the corresponding index set $\mathcal{Q}$ and hysteresis gap $\delta$ and, accordingly, show how to express the above hybrid observer in terms of the available inertial vectors $(a_i)_{1 \leq i \leq n}$ and their corresponding body-frame measurements $(b_i)_{1 \leq i \leq n}$.

Also, note that although the hybrid attitude observer proposed above exhibits jump transitions, the discrete jumps are hidden by the integration process since only the correction term is being subject to jumps and not the states (attitude and gyro bias) of the observer. This is desirable in practice since the discrete transitions in the attitude estimates may excite undesirable and unmodelled dynamics when used in a control input. To analyze the convergence properties of the proposed hybrid observer, the closed-loop system is written as an autonomous hybrid system with state $X = (\tilde{R}, q, \tilde{b}_\omega, \hat{R}, \omega) \in \mathbb{SO}(3) \times \mathcal{Q} \times \mathbb{R}^3 \times \mathbb{SO}(3) \times \mathbb{R}^3$ and data given by (C.51)-(C.54). The objective is to establish global exponential stability of the closed set $\mathcal{A}$ defined by

$$\mathcal{A} = \{(\tilde{R}, q, \tilde{b}_\omega, \hat{R}, \omega) : \tilde{R} = I, \tilde{b}_\omega = 0\}$$

**Theorem 4.2.3** *Consider the attitude kinematics* (4.1) *coupled with the hybrid observer* (4.7)-(4.10) *where Assumptions 4.2.1-4.2.2 are satisfied. If the potential function* $\Phi$ *is exp-synergistic with gap exceeding* $\delta$ *then the number of discrete jumps is finite and the*

*set $\mathcal{A}$ is globally exponentially stable.*

**Proof** See Appendix C.6.

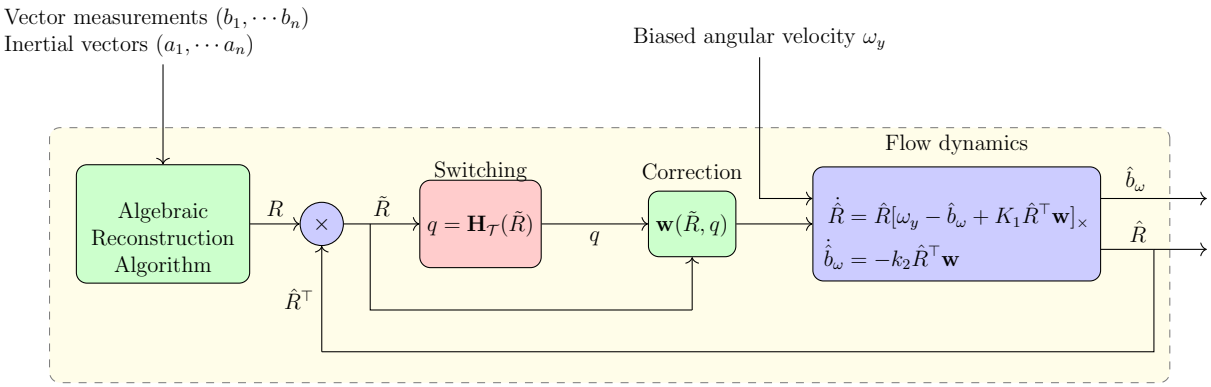


Figure 4.1: Schematic of the synergistic-based hybrid attitude and gyro bias observer using algebraic attitude reconstruction. This estimation scheme can be implemented using any exp-synergistic potential function $\Phi$.

Note that, according to the result of Theorem 4.2.3, the hybrid attitude estimation algorithm (4.7)-(4.9) can be implemented by picking any exp-synergistic potential function. Example of such choices are the exp-synergistic potential functions designed in Proposition (3.3.10) and Proposition 3.3.16. However, since the attitude error $\tilde{R} = R\hat{R}^\top$ is not available to the attitude estimation algorithm, one needs to express the proposed estimation scheme in terms of vector measurements $(b_i)_{1 \leq i \leq n}$. An intuitive remedy is to first use a static reconstruction algorithm (such as SVD or TRIAD) to recover a noisy attitude $R_y$ from the inertial vector measurements and then feed this reconstructed attitude to the hybrid algorithm (4.7)-(4.9) as if $R_y$ corresponds to the true attitude matrix. This results in the estimation scheme depicted in Figure 4.1. Note that in using the reconstruction algorithm, there is no restriction on the inertial vectors $a_1, \cdots, a_n$ to be constant as long as they are known.

**Formulation in the case of constant inertial vectors $(a_i)_{1 \leq i \leq n}$**

The reconstruction algorithm is computationally expensive to execute at each iteration of the estimation algorithm and might introduce another type of noise which would degrade the performance of the algorithm. To avoid these problems and complications introduced by the algebraic reconstruction algorithm, an explicit formulation of the attitude observer using body-frame measurements of known constant inertial vectors is proposed as follows.

Take the matrix $A = \sum_{i=1}^{n} \rho_i a_i a_i^\top$ where $\rho_i > 0, i = 1, \cdots, n$. This ensures that $A$ is positive definite provided that at least 3 inertial vectors, say $a_1, a_2$ and $a_3$, are non-collinear. In the case where only two non-collinear vectors $a_1$ and $a_2$ are available, it is always possible to consider a third vector $a_3 = a_1 \times a_2$, corresponding to the body-frame measurement $b_3 = b_1 \times b_2$. Moreover, there exist positive scalars $\rho_i$ such that $A$ has distinct eigenvalues. In this case, one can construct the potential function $\Phi \equiv \Psi_{1,A} \circ \Gamma$ where $\Psi_{1,A}$ and $\Gamma$ are defined in (3.28) and (3.63). Select the corresponding parameters such as in Proposition (3.3.16) to ensure that $\Phi$ is exp-synergisitic with gap exceeding $\bar{\delta}_1$ given in Proposition (3.3.16). Interstingly, this potential function as well as its gradient can be computed directly using the vector measurements without the need for the attitude matrix $R$. Using Lemma 2.2.7 and the definition of $\Gamma$ in (3.63), one can show that the potential function $\Phi(\tilde{R}, q) = \Psi_{1,A} \circ \Gamma(\tilde{R}, q)$ is expressed using vector measurements as follows:

$$\hat{\Phi}((a_i, b_i)_{1 \leq i \leq n}, \hat{R}, q) = \frac{1}{4} \sum_{i=1}^{n} \rho_i \|b_i - \hat{b}_i^q\|^2, \tag{4.11}$$

where $\hat{\Phi}((a_i, b_i)_{1 \leq i \leq n}, \hat{R}, q) \equiv \Phi(\tilde{R}, q)$, $\hat{b}_i^q = \hat{R}^\top \mathbf{R}_a(2 \arcsin(k\bar{\Psi}), u_q) a_i$ and $\bar{\Psi} = \frac{1}{2} \sum_{i=1}^{n} \rho_i \|b_i - \hat{R}^\top a_i\|^2$. Using this explicit formulation of the potential function $\Phi(\tilde{R}, q)$, the hybrid switching mechanism $\mathbf{H}_\mathcal{T}$ defined in (3.48) can be implemented directly using vector measurements by replacing $\Phi(\tilde{R}, q)$ with $\hat{\Phi}(a_1, \cdots, a_n, b_1, \cdots, b_n, \hat{R}, q)$. Let us denote by $\hat{\mathbf{H}}_\mathcal{T}$ the explicit implementation of the hybrid dynamical system $\mathbf{H}_\mathcal{T}$ so that

$$q = \hat{\mathbf{H}}_\mathcal{T}((a_i, b_i)_{1 \leq i \leq n}, \hat{R}). \tag{4.12}$$

Moreover, in view of (3.69)-(3.70) and using again the result of Lemma 2.2.7 the gradient of $\Phi$ can also be formulated using vector measurements as follows

$$\hat{\mathbf{w}}((a_i, b_i)_{1 \leq i \leq n}, \hat{R}, q) = \frac{1}{4} \bar{\Theta}^\top \sum_{i=1}^{n} \rho_i (b_i \times \hat{b}_i^q), \tag{4.13}$$

where $\hat{\mathbf{w}}((a_i, b_i)_{1 \leq i \leq n}, \hat{R}, q) \equiv \hat{R}^\top \mathbf{w}(\tilde{R}, q)$ and $\bar{\Theta} = I + 2k[1 - (k\bar{\Psi})^2]^{\frac{1}{2}} \hat{R}^\top u_q \sum_{i=1}^{n} \rho_i (b_i \times \hat{R}^\top a_i)^\top$. To sum up, the proposed hybrid observer can be implemented according to Algorithm 1. It should be mentioned that another hybrid observer can be derived when considering the potential function $\Phi = \Psi_{2,A} \circ \Gamma$ instead, where $\Psi_{2,A}$ is defined in (3.60).

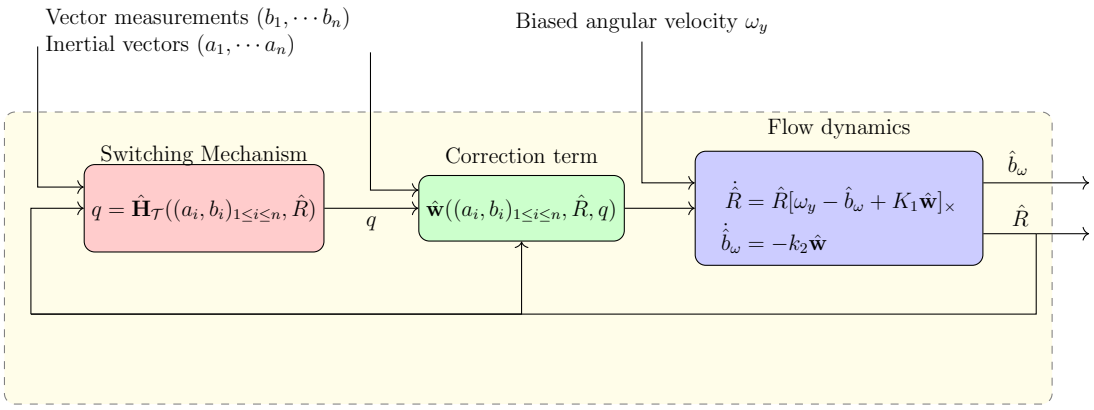


Figure 4.2: Schematic of the synergistic-based hybrid attitude and gyro bias observer using directly vector measurements (without the need to algebraically reconstruct the attitude).

**Algorithm 1** Synergistic-based observer using constant inertial vectors

Pick $A = \sum_{i=1}^{n} \rho_i a_i a_i^\top$ where $\rho_i > 0, i = 1, \cdots, n$.
Choose a scalar $k$ to satisfy (3.64), a unit vector $u$ as in Proposition 3.3.15 and $\mathcal{Q} = \{1, 2\}$.
Initialize the observer states $\hat{R}(0,0) \in \mathbb{SO}(3)$, $\hat{b}_\omega(0,0) \in \mathbb{R}^3$ and $q(0,0) \in \mathcal{Q}$ and pick the observer gains $K_1$ and $k_2$ to obtain the desirable performance.

1: **for** each set of measurements $(b_i)_{1\leq i\leq n}$ **do**
2: Calculate $\Phi(\tilde{R}, q)$ and $\min_{p\in\mathcal{Q}} \Phi(\tilde{R}, p)$ using (4.11).
3: **while** $(\tilde{R}, q) \in \mathcal{J}_{\mathcal{T}}$ **do**
4: Update $q = \arg\min_{p\in\mathcal{Q}} \Phi(\tilde{R}, p)$.
5: **end while**
6: Calculate the correction term $\mathbf{w}(\tilde{R}, q)$ using (4.13).
7: Update the states $\hat{R}$ and $\hat{b}_\omega$ according to (4.7)-(4.8).
8: **end for**

### 4.2.3 Reset-Based Approach

The synergistic-based approach for the design of hybrid observers discussed in the previous section is inspired from the hybrid control approach proposed in Chapter 3. In this section, an alternative hybrid approach for the design of attitude observers is proposed by allowing the estimation state to be *reset* to a certain value whenever it leaves the flow set and enters the jump set.

Consider a potential function $\Phi \in \mathcal{P}_{\mathcal{D}_\Phi}$ with $\mathcal{D}_\Phi \subseteq \mathbb{SO}(3)$ and $\Xi : \mathbb{SO}(3)\times\mathbb{R}_{\geq 0} \to \mathbb{R}_{\geq 0}$ a possibly time-varying potential function continuous and differentiable on the set $\mathcal{D}_\Xi \times \mathbb{R}_{\geq 0}$ where $\mathcal{D}_\Xi \subseteq \mathbb{SO}(3)$. Consider the following hybrid attitude and gyro-bias estimation

scheme

$$\begin{cases} \dot{\hat{R}} = \hat{R}\left[\omega_y - \hat{b}_\omega + k_1 \hat{R}^\top \mathbf{w}(t,\tilde{R})\right]_\times \\ \dot{\hat{b}}_\omega = \mathbf{P}_{c_b}(\hat{b}_\omega, -k_2 \hat{R}^\top \mathbf{w}(t,\tilde{R})) \\ \mathbf{w}(t,\tilde{R}) = \psi\big(\tilde{R}^\top \nabla \Xi(t,\tilde{R})\big) \end{cases} \qquad \tilde{R} \in \hat{\mathcal{F}}, \tag{4.14}$$

$$\begin{cases} \hat{R}^+ = \mathbf{R}_a(\theta, u_q)^\top \hat{R} \\ \hat{b}_\omega^+ = \hat{b}_\omega \end{cases} \qquad \tilde{R} \in \hat{\mathcal{J}}, \tag{4.15}$$

where $k_1, k_2, c_b > 0$, $q \in \arg\min_{p\in\mathcal{Q}} \Phi(\tilde{R}\mathbf{R}_a(\theta, u_p))$, $\mathcal{Q} \subset \mathbb{N}$, $\{u_p\}_{q\in\mathcal{Q}}$ is a set of real unit vectors in $\mathbb{S}^2$ and $\mathbf{P}_{c_b}(\cdot,\cdot)$ is the parameter projection function defined in (2.3). The flow and jump sets are defined, for some $\delta > 0$, as

$$\hat{\mathcal{F}} = \{\tilde{R} \in \mathbb{SO}(3) : \Phi(\tilde{R}) - \min_{p\in\mathcal{Q}} \Phi(\tilde{R}\mathbf{R}_a(\theta, u_p)) \leq \delta\}, \tag{4.16}$$

$$\hat{\mathcal{J}} = \{\tilde{R} \in \mathbb{SO}(3) : \Phi(\tilde{R}) - \min_{p\in\mathcal{Q}} \Phi(\tilde{R}\mathbf{R}_a(\theta, u_p)) \geq \delta\}. \tag{4.17}$$

The design of the reset-based hybrid observer (4.14)-(4.17) is somehow simpler thanks to the fact that only one single potential function $\Phi(\tilde{R})$ is being employed compared to a family of potential functions $\{\Phi(\tilde{R}, q)\}_{q\in\mathcal{Q}}$ used in the design of the synergistic-based hybrid observer (4.7)-(4.10). This comes at the cost of a discrete transition of the attitude state $\hat{R}$ in (4.15). To analyze the convergence properties of the proposed hybrid observer, the closed-loop system is written as an autonomous hybrid system with state $X = (\tilde{R}, \tilde{b}_\omega, \hat{R}, \hat{b}_\omega, \omega, t) \in \mathbb{SO}(3) \times \mathbb{R}^3 \times \mathbb{SO}(3) \times \mathbb{R}^3 \times \mathbb{R}^3 \times \mathbb{R}_{\geq 0}$ and data given by (C.62)-(C.65). The objective is to establish global exponential stability of the closed set $\mathcal{A}$ defined by

$$\mathcal{A} = \{(\tilde{R}, \tilde{b}_\omega, \hat{R}, \hat{b}_\omega, \omega, t) : \tilde{R} = I, \tilde{b}_\omega = 0\}$$

Note that the set $\mathcal{A}$ is only closed (non-compact) due to the presence of the time variable $t$ that grows unbounded. The following theorem gives sufficient conditions for the global exponentially stability of the set $\mathcal{A}$.

**Theorem 4.2.4** *Consider the attitude kinematics* (4.1) *coupled with the hybrid observer* (4.14)-(4.17) *where Assumptions 4.2.1-4.2.2 are satisfied. If the potential functions* $\Phi, \Xi$*, and the corresponding parameters of the hybrid observer* $\theta, \delta$ *and* $\{u_q\}_{q\in\mathcal{Q}}$*, satisfy the following properties:*

*i)* $\exists \alpha_1, \alpha_2 > 0$ *such that* $\alpha_1 |\tilde{R}|_I^2 \leq \Phi(\tilde{R}) \leq \alpha_2 |\tilde{R}|_I^2$ *for all* $\tilde{R} \in \mathbb{SO}(3)$*,*

*ii)* $\exists \alpha_3, \alpha_4 > 0$ *such that* $\alpha_3 |\tilde{R}|_I^2 \leq \langle\langle \nabla\Phi(\tilde{R}), \nabla\Xi(t,\tilde{R})\rangle\rangle \leq \alpha_4 |\tilde{R}|_I^2$ *for all* $\tilde{R} \in \hat{\mathcal{F}}$*,*

*iii)* $\hat{\mathcal{F}} \subseteq \mathcal{D}_\Xi$,

*iv)* $\exists \alpha_5, \alpha_6 > 0$ *such that* $\|\nabla \Xi(t, \tilde{R})\|_F \leq \alpha_5 |\tilde{R}|_I$ *and* $\|\nabla \Phi(\tilde{R})\|_F \leq \alpha_6 |\tilde{R}|_I$.

*Then the number of discrete jumps is finite and the set* $\mathcal{A} = \{(\tilde{R}, \tilde{b}_\omega, \hat{R}, \omega, t) : \tilde{R} = I, \tilde{b}_\omega = 0\}$, *for the hybrid system with data* (C.62)-(C.65), *is globally exponentially stable if* $k_1 > \bar{k}_1 > 0$ *for some gain* $\bar{k}_1$ *provided in the proof.*

**Proof** See Appendix C.7.

The stability result of Theorem 4.2.4 is equivalent to the one obtained in Theorem 4.2.3 for the hybrid observer (4.7)-(4.10). However, in Theorem 4.2.4, a condition on the gain $k_1$ is imposed. This condition, as shown in the proof of Theorem 4.2.4, comes from the fact that the correction term is allowed to be dependent on a possibly time-varying potential function $\Xi$. If one takes $\Xi = \Phi$ (although not shown here) it can be verified that the condition on the gain $k_1$ is no longer needed to establish global exponential stability. In some applications, as the case when the vector measurements are time-varying, the functions $\Phi(\tilde{R})$ and $\Xi(t, \tilde{R})$ may be chosen to be different [Grip *et al.*, 2012a].

Moreover, compared to the synergistic-based observer, the use of the projection operator in the bias adaptation law is necessary to establish the proof of Theorem 4.2.4 in the case where $\Xi$ is time-varying. If one takes $\Xi = \Phi$ (time-invariant), one can still guarantee global exponential stability without the use of the projection operator. Note that restricting the bias estimates to lie inside a predefined ball is desirable in practice to avoid unbounded growth due to the integration of measurement noise. The projection operator can also be used in (4.8) for practical considerations although it was not needed to establish the proof of exponential stability.

**Remark 4.2.5** *Note that in view of the definition of the jump set* $\hat{\mathcal{J}}$ *in* (4.17) *and item i) of Theorem 4.2.4 one has* $\tilde{R} \in \hat{\mathcal{J}}$ *implies that*

$$\delta \leq \Phi(\tilde{R}) - \min_{p \in \mathcal{Q}} \Phi(\tilde{R}\mathbf{R}_a(\theta, u_p)) \leq \Phi(\tilde{R}) \leq \alpha_2 |\tilde{R}|_I^2 \leq \alpha_2. \tag{4.18}$$

*Therefore, in the case where* $\delta > \alpha_2$, *it is clear that* $\hat{\mathcal{J}} = \emptyset$ *and* $\hat{\mathcal{F}} = \mathbb{SO}(3)$. *In this case the reset-base observer is continuous since the jump mechanism is never executed. In this case, the result of Theorem 4.2.4 cannot hold since the topological obstruction on* $\mathbb{SO}(3)$ *prevents a continuous observer to guarantee global exponential stability. In fact, item ii) cannot hold for all* $\tilde{R} \in \mathbb{SO}(3)$ *since the gradient of* $\Phi$ *needs to vanish at some critical points other than* $\tilde{R} = I$ *only.*

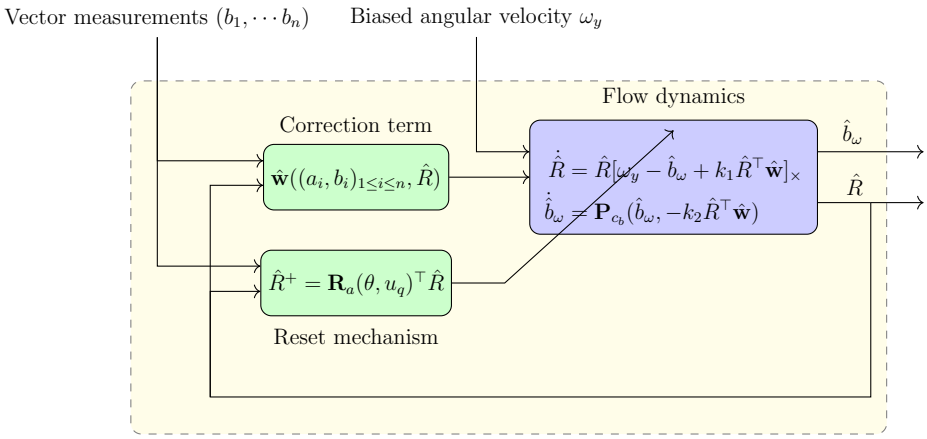


Figure 4.3: Schematic of the reset-based hybrid attitude and gyro bias observer

Now, let us look for a potential function and the parameters of the hybrid observer satisfying the conditions of Theorem 4.2.4.

**Formulation in the case of constant inertial vectors** $(a_i)_{1\leq i\leq n}$

Before formulating the reset-based observer using body-frame measurements of constant and known inertial vectors, one needs the following important result.

**Proposition 4.2.6** *Let $A \in \mathbb{R}^{3\times 3}$ be a constant positive semidefinite matrix, $\mathcal{Q} = \{1, 2, 3\}$ and $\theta \in (-\pi, \pi) \setminus \{0\}$. Let $\{u_1, u_2, u_3\}$ be an orthonormal basis for the eigenvectors' set $\mathcal{E}_v^{\mathbb{R}}(A)$. Choose $0 < \delta < \bar{\delta}$ in (4.16)-(4.17) such that*

- $\bar{\delta} = 2\sin^2(\theta/2)\lambda/3$ *if* $A = \lambda I > 0$.
- $\bar{\delta} = 2\sin^2(\theta/2)\min\{\lambda_1^A, \lambda_3^A/3\}$ *if $A$ has two distinct eigenvalues where $\lambda_1^A > 0$ has algebraic multiplicity equals to 2 and $\lambda_3^A > 0$ has algebraic multiplicity equals to 1.*
- $\bar{\delta} = \sin^2(\theta/2)(\lambda_1^A + \lambda_2^A)$ *if $A$ has three distinct eigenvalues $0 \leq \lambda_1^A < \lambda_2^A < \lambda_3^A$.*

*Then the conditions of Theorem 4.2.4 are satisfied when considering $\Phi = \Xi = \Psi_{1,A}$.*

**Proof** See Appendix B.7.

The trace function $\Psi_{1,A}$, defined in (3.28) for some $A$ such that $\mathbf{E}(A) > 0$, can be, therefore, used to design the reset-based hybrid attitude observer (4.14)-(4.17) by letting $\Phi = \Xi = \Psi_{1,A}$. If one sets $A = \sum_{i=1}^n \rho_i a_i a_i^\top$ for some $\rho_1, \cdots, \rho_n > 0$ the observer can be written explicitly using the available vector measurements by noticing that (in view of

Lemma 2.2.7)

$$\Phi(\tilde{R}) = \frac{1}{4}\sum_{i=1}^{n} \rho_i \|b_i - \hat{R}^\top a_i\|^2, \tag{4.19}$$

$$\Phi(\tilde{R}\mathbf{R}_a(\theta,u)) = \frac{1}{4}\sum_{i=1}^{n} \rho_i \|b_i - \hat{R}^\top \mathbf{R}_a(\theta,u) a_i\|^2, \tag{4.20}$$

$$\mathbf{w}(t,\tilde{R}) = \frac{1}{4}\hat{R}\sum_{i=1}^{n} \rho_i (b_i \times \hat{R}^\top a_i). \tag{4.21}$$

**Algorithm 2** Reset-based hybrid observer using constant inertial vectors

Pick scalars $\rho_i > 0, i = 1, \cdots, n$ such that $A = \sum_{i=1}^{n} \rho_i a_i a_i^\top$ has distinct eigenvalues.
Pick $\theta \in \mathbb{R} \setminus \{0\}$ and $0 < \delta < \sin^2(\theta/2)(\lambda_1^A + \lambda_2^A)$.
Let $\mathcal{Q} = \{1,2,3\}$ and $\{u_1, u_2, u_3\}$ an orthonormal basis for $\mathcal{E}_v^{\mathbb{R}}(A)$.
Initialize the observer states $\hat{R}(0,0) \in \mathbb{SO}(3)$, $\hat{b}_\omega(0,0) \in \mathbb{R}^3$
Pick the observer gains $k_1$ and $k_2$ to obtain the desirable performance.

1: **for** each set of measurements $(b_i)_{1\le i\le n}$ and $(a_i)_{1\le i\le n}$ **do**
2: Calculate $\Phi(\tilde{R})$ and $\min_{p\in\mathcal{Q}} \Phi(\tilde{R}\mathbf{R}_a(\theta,u_p))$ using (4.19) and (4.20).
3: **while** $\tilde{R} \in \hat{\mathcal{J}}$ **do**
4: Update $\hat{R}^+ = \mathbf{R}_a(\theta,u_q)^\top \hat{R}$ where $q \in \arg\min_{p\in\mathcal{Q}} \Phi(\tilde{R}\mathbf{R}_a(\theta,u_p))$.
5: **end while**
6: Calculate the correction term $\mathbf{w}(t,\tilde{R})$ using (4.21).
7: Update the states $\hat{R}$ and $\hat{b}_\omega$ according to (4.14).
8: **end for**

**Formulation in the case of time-varying inertial vectors** $(a_i)_{1\le i\le n}$

In the case where the inertial vectors are time-varying, the matrix $A$ becomes time-varying and thus the potential function $\Psi_{1,A}$ depends on time as well. It can not be used as $\Phi = \Psi_{1,A}$ since $\Phi$ in Theorem 4.2.4 was assumed to be state dependent only. In this case, we construct a potential function $\Phi$ that does not depend on time. Let $a_1$ and $a_2$ be any two noncollinear inertial vectors which are guaranteed to exist thanks to Assumption 4.2.1. Construct the following three orthonormal vectors $r_1 = a_1/\|a_1\|, r_2 = (a_1 \times a_2)/\|a_1 \times a_2\|$ and $r_3 = r_1 \times r_2$. The corresponding body-frame measurements of $r_1, r_2$ and $r_3$ are given by $s_1 = b_1/\|b_1\|, s_2 = (b_1 \times b_2)/\|b_1 \times b_2\|$ and $s_3 = s_1 \times s_2$. Then, in view of Lemma 2.2.7 and the fact that $\sum_{i=1}^{3} r_i r_i^\top = I$ one obtains

$$\Psi_1(\tilde{R}) = \frac{1}{4}\sum_{i=1}^{3} \|s_i - \hat{R}^\top r_i\|. \tag{4.22}$$

Now consider $\Phi = \Psi_1$ and $\Xi = \Psi_{1,A}$ with $A = \sum_{i=1}^{n} \rho_i a_i a_i^\top$ for some $\rho_1, \cdots, \rho_n > 0$.

**Proposition 4.2.7** *Let $\mathcal{Q} = \{1, 2, 3\}$ and $\theta \in (-\pi, \pi) \setminus \{0\}$. Let $\{u_1, u_2, u_3\}$ be an orthonormal basis for $\mathbb{R}^3$. Choose $0 < \delta < \bar{\delta}$ in (4.16)-(4.17) such that $\bar{\delta} = 2\sin^2(\theta/2)/3$. Then the conditions of Theorem 4.2.4 are satisfied when considering $\Phi = \Psi_1$ and $\Xi = \Psi_{1,A}$.*

**Proof** See Appendix B.8.

Therefore, under the design choices of Proposition 4.2.7, the hybrid observer (4.14)-(4.17) can be implemented using time-varying inertial vector measurements by letting

$$\Phi(\tilde{R}) = \frac{1}{4}\sum_{i=1}^{3} \|s_i - \hat{R}^\top r_i\|^2, \tag{4.23}$$

$$\Phi(\tilde{R}\mathbf{R}_a(\theta, u)) = \frac{1}{4}\sum_{i=1}^{3} \|s_i - \hat{R}^\top \mathbf{R}_a(\theta, u) r_i\|^2, \tag{4.24}$$

$$\hat{\mathbf{w}}((a_i, b_i)_{1\le i\le n}, \hat{R}) = \mathbf{w}(t, \tilde{R}) = \frac{1}{4}\hat{R}\sum_{i=1}^{n} \rho_i (b_i \times \hat{R}^\top a_i). \tag{4.25}$$

**Algorithm 3** Reset-based hybrid observer using time-varying inertial vectors

Choose scalars $\rho_i > 0, i = 1, \cdots, n$, $\theta \in \mathbb{R} \setminus \{0\}$ and $0 < \delta < 2\sin^2(\theta/2)/3$.
Let $\mathcal{Q} = \{1, 2, 3\}$ and $\{u_1, u_2, u_3\}$ an orthonormal basis for $\mathbb{R}^3$.
Initialize the observer states $\hat{R}(0, 0) \in \mathbb{SO}(3)$, $\hat{b}_\omega(0, 0) \in \mathbb{R}^3$ and pick the observer gains $k_1$ and $k_2$ to obtain the desirable performance.

1: **for** each set of measurements $(b_i)_{1\le i\le n}$ and $(a_i)_{1\le i\le n}$ **do**
2: Calculate $\Phi(\tilde{R})$ and $\min_{p\in\mathcal{Q}} \Phi(\tilde{R}\mathbf{R}_a(\theta, u_p))$ using (4.23) and (4.24).
3: **while** $\tilde{R} \in \hat{\mathcal{J}}$ **do**
4: Update $\hat{R}^+ = \mathbf{R}_a(\theta, u_q)^\top \hat{R}$ where $q \in \arg\min_{p\in\mathcal{Q}} \Phi(\tilde{R}\mathbf{R}_a(\theta, u_p))$.
5: **end while**
6: Calculate the correction term $\mathbf{w}(t, \tilde{R})$ using (4.25).
7: Update the states $\hat{R}$ and $\hat{b}_\omega$ according to (4.14).
8: **end for**

### 4.2.4 Simulations

We consider a rigid body motion with inertia matrix $J = \mathrm{diag}(1, 2, 3)(\mathrm{kg.m}^2)$ initialized at a zero angular velocity $\omega(0) = 0$ $(\mathrm{rad.s}^{-1})$. We assume that the rigid body is subject

to the following external body-frame torque vector

$$\tau = \begin{bmatrix} \sin(0.1t) \\ 2\sin(0.05t + \pi) \\ 0.5\sin(0.03t + \pi/3) \end{bmatrix} \times 10^{-2}(\text{N.m}). \tag{4.26}$$

The simulation of the attitude trajectory for the above described rigid body configuration is done by first integrating the Euler's equation $J\dot{\omega} = J\omega \times \omega + \tau$ using a fourth-order Runge-Kutta method over a time span of 100 seconds to obtain the angular velocity vector $\omega(t)$, see Figure 4.4. For our estimation purpose, we assume that the angular

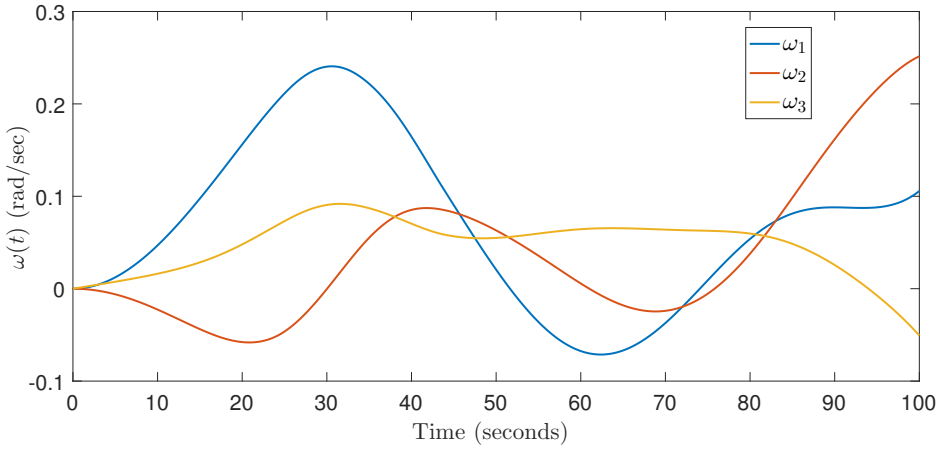


Figure 4.4: Angular velocity $\omega(t)$.

velocity is obtained at high frequency (quasi continuous) of around 200 Hz.

We assume available two sensors that provide two body-frame vector measurements $b_1 = R^\top a_1$ and $b_2 = R^\top a_2$ such that $a_1 = [1, -1, 1]^\top/\sqrt{3}$ and $a_2 = [0, 0, 1]^\top$. We construct a third vector measurement by letting $b_3 = b_1 \times b_2$ and $a_3 = a_1 \times a_3$. We assume that the angular velocity measurements are biased with a constant bias $b_\omega = [5, 5, 5]^\top \times 10^{-3}$ (rad/sec). The true attitude of the rigid body is initialized at $R(0) = \mathbf{R}_a(\pi, [0, 0, 1]^\top)$. We implement the smooth observer (4.4)-(4.6), the synergistic-based hybrid observer (4.7)-(4.10) with its explicit formulation (4.11)-(4.13) and the reset-based hybrid observer (4.14)-(4.17) with its explicit formulation in (4.19)-(4.21). All the observers states are initialized at $\hat{R}(0, 0) = 0$ and $\hat{b}_\omega(0, 0) = [0, 0, 0]^\top$. Since all the observers are locally similar, we use the same following gains $\rho_1 = 2, \rho_2 = 1, \rho_3 = 0.25, k_1 = 7$ and $k = 5$. The synergistic-based hybrid observer is implemented with the initial configuration $q(0, 0) = 1$ and the parameters $\delta = 3 \times 10^{-3}, k = 0.07$ and $u = [0.18, 0.18, 0.97]^\top$ which satisfy the exp-synergism condition of Proposition 3.3.16 by setting $A = \sum_{i=1}^{3} \rho_i a_i a_i^\top$. Since the inertial vectors are constant, we implement the reset-based hybrid observer without the

projection function $\mathbf{P}_{c_b}(\cdot)$ which has been added only to deal with the possibility of having time-varying inertial vectors. For the reset-based hybrid observer, we pick $\theta = \pi/2$ and $\delta = 0.3$ and $\{u_1, u_2, u_3\}$ as the eigenvectors of $A$. The performance of these estimation schemes is depicted in Figures 4.5-(4.6). As expected the smooth observer takes some warm-up time (around $5-6$ seconds) before it convergence due to the undesired critical points of the cost function used to derive the observer. The reset-based hybrid observer immediately corrects the attitude estimate to reduce the total attitude error from 180° to around 90° of angle and then flows till it converges. The synergistic-based hybrid observer however changes the innovation term from $q = 1$ to $q = 2$ at around $t = 3$ seconds and then flows until it converges to zero estimation error. Both hybrid observers exhibit lower settling times compared to the smooth observer which illustrates the advantage of the proposed hybrid estimation schemes compared to the traditional smooth explicit complementary filter.

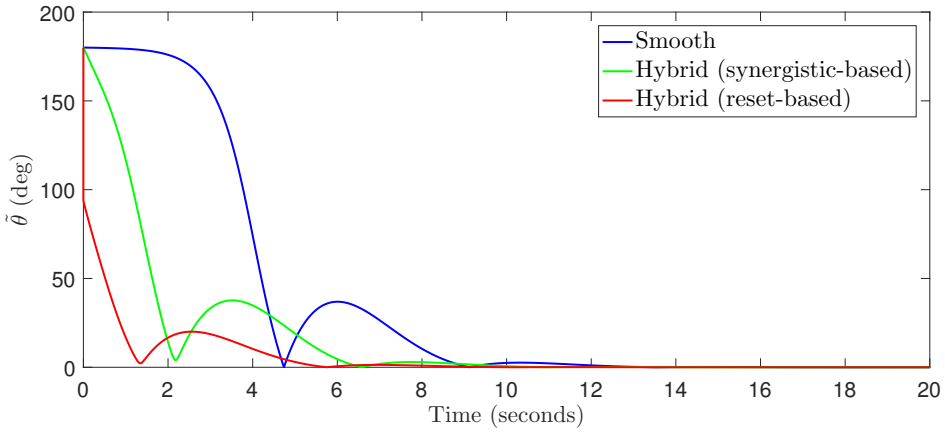


Figure 4.5: Attitude estimation error for the proposed hybrid observers.

## 4.3 Attitude Estimation Using Intermittent Vector Measurements

In this section, we consider the problem of attitude observers design on $\mathbb{SO}(3)$ with a measurement-triggered behaviour. The angular velocity measurements are used to continuously predict the attitude on $\mathbb{SO}(3)$ which is corrected, via an instantaneous jump mechanism, upon the arrival of new measurements. A hybrid model that captures the dynamic behaviour of the interconnection of the attitude estimator and the attitude kinematics is proposed. We consider both cases where the body-frame vector measurements

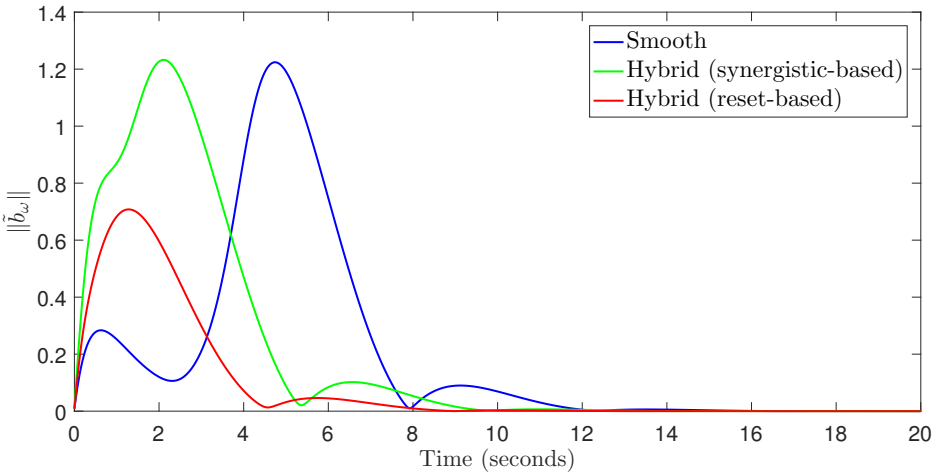


Figure 4.6: Gyro-bias estimation error for the proposed hybrid observers.

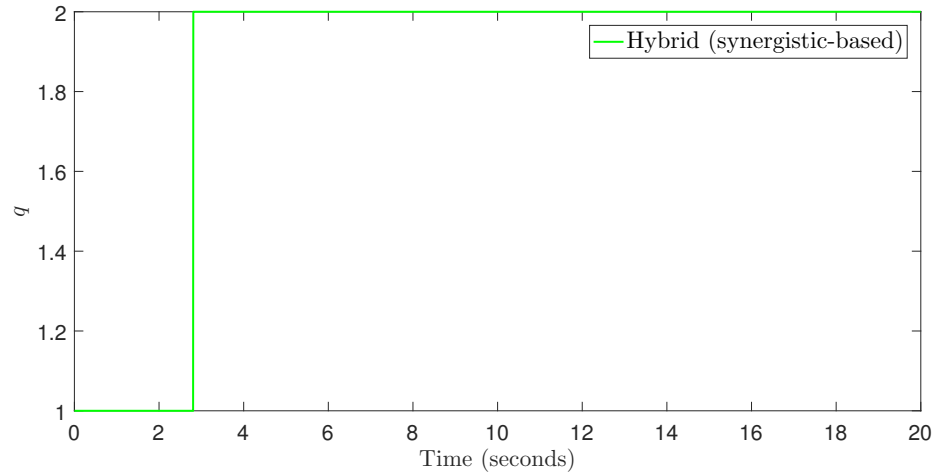


Figure 4.7: Switching variable $q$ for the synergistic-based hybrid observer.

are collected synchronously and asynchronously. Some practical considerations such as discrete-time implementation, noise filtering and gyro-bias compensation are discussed.

### 4.3.1 Problem Formulation

Consider the attitude kinematics for a rigid body

$$\dot{R}(t) = R(t)[\omega(t)]_\times, \tag{4.27}$$

where $R(t) \in \mathbb{SO}(3)$ represents the instantaneous rotation matrix describing the orientation of a body-attached frame with respect to an inertial frame. The vector $\omega(t) \in \mathbb{R}^3$

represents the instantaneous angular velocity of the rigid body expressed in the body-attached frame. We consider that the angular velocity vector $\omega(t)$ is measured continuously for all $t \geq 0$. Also, we consider available some "intermittent" or sporadic vector measurements $b_i = R^\top a_i, i = 1, \cdots, n$ arriving at some instant of times $t_k^i, k \in \mathbb{N}$ and $i = 1, \cdots, n$. The inertial vectors $a_i$ are assumed to be constant, known and satisfying Assumption 4.2.1. Assume moreover that each sequence $\{t_k^i\}_{k\in\mathbb{N}}$, for $i = 1, \cdots, n$, is strictly increasing and unbounded and that there exist $0 < T_1^i \leq T_2^i$ such that

$$0 \leq t_0^i \leq T_2^i, \tag{4.28}$$

$$T_1^i \leq t_{k+1}^i - t_k^i \leq T_2^i, \qquad \forall k \in \mathbb{N}, \forall i = 1, \cdots, n. \tag{4.29}$$

The formulation of the available measurements above is very generic and allows for measurements with irregular and different sampling periods. We can derive particular cases from the above formulation of measurements as follows:

1. If $T_1^1 = \cdots = T_1^n = T_2^1 = \cdots = T_2^n = T$ and $t_0^1 = \cdots = t_0^n$ then the measurements are *synchronous* with *regular* (constant) sampling period equals $T$.

2. If the sequences $\{t_k^i\}_{k\in\mathbb{N}}$ are identical for all $i = 1, \cdots, n$, then the measurements are *synchronous* with *irregular* sampling.

3. If $T_1^i = T_2^i = T^i$, for $i = 1, \cdots, n$, without necessarily having $T^1, \cdots, T^n$ being all equal, then the measurements are *asynchronous* with different *regular* sampling periods (each measurement has a constant sampling rate).

4. In the general case the measurements are *asynchronous* with *irregular* sampling.

The objective of this work is to develop attitude estimation algorithms in the presence of constraints on the vector measurements as defined above. In particular, we will first solve the attitude estimation problem with synchronous measurements and irregular sampling (item 2 above) which can be also considered as a solution to the attitude estimation problem with synchronous measurements and regular sampling (item 1) since the later is a particular case. Next, we will develop an estimation algorithm that solves the general case with *asynchronous* measurements and *irregular* sampling (item 4) which covers all the particular cases mentioned above.

### 4.3.2 Attitude Estimation Using Synchronous Vector Measurements

In this subsection, we assume that the vector measurements are synchronized, which means that the time sequences $\{t_k^i\}_{k\in\mathbb{N}}$ are identical for all $i = 1, \cdots, n$ and can be denoted as $\{t_k\}_{k\in\mathbb{N}}$ by removing the index $i$. In this case, the lower and upper bound on the transmission times $T_1^i$ and $T_2^i$ are also denoted by $T_1$ and $T_2$ for short. Observers with impulsive-like dynamics for linear time invariant systems and some special classes of nonlinear systems with Lipschitz nonlinearities have been discussed in [Raff and Allgöwer, 2007, Andrieu *et al.*, 2013, Ferrante *et al.*, 2016]. Motivated by these works, we propose the following estimation scheme on $\mathbb{SO}(3)$

$$\dot{\hat{R}}(t) = \hat{R}(t)[\omega(t)]_\times, \qquad t \in [t_{k-1}, t_k),\ k \in \mathbb{N}, \tag{4.30}$$

$$\hat{R}(t^+) = \mathbf{R}_r\left(\sigma(t)\right)\hat{R}(t), \qquad t = t_k,\ k \in \mathbb{N}, \tag{4.31}$$

$$\sigma = \sum_{i=1}^{n} \rho_i(\hat{R}b_i \times a_i), \quad \rho_i > 0, \tag{4.32}$$

where the notation $\hat{R}(t^+)$ is used such that $\hat{R}(t^+) = \lim_{h\to 0}\hat{R}(t+h)$ and, without loss of generality, it is assumed that $\hat{R}(t) = \hat{R}(t^-) = \lim_{h\to 0}\hat{R}(t-h)$. Between two instants of time $t_{k-1}$ and $t_k$, the attitude observer is a copy of the attitude kinematics (4.27). This is similar to the "prediction step" in the traditional Kalman filtering technique. The estimated attitude $\hat{R}(t)$ is updated (corrected) at each instant of time $t_k$ when a new measurement becomes available. This correction step uses matrix multiplication to preserve attitude estimates on $\mathbb{SO}(3)$ since the group $\mathbb{SO}(3)$ is closed under the matrix multiplication operation. Specifically, we use a correction matrix that is built from the error vector $\sigma$ used in many continuous attitude estimation schemes [Mahony *et al.*, 2008, Berkane and Tayebi, 2016, Zlotnik and Forbes, 2017]. Note that in [Barrau and Bonnabel, 2015] a similar observer structure has been proposed in the case of two vector measurements, with the use of the exponential map $\exp(\sigma)$ as a correction rotation instead of $\mathbf{R}_r(\sigma)$. The advantage of using $\mathbf{R}_r(\sigma)$ over $\exp(\sigma)$ is the computational efficiency since $\mathbf{R}_r(\sigma)$ does not require the calculation of trigonometric functions. Moreover, this choice facilitates considerably the proof of convergence which is conducted for a set of $n \geq 2$ vector measurements compared to [Barrau and Bonnabel, 2015] where only two vector measurements are used.

To analyze the stability of the proposed attitude estimation scheme, we define the

following (left-invariant) attitude estimation error

$$\tilde{R} = R\hat{R}^\top. \tag{4.33}$$

During the flows of (4.30) the evolution of the attitude estimation error satisfies $\dot{\tilde{R}} = \dot{R}\hat{R}^\top + R\dot{\hat{R}}^\top = R[\omega]_\times \hat{R}^\top - R[\omega]_\times \hat{R}^\top = 0$. This implies that the attitude error is kept constant while waiting for the arrival of a new measurement. Note that this property holds true only when considering perfect angular velocity readings. In fact if the angular velocity reading is biased or noisy then we would accept slight drift of the attitude estimation error during the intervals of time where no measurements are available. For sufficiently small measurement intervals and accurate enough gyros we expect that this drift will be maintained small enough and stable. The interconnection of the jump-free kinematic model (4.27) and the attitude observer (4.30)-(4.31) leads naturally to the following closed-loop system

$$\dot{\tilde{R}}(t) = 0, \qquad t \in [t_{k-1}, t_k),\ k \in \mathbb{N}, \tag{4.34}$$

$$\tilde{R}(t^+) = \tilde{R}(t)\mathbf{R}_r\left(-\sigma(t)\right), \qquad t = t_k,\ k \in \mathbb{N}, \tag{4.35}$$

where we have used the fact that during the jumps the true attitude $R(t)$ is unchanged and thus $R(t^+) = R(t)$. The correction term $\sigma(t)$ in (4.32) can be expressed in terms of the attitude error as $\sigma = \sum_{i=1}^{n} \rho_i [\tilde{R}^\top a_i]_\times a_i$. Note that the dynamics of the attitude error $\tilde{R}$ is independent from the attitude trajectory in (4.27). This is a desirable behaviour since the gains can be tuned and optimized off-line to yield the desirable behaviour in real-time, independently from the trajectory of the attitude system dictated by the angular velocity vector $\omega(t)$.

Now, we map the closed-loop system (4.34)-(4.35) into a hybrid model by augmenting the system with a "hidden" timer (see [Jentzen *et al.*, 2010]) as follows

$$\begin{cases} \dot{\tilde{R}} = 0 \\ \dot{\tau} = 1 \end{cases} \qquad (\tilde{R}, \tau) \in \mathcal{F}, \tag{4.36}$$

$$\begin{cases} \tilde{R}^+ = \tilde{R}\mathbf{R}_r\left(-\sigma\right) \\ \tau^+ = 0 \end{cases} \qquad (\tilde{R}, \tau) \in \mathcal{J}, \tag{4.37}$$

where the flow set $\mathcal{F}$ and jump set $\mathcal{J}$ are defined as

$$\mathcal{F} = \left\{(\tilde{R}, \tau) \in \mathbb{SO}(3) \times \mathbb{R}_{\geq 0} :\ \tau \in [0, T_2]\right\}, \tag{4.38}$$

$$\mathcal{J} = \left\{(\tilde{R}, \tau) \in \mathbb{SO}(3) \times \mathbb{R}_{\geq 0} :\ \tau \in [T_1, T_2]\right\}. \tag{4.39}$$

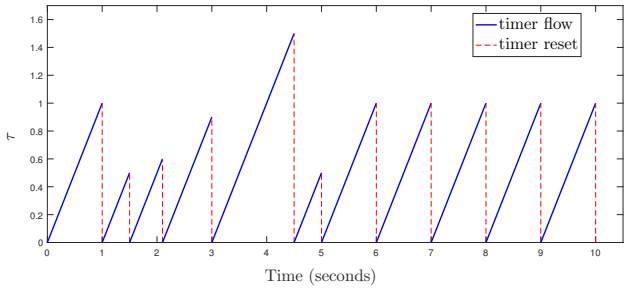


Figure 4.8: Behaviour of the virtual variable $\tau$ (timer) introduced in (4.36)-(4.37). At the arrival of a new measurement, the timer is reset back to zero (dashed red) and flows linearly otherwise (blue solid).

The extra variable introduced (timer $\tau$ with $\tau(0,0) \in [T_1, T_2]$) allows to capture the *time-triggered* behaviour of (4.34)-(4.35) which results in an autonomous hybrid system capturing all the solutions of (4.34)-(4.35). In fact, as the ordinary time $t$ increases the timer $\tau$ increases up to a certain value in $[0, T_2]$. Thus, the system can flow when $\tau \in [0, T_2]$ and flows are not allowed after $\tau = T_2$. On the other hand, after each jump the timer $\tau$ is reset to zero and the next jump can not happen except after the minimum time $T_1$ has elapsed. This reflects the condition (4.28)-(4.29) on the communication protocol between the sensors and the CPU, see Figure 4.8 for an illustration. Our objective is to achieve almost global exponential stability of the set

$$\mathcal{A}_s = \{I\} \times [0, T_2]. \tag{4.40}$$

The set $\mathcal{A}_s$ is forward invariant for the hybrid system (4.36)-(4.39). In fact, for $\tilde{R} = I$, one has $\sigma = \sum_{i=1}^{n} \rho_i [\hat{R} b_i]_\times a_i = \sum_{i=1}^{n} \rho_i [\tilde{R}^\top a_i]_\times a_i = 0$ which implies that $\mathbf{R}_r(\sigma) = I$ and hence $\tilde{R}^+ = I$. This leads to conclude that the set $\mathcal{A}_s$ is an equilibrium of (4.36)-(4.39) since it is invariant under both the flows and the jumps. In the following theorem, we provide a sufficient condition for the set $\mathcal{A}_s$ to be exponentially stable for the hybrid system (4.36)-(4.39).

**Theorem 4.3.1** *Consider the kinematic system* (4.27) *coupled with the estimator* (4.30)-(4.32). *The set* $\mathcal{A}_s$ *defined in* (4.40) *is almost globally exponentially stable for the closed-loop hybrid system* (4.36)-(4.39) *if*

$$0 < \mathbf{tr}(A) - \lambda_{\min}^{A} < 1, \tag{4.41}$$

*where* $A = \sum_{i=1}^{n} \rho_i a_i a_i^\top$. *The region of exponential stability is defined by the set* $\Pi_{\mathbb{SO}(3)} \times [0, T_2]$. *Moreover, the set* $\mathbf{R}_a(\pi, \mathbb{S}^2) \times [0, T_2]$ *is forward invariant.*

**Proof** See Appendix C.8.

Note that the domain of exponential stability of the closed-loop system (4.36)-(4.39) covers all attitude errors $\tilde{R} \in \mathbb{SO}(3)$ that have an angle of rotation strictly less than 180°. This manifold is formally characterized by the condition $\mathbf{tr}(\tilde{R}) = -1$ and has Lebesgue measure zero in the state space.

### 4.3.3 Attitude Estimation Using Asynchronous Vector Measurements

In a general setting of attitude estimation using intermittent asynchronous measurements, the sensors' readings are obtained at different instants of time for each sensor according to the communication constraint (4.28)-(4.29). The challenge with this situation is that at a given transmission time $t_k^i$ for sensor $i$ there is no guarantee that another sensor $l$ has transmitted an information (or equivalently $t_k^l = t_k^i$). Therefore, since each vector measurement $b_i$ represents only a partial attitude information, there is no mean to obtain a full information about the attitude since at least two non-collinear vector measurements are needed to recover the full attitude. Nevertheless, it is possible to use this partial attitude information to correct the attitude whenever a sensor measurement is available. We propose the following attitude estimation scheme

$$\dot{\hat{R}}(t) = \hat{R}(t)[\omega(t)]_\times, \qquad t \neq t_k^i, k \in \mathbb{N}, i = 1, \cdots, n, \tag{4.42}$$

$$\hat{R}(t^+) = \mathbf{R}_r(\sigma_i(t))\hat{R}(t), \qquad t = t_k^i, k \in \mathbb{N}, i = 1, \cdots, n, \tag{4.43}$$

where $\sigma_i = \rho_i(\hat{R}b_i \times a_i)$ and $\rho_i, i = 1, \cdots, n$ are some positive scalars. This attitude estimation scheme allows to correct the attitude estimates only at times where we receive a measurement. Note that we can have multiple jumps (consecutive updates of the state) at the same instant of time if two or more measurements arrive at this instant of time ($t_k^l = t_k^i$ with $l \neq i$). In this case the order of priority of the updates (which sensor's reading to use first) can be arbitrary but in practical applications, the user might establish a priority protocol according to the reliability of each sensor.

To capture the behaviour of the event-triggered system (4.42)-(4.43) one needs to introduce a timer $\tau_i$ for each sensor measuring the body-frame vector $b_i$. At the arrival of a measurement $b_i(t_k^i)$ the timer $\tau_i$ is reset to zero. The timer $\tau_i$ will keep increasing until it reaches a value in the interval $[T_1^i, T_2^i]$ where its reset is triggered by the arrival of a new measurement $b_i(t_{k+1}^i)$. This behaviour is depicted in Figure 4.9 in the case of two vector measurements with asynchronous transmission times. Following similar steps as

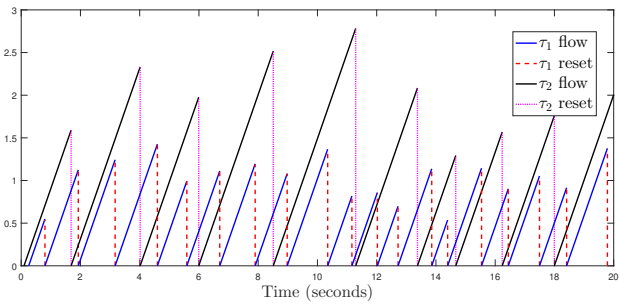


Figure 4.9: Behaviour of the virtual variables $\tau_1$ and $\tau_2$ (timers) introduced in (4.42)-(4.49). The transmission (measurement) times $t_k^i$ with $i \in \{1, 2\}$ satisfy the constraints (4.28)-(4.29) with $T_1^1 = 0.5, T_2^1 = 1.5, T_1^2 = 1$ and $T_2^2 = 3$. At the arrival of a measurement $b_i$ the corresponding timer $\tau_i$ is reset back to zero.

(4.34)-(4.39), we derive the hybrid model that captures the dynamics of the closed-loop system as follows. Let us define the state $X := (\tilde{R}, \tau_1, \cdots, \tau_n) \in \mathbb{SO}(3) \times \mathbb{R}^n_{\geq 0}$. The closed-loop system is governed by the hybrid dynamical model

$$\dot{X} = \mathbf{F}(X), \qquad X \in \mathcal{F}, \tag{4.44}$$

$$X^+ \in \mathbf{J}(X), \qquad X \in \mathcal{J}, \tag{4.45}$$

where the single-valued flow map $\mathbf{F}$ and set-valued jump map $\mathbf{J}$ are defined by

$$\mathbf{F}(X) = (0_{3\times 3}, 1, \cdots, 1), \tag{4.46}$$

$$\mathbf{J}(X) = \{\mathbf{J}_i(X), X \in \mathcal{J}_i\}, \tag{4.47}$$

where $\mathbf{J}_i(X) = (\tilde{R}\mathbf{R}_r(-\sigma_i), \tau_1, \cdots, \tau_{i-1}, 0, \tau_{i+1}, \cdots, \tau_n)$ and $\mathcal{J}_i = \{X \in \mathbb{SO}(3) \times \mathbb{R}^n_{\geq 0} : \tau_i \in [T_1^i, T_2^i]\}$. The flow set $\mathcal{F}$ and jump set $\mathcal{J}$ are given by

$$\mathcal{F} = \mathbb{SO}(3) \times [0, T_2^1] \times \cdots \times [0, T_2^n], \tag{4.48}$$

$$\mathcal{J} = \mathcal{J}_1 \cup \cdots \cup \mathcal{J}_n. \tag{4.49}$$

Note that the jumps in (4.43) are modelled by an inclusion and therefore the updated state $X^+$ can take any of the values from the set $\mathbf{J}(X)$. This captures the behaviour when multiple measurements from different sensors arrive at the same instant of time. In this case the closed-loop system is allowed to experience multiple consecutive jumps in any order. The objective is to achieve almost global asymptotic stability of the set

$$\mathcal{A}_a = \{I\} \times [0, T_2^1] \times \cdots \times [0, T_2^n].$$

**Theorem 4.3.2** *Consider the kinematic system* (4.27) *coupled with the estimator* (4.42)-(4.43). *The set* $\mathcal{A}_a$ *is almost globally asymptotically stable for the closed-loop hybrid system* (4.36)-(4.39) *if the scalars* $\rho_i$ *satisfy*

$$0 < \rho_i < \frac{1}{\|a_i\|^2}, \quad i \in \{1, \cdots, n\}. \tag{4.50}$$

*The region of asymptotic stability is defined by the set* $\Pi_{\mathbb{SO}(3)} \times [0, T_2^1] \times \cdots \times [0, T_2^n]$.

**Proof** See Appendix C.9.

Note that the attitude estimation scheme (4.42)-(4.43), although developed for the general case of asynchronous measurements, can also be used in the particular case of synchronous measurements. In this case $t_k^1 = \cdots = t_k^i = \cdots = t_k^n$ and equations (4.42)-(4.43) can be rewritten as follows

$$\dot{\hat{R}}(t) = \hat{R}(t)[\omega(t)]_\times, \qquad t \neq t_k, k \in \mathbb{N}, \tag{4.51}$$

$$\hat{R}^+(t) = \Pi_{i=1}^n \mathbf{R}_r(\sigma_i(t))\hat{R}(t), \qquad t = t_k, k \in \mathbb{N}. \tag{4.52}$$

The obtained algorithm is different from the one proposed in (4.30)-(4.31) for synchronous measurements. The difference resides in the correction attitude matrix which is defined by the product $\Pi_{i=1}^n \mathbf{R}_r(\sigma_i)$ in (4.51)-(4.52) while in (4.30)-(4.31) it is defined by the single rotation matrix $\mathbf{R}_r(\sum_{i=1}^n \sigma_i)$. The latter requires less computational power and this argument has motivated the introduction of algorithm (4.30)-(4.31) which suites better the case of synchronous measurements.

### 4.3.4 Practical Considerations

In this section, we discuss some practical issues and improvements to the raw algorithms presented in the previous sections.

#### 4.3.4.1 Discrete-Time Implementation

The attitude estimation scheme proposed in (4.30)-(4.31) relies on continuous flow dynamics between each two instant of measurements $t_k$ and $t_{k+1}$. The observer state is updated (via instantaneous jumps) at each instant of time $t_k$ when a new measurement arrives. To implement this attitude observer, we propose a discrete-time integration scheme that emulates the behaviour of the observer during the continuous flow. Assume

that the unbounded continuous time interval $[0, \infty)$ is sampled with a sampling period $T_s > 0$. We obtain a series of discrete times $\{s_m\}_{m\in\mathbb{N}}$ such that $s_m = mT_s$. We assume that the sampling period $T_s$ is small enough such that the angular velocity is constant during each sampling period, *i.e.,*

$$\omega(t) = \omega(s_m), \quad t \in [s_m, s_{m+1}), m \in \mathbb{N}. \tag{4.53}$$

Consequently, in view of the flow dynamics (4.30), the following holds for all $t \in [s_m, s_{m+1})$ and $m \in \mathbb{N}$

$$\frac{d}{dt}\left(\hat{R}\exp([\omega(s_m)t]_\times)\right) = 0. \tag{4.54}$$

An exact integration of the above equation, between the instants of time $s_m^+$ and $s_{m+1}^- \equiv s_{m+1}$, leads to the following discrete-time update rule for the estimated attitude $\hat{R}$, during the flows of (4.30):

$$\hat{R}(s_{m+1}) = \hat{R}(s_m^+)\exp([\omega(s_m)T_s]_\times). \tag{4.55}$$

The above prediction rule preserves the $\mathbb{SO}(3)$ structure since the group $\mathbb{SO}(3)$ is closed under matrix multiplication and the exponential matrix $\exp([\omega(s_m)T_s]_\times)$ is indeed an element of $\mathbb{SO}(3)$. It corresponds to the Euler-Lie method for numerical integration on Lie groups [Celledoni *et al.*, 2014]. Note that $\hat{R}(s_m^+) = \lim_{h\to 0}\hat{R}(s_m + h)$ which represents the state of the observer after a "possible" jump in (4.31). For sufficiently small $T_s$, it is reasonable to assume that the intermittent instants of time $t_k$, where the measurements are available, are elements of the discrete-time interval, *i.e.,* $t_k \in \{s_m\}_{m\in\mathbb{N}}$ for all $k \in \mathbb{N}$. That is to say that for all $k \in \mathbb{N}$, there exists $m \in \mathbb{N}$ such that $t_k = s_m = mT_s$. Only at these particular instants of time, the attitude estimate $\hat{R}$ is updated according to (4.31). Therefore, one has

$$\hat{R}(s_m^+) = \mathbf{R}_r(\sigma(s_m))\hat{R}(s_m), \qquad s_m = t_k,\ k \in \mathbb{N}, \tag{4.56}$$

$$\hat{R}(s_m^+) = \hat{R}(s_m), \qquad s_m \neq t_k,\ k \in \mathbb{N}. \tag{4.57}$$

Equations (4.55)-(4.57) define the discrete-time implementation of the proposed attitude estimation scheme (4.30)-(4.31). Compared to the traditional methods, the discrete version of our proposed attitude estimation scheme is also asymptotically stable when connected to a good discrete approximation model for the attitude kinematics (4.27). To clarify this idea, let us exactly discretize the kinematic model (4.27) under assumption

(4.53). Following similar steps as in (4.54)-(4.55), one obtains the following discrete kinematic model:

$$R(s_{m+1}) = R(s_m)\exp([\omega(s_m)T_s]_\times), \quad m \in \mathbb{N}. \tag{4.58}$$

For a small enough sampling period $T_s$, the above discrete model is a good approximation of the original continuous time kinematic model (4.27). We now state the following theorem whose proof is given in Appendix C.10.

**Theorem 4.3.3** *Consider the discrete kinematic model* (4.58) *coupled with the discrete attitude estimation scheme* (4.55)-(4.57) *under the conditions of Theorem 4.3.1. Then for all initial attitude errors* $\tilde{R}(0) \in \Pi_{\mathbb{SO}(3)}$ *one has* $\lim_{m\to\infty} \tilde{R}(mT_s) = I$.

Following similar steps as in (4.53)-(4.57) we can derive the discrete version of (4.42)-(4.43) which is suitable for the case of asynchronous vector measurements as follows

$$\hat{R}(s_{m+1}) = \hat{R}(s_m^+)\exp([\omega(s_m)T_s]_\times) \tag{4.59}$$
$$\hat{R}(s_m^+) = \mathbf{R}_r(\sigma_i(s_m))\hat{R}(s_m), \qquad s_m = t_k^i, \tag{4.60}$$
$$\hat{R}(s_m^+) = \hat{R}(s_m), \qquad s_m \neq t_k^i, \tag{4.61}$$

such that $m, k \in \mathbb{N}$ and $i \in \{1, \cdots, n\}$. Moreover, the interconnection of the discrete attitude kinematic model (4.58) and the discrete scheme (4.59)-(4.61) can be shown to retain the almost global asymptotic convergence result under the conditions of Theorem 4.3.2. The proof follows similar lines as in the proof of Theorem 4.3.3 thus omitted.

#### 4.3.4.2 Estimation Algorithms with Enhanced Filtering

We introduce recursive states to the observer (4.30)-(4.31) which, when averaged, yield a better filtered attitude estimate. This can be done by using $N \in \mathbb{N}_{>0}$ attitude states in the following attitude estimation scheme:

- **Flow dynamics** (Prediction step): for all $h \in \{1, \cdots, N\}$ the $h$-th state of the observer flows according to the kinematic equation

$$\dot{\hat{R}}_h(t) = \hat{R}_h(t)[\omega(t)]_\times, \qquad t \in [t_{k-1}, t_k),\ k \in \mathbb{N}. \tag{4.62}$$

- **Jump dynamics** (Update step): during the instants of time $t = t_k, k \in \mathbb{N}$ the observer states are updated as follows

$$\hat{R}_1(t^+) = \mathbf{R}_r\left(\sigma(t)\right)\hat{R}_1(t), \tag{4.63}$$
$$\hat{R}_h(t^+) = \hat{R}_{h-1}(t), \qquad h \in \{2, \cdots, N\}, \tag{4.64}$$

  where the correction term $\sigma$ is defined as $\sigma = \sum_{i=1}^{n} \rho_i(\hat{R}_1 b_i \times a_i)$ and $\rho_1, \cdots, \rho_n$ are positive scalars.

- **Attitude estimate** (averaged rotation): the final attitude estimate is obtained by averaging all the observer states on $\mathbb{SO}(3)$ and is given by

$$\hat{R} = \mathbf{P}_{\mathbb{SO}(3)}\left(\sum_{i=1}^{N} \alpha_h \hat{R}_h\right), \tag{4.65}$$

  where $\alpha_h$ are scalars satisfying, without loss of generality, the equality $\sum_{h=1}^{N} \alpha_h = 1$, and the projection map $\mathbf{P}_{\mathbb{SO}(3)}(\cdot)$ is given in (2.12).

The idea of the attitude estimation scheme (4.62)-(4.65) is to expand the estimation scheme (4.30)-(4.31) with $(N-1)$ additional states which are averaged at the end to give the final attitude state. At each measurement time $t = t_k$, the attitude states $\hat{R}_h$ are shifted one step with respect to the index $h$ (*i.e.* each state $\hat{R}_h$ receives the value of the state $\hat{R}_{h-1}$) which implies that the "error" presented between the state $\hat{R}_{h-1}$ and the true attitude $R$ is shifted to $\hat{R}_h$ for all $i \in \{2, \cdots, N\}$. Therefore, by averaging all the states $\hat{R}_h, i \in \{1, \cdots, N\}$, we aim to reduce the noise level compared to the use of a single observer state. During the flows (when no measurements are available) all the states of the observer are predicted using the continuous-time angular velocity measurements which allows to maintain constant errors between each states of the observer and the true attitude $R$.

The asymptotic convergence of the observer, under the conditions of Theorem 4.3.1, can be argued in straightforward manner as follows. In view of Theorem 4.3.1 the attitude error $\tilde{R}_1 = R\hat{R}_1 = I$ is almost globally exponentially stable which implies that $\lim_{t_k \to \infty} R(t_k)\hat{R}_1^\top(t_k^-) = I$. Since $\hat{R}_2(t_k^+) = \hat{R}_1(t_k^-)$ implies that $\lim_{t_k \to \infty} R(t_k)\hat{R}_2^\top(t_k^+) = I$ and therefore $\hat{R}_2$ also converges to $R$ when time goes to infinity. The same argument can be used to show that all the observer states will converge to $R$ as time goes to infinity.

Consequently

$$\lim_{t\to\infty}\hat{R}(t)=\lim_{t\to\infty}\mathbf{P}_{\mathbb{SO}(3)}\left(\sum_{h=1}^{N}\alpha_h\hat{R}_h\right)=\sum_{h=1}^{N}\alpha_h\mathbf{P}_{\mathbb{SO}(3)}\left(R\right)=R,$$

where we used the fact that $\sum_{h=1}^{N}\alpha_h=1$ and $\mathbf{P}_{\mathbb{SO}(3)}(R)=R\in\mathbb{SO}(3)$. Therefore, the estimation scheme (4.62)-(4.65) is also almost globally asymptotically stable under the same conditions of Theorem 4.3.1.

Furthermore, thanks to the symmetry of the group $\mathbb{SO}(3)$, it is possible to considerably reduce the computational complexity of the estimation scheme (4.62)-(4.65). Observe that $\hat{R}_h$ evolves according to the same kinematic equation (4.62). Hence, the estimation error $\hat{R}_h\hat{R}_1^\top$ is constant during the flows of the observer for $t\in[t_{k-1},t_k)$. Consequently, one can write, for all $h\in\{2,\cdots,N\}$,

$$\int_{t_{k-1}^+}^{t}(\hat{R}_h\hat{R}_1^\top)(\tau)d\tau=0,\quad t\in[t_{k-1},t_k). \tag{4.66}$$

By completing the above integral one obtains

$$\hat{R}_h(t)=\hat{R}_h(t_{k-1}^+)\hat{R}_1(t_{k-1}^+)^\top\hat{R}_1(t),t\in[t_{k-1},t_k). \tag{4.67}$$

Therefore, the value of $\hat{R}_h$ at a given time $t\in[t_{k-1},t_k)$ can be directly obtained from the value of $\hat{R}_1$ at $t$ and past values of $\hat{R}_h$ and $\hat{R}_1$ at time $t=t_{k-1}^+$ just after the last jump has occurred. By creating an $N$ dimensional register containing the values of $\hat{R}_1(t_{k-1}^+),\cdots,\hat{R}_N(t_{k-1}^+)$, it is possible to calculate the values of the individual state variables at any time $t\in[t_{k-1},t_k)$ without performing $N$ integrations in (4.62) but only once for the $\hat{R}_1$ attitude state. Moreover, the computation of the averaged rotation (4.65) can be simplified by observing that for all $t\in[t_{k-1},t_k)$ one has

$$\begin{aligned}\hat{R}(t)&=\mathbf{P}_{\mathbb{SO}(3)}\left(\sum_{h=1}^{N}\alpha_h\hat{R}_h(t)\right)=\mathbf{P}_{\mathbb{SO}(3)}\left(\sum_{h=1}^{N}\alpha_h\hat{R}_h(t_{k-1}^+)\hat{R}_1(t_{k-1}^+)^\top\hat{R}_1(t)\right)\\&=\mathbf{P}_{\mathbb{SO}(3)}\left(\sum_{h=1}^{N}\alpha_h\hat{R}_h(t_{k-1}^+)\right)\hat{R}_1(t_{k-1}^+)^\top\hat{R}_1(t)\\&:=P(k-1)\hat{R}_1(t)\end{aligned} \tag{4.68}$$

where we used the fact that $\mathbf{P}_{\mathbb{SO}(3)}(XR)=\mathbf{P}_{\mathbb{SO}(3)}(X)R$ for all $X\in\mathbb{R}^{3\times3}$ and $R\in\mathbb{SO}(3)$. Therefore the projection operation $\mathbf{P}_{\mathbb{SO}(3)}\left(\sum_{h=1}^{N}\alpha_h\hat{R}_h(t_{k-1}^+)\hat{R}_1(t_{k-1}^+)^\top\right)$ needs

to be executed at the discrete jump times $t_{k-1}$ only. This resulting matrix $P(k-1) \in \mathbb{SO}(3)$ is stored and then used in (4.68) to provide a correction to $\hat{R}_1(t)$. This avoids to continuously project the mean of rotations in (4.65) for all $t \in [t_{k-1}, t_k)$. Since the attitude state $\hat{R}_h$ needs to be evaluated only at times $t_k^+$, we can define $P_h(k) = \hat{R}_h(t_k^+)$ and use (4.67) to derive the following propagation equation for $P_h(k)$

$$P_h(k) = P_{h-1}(k-1)P_1(k-1)^\top \hat{R}_1(t_k^-), \tag{4.69}$$

for all $h \in \{2, \cdots, N\}$. The new update for $\hat{R}_1$ is given by (4.63). The obtained estimation algorithm is summarized in Algorithm 4.

**Algorithm 4** Attitude Estimation Using Intermittent Synchronized Measurements

Initialize the states $P_1(0), \cdots, P_N(0) \in \mathbb{SO}(3)$.
Compute $P(0) = \mathbf{P}_{\mathbb{SO}(3)}(\sum_{h=1}^N \alpha_h P_h(0)) P_1(0)^\top$.
Set $k = 1$ and $\hat{R}_1(0) = P_1(0)$.

1: **for** each $t \in \mathbb{R}_{\geq 0}$ **do**
2: **if** $t = t_k$ **then**
3: $\hat{R}_1(t^+) = \mathbf{R}_r(\sigma(t))\hat{R}_1(t)$ with $\sigma = \sum_{i=1}^n \rho_i(\hat{R}_1 b_i \times a_i)$.
4: $P_1(k) = \hat{R}_1(t^+)$.
5: **for** each $h \in \{2, \cdots, N\}$ **do**
6: $P_h(k) = P_{h-1}(k-1)P_1(k-1)^\top \hat{R}_1(t)$
7: **end for**
8: $P(k) = \mathbf{P}_{\mathbb{SO}(3)}(\sum_{h=1}^N \alpha_h P_h(k)) P_1(k)^\top$
9: Update $k = k+1$
10: **end if**
11: Predict $\hat{R}_1(t)$ according to $\dot{\hat{R}}_1(t) = \hat{R}_1(t)[\omega(t)]_\times$.
12: Calculate the estimate $\hat{R}(t) = P(k-1)\hat{R}_1(t)$.
13: **end for**

Furthermore, we can also improve the filtering capabilities of the attitude estimation scheme (4.42)-(4.43) which is developed for the case of asynchronous measurements. We follow similar steps as above to derive Algorithm 5. Note that for practical implementation purposes the prediction step in Algorithm 4 or 5 (line 12 or 13) can be discretized as in subsection 4.3.4.1 using Euler-Lie numerical integration method.

#### 4.3.4.3 Smoothing of the Estimator Output

The discrete transitions of the attitude estimates in (4.31) or (4.43) can be undesirable when feeding these states to a controller for feedback. As a remedy, we propose to cascade the proposed attitude estimation algorithms with an attitude "smoother" on $\mathbb{SO}(3)$ to

**Algorithm 5** Attitude Estimation Using Intermittent Asynchronous Measurements

Initialize the states $P_1(0), \cdots, P_N(0) \in \mathbb{SO}(3)$.
Compute $P(0) = \mathbf{P}_{\mathbb{SO}(3)}(\sum_{h=1}^{N} \alpha_h P_h(0)) P_1(0)^\top$.
Set $j = 1$ and $\hat{R}_1(0) = P_1(0)$.

**for** each $t \in \mathbb{R}_{\geq 0}$ **do**
  **if** $t = t_k^i$ for some $k \in \mathbb{N}$ and $i \in \{1, \cdots, n\}$ **then**
    Get $i \in \{1, \cdots, n\}$ s.t. $\exists k \in \mathbb{N}$ and $t = t_k^i$.
    $\hat{R}_1(t^+) = \mathbf{R}_r(\sigma_i)\hat{R}_1(t)$ s.t. $\sigma_i = \rho_i(\hat{R}_1 b_i \times a_i)$.
    $P_1(j) = \hat{R}_1(t^+)$.
    **for** each $h \in \{2, \cdots, N\}$ **do**
      $P_h(j) = P_{h-1}(j-1) P_1(j-1)^\top \hat{R}_1(t)$
    **end for**
    $P(j) = \mathbf{P}_{\mathbb{SO}(3)}(\sum_{h=1}^{N} \alpha_h P_h(j)) P_1(j)^\top$
    Update $j = j + 1$
  **end if**
  Predict $\hat{R}_1(t)$ according to $\dot{\hat{R}}_1(t) = \hat{R}_1(t)[\omega(t)]_\times$.
  Calculate the final estimate $\hat{R}(t) = P(j-1)\hat{R}_1(t)$.
**end for**

obtain a smooth attitude $\hat{R}_s(t)$ that does not involve jumps. The smoother is given by

$$\dot{\hat{R}}_s = \hat{R}_s[\omega + k\psi(\hat{R}_s^\top \hat{R})]_\times, \ \hat{R}_s(0) = \hat{R}(0), \ k > 0, \tag{4.70}$$

where $\hat{R}$ is either the output of Algorithm 1 or Algorithm 2 depending on the application. It is not difficult to show that $\hat{R}_s$ converges to $\hat{R}$ from all initial conditions except those attitudes satisfying $\mathbf{tr}(\hat{R}\hat{R}_s^\top) = -1$ which are characterized by errors of angle strictly less than 180°. Due to the knowledge of $\hat{R}(0)$ (accessible to the designer), the smoother state $\hat{R}_s$ can be initialized to $\hat{R}(0)$ and therefore the initial error between the smoothed attitude $\hat{R}_s$ and the intermittent observer attitude $\hat{R}$ is zero. This implies that the smoother starts inside the region of convergence. Moreover, during the jumps of (4.31), the correction attitude $\mathbf{R}_r(\sigma)$ has an angle which is strictly less than 180°. Therefore, it is guaranteed that the error $\hat{R}\hat{R}_s^\top$ never reaches an attitude of angle 180° which, consequently, shows that the interconnection of the observer-smoother preserves the convergence properties, given in Theorem 4.3.1 and Theorem 4.3.2, for the standalone intermittent observers.

#### 4.3.4.4 Gyro Bias Compensation

The algorithms developed in this section assumed continuous and perfect angular velocity measurements. However, in practice, gyro rates measurements are subject to noise and

bias. If $\omega_y$ is the output of the gyro sensor then one has

$$\omega_y = \omega + b_\omega + n_\omega, \tag{4.71}$$

where $b_\omega$ is a constant bias and $n_\omega$ is a noise vector. Assuming Gaussian processes the uncorrelated noise $n_\omega$ is filtered by the forward integration of the angular velocity and therefore it has a little effect on the attitude estimates. However, bias in the angular rates may cause the attitude estimates to drift over time especially if the sampling of the vector measurements is not fast enough to correct the attitude before it drifts. It is therefore, desirable from a practical point of view and for long run-time applications, to be able to compensate for constant or slowly varying biases in the angular velocity measurements. In the case of *synchronous measurements with regular sampling* equals $T > 0$, we propose the following attitude estimation scheme with bias compensation:

$$\left.\begin{array}{rcl} \dot{\hat{R}}(t) & = & \hat{R}(t)[\omega_y(t) - \hat{b}_\omega(t)]_\times \\ \dot{\hat{b}}_\omega(t) & = & 0 \end{array}\right\} \qquad t \in [t_{k-1}, t_k), \tag{4.72}$$

$$\left.\begin{array}{rcl} \hat{R}(t^+) & = & \mathbf{R}_r\left(\sigma(t)\right)\hat{R}(t) \\ \hat{b}_\omega(t^+) & = & \hat{b}_\omega(t) - \gamma_b T^{-1}\hat{R}(t)^\top \sigma(t) \end{array}\right\} \qquad t = t_k, \tag{4.73}$$

where $k \in \mathbb{N}$, $\gamma_b > 0$ and $\sigma$ is defined in (4.32). Consider the attitude estimations error $\tilde{R} = R\hat{R}^\top$ and the bias estimation error $\tilde{b}_\omega = b_\omega - \hat{b}_\omega$. By introducing the virtual timer variable as in (4.36)-(4.37) and adding $\hat{R}$ and $\omega$ as states variables, the closed-loop system can be written as a hybrid autonomous system as follows

$$\left\{\begin{array}{rcll} \dot{\tilde{R}} & = & \tilde{R}[-\hat{R}\tilde{b}_\omega]_\times & \\ \dot{\tau} & = & 1 & \\ \dot{\tilde{b}}_\omega & = & 0 & (\tilde{R}, \tau, \tilde{b}_\omega, \hat{R}, \omega) \in \mathbb{SO}(3) \times [0, T] \times \mathbb{R}^3 \times \mathbb{SO}(3) \times \mathbb{R}^3, \\ \dot{\hat{R}} & = & \hat{R}[\omega + \tilde{b}_\omega]_\times & \\ \dot{\omega} & \in & c_{\dot{\omega}}\mathbb{B} & \end{array}\right. \tag{4.74}$$

$$\left\{\begin{array}{rcll} \tilde{R}^+ & = & \tilde{R}\mathbf{R}_r(-\sigma), & \\ \tau^+ & = & 0 & \\ \tilde{b}_\omega^+ & = & \tilde{b}_\omega + \gamma_b T^{-1}\hat{R}^\top\sigma & (\tilde{R}, \tau, \tilde{b}_\omega, \hat{R}, \omega) \in \mathbb{SO}(3) \times \{T\} \times \mathbb{R}^3 \times \mathbb{SO}(3) \times \mathbb{R}^3, \\ \hat{R}^+ & = & \mathbf{R}_r(\sigma)\hat{R} & \\ \omega^+ & = & \omega & \end{array}\right. \tag{4.75}$$

where we have used the fact that the angular velocity $\omega$ satisfies Assumption 4.2.2 so that we can write the inclusion $\dot{\omega} \in c_{\dot{\omega}}\mathbb{B}$. The objective of the next Theorem is to state exponential stability of the set

$$\mathcal{A} = \{I\} \times [0, T] \times \{0\} \times \mathbb{SO}(3) \times \mathbb{R}^3. \tag{4.76}$$

**Theorem 4.3.4** *Consider the kinematic system* (4.27) *coupled with the estimator* (4.72)-(4.73) *where Assumptions 4.2.1-4.2.2 are satisfied. Pick the gains $\rho_i$ and $\gamma_b$ such that*

$$0 < \lambda_{\max}^{\mathbf{E}(A)} < \frac{1}{2} \tag{4.77}$$

$$0 < \gamma_b < \frac{2(1 - 2\lambda_{\max}^{\mathbf{E}(A)})}{\lambda_{\max}^{\mathbf{E}(A)}} \tag{4.78}$$

*where $A = \sum_{i=1}^{n} \rho_i a_i a_i^\top$. Then there exists an upper bound $\bar{T}(A, \gamma_b, c_\omega)$ such that if the sampling period $T$ satisfies $0 < T < \bar{T}(A, \gamma_b, c_\omega)$ then the set $\mathcal{A}$ is locally exponentially stable for the closed-loop system* (4.74)-(4.75).

**Proof** Appendix C.11.

Theorem 4.3.4 shows that the attitude and bias estimation scheme in (4.72)-(4.73) is locally exponentially stable if the maximum waiting time interval between two measurements is less than an upper bound which is function of the gains and the bound on the angular velocity. From the proof of Theorem 4.3.4, the upper bound on $T$ can be explicitly computed as follows:

$$\bar{T}(A, \gamma_b, c_\omega) = \frac{-\ln(1 - \lambda_{\min}^{L}/\lambda_{\max}^{P})}{4c_\omega(\lambda_{\max}^{P}/\lambda_{\min}^{P})} \tag{4.79}$$

where $L \in \mathbb{R}^{6\times 6}$ is any positive definite matrix and $P$ is solution to the following discrete Lyapunov equation

$$A_d^\top P A_d - P = -L,$$

such that the matrix $A_d$ is as defined in (C.109). The exact computation of the upper bound $\bar{T}(A, \gamma_b, c_\omega)$ requires to solve the Lyapunov discrete equation for $P$ using knowledge of the stable matrix $A_d$. This computation might be avoided if one uses lower and upper bounds on the eigenvalues of $P$ such as those reported in [Tippett, 1998] which allows to obtain a tighter bound for $T$ than $\bar{T}(A, \gamma_b, c_\omega)$.

The proposed solution to the attitude and gyro bias estimation using intermittent measurements given in this subsection is, to the author's knowledge, unique since the existing litterature on the topic, such as [Barrau and Bonnabel, 2015] and [Khosravian *et al.*, 2015], did not consider the bias in the angular velocity measurements. It is yet an open problem to derive a similar solution for the other more general cases where the measurements are synchronous irregular and/or asynchronous.

### 4.3.5 Simulations

In this section we conduct some simulation scenarios to illustrate the effectiveness of the proposed attitude estimation algorithms in the presence of intermittent vector measurements. We consider a rigid body subject to the angular velocity provided in Figure 4.4.

#### Synchronous measurements

In the first simulation scenario we assume available two sensors that provide two body-frame vector measurements $b_1 = R^\top a_1$ and $b_2 = R^\top a_2$ such that $a_1 = [1, 0, 0]^\top$ and $a_2 = [0, 1, 0]^\top$. The true attitude of the rigid body is initialized at an attitude angle of $150^\circ$ in the $z-$direction, *i.e.,* $R(0) = \exp([\theta u]_\times)$ where $\theta = 10\pi/12$ and $u = [0, 0, 1]^\top$. The actual attitude trajectory is generated using the discrete-kinematic model (4.58) with a sampling period of 1 ms. The measurements are corrupted by a Gaussian white noise of zero mean and variance equals 0.1 in each axis. The information transmission between the sensors and the CPU is done synchronously at a low sampling frequency of 1 Hz which corresponds to a time period of 1 $s$. We also assume that information is lost during the time interval $[40, 60]$ seconds, see Figure 4.10. Now, we need to set the scalar gains $\rho_1$ and $\rho_2$ in (4.32) such that condition (4.41) is satisfied. It can be verified that the maximum eigenvalue of $\mathbf{E}(A)$ corresponds to $(\rho_1 + \rho_2)/2$. Therefore, it is sufficient to pick $(\rho_1 + \rho_2) < 1$ to verify the condition. Here we chose $\rho_1 = \rho_2 = 1/4$. Recursive Algorithm 1 is implemented for different values of $N$ (number of states). The values of the coefficients $\alpha_h$ are selected arbitrary as $\alpha_1 = \cdots = \alpha_N = 1/N$. All the states $P_0, \cdots, P_N, \hat{R}_1$ and $\hat{R}$ are initialized at the identity rotation $I$. Figure 4.11 depicts the evolution of the attitude estimation error, given by the angle of the rotation matrix $\tilde{R}$ in degrees, versus time. For different values of $N$ the proposed algorithm is capable of forgetting the initial attitude error despite the blackout interval (information loss) and the intermittent nature of the measurements. Moreover, it can be seen that as $N$ increases the level of noise in the attitude estimation error is reduced. However, it should

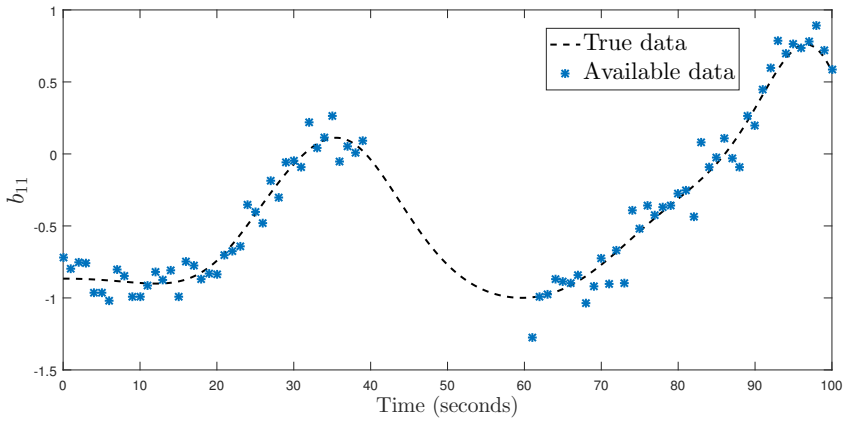


Figure 4.10: Plot of the available information for the x-axis component of $b_1$. Both measurements of $b_1$ and $b_2$ are synchronously obtained at the same instants of time.

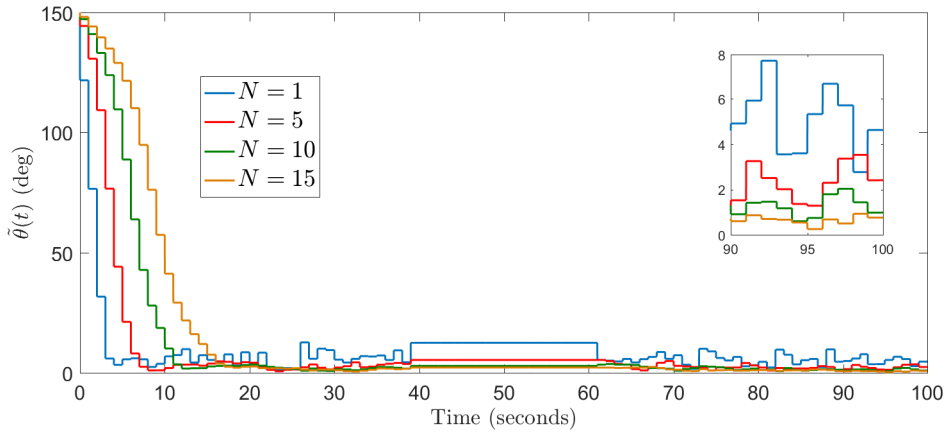


Figure 4.11: Time evolution of the attitude estimation error (angle of rotation) of the attitude estimation scheme proposed in Algorithm 1 using different values of $N$. The region between 90s and 100s is enlarged.

be acknowledged that as $N$ increases the transient response of the estimation algorithm becomes slower. In fact, according to Algorithm 1, in the ideal case when $\hat{R}_1$ converges to $R$, we need $N$ additional steps to guarantee that all the register states $P_1, \cdots, P_N$ converge to $R$ and therefore $\hat{R}$ converges to $R$ as well. Of course these steps depend on the sampling rate of the measurements since the register is updated at each measurement. The smaller the sampling period the smaller the lag introduced by increasing the value of $N$.

**Asynchronous measurements**

In the second simulation scenario we assume available two sensors that provide two body-frame vector measurements $b_1 = R^\top a_1$ and $b_2 = R^\top a_2$ such that $a_1 = [1, 0, 0]^\top$ and $a_2 = [1, 1, 0]^\top/\sqrt{2}$. The true attitude of the rigid body is initialized at $R(0) = \exp([\theta u])$ where $\theta = 10\pi/12 \equiv 150^\circ$ and $u = [1, 1, 1]^\top/\sqrt{3}$. The actual attitude trajectory is generated using the discrete-kinematic model (4.58) with a sampling period of 1 ms. The measurements of $b_1$, respectively $b_2$, are corrupted by a Gaussian white noise of zero mean and standard deviation equals 0.1, respectively 0.01, in each axis. The first sensor provides readings of $b_1$ at a frequency of 10 Hz while the second sensor has a very low sampling rate of 0.1 Hz, see Figure 4.12. The scalar gains $\rho_1$ and $\rho_2$ are chosen to

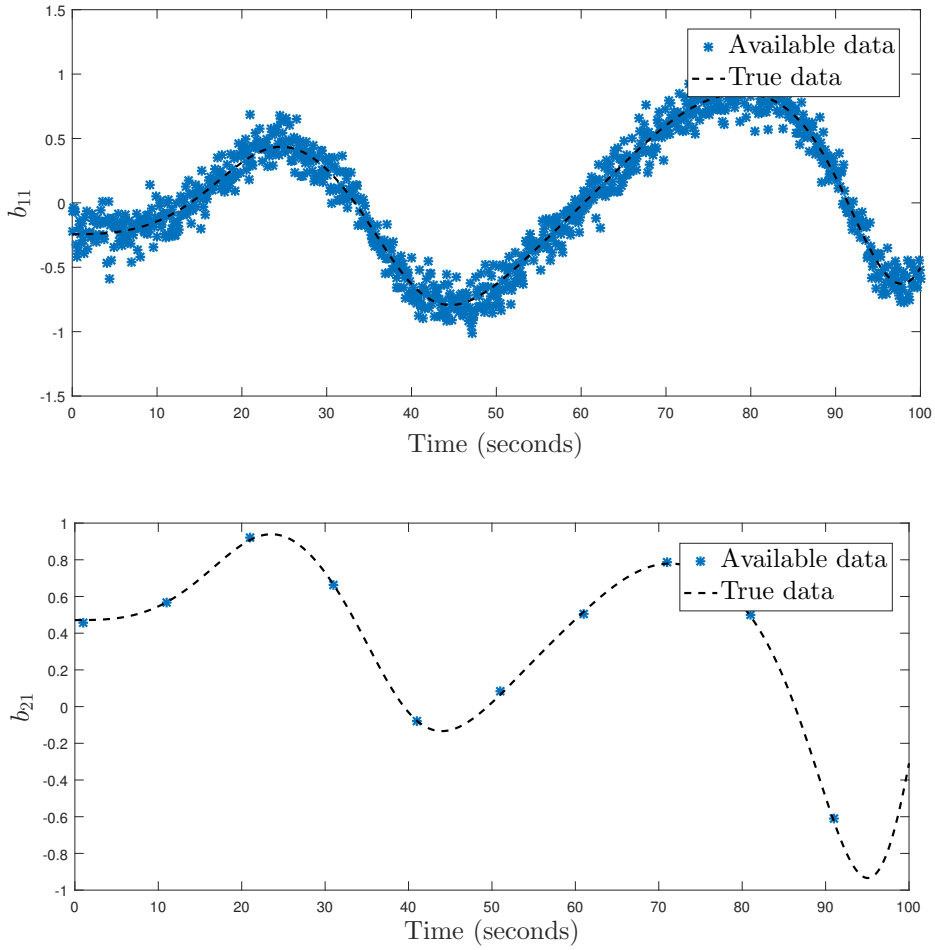


Figure 4.12: Plot of the available information for the x-axis component of $b_1$ (top) and $b_2$ (bottom). The measurements are collected asynchronously at different sampling rates.

satisfy the condition (4.50). We thus set $\rho_1 = 1/4$ and $\rho_2 = 2/3$. The gain $\rho_2$ associated

to the measurements of $b_2$ is set relatively higher than $\rho_1$ since the measurements of $b_2$ are more reliable (less noisy). Recursive Algorithm 2 is implemented for different values of $N$ (number of states). The values of the coefficients $\alpha_h$ are selected arbitrary as $\alpha_1 = \cdots = \alpha_N = 1/N$. All the states $P_0, \cdots, P_N, \hat{R}_1$ and $\hat{R}$ are initialized at the identity rotation $I$. Figure 4.13 depicts the evolution of the attitude estimation error, given by

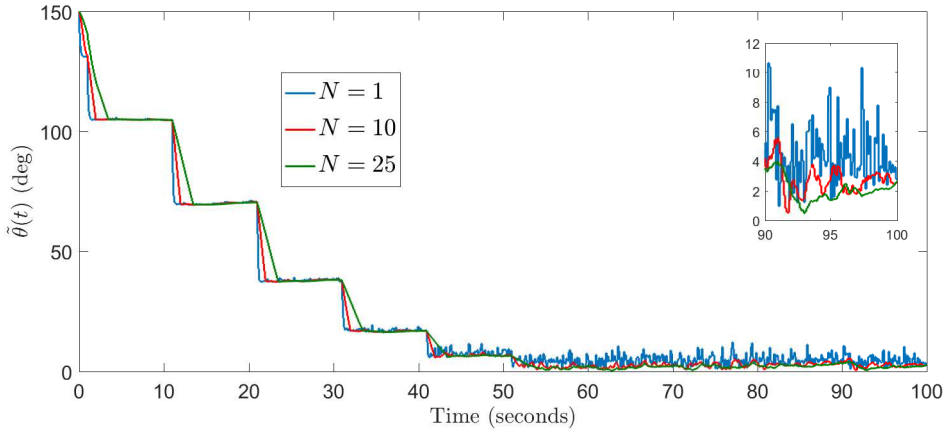


Figure 4.13: Time evolution of the attitude estimation error (angle of rotation) of the attitude estimation scheme proposed in Algorithm 2 using different values of $N$. The region between 90s and 100s is enlarged.

the angle of the rotation matrix $\tilde{R}$ in degrees, against time. For different values of $N$ the proposed algorithm is capable of forgetting the initial attitude error despite the fact that the measurements have different sampling periods (angular velocity $\omega$ at 200 Hz, vector measurement $b_1$ at 10 Hz and $b_2$ at 0.1 Hz). Note that the use of a single sensor is not enough to correct the attitude. Although sensor $b_2$ has a very large sampling period of 10 seconds, it helps to reduce the attitude error in the direction parallel to $a_1$ since the latter direction can not be corrected using measurements of $b_1$. In fact, when $\tilde{R}$ has a rotation axis parallel to $a_1$ then we have $\sigma_1 = \rho_1(\hat{R}b_1 \times a_1) = 0$ which implies that no correction occurs using this measurement. Note that the register states $P_1, \cdots, P_N$ are updated at each measurement step (readings of $b_1$ or $b_2$) thus the update has a frequency greater than or equal to the largest measurements frequency (in our case 10 Hz). In other words, the lag introduced by increasing $N$ is proportional to the smallest sampling period. As a consequence the transient response when $N = 25$ is not very slow compared to $N = 1$ while the level of steady state noise is largely reduced ($10^\circ$ for $N = 1$ compared to $2^\circ$ for $N = 25$). Future work may include the search for the best value of $N$ as well as the corresponding coefficients $\alpha_1, \cdots, \alpha_N$ in order to optimize the performance of the algorithm with respect to the sensors' characteristics.

**Biased angular velocity measurements**

In this simulation scenario we assume that the angular velocity measurements are biased with a constant bias $b_\omega = [0.05, 0.05, 0.05]^\top$ (rad/sec). We assume available two sensors that provide two body-frame vector measurements $b_1 = R^\top a_1$ and $b_2 = R^\top a_2$ such that $a_1 = [1, 0, 0]^\top$ and $a_2 = [0, 1, 0]^\top$. The true attitude of the rigid body is initialized at an attitude angle of 45° in the $z-$direction, *i.e.,* $R(0) = \exp([\theta u]_\times)$ where $\theta = \pi/4$ and $u = [0, 0, 1]^\top$. The actual attitude trajectory is generated using the discrete-kinematic model (4.58) with a sampling period of 1 ms. The observers states are initialized at $\hat{R}(0) = I$ and $\hat{b}_\omega = [0, 0, 0]^\top$ (rad/sec). Note that although in Theorem 4.3.4 we provide only a proof of local exponential convergence for the observer (4.72)-(4.73), the chosen initial attitude error (45° angle) is large which suggests that the region of convergence of the proposed estimation scheme is large. Now, we set the the observer gains as $\rho_1 = \frac{1}{4}$, $\rho_2 = \frac{1}{2}$ and $\gamma_b = 0.5$ which satisfy the conditions of Theorem 4.3.4. To find the maximum allowed sampling period $T$ we compute the upper bound $\bar{T}$ in (4.79). The corresponding matrix $A_d$ can be computed form (C.109) and the solution of the discrete Lyapunov equation is derived by pick $L = I$. We obtain a matrix $P$ such that $\lambda^P_{\max} = 4.8895$ and $\lambda^P_{\min} = 1$. The angular velocity bound $c_\omega$ is chosen as $c_\omega = 0.5$ which is a very conservative bound on the norm of the angular velocity. Therefore on obtains the condition on $T$

$$T < \bar{T}(A, \gamma_b, c_\omega) = 0.0234 \text{ seconds.} \tag{4.80}$$

The above is a conservative bound on the allowable sampling period which guarantees local convergence of the attitude observer. To show that our observer works even when the above bound is not satisfied, we pick different values of $T$ between 0.02 and 5 seconds. Simulation results are plotted in Figure 4.14 and (4.15) which shows convergences of the attitude and bias estimation errors as zero. These simulation results suggest that a larger bound on the allowable sampling period $T$ exists, however it remains an open problem to find the least conservative bound. Of course for larger values of the sampling period $T$, the convergence is slower since fewer correction steps are executed in (4.72)-(4.73).

## 4.4 Conclusion

We dealt with the problem of attitude estimation on $\mathbb{SO}(3)$ using intermittent synchronous and asynchronous vector measurements. The problem formulation takes into account some practical constraints related to the sensors bandwidth and measurements loss. The proposed hybrid attitude estimation scheme has a measurement-triggered struc-

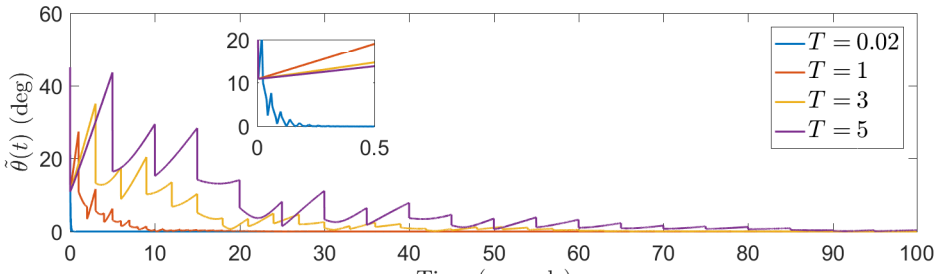


Figure 4.14: Time evolution of the attitude estimation error (angle of rotation) for the observer proposed in (4.72)-(4.73) using different sampling periods $T$.

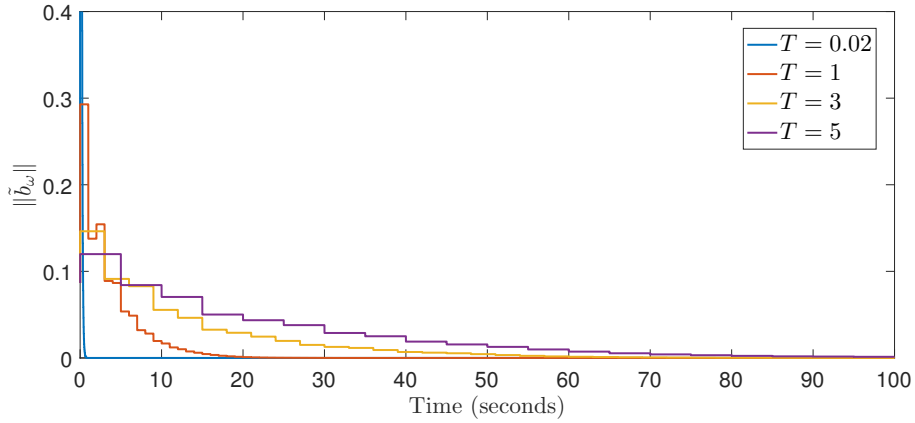


Figure 4.15: Time evolution of the bias estimation error for the observer proposed in (4.72)-(4.73) using different sampling periods $T$. The region between 0 and 0.5 seconds is enlarged.

ture where the continuous-time angular velocity is used to predict the rotation matrix which is corrected by the discrete vector measurements upon their arrival. Virtual timers are introduced to capture the behaviour of the closed-loop system by a time-invariant hybrid dynamical model, and almost global asymptotic stability results are established under some sufficient conditions on the gains that are independent from the communication protocol between the CPU and the sensors (sampling constraints). Discrete integration an filtering techniques have also been proposed to improve the computational efficiency and noise attenuation of the proposed attitude estimation schemes.

# Chapter 5

# Conclusion

## 5.1 Summary

In Chapter 2, some preliminary results and useful lemmas on the rotation group $\mathbb{SO}(3)$ have been presented. Some of these results are newly derived in this thesis and can be used for the design and analysis of control systems on $\mathbb{SO}(3)$. Moreover, the hybrid systems framework, used in this thesis, which is mainly inspired from [Goebel *et al.*, 2012] and related works has been recalled. A new result concerning exponential stability of general hybrid systems is derived. Our proposed theorem relaxed, for certain class of hybrid systems, some previously developed Lyapunov-based sufficient conditions for exponential stability. These derived sufficient conditions for exponential stability are then used in the thesis to analysis the stability of some closed-loop systems.

Chapter 3 was devoted to the problem of attitude control on $\mathbb{SO}(3)$. The simple example of the unit circle $\mathbb{S}^1$, which is a submanifold of $\mathbb{SO}(3)$, was used as a motivation. It helped to explain the limitations of existing smooth and discontinuous feedbacks and motivated the use of hybrid controllers to solve the problem of global exponential stabilization on compact manifolds such as $\mathbb{SO}(3)$. The new definition of "exp-synergistic" potential functions has been proposed which, roughly speaking, means a family of (smooth or nonsmooth) potential functions on $\mathbb{SO}(3)$ that enjoys the following properties: (1) being quadratic (as well as their gradients) with respect to an attitude distance, and (2) being synergistic[1] with respect to the gradient's singular and/or critical points. Then, we showed that exp-synergistic potential functions are sufficient to design a hybrid controller guaranteeing global exponential stability on $\mathbb{SO}(3)$. The proposed hybrid controller, which is inspired from [Mayhew and Teel, 2011c], consists of a family of control

[1]The definition of "synergistic" potential functions is given in Definition 3.3.6 and can be found in reference [Mayhew and Teel, 2011c, Mayhew and Teel, 2013a].

laws (each derived from a potential function within the family of exp-synergistic potential functions) which are coordinated in a suitable manner. The hybrid controller selects the control law corresponding to the potential function which has the minimal value among the family. The min-switch mechanism has a hysteresis property that guarantees some level of robustness to measurement noise. We proposed a systematic methodology to construct exp-synergistic potential functions from existing (traditional) smooth and non-smooth potential functions on $\mathbb{SO}(3)$. The construction is done by applying an adequate transformation on $\mathbb{SO}(3)$ that stretches and compresses the manifold in a way to relocate the undesired critical and singular points. This transformation is different from the one proposed in [Mayhew and Teel, 2011d] and allows to explicitly derive the parameters of the hybrid controller (*e.g.,* synergistic gap). Finally, the proposed control strategy is applied to the attitude tracking problem for rigid body systems. The resulting hybrid tracking algorithm is made continuous by filtering the discrete transitions in the controller using a first order low pass filter. We proved that global exponential convergence of the tracking errors to zero is preserved.

The attitude estimation problem has been investigated in Chapter 4. The first objective in this chapter was to derive globally exponentially stable hybrid attitude and gyro bias observers, developed directly on $\mathbb{SO}(3)$, using continuous sensor measurements. Our motivation was driven by the fact that existing attitude observers on $\mathbb{SO}(3)$ are limited in terms of their domain of convergence (local or almost global) and exhibit some robustness and performance issues such as those discussed in our paper [Berkane and Tayebi, 2017a]. To achieve this first objective, we propose two hybrid attitude estimation schemes. The first scheme uses the concept of exp-synergistic potential functions, discussed in Chapter 3, to derive a family of innovation (correction) terms for an attitude observer that has a similar structure as the nonlinear complementary filter on $\mathbb{SO}(3)$. It is shown that the exp-synergistic potential functions and their gradients, derived in Chapter 3, can be explicitly written in terms of body-frame vector measurements of known constant inertial vectors. Therefore, the proposed hybrid observer can be readily implemented using available sensors depending on the application at hand. The second scheme uses rather a fixed innovation term for the attitude observer but, however, allows the attitude state to experience jumps. This reset behaviour of the attitude estimated matrix is done adequately to guarantee that, after a jump, a given cost function is within the flow set. The main purpose behind this reset-based approach is to avoid the undesired critical/singular points of the cost function on $\mathbb{SO}(3)$ by simply jumping the attitude estimate to a region where these undesired points do not belong. The advantage of the reset-based technique over the synergistic-based technique resides in the design simplicity and the possibility of

using time-varying inertial vectors. However, the reset-based approach comes at the cost of having possible discrete transitions in the observer output which might be undesirable in practice when connecting the observer to the controller. The good news is that this potential jumps are not likely to occur when the attitude estimation errors are small (an observer operating near the true state values).

The second objective of Chapter 4 was to design attitude estimation schemes on $\mathbb{SO}(3)$ that deal with the problem where the measurements are allowed to have different bandwidths with possible information loss between the sensor and the control processing unit. There are very few references that have dealt with this problem [Khosravian *et al.*, 2015, Barrau and Bonnabel, 2015]. At a first step, we have considered the simplified problem where the measurements are collected synchronously at possibly irregular sampling periods. We also assumed that the angular velocity measurements are unbiased and available continuously. The last assumption is motivated by the high sampling frequency of most existing commercial gyroscopes compared to other sensors such as landmarks, GPS,...*etc.* We proposed a measurement-triggered observer which consists of forward integration on $\mathbb{SO}(3)$ of the continuous angular velocity and intermittent correction of the attitude estimate at the arrival of the new measurements. Both the integration (prediction) and the correction steps are done in a way to keep the attitude estimates within the rotation group $\mathbb{SO}(3)$. To analyze the stability of the closed-loop system, we proposed to extend the system with a virtual timer to capture the behaviour of the communication protocol. The virtual time is reset at each time when the measurements are received. The extended closed-loop system is modelled as an autonomous hybrid system which allowed for hybrid systems tools to be applied to conduct the stability proofs. We showed that the zero estimation error is almost globally exponentially stable. Secondly, we considered the more general case where the measurements are collected asynchronously (at different sampling periods). In this case the observer state is updated at the arrival of each single measurement. A virtual timer is introduced for each sensor to model the communication protocol between that sensor and the processing unit. Again the closed-loop system is modelled as a hybrid system and almost global asymptotic stability is concluded using the invariance principle for hybrid systems. Finally, some practical issues have been considered. First, when the gyro readings are biased we proposed an extended measurement-triggered observer on $\mathbb{SO}(3) \times \mathbb{R}^3$ to estimate both the attitude state and the gyro bias vector. We were able to prove local exponential convergence to zero of the estimation errors only in the case where the measurements are synchronously collected at a constant sampling period. A second practical consideration is the effect of measurement noise on the output of the observer. We extended the observer with $N \geq 1$

states on $\mathbb{SO}(3)$ which are recursively updated and averaged to yield a better estimate. We also proposed a discrete version of the observer which is obtained by discretizing the integrator on $\mathbb{SO}(3)$ using a first order Lie group integration method. The discrete version of the observer preserves the convergence properties of the original version of the observer which is an advantage over most existing attitude estimation schemes on $\mathbb{SO}(3)$.

## 5.2 Perspectives

In many systems of practical and theoretical interest, the configuration space of the system can be given the structure of a Lie group. Examples include unmanned aerial vehicles, underwater vehicles, satellites and surface vessels. A future direction is to extend the synergistic hybrid control strategy, developed on $\mathbb{S}^1, \mathbb{S}^2$ and $\mathbb{SO}(3)$ to fully-actuated mechanical systems, when the configuration space is a general class of Lie groups, in a differential geometric setting such as in [Maithripala *et al.*, 2006, Chaturvedi *et al.*, 2006]. This requires to define intrinsic potential functions on a Lie group and propose an efficient way to obtain the corresponding synergistic family via angular warping. This task is challenging due to the difficulty in proving the synergism property on a general Lie group and the fact that most compact identities used on $\mathbb{SO}(3)$, for instance, are not available on a general Lie group. We wish as well to propose a unified framework for the construction of hybrid, continuous and possibly smooth controllers for general mechanical systems evolving on a Lie group.

In addition to the above future directions, the following are few perspectives "closely" related to this thesis:

- In Section 3.3.5, we have successfully constructed two exp-synergistic families of weighted potential functions but under the full knowledge of the eigenvalues and eigenvectors of the matrix $A$. It would be interesting to derive weighted exp-synergistic functions without requiring information about the spectrum of the weighting matrix which might simplify the design process. Also, recall that these exp-synergistic potential functions were used in Section 4.2 to derive attitude observers using directly vector measurements. The weighting matrix $A$ was directly related to the known and constant inertial vectors. In some applications, these vectors are unknown or time varying which is obstacle towards the use of this class of exp-synergistic potential functions.

- In certain applications, the information about the inertia matrix is uncertain. An interesting direction is to make robust the proposed hybrid tracking control algo-

rithms using some adaptation laws for the inertia matrix while maintaining the strong stability results.

- The proposed measurement-triggered observers are shown to have almost global convergence properties. It is possible to extend these observers with a switching mechanism (such as the reset-based approach) to enlarge the domain of convergence to global. Moreover, it remains an open problem to estimate the region of convergence of the proposed intermittent observer with bias estimation. We have shown local exponential convergence only in the particular case of synchronous measurement with constant sampling rate. Other more general cases where the measurements are asynchronous and/or the sampling rate is irregular remains unsolved. Simulations results, however, are very promising.

# Bibliography

[Andrieu *et al.*, 2013] Andrieu, V., Nadri, M., Serres, U., and Vivalda, J.-C. (2013). Continuous Discrete Observer with Updated Sampling Period. In *Proceedings of the IFAC Symposium on Nonlinear Control System*, pages 439–444.

[Arfken *et al.*, 1999] Arfken, G. B., Weber, H. J., and Spector, D. (1999). Mathematical methods for physicists. *American Journal of Physics*, 67(2):165–169.

[Barrau and Bonnabel, 2015] Barrau, A. and Bonnabel, S. (2015). Intrinsic Filtering on Lie Groups With Applications to Attitude Estimation. *IEEE Transactions on Automatic Control*, 60(2):436–449.

[Barrau and Bonnabel, 2017] Barrau, A. and Bonnabel, S. (2017). The Invariant Extended Kalman Filter as a Stable Observer. *IEEE Transactions on Automatic Control*, 62(4):1797–1812.

[Batista *et al.*, 2012a] Batista, P., Silvestre, C., and Oliveira, P. (2012a). Globally exponentially stable cascade observers for attitude estimation. *Control Engineering Practice*, 20(2):148–155.

[Batista *et al.*, 2012b] Batista, P., Silvestre, C., and Oliveira, P. (2012b). Sensor-based globally asymptotically stable filters for attitude estimation: Analysis, design, and performance evaluation. *IEEE Transactions on Automatic Control*, 57(8):2095–2100.

[Bayadi and Banavar, 2014] Bayadi, R. and Banavar, R. N. (2014). Almost global attitude stabilization of a rigid body for both internal and external actuation schemes. *European Journal of Control*, 20(1):45–54.

[Berkane *et al.*, 2017a] Berkane, S., Abdessameud, A., and Tayebi, A. (2017a). Hybrid Attitude and Gyro-bias Observer Design on $SO(3)$. *IEEE Transactions on Automatic Control.*, 62(11):6044 – 6050.

[Berkane *et al.*, 2017b] Berkane, S., Abdessameud, A., and Tayebi, A. (2017b). Hybrid Global Exponential Stabilization on $SO(3)$. *Automatica*, 81:279–285.

[Berkane and Tayebi, 2015a] Berkane, S. and Tayebi, A. (2015a). On the Design of Synergistic Potential Functions on $SO(3)$. In *Proceedings of the Conference on Decision and Control*, volume 1, pages 270–275.

[Berkane and Tayebi, 2015b] Berkane, S. and Tayebi, A. (2015b). Some Optimization Aspects on the Lie Group $SO(3)$. In *IFAC Symposium on Information Control in Manufacturing , Ottawa*, pages 1173–1177.

[Berkane and Tayebi, 2016] Berkane, S. and Tayebi, A. (2016). On Deterministic Attitude Observers on the Special Orthogonal Group $SO(3)$. In *Proceedings of the Conference on Decision and Control*, pages 1165–1170.

[Berkane and Tayebi, 2017a] Berkane, S. and Tayebi, A. (2017a). On the Design of Attitude Complementary Filters on $SO(3)$. *IEEE Transactions on Automatic Control (to appear).*

[Berkane and Tayebi, 2017b] Berkane, S. and Tayebi, A. (2017b). Attitude and Gyro-bias Estimation Using GPS and IMU Measurements. In *Proceedings of the Conference on Decision and Control*.

[Berkane and Tayebi, 2017c] Berkane, S. and Tayebi, A. (2017c). Attitude Estimation With Intermittent Measurements. *Submitted to Automatica*.

[Berkane and Tayebi, 2017d] Berkane, S. and Tayebi, A. (2017d). Attitude Observer Using Synchronous Intermittent Vector Measurements. In *Proceedings of the Conference on Decision and Control*.

[Berkane and Tayebi, 2017e] Berkane, S. and Tayebi, A. (2017e). Construction of Synergistic Potential Functions on $SO(3)$ with Application to Velocity-Free Hybrid Attitude Stabilization. *IEEE Transactions on Automatic Control*, 62(1):495–501.

[Brodtkorb *et al.*, 2015] Brodtkorb, A. H., Teel, A. R., and Sørensen, A. J. (2015). Sensor-based Hybrid Observer for Dynamic Positioning. In *Proceedings of the Conference on Decision and Control*, pages 948–953.

[Bullo, 2005] Bullo, F. (2005). *Geometric control of mechanical systems*, volume 49. Springer Science & Business Media.

[Bullo and Murray, 1995] Bullo, F. and Murray, R. (1995). Proportional derivative (pd) control on the euclidean group. In *Proceedings of the European Control Conference*, volume 2, pages 1091–1097.

[Bullo and Murray, 1999] Bullo, F. and Murray, R. M. (1999). Tracking for fully actuated mechanical systems : a geometric framework. *Automatica*, 35:17–34.

[Cai and Teel, 2009] Cai, C. and Teel, A. R. (2009). Characterizations of input-to-state stability for hybrid systems. *Systems & Control Letters*, 58(1):47–53.

[Casau *et al.*, 2015a] Casau, P., Mayhew, C. G., Sanfelice, R. G., and Silvestre, C. (2015a). Global exponential stabilization on the n-dimensional sphere. In *Proceedings of the American Control Conference*, pages 3218–3223.

[Casau *et al.*, 2015b] Casau, P., Sanfelice, R. G., Cunha, R., and Silvestre, C. (2015b). A globally asymptotically stabilizing trajectory tracking controller for fully actuated rigid bodies using landmark-based information. *International Journal of Robust and Nonlinear Control*, 25(18):3617–3640.

[Celledoni *et al.*, 2014] Celledoni, E., Marthinsen, H., and Owren, B. (2014). An introduction to Lie group integrators C basics , new developments and applications. *Journal of Computational Physics*, 257:1040–1061.

[Chaturvedi *et al.*, 2011] Chaturvedi, N., Sanyal, A., and McClamroch, N. (2011). Rigid-body attitude control. *IEEE Control Systems Magazine*, 31(3):30 – 51.

[Chaturvedi *et al.*, 2006] Chaturvedi, N. A., Bloch, A. M., and McClamroch, N. H. (2006). Global stabilization of a fully actuated mechanical system on a riemannian manifold: controller structure. In *Proceedings of the American Control Conference*, pages 3612–3617.

[Choukroun, 2009] Choukroun, D. (2009). Novel stochastic modeling and filtering of the attitude quaternion. *The Journal of the Astronautical Sciences*, 57(1-2):167–189.

[Crassidis *et al.*, 2007] Crassidis, J., Markley, F., and Cheng, Y. (2007). Survey of nonlinear attitude estimation methods. *Journal of Guidance Control and Dynamics*, 30(1):12.

[Crouch and Grossman, 1993] Crouch, P. E. and Grossman, R. (1993). Numerical Integration of Ordinary Differential Equations on Manifolds. *J. Nonlinear Sci.*, 3:1–33.

[Darryl D. Holm and Stoica, 2009] Darryl D. Holm, T. S. and Stoica, C. (2009). *Geometric Mechanics and Symmetry. From Finite to Infinite Dimensions*. Oxford University Press.

[Davatzikos, 1997] Davatzikos, C. (1997). Spatial transformation and registration of brain images using elastically deformable models. *Computer Vision and Image Understanding*, 66(2):207–222.

[Egeland and Godhavn, 1994] Egeland, O. and Godhavn, J. M. (1994). Passivity-Based Adaptive Attitude Control of a Rigid Spacecraft. *IEEE Transactions on Automatic Control*, 39(4):842–846.

[Elger and Roberson, 2013] Elger, D. F. and Roberson, J. A. (2013). *Engineering fluid mechanics*. Wiley Hoboken (NJ).

[Ferrante *et al.*, 2016] Ferrante, F., Gouaisbaut, F., Sanfelice, R. G., and Tarbouriech, S. (2016). State estimation of linear systems in the presence of sporadic measurements. *Automatica*, 73:101–109.

[Fjellstad and Fossen, 1994] Fjellstad, O. E. and Fossen, T. I. (1994). Quaternion feedback regulation of underwater vehicles. In *Proceedings of International Conference on Control and Applications*, pages 857–862 vol.2.

[Forbes, 2013] Forbes, J. R. (2013). Passivity-Based Attitude Control on the Special Orthogonal Group of Rigid-Body Rotations. *Journal of Guidance, Control, and Dynamics*, 36(6):1596–1605.

[Goebel *et al.*, 2009] Goebel, R., Sanfelice, R. G., and Teel, A. R. (2009). Hybrid dynamical systems. *IEEE Control Systems Magazine*, 29(2):28–93.

[Goebel *et al.*, 2012] Goebel, R., Sanfelice, R. G., and Teel, A. R. (2012). *Hybrid Dynamical Systems: modeling, stability, and robustness*. Princeton University Press.

[Goebel and Teel, 2006] Goebel, R. and Teel, A. (2006). Solutions to hybrid inclusions via set and graphical convergence with stability theory applications. *Automatica*, 42:573–587.

[Grip *et al.*, 2012a] Grip, H. F., Fossen, T., Johansen, T. A., Saberi, A., et al. (2012a). Attitude estimation using biased gyro and vector measurements with time-varying reference vectors. *IEEE Transactions on Automatic Control*, 57(5):1332–1338.

[Grip *et al.*, 2012b] Grip, H. F., Fossen, T. I., Johansen, T. a., and Saberi, A. (2012b). A nonlinear observer for integration of GNSS and IMU measurements with gyro bias estimation. In *Proceedings of the American Control Conference*, pages 4607–4612.

[Hadidi and Schwartz, 1979] Hadidi, M. and Schwartz, S. (1979). Linear recursive state estimators under uncertain observations. *IEEE Transactions on Automatic Control*, 24(6):944–948.

[Hartley *et al.*, 2013] Hartley, R., Trumpf, J., Dai, Y., and Li, H. (2013). Rotation Averaging. *International journal of computer vision*, 103(3):267–305.

[Helmke and Moore, 1994] Helmke, U. and Moore, J. (1994). *Optimization and Dynamical Systems*. New york: Springer.

[Hoag, 1963] Hoag, D. (1963). Apollo guidance and Navigation: Considerations of apollo imu gimbal lock. *Canbridge: MIT Instrumentation Laboratory*, pages 1–64.

[Hua, 2010] Hua, M. D. (2010). Control Engineering Practice Attitude estimation for accelerated vehicles using GPS / INS measurements. *Control Engineering Practice*, 18(7):723–732.

[Hughes, 1986] Hughes, P. (1986). *Spacecraft attitude dynamics*. John Wiley & Sons Inc.

[Itô, 1993] Itô, K. (1993). *Encyclopedic dictionary of mathematics*, volume 1. MIT press.

[Izadi and Sanyal, 2014] Izadi, M. and Sanyal, A. K. (2014). Rigid body attitude estimation based on the lagrange–dalembert principle. *Automatica*, 50(10):2570–2577.

[Jentzen *et al.*, 2010] Jentzen, A., Leber, F., Schneisgen, D., Berger, A., and Siegmund, S. (2010). An improved maximum allowable transfer interval for Lp-Stability of networked control systems. *IEEE Transactions on Automatic Control*, 55(1):179–184.

[Joshi *et al.*, 1995] Joshi, S., Kelkar, A., and Wen, J.-Y. (1995). Robust attitude stabilization of spacecraft using nonlinear quaternion feedback. *IEEE Transactions on Automatic Control*, 40(10):1800–1803.

[Khosravian *et al.*, 2015] Khosravian, A., Trumpf, J., Mahony, R., and Hamel, T. (2015). Recursive Attitude Estimation in the Presence of Multi-rate and Multi-delay Vector Measurements. In *Proceedings of the American Control Conference*, pages 3199–3205.

[Koditschek, 1988] Koditschek, D. E. (1988). Application of a new lyapunov function to global adaptive attitude tracking. In *Proceedings of the Conference on Decision and Control*, pages 63–68.

[Kreutz and Wen, 1988] Kreutz, K. and Wen, J. T. (1988). Attitude control of an object commonly held by multiple robot arms: A lyapunov approach. In *Proceedings of the American Control Conference*, pages 1790–1794.

[Krstic *et al.*, 1995] Krstic, M., Kanellakopoulos, I., and Kokotovic, P. V. (1995). *Nonlinear and adaptive control design*. Wiley.

[Lang, 1987] Lang, S. (1987). *Linear Algebra, 3rd Edition*. Springer-Verlag.

[Lee, 2012] Lee, T. (2012). Exponential stability of an attitude tracking control system on $SO(3)$ for large-angle rotational maneuvers. *Systems & Control Letters*, 61(1):231–237.

[Lee, 2015] Lee, T. (2015). Global exponential attitude tracking controls on $SO(3)$. *IEEE Transactions on Automatic Control*, 60(10):2837–2842.

[Lizarralde and Wen, 1996] Lizarralde, F. and Wen, J. (1996). Attitude control without angular velocity measurement: A passivity approach. *IEEE Transations on Automatic Control*, 41(3):46817–472.

[Mahony *et al.*, 2008] Mahony, R., Hamel, T., and Pflimlin, J.-M. (2008). Nonlinear complementary filters on the special orthogonal group. *IEEE Transactions on Automatic Control*, 53(5):1203–1218.

[Maithripala *et al.*, 2006] Maithripala, D. S., Berg, J. M., and Dayawansa, W. P. (2006). Almost-global tracking of simple mechanical systems on a general class of lie groups. *IEEE Transactions on Automatic Control*, 51(2):216–225.

[Markley, 1988] Markley, F. (1988). Attitude determination using vector observations and the singular value decomposition. *Journal of the Astronautical Sciences*, 36:245–258.

[Markley, 2003] Markley, F. (2003). Attitude error representations for kalman filtering. *Journal of Guidance, Control, and Dynamics*, 63(2):311–317.

[Markley, 2006] Markley, F. L. (2006). Attitude filtering on $SO(3)$. *The Journal of the Astronautical Sciences*, 54(3):391–413.

[Martin and Salaün, 2008] Martin, P. and Salaün, E. (2008). An Invariant Observer for Earth-Velocity-Aided Attitude Heading Reference Systems. *Proceedings of the 17th IFAC World Congress*, pages 9857–9864.

[Masten, 2008] Masten, M. (2008). Inertially stabilized platforms for optical imaging systems. *IEEE Control Systems Magazine*, 28(1):47–64.

[Mayhew, 2010] Mayhew, C. G. (2010). *Hybrid Control for Topologically Constrained Systems*. PhD thesis, UC Santa Barbara.

[Mayhew *et al.*, 2008] Mayhew, C. G., Sanfelice, R. G., and Teel, A. R. (2008). Robust hybrid source-seeking algorithms based on directional derivatives and their approximations. In *Proceedings of the Conference on Decision and Control*, pages 1735–1740.

[Mayhew *et al.*, 2011] Mayhew, C. G., Sanfelice, R. G., and Teel, A. R. (2011). Quaternion-based hybrid control for robust global attitude tracking. *IEEE Transactions on Automatic Control*, 56:2555–2566.

[Mayhew and Teel, 2011a] Mayhew, C. G. and Teel, A. (2011a). On the topological structure of attraction basins for differential inclusions. *Systems & Control Letters*, 60(12):1045–1050.

[Mayhew and Teel, 2013a] Mayhew, C. G. and Teel, A. (2013a). Synergistic hybrid feedback for global rigid-body attitude tracking on $SO(3)$. *IEEE Transactions on Automatic Control*, 58(11):2730–2742.

[Mayhew and Teel, 2010] Mayhew, C. G. and Teel, A. R. (2010). Hybrid control of planar rotations. In *Proceedings of the American Control Conference*, pages 154–159.

[Mayhew and Teel, 2011b] Mayhew, C. G. and Teel, A. R. (2011b). Hybrid control of rigid-body attitude with synergistic potential functions. In *Proceedings of the American Control Conference*, pages 287–292.

[Mayhew and Teel, 2011c] Mayhew, C. G. and Teel, A. R. (2011c). Hybrid control of rigid-body attitude with synergistic potential functions. In *Proceedings of the American Control Conference*, pages 287–292.

[Mayhew and Teel, 2011d] Mayhew, C. G. and Teel, A. R. (2011d). Synergistic potential functions for hybrid control of rigid-body attitude. In *Proceedings of the American Control Conference*, pages 875–880.

[Mayhew and Teel, 2013b] Mayhew, C. G. and Teel, A. R. (2013b). Global stabilization of spherical orientation by synergistic hybrid feedback with application to reduced-attitude tracking for rigid bodies. *Automatica*, 49(7):1945–1957.

[Meyer, 1971] Meyer, G. (1971). *Design and global analysis of spacecraft attitude control systems*. National Aeronautics and Space Administration, Ames Research Center.

[Morse, 1934] Morse, M. (1934). *The calculus of variations in the large*, volume 18. American Mathematical Soc.

[Mueller *et al.*, 2016] Mueller, M. W., Hehn, M., and DAndrea, R. (2016). Covariance correction step for kalman filtering with an attitude. *Journal of Guidance, Control, and Dynamics*.

[Munthe-Kaas, 1995] Munthe-Kaas, H. (1995). LIE-BUTCHER THEORY FOR RUNGE-KUTTA METHODS. *BIT*, 35:572–587.

[Munthe-Kaas, 1998] Munthe-Kaas, H. (1998). RUNGE-KUTTA METHODS ON LIE GROUPS. *BIT*, 381:92–111.

[Munthe-Kaas, 1999] Munthe-Kaas, H. (1999). High order Runge-Kutta methods on manifolds. *Applied Numerical Mathematics*, 29:115–127.

[Murray *et al.*, 1994] Murray, R., Li, Z., and Sastry, S. (1994). *A mathematical introduction to robotic manipulation*. CRC press.

[Nahi, 1969] Nahi, N. (1969). Optimal recursive estimation with uncertain observation. *IEEE Transactions on Information Theory*, 15(4):457–462.

[Osborne *et al.*, 2008] Osborne, J., Hicks, G., and Fuentes, R. (2008). Global analysis of the double-gimbal mechanism. *IEEE Control Systems Magazine*, 28(4):44–64.

[Pettersen and Egeland, 1999] Pettersen, K. Y. and Egeland, O. (1999). Time-Varying Exponential Stabilization of the Position and Attitude of an Underactuated Autonomous Underwater Vehicle. *IEEE Transactions on Automatic Control*, 44(1):112–115.

[Plarre and Bullo, 2009] Plarre, K. and Bullo, F. (2009). On Kalman Filtering for Detectable Systems With Intermittent Observations. *IEEE Transactions on Automatic Control*, 54(2):386–390.

[Prieur *et al.*, 2014] Prieur, C., Teel, A. R., and Zaccarian, L. (2014). Relaxed persistent flow/jump conditions for uniform global asymptotic stability. *IEEE Transactions on Automatic Control*, 59(10):2766–2771.

[Raff and Allgöwer, 2007] Raff, T. and Allgöwer, F. (2007). Observers with impulsive dynamical behavior for linear and nonlinear continuous-time systems. In *Proceedings of the Conference on Decision and Control*, pages 4287–4292.

[Repoulias and Papadopoulos, 2007] Repoulias, F. and Papadopoulos, E. (2007). Planar trajectory planning and tracking control design for underactuated AUVs. *Ocean Engineering*, 34:1650–1667.

[Roberts and Tayebi, 2011] Roberts, A. and Tayebi, A. (2011). On the attitude estimation of accelerating rigid-bodies using gps and imu measurements. In *Proceedings of the Conference on Decision and Control and European Control Conference*.

[Rue, 1969] Rue, A. K. (1969). Stabilization of Precision Electrooptical Pointing and Tracking Systems. *IEEE Transactions on Aerospace and Electronic Systems*, AES-5(5):805–819.

[Saccon *et al.*, 2010] Saccon, A., Hauser, J., and Aguiar, A. P. (2010). Exploration of kinematic optimal control on the Lie group $SO(3)$. In *Proceedings of the 8th IFAC Symposium on Nonlinear Control Systems*, pages 1302–1307.

[Salcudean, 1988] Salcudean, S. (1988). On the control of magnetically levitated robot wrists. In *Proceedings of the Conference on Decision and Control*, pages 186–191.

[Sanfelice *et al.*, 2007] Sanfelice, R. G., Goebel, R., and Teel, A. (2007). Invariance principles for hybrid systems with connections to detectability and asymptotic stability. *IEEE Transactions on Automatic Control*, 52(12):2282–2297.

[Sanfelice and Teel, 2006] Sanfelice, R. G. and Teel, A. R. (2006). On the Continuity of Asymptotically Stable Compact Sets for Simulations of Hybrid Systems. In *Proceeding of the Conference on Decision and Control*, pages 270–275.

[Sanjay P. Bhat, 2000] Sanjay P. Bhat, D. S. B. (2000). A topological obstruction to continuous global stabilization of rotational motion and the unwinding phenomenon. *Systems & Control Letters*, 39:63–70.

[Sanyal *et al.*, 2009] Sanyal, A., Fosbury, A., Chaturvedi, N., and Bernstein, D. (2009). Inertia-free spacecraft attitude tracking with disturbance rejection and almost global stabilization. *Journal of Guidance, Control, Dynamics*, 32(4):1167–1178.

[Shuster, 1993] Shuster, M. (1993). A survey of attitude representations. *The Journal of the Astronautical Sciences*, 41(4):439–517.

[Shuster and Oh, 1981] Shuster, M. D. and Oh, S. D. (1981). Three-axis attitude determination from vector observations. *Journal of Guidance and Control*, 4:70–77.

[Sinopoli *et al.*, 2004] Sinopoli, B., Schenato, L., Franceschetti, M., Poolla, K., Jordan, M. I., and Sastry, S. S. (2004). Kalman filtering with intermittent observations. *IEEE Transactions on Automatic Control*, 49(9):1453–1464.

[Smith and Seiler, 2003] Smith, S. C. and Seiler, P. (2003). Estimation with lossy measurements: jump estimators for jump systems. *IEEE Transactions on Automatic Control*, 48(12):2163–2171.

[Sprinkle *et al.*, 2005] Sprinkle, J., Ames, A. D., Pinto, A., Zheng, H., and Sastry, S. S. (2005). On the partitioning of syntax and semantics for hybrid systems tools. In *Proceedings of the Conference on Decision and Control and the European Control Conference,*, pages 4694–4699.

[Stuelpnagel, 1964] Stuelpnagel, J. (1964). On the parametrization of the three-dimensional rotation group. *SIAM review*, 6(4):422–430.

[Tayebi, 2008] Tayebi, A. (2008). Unit quaternion-based output feedback for the attitude tracking problem. *IEEE Transactions on Automatic Control*, 53(6):1516–1520.

[Tayebi and McGilvray, 2006] Tayebi, A. and McGilvray, S. (2006). Attitude stabilization of a vtol quadrotor aircraft. *IEEE Transactions on Control Systems Technology*, 14(3):562–571.

[Teel *et al.*, 2013] Teel, A. R., Forni, F., and Zaccarian, L. (2013). Lyapunov-based sufficient conditions for exponential stability in hybrid systems. *IEEE Transactions on Automatic Control*, 58(6):1591–1596.

[Terzopoulos *et al.*, 1987] Terzopoulos, D., Platt, J., Barr, A., and Fleischer, K. (1987). Elastically deformable models. *ACM Siggraph Computer Graphics*, 21(4):205–214.

[Thienel and Sanner, 2003] Thienel, J. and Sanner, R. (2003). A coupled nonlinear spacecraft attitude controller and observer with an unknown constant gyro bias and gyro noise. *IEEE Transactions on Automatic Control*, 48(11):2011–2015.

[Tippett, 1998] Tippett, M. K. (1998). Bounds for the solution of the discrete algebraic Lyapunov equation. *Automatica*, 34(2):275–277.

[Tse-Huai Wu and Lee, 2015] Tse-Huai Wu, E. K. and Lee, T. (2015). Globally asymptotically stable attitude observer on $SO(3)$. In *Proceedings of the Conference on Decision and Control*, pages 2164–2168.

[Vanderbei, 1996] Vanderbei, R. J. (1996). *Linear Programming: Foundations and Extensions*. Citeseer.

[Wahba, 1965] Wahba, G. (1965). A least squares estimate of spacecraft attitude. *SIAM Review*, 7(3):409.

[Wen and Kreutz-Delgado, 1991] Wen, J.-Y. and Kreutz-Delgado, K. (1991). The Attitude Control Problem. *IEEE Transactions on Automatic Control*, 36(10):1148–1162.

[Wie and Barba, 1985] Wie, B. and Barba, P. M. (1985). Quaternion feedback for spacecraft large angle maneuvers. *Journal of Guidance*, 8(3):360–365.

[Wie *et al.*, 1989] Wie, B., Weiss, H., and Arapostathis, A. (1989). A quaternion feedback regulator for spacecraft eigenaxis rotations. In *Proceedings of the Guidance, Navigation and Control Conference*, page 4128.

[Yasuda and Hirai, 1979] Yasuda, K. and Hirai, K. (1979). Upper and lower bounds on the solution of the algebraic Riccati equation. *IEEE Transactions on Automatic Control*, 24(3):483–487.

[Yuan, 1988] Yuan, J. (1988). Closed-loop manipulator control using quaternion feedback. *IEEE Journal on Robotics and Automation*, 4(4):434–440.

[Zlotnik and Forbes, 2016] Zlotnik, D. E. and Forbes, J. R. (2016). Exponential convergence of a nonlinear attitude estimator. *Automatica*, 72:11–18.

[Zlotnik and Forbes, 2017] Zlotnik, D. E. and Forbes, J. R. (2017). Nonlinear estimator design on the special orthogonal group using vector measurements directly. *IEEE Transactions on Automatic Control*, 62:149–160.

# Appendix A

# Proofs of Lemmas

## A.1 Proof of Lemma 2.2.1

Using (2.62) and identities (2.41)-(2.44) of the trace function one has

$$\begin{aligned}\mathbf{tr}(M(I-R^2)) &= \mathbf{tr}(M) - \mathbf{tr}(M(R^\top + \mathbf{tr}(R)R - \mathbf{tr}(R)I)) \\ &= \mathbf{tr}(M) - \mathbf{tr}(MR^\top) - \mathbf{tr}(R)\mathbf{tr}(MR) + \mathbf{tr}(R)\mathbf{tr}(M) \\ &= \mathbf{tr}(M) - \mathbf{tr}(MR) + \mathbf{tr}(R)(\mathbf{tr}(M) - \mathbf{tr}(MR)) \\ &= (1+\mathbf{tr}(R))\mathbf{tr}(M(I-R)).\end{aligned}$$

Moreover, using the fact that $\mathbf{P}_{\mathfrak{so}(3)}(A) = (A - A^\top)/2$ and relation (2.62) one obtains

$$\begin{aligned}\mathbf{P}_{\mathfrak{so}(3)}(MR^2) &= \frac{1}{2}(MR^2 - (R^2)^\top M) \\ &= \frac{1}{2}M(R^\top + \mathbf{tr}(R)R - \mathbf{tr}(R)I) - \frac{1}{2}(R + \mathbf{tr}(R)R^\top - \mathbf{tr}(R)I)M \\ &= \frac{1}{2}(MR^\top - RM) + \frac{1}{2}\mathbf{tr}(R)(MR - R^\top M) \\ &= \mathbf{tr}(R)\mathbf{P}_{\mathfrak{so}(3)}(MR) + \mathbf{P}_{\mathfrak{so}(3)}(MR^\top).\end{aligned}$$

Finally, using the fact that $\mathbf{tr}(R^\top MR) = \mathbf{tr}(MRR^\top) = \mathbf{tr}(M)$ and $\mathbf{tr}(RMR) = \mathbf{tr}(MR^2)$ one has

$$\begin{aligned}\langle\langle \mathbf{P}_{\mathfrak{so}(3)}(R), \mathbf{P}_{\mathfrak{so}(3)}(MR)\rangle\rangle &= \frac{1}{4}\mathbf{tr}((R^\top - R)(MR - R^\top M)) \\ &= \frac{1}{4}\mathbf{tr}(R^\top MR) - \frac{1}{4}\mathbf{tr}(RMR) - \frac{1}{4}\mathbf{tr}((R^\top)^2 M) + \frac{1}{4}\mathbf{tr}(M) \\ &= \frac{1}{2}\mathbf{tr}(M) - \frac{1}{4}\mathbf{tr}(MR^2) - \frac{1}{4}\mathbf{tr}((R^\top)^2 M) = \frac{1}{2}\mathbf{tr}(M(I-R^2)).\end{aligned}$$

## A.2 Proof of Lemma 2.2.2

Using the definition of the map $\mathbf{E}(\cdot)$ in (2.66) one can verify that $\mathbf{E}^{-1}(\mathbf{E}(M)) = M$ and $\mathbf{E}(\mathbf{E}^{-1}(M)) = M$ for any $M \in \mathbb{R}^{3\times 3}$. Let $v$ be an eigenvector such that $M^\top v = \lambda_v^{M^\top} v$. This implies, using the definition of the map $\mathbf{E}(\cdot)$, that

$$\begin{aligned}\mathbf{E}(M)v &= \frac{1}{2}(\mathbf{tr}(M)I - M^\top)v = \frac{1}{2}\mathbf{tr}(M)v - \frac{1}{2}\lambda_v^{M^\top} v = \frac{1}{2}(\mathbf{tr}(M) - \lambda_v^{M^\top})v = \lambda_v^{\mathbf{E}(M)} v,\\ \mathbf{E}^{-1}(M)v &= (\mathbf{tr}(M)I - 2M^\top)v = \mathbf{tr}(M)v - 2\lambda_v^{M^\top} v = (\mathbf{tr}(M) - 2\lambda_v^{M^\top})v = \lambda_v^{\mathbf{E}^{-1}(M)} v.\end{aligned}$$

## A.3 Proof of Lemma 2.2.3

If $M$ is symmetric and $R \in \mathbb{SO}(3), x \in \mathbb{R}^3$ one has

$$\begin{aligned}x^\top[\lambda_{\min}^{\mathbf{E}(M)} I - \mathbf{E}(MR)]x =& x^\top[\lambda_{\min}^{\mathbf{E}(M)} I - \frac{1}{2}(\mathbf{tr}(MR)I - R^\top M)]x\\ =& (\lambda_{\min}^{\mathbf{E}(M)} - \frac{1}{2}\mathbf{tr}(MR))\|x\|^2 + \frac{1}{2}x^\top R^\top M x\\ \leq& (\lambda_{\min}^{\mathbf{E}(M)} - \frac{1}{2}\mathbf{tr}(MR))\|x\|^2 + \frac{1}{2}\lambda_{\max}^{M}\|x\|^2\\ =& \frac{1}{2}\mathbf{tr}(M(I-R))\|x\|^2,\end{aligned}$$

where the fact $\lambda_{\min}^{\mathbf{E}(M)} = \frac{1}{2}(\mathbf{tr}(M) - \lambda_{\max}^M)$, from Lemma 2.2.2, has been used. Moreover, for all $x, y \in \mathbb{R}^3$

$$\begin{aligned}x^\top[\mathbf{E}(M) - \mathbf{E}(MR)]y &= x^\top \mathbf{E}(M(I-R))y\\ &= \frac{1}{2}\mathbf{tr}(M(I-R))x^\top y + \frac{1}{2}x^\top(I - R^\top)M^\top y,\\ &\leq \frac{1}{2}\mathbf{tr}(M(I-R))x^\top y + \frac{1}{2}\|M(I-R)\|_F\|x\|\|y\|.\end{aligned}$$

In view of (2.75) and item *ii)* of Lemma 2.2.2 one has

$$\mathbf{tr}(M) - \mathbf{tr}(MR) = 4\epsilon^\top \mathbf{E}(M)\epsilon \leq 4\lambda_{\max}^{\mathbf{E}(M)} = 2(\mathbf{tr}(M) - \lambda_{\min}^M), \tag{A.1}$$

where $\epsilon$ is the vector part of the unit quaternion associated to $R$ (hence by definition one has $0 \leq \|\epsilon\| \leq 1$). Similarly, one can write

$$\begin{aligned}\mathbf{tr}(M) - \mathbf{tr}(MR) \geq \min(0, 4\lambda_{\min}^{\mathbf{E}(M)}) &= \mathbf{tr}(M) - \max(\mathbf{tr}(M), \mathbf{tr}(M) - 4\lambda_{\min}^{\mathbf{E}(M)})\\ &= \mathbf{tr}(M) - \max(\mathbf{tr}(M), 2\lambda_{\max}^M - \mathbf{tr}(M)),\end{aligned} \tag{A.2}$$

which leads to (2.69). Finally, from (2.69) one deduces that $\mathbf{tr}(MR) \leq \mathbf{tr}(M)$ for all $R \in \mathbb{SO}(3)$ if $\mathbf{E}(M) \geq 0$ since $2\lambda_{\min}^{\mathbf{E}(M)} = \mathbf{tr}(M) - \lambda_{\max}^{M} \geq 0$ which implies that $\max(\mathbf{tr}(M), 2\lambda_{\max}^{M} - \mathbf{tr}(M)) = \mathbf{tr}(M)$. Using this fact, one has

$$\begin{aligned}
\|\mathbf{E}(MR)\|_F^2 &= \mathbf{tr}\left(\mathbf{E}(MR)^\top \mathbf{E}(MR)\right) \\
&= \frac{1}{4}\mathbf{tr}\left(M^2 + \mathbf{tr}^2(MR)I - \mathbf{tr}(MR)(MR + R^\top M)\right) \\
&= \frac{1}{4}(\mathbf{tr}(M^2) + \mathbf{tr}^2(MR)) \\
&\leq \frac{1}{4}(\mathbf{tr}(M^2) + \mathbf{tr}^2(M)) \\
&= \frac{1}{4}\mathbf{tr}\left((\mathbf{tr}(M)I - M)(\mathbf{tr}(M)I - M)\right) \\
&= \|\mathbf{E}(M)\|_F^2.
\end{aligned}$$

## A.4 Proof of Lemma 2.2.4

Consider the trajectories of $\dot{R}(t) = R(t)[\omega(t)]_\times$ with $R(0) \in \mathbb{SO}(3)$ and $\omega(t) \in \mathbb{R}^3$ for all $t \geq 0$. Then, for all $M \in \mathbb{R}^{3\times 3}$ one has

$$\begin{aligned}
\frac{d}{dt}\mathbf{tr}(M(I - R(t))) = -\mathbf{tr}(M\dot{R}(t)) &= -\mathbf{tr}(MR(t)[\omega(t)]_\times) = \langle\langle [\omega(t)]_\times, MR(t)\rangle\rangle \\
&= \langle\langle [\omega(t)]_\times, \mathbf{P}_{\mathfrak{so}(3)}(MR(t))\rangle\rangle = 2\omega(t)^\top \psi(MR(t)),
\end{aligned}$$

where (2.56)-(2.57) have been used. Also, by the definition of the gradient in (2.7) one has

$$\begin{aligned}
\frac{d}{dt}\mathbf{tr}(M(I - R(t))) = \langle\langle \nabla\mathbf{tr}(M(I - R(t))), \dot{R}(t)\rangle\rangle &= \langle\langle R(t)^\top \nabla\mathbf{tr}(M(I - R(t))), [\omega(t)]_\times\rangle\rangle \\
&= \langle\langle [\omega(t)]_\times, \mathbf{P}_{\mathfrak{so}(3)}(MR(t))\rangle\rangle,
\end{aligned}$$

which leads to the gradient expression given in (2.71). Moreover, using (2.59) one has

$$\begin{aligned}
\frac{d}{dt}\psi(MR(t)) = \frac{d}{dt}\mathbf{vex}(\mathbf{P}_{\mathfrak{so}(3)}(MR(t))) &= \frac{1}{2}\mathbf{vex}(MR(t)[\omega(t)]_\times + [\omega(t)]_\times R(t)^\top M^\top), \\
&= \frac{1}{2}[\mathbf{tr}(MR(t))I - R(t)^\top M^\top]\omega(t) = \mathbf{E}(MR(t))\omega(t).
\end{aligned}$$

## A.5 Proof of Lemma 2.2.5

Let $(\eta, \epsilon) \in \mathbb{Q}$ be a unit quaternion representation. Using (2.26) and (2.57) one obtains

$$\begin{aligned}\mathbf{tr}(M(I - \mathbf{R}_u(\eta,\epsilon))) = \mathbf{tr}(M(-2[\epsilon]_\times^2 - 2\eta[\epsilon]_\times)) &= -2\mathbf{tr}(M[\epsilon]_\times^2) + 2\eta\langle\langle[\epsilon]_\times, M\rangle\rangle \\ &= -2\mathbf{tr}(M[\epsilon]_\times^2) + 2\eta\langle\langle[\epsilon]_\times, \mathbf{P}_{\mathfrak{so}(3)}(M)\rangle\rangle \\ &= -2\mathbf{tr}(M[\epsilon]_\times^2)\end{aligned}$$

where $\mathbf{P}_{\mathfrak{so}(3)}(M) = 0$ is used since $M$ is symmetric. Now, using (2.53) and then (2.48), the above equation leads to

$$\mathbf{tr}(M(I - \mathbf{R}_u(\eta,\epsilon))) = 2\mathbf{tr}(\epsilon^\top\epsilon M - M\epsilon\epsilon^\top) = 2\epsilon^\top(\mathbf{tr}(M)I - M)\epsilon = 4\epsilon^\top\mathbf{E}(M)\epsilon.$$

Equation (2.74) (respectively (2.76)) can be inferred from (2.75) by noticing that $\mathbf{R}_u(\eta,\epsilon) = \mathbf{R}_a(\theta,u)$ (respectively $\mathbf{R}_u(\eta,\epsilon) = \mathbf{R}_r(z)$) if $\eta = \cos(\theta/2)$ and $\epsilon = \sin(\theta/2)u$ (respectively $z = \epsilon/\eta$). Again, using (2.26) and (2.50), one has

$$\begin{aligned}\mathbf{P}_{\mathfrak{so}(3)}(M\mathbf{R}_u(\eta,\epsilon)) &= \frac{1}{2}(M\mathbf{R}_u(\eta,\epsilon) - \mathbf{R}_u(\eta,\epsilon)^\top M) \\ &= M\epsilon\epsilon^\top - \epsilon\epsilon^\top M + \eta M[\epsilon]_\times + \eta[\epsilon]_\times M \\ &= [\epsilon \times M\epsilon]_\times + 2\eta[\mathbf{E}(M)\epsilon]_\times,\end{aligned}$$

where (2.51) and (2.55) have been used. Consequently, one obtains

$$\psi(M\mathbf{R}_u(\eta,\epsilon)) = \epsilon \times M\epsilon + \eta\mathbf{E}(M)\epsilon = 2(\eta I - [\epsilon]_\times)\mathbf{E}(M)\epsilon.$$

Equation (2.77) (respectively (2.79)) can be inferred from (2.78) by noticing that $\mathbf{R}_u(\eta,\epsilon) = \mathbf{R}_a(\theta,u)$ (respectively $\mathbf{R}_u(\eta,\epsilon) = \mathbf{R}_r(z)$) if $\eta = \cos(\theta/2)$ and $\epsilon = \sin(\theta/2)u$ (respectively $z = \epsilon/\eta$).

## A.6 Proof of Lemma 2.2.6

Let $(\eta, \epsilon) \in \mathbb{Q}$ be the quaternion representation of the attitude matrix $R$. In view of (2.38) and (2.75), it is clear that $|R|_I^2 = \|\epsilon\|^2$. Moreover, using again (2.75), one has

$$4\lambda_{\min}^{\mathbf{E}(M)}|R|_I^2 = 4\lambda_{\min}^{\mathbf{E}(M)}\|\epsilon\|^2 \leq \mathbf{tr}(M(I-R)) \leq 4\lambda_{\max}^{\mathbf{E}(M)}\|\epsilon\|^2 = 4\lambda_{\max}^{\mathbf{E}(M)}|R|_I^2.$$

Making use of (2.78) and (2.53), one obtains

$$\begin{aligned}\|\psi(MR)\|^2 &= 4\epsilon^\top \mathbf{E}(M)(\eta I + [\epsilon]_\times)(\eta I - [\epsilon]_\times)\mathbf{E}(M)\epsilon \\ &= 4\epsilon^\top \mathbf{E}(M)\eta^2 I - [\epsilon]_\times^2)\mathbf{E}(M)\epsilon \\ &= 4\epsilon^\top \mathbf{E}(M)(I - \epsilon\epsilon^\top)\mathbf{E}(M)\epsilon \\ &= 4\epsilon^\top \mathbf{E}(M)^2\epsilon(1 - \|\epsilon\|^2\cos^2(\phi)),\end{aligned}$$

where the facts $\eta^2 + \epsilon^\top\epsilon = 1$ and $\epsilon^\top\mathbf{E}(M)\epsilon = \|\epsilon\|\|\mathbf{E}(M)\epsilon\|\cos(\phi)$ with $\phi = \angle(\epsilon, \mathbf{E}(M)\epsilon)$, have been used. Finally, in view of (2.75), one has

$$\mathbf{tr}(\mathbf{E}^{-1}(\mathbf{E}(M)^2)(I - R)) = 4\epsilon^\top\mathbf{E}(M)^2\epsilon,$$

which proves (2.81). Furthermore, (2.82) follows from the fact that for any positive definite matrix $\mathbf{E}(M)$ one has

$$0 < \frac{\lambda_{\min}^{\mathbf{E}(M)}}{\lambda_{\max}^{\mathbf{E}(M)}} \leq \cos(u, \mathbf{E}(M)u) \leq 1.$$

Now, to show (2.84) one needs the following lemma.

**Lemma A.6.1** *Consider the function $f : [0,1] \times [0,1] \to \mathbb{R}_{\geq 0}$ defined as*

$$f(x, y) = x(1 - yx). \tag{A.3}$$

*Then, one has*

$$\max_{x\in[0,1]} f(x, y) = \begin{cases} \frac{1}{4y} & \text{if} \quad \frac{1}{2} \leq y \leq 1, \\ 1 - y & \text{if} \quad 0 \leq y < \frac{1}{2}. \end{cases} \tag{A.4}$$

**Proof** The partial derivative of $f$ with respect to $x$ satisfies

$$\frac{\partial f(x, y)}{\partial x} = 1 - 2xy. \tag{A.5}$$

If $y < \frac{1}{2}$ then $2xy < 1$ which implies that $\frac{\partial f(x,y)}{\partial x} > 0$ for all $x \in [0, 1]$ and therefore the maximum of $f(x, y)$ is reached at $x = 1$ and is equal to $f(1, y) = 1 - y$. In the case where $\frac{1}{2} \leq y \leq 1$ one has $\frac{\partial f(x,y)}{\partial x} = 0$ at $x = \frac{1}{2y}$ which is the point where $f$ attains its maximum given by $f(\frac{1}{2y}, y) = \frac{1}{2y}(1 - y\frac{1}{2y}) = \frac{1}{4y}$. The proof is complete.

Using (2.80)-(2.82) one has

$$\|\psi(MR)\|^2 \leq 4(\lambda_{\max}^{\mathbf{E}(M)})^2(1-\xi^2|R|_I^2)|R|_I^2 = 4(\lambda_{\max}^{\mathbf{E}(M)})^2 f(|R|_I^2, \xi^2). \tag{A.6}$$

Using the result of Lemma A.6.1 one obtains $\max_{R\in\mathbb{SO}(3)} f(|R|_I^2, \xi^2) = \max_{|R|_I^2\in[0,1]} f(|R|_I^2, \xi^2) = \bar{\psi}(\xi^2)/4$ which implies that (2.84) holds.

### A.6.1 Proof of Lemma 2.2.7

Making use of (2.48), one has

$$\mathbf{tr}(x_i x_i^\top (I - RP^\top)) = \frac{1}{2}\|R^\top x_i - P^\top x_i\|^2. \tag{A.7}$$

Therefore, using the linear property of the trace function one obtains

$$\mathbf{tr}\left(\sum_{i=1}^n \rho_i x_i x_i^\top (I - RP^\top)\right) = \frac{1}{2}\sum_{i=1}^n \rho_i \|R^\top x_i - P^\top x_i\|^2. \tag{A.8}$$

Furthermore, making use of (2.54) and (2.61) one has

$$\psi(x_i x_i^\top RP^\top) = \frac{1}{2}([PR^\top x_i]_\times x_i) = \frac{1}{2}PR^\top [x_i]_\times RP^\top x_i = \frac{1}{2}P(R^\top x_i \times P^\top x_i), \tag{A.9}$$

which leads to

$$\psi\left(\sum_{i=1}^n \rho_i x_i x_i^\top RP^\top\right) = \frac{1}{2}P\sum_{i=1}^n \rho_i (R^\top x_i \times P^\top x_i). \tag{A.10}$$

## A.7 Proof of Lemma 2.2.8

Let $(\eta, \epsilon) \in \mathbb{Q}$ be a quaternion representation of the rotation matrix $\mathbf{R}_a(\pi, v)\mathbf{R}_a(\theta, u)$. Using the quaternion multiplication rule (2.28) and the facts that $\mathbf{R}_a(\pi, v) = \mathbf{R}_u(0, v)$ and $\mathbf{R}_a(\theta, u) = \mathbf{R}_u(\cos(\theta/2), \sin(\theta/2)u)$, one obtains

$$\epsilon = \cos(\theta/2)v + \sin(\theta/2)(v \times u). \tag{A.11}$$

Hence, in view of (2.75) and the assumption that $v$ is an eigenvector of $M$, one has

$$\begin{aligned}
&\mathbf{tr}(M(I - \mathbf{R}_a(\pi, v)\mathbf{R}_a(\theta, u))) \\
&= 4\epsilon^\top \mathbf{E}(M)\epsilon \\
&= 4\left(\cos(\theta/2)v + \sin(\theta/2)(v \times u)\right)^\top \mathbf{E}(M)\left(\cos(\theta/2)v + \sin(\theta/2)(v \times u)\right) \\
&= 4\cos^2(\theta/2)v^\top \mathbf{E}(M)v + 4\sin^2(\theta/2)(v \times u)^\top \mathbf{E}(M)(v \times u) \\
&= 4v^\top \mathbf{E}(M)v - 4\sin^2(\theta/2)v^\top \left(\mathbf{E}(M) + [u]_\times \mathbf{E}(M)[u]_\times\right) v \\
&= 4\lambda_v^{\mathbf{E}(M)} - 4\sin^2(\theta/2)\Delta(v, u),
\end{aligned}$$

where the fact that $(v \times u)^\top \mathbf{E}(M)v = \lambda_v^{\mathbf{E}(M)}(v \times u)^\top v = 0$ has been used to obtain the third equality above.

## A.8 Proof of Lemma 3.3.9

First, using the derivation product rule and (2.61), it is straightforward to show that if $\dot{R}_i = R_i[\omega_i]_\times$, $i = 1, 2$, then

$$\frac{d}{dt}(R_1 R_2) = R_1 R_2 \left[R_2^\top \omega_1 + \omega_2\right]_\times. \tag{A.12}$$

On the other hand, using (2.13) and (2.56), one has

$$\dot{\theta}_q(R) = \langle \nabla\theta_q(R), R[\omega]_\times \rangle_R = 2\ \psi(R^\top \nabla\theta_q(R))^\top \omega,$$

which, using the fact that $\frac{d}{dt}e^{\theta(t)M} = e^{\theta(t)M}\dot{\theta}(t)M$ for any $M \in \mathbb{R}^{3\times 3}$, yields

$$\dot{\mathbf{R}}_a(\theta_q(R), u_q) = \mathbf{R}_a(\theta_q(R), u_q)\dot{\theta}_q(R)[u_q]_\times = \mathbf{R}_a(\theta_q(R), u_q)\left[2u_q\ \psi(R^\top \nabla\theta_q(R))^\top \omega\right]_\times. \tag{A.13}$$

Since $\Gamma(R, q) = R\mathbf{R}_a(\theta_q(R), u_q)$ then, in view of (A.12) and (A.13), one obtains $\dot{\Gamma}(R, q) = \Gamma(R, q)\left[\Theta(R, q)\omega\right]_\times$ where $\Theta(R, q) = \mathbf{R}_a(\theta_q(R), u_q)^\top + 2u_q\psi(R^\top \nabla\theta_q(R))^\top$.

For some $q \in \mathcal{Q}$, let us define the mapping $\mathbf{T}^q(R) = \Gamma(R, q)$. The time-derivative of the map $\mathbf{T}^q$ is nothing but the differential of $\mathbf{T}^q$ in the tangent direction $\xi = \dot{R} = R[\omega]_\times$. Replacing $\omega = \mathbf{vex}(R^\top \xi)$ in equation (3.51) shows that

$$d\mathbf{T}_R^q(\xi) = \mathbf{T}^q(R)[\Theta(R, q)\mathbf{vex}(R^\top \xi)]_\times, \quad \xi \in \mathsf{T}_R\mathbb{SO}(3).$$

It is clear that when the inverse of the matrix $\Theta(R, q)$ exists for all $R \in \mathbb{SO}(3)$ the map

$d\mathbf{T}_R^q(\cdot)$ is an isomorphism. In fact, for all $y := d\mathbf{T}_R^q(\xi) \in T_{\mathbf{T}^q(R)}\mathbb{SO}(3)$, the inverse is explicitly given by

$$\xi = R\left[(\Theta(R,q))^{-1}\,\mathbf{vex}\left(\mathbf{T}^q(R)^\top y\right)\right]_\times \in \mathsf{T}_R\mathbb{SO}(3).$$

Consequently, the inverse function theorem [Helmke and Moore, 1994] guarantees that $\mathbf{T}_q(R)$ is a local diffeomorphism for all $R \in \mathbb{SO}(3)$. Therefore, $\Gamma$ is everywhere a local diffeomorphism on $\mathbb{SO}(3) \times \mathcal{Q}$ which implies that if $\Psi \in \mathsf{C}^1(\mathcal{D}_\Psi, \mathbb{R}_{\geq 0})$ then one has $\Psi \circ \Gamma \in \mathsf{C}^1(\Gamma^{-1}(\mathcal{D}_\Psi), \mathbb{R}_{\geq 0})$. If in addition $\Gamma^{-1}(\{I\}) = \mathcal{A}$ then $\Psi \circ \Gamma(R,q) = 0$ if and only if $(R,q) \in \mathcal{A}$ which shows that $\Psi \circ \Gamma \in \mathcal{P}_{\Gamma^{-1}(\mathcal{D}_\Psi),}$. In this case, the time-derivative of $\Psi \circ \Gamma$ can be computed as follows

$$\begin{aligned}
\frac{d}{dt}\Psi \circ \Gamma(R,q) &= \langle \nabla\Psi(\Gamma(R,q)), \dot{\Gamma}(R,q)\rangle_{\Gamma(R,q)} \\
&= 2\,\psi\left(\Gamma(R,q)^\top \nabla\Psi(\Gamma(R,q))\right)^\top \psi\left(\Gamma(R,q)^\top \dot{\Gamma}(R,q)\right) \\
&= 2\,\psi\left(\Gamma(R,q)^\top \nabla\Psi(\Gamma(R,q))\right)^\top \Theta(R,q)\omega \\
&= \langle\langle \left[\Theta(R,q)^\top \psi\left(\Gamma(R,q)^\top \nabla\Psi(\Gamma(R,q))\right)\right]_\times, [\omega]_\times\rangle\rangle \\
&= \langle\langle R\left[\Theta(R,q)^\top \psi\left(\Gamma(R,q)^\top \nabla\Psi(\Gamma(R,q))\right)\right]_\times, \dot{R}\rangle\rangle
\end{aligned}$$

where (2.13), (2.56) and (3.51) have been used. Consequently, in view of (2.7), the gradient of $\Psi \circ \Gamma(R,q)$, with respect to the first argument $R$, is given by

$$\nabla(\Psi \circ \Gamma)(R,q) = R\left[\Theta(R,q)^\top \psi\left(\Gamma(R,q)^\top \nabla\Psi(\Gamma(R,q))\right)\right]_\times. \tag{A.14}$$

Moreover, since the matrix $\Theta(R,q)$ is full rank, the set of critical points of $\Psi \circ \Gamma$ is

$$\mathcal{C}_{\Psi\circ\Gamma} = \{(R,q) \in \mathbb{SO}(3) \times \mathcal{Q} : \nabla\Psi(\Gamma(R,q)) = 0\} = \Gamma^{-1}(\mathcal{C}_\Psi).$$

## A.9 Proof of Lemma 3.3.12

Let us define the angle function $\theta(R) = 2\arcsin\left(k\mathbf{tr}(A(I-R))\right)$. Note that $\theta(\cdot)$ is well defined and differentiable on $\mathbb{SO}(3)$ thanks to the fact that $k\mathbf{tr}(A(I-R) \leq 4k\lambda_{\max}^{\mathbf{E}(A)} < 1$ where (2.80) and (3.64) have been used. The gradient of the function $\theta(R)$ satisfies

$$\nabla\theta(R) = \frac{2k\nabla\mathbf{tr}(A(I-R))}{\sqrt{1-k^2\mathbf{tr}^2(A(I-R))}} = \frac{2kR\mathbf{P}_{\mathfrak{so}(3)}(AR)}{\sqrt{1-k^2\mathbf{tr}^2(A(I-R))}},$$

where (2.71) has been used. Therefore, for this choice of $\Gamma$, the function $\Theta(R,q)$ which appears in Lemma 3.3.9 is written as

$$\begin{aligned}\Theta(R,q) &= \mathbf{R}_a(\theta(R),u_q)^\top + 2u_q\psi(R^\top\nabla\theta_q(R))^\top \\ &= \mathbf{R}_a(\theta(R),u_q)^\top + \frac{4ku_q\psi(AR)^\top}{\sqrt{1-k^2\mathbf{tr}^2(A(I-R))}},\end{aligned} \tag{A.15}$$

which leads, using the facts that $\mathbf{R}_a(\theta(R),u_q)^\top u_q = u_q$ and $\mathbf{det}(\mathbf{R}_a(\theta(R),u_q)^\top) = 1$, to

$$\mathbf{det}(\Theta(R,q)) = \mathbf{det}\left(\mathbf{R}_a(\theta(R),u_q)^\top\left(I + \frac{4ku_q\psi(AR)^\top}{\sqrt{1-k^2\mathbf{tr}^2(A(I-R))}}\right)\right) \tag{A.16}$$

$$= \mathbf{det}\left(I + \frac{4ku_q\psi(AR)^\top}{\sqrt{1-k^2\mathbf{tr}^2(A(I-R))}}\right) \tag{A.17}$$

$$= 1 + \frac{4ku_q^\top\psi(AR)}{\sqrt{1-k^2\mathbf{tr}^2(A(I-R))}}, \tag{A.18}$$

where (2.46)-(2.47) have been used. Note that, in view of (2.80) and (2.84), one has

$$\frac{16k^2|u_q^\top\psi(AR)|^2}{1-k^2\mathbf{tr}^2(A(I-R))} \leq \frac{16k^2\|\psi(AR)\|^2}{1-k^2\mathbf{tr}^2(A(I-R))} \leq \frac{16k^2(\lambda_{\max}^{\mathbf{E}(A)})^2\bar{\psi}(\xi^2)}{1-16k^2(\lambda_{\max}^{\mathbf{E}(A)})^2} < 1, \tag{A.19}$$

when $k$ satisfies the bound (3.64). Finally, one concludes that $\mathbf{det}(\Theta(R,q)) \neq 0$ for all $(R,q) \in \mathbb{SO}(3)$. Let $(R,q) \in \mathbb{SO}(3)\times\mathcal{Q}$ such that $\Gamma(R,q) = I$ which implies that $R = \mathbf{R}_a(\theta(R),u_q)^\top = \mathbf{R}_u(\sqrt{1-k^2\mathbf{tr}^2(A(I-R))}, -k\mathbf{tr}(A(I-R))u_q)$. Using (2.75), one obtains

$$\mathbf{tr}(A(I-R)) = 4k^2\mathbf{tr}^2(A(I-R))u_q^\top\mathbf{E}(A)u_q. \tag{A.20}$$

However, using again (2.80) and (3.64) one has $4k^2\mathbf{tr}(A(I-R))u_q^\top\mathbf{E}(A)u_q \leq 16k^2(\lambda_{\max}^{\mathbf{E}(A)})^2 \leq 1/(1+\bar{\psi}(\xi^2)) < 1$. This implies that the only solution to the above equation is $R = I$. Thus, one has $\Gamma^{-1}(\{I\}) = \{I\}\times\mathcal{Q} = \mathcal{A}$.

## A.10 Proof of Lemma 3.3.13

Invoking Lemma 3.3.9, the set of critical points for $\Phi = \Psi_{1,A}\circ\Gamma$ is given by

$$\mathcal{C}_\Phi = \Gamma^{-1}(\mathcal{C}_{\Psi_{1,A}}) = \mathcal{A}\cup\Gamma^{-1}(\mathbf{R}_a(\pi,\mathcal{E}_v^{\mathbb{R}}(A))). \tag{A.21}$$

Let $v_i \in \mathcal{E}_v^{\mathbb{R}}(A) = \{v_1, v_2, v_3\}$ and let $(R, q) = \Gamma^{-1}(\mathbf{R}_a(\pi, v_i))$. Thus, $\Gamma(R, q) = \mathbf{R}_a(\pi, v_i)$, which in view of (3.63), implies that the rotation matrix $R$ satisfies

$$R = \mathbf{R}_a(\pi, v_i)\mathbf{R}_a(2\arcsin\left(k\mathbf{tr}(A(I-R))\right), u_q)^\top. \tag{A.22}$$

Therefore, for a given $p \in \mathcal{Q}$ such that $p \neq q$, one has

$$\begin{aligned}\Gamma(R,p) &= R\mathbf{R}_a(2\arcsin\left(k\mathbf{tr}(A(I-R))\right), u_p)\\ &= \mathbf{R}_a(\pi, v_i)\mathbf{R}_a(2\arcsin\left(k\mathbf{tr}(A(I-R))\right), -u_q)\mathbf{R}_a(2\arcsin\left(k\mathbf{tr}(A(I-R))\right), u_p)\\ &= \mathbf{R}_a(\pi, v_i)\mathbf{R}_a(4\arcsin\left(k\mathbf{tr}(A(I-R))\right), u_p)\end{aligned}$$

where the fact that $u_q = -u_p$ has been used along with (2.21). Let $\theta = 2\arcsin\left(k\mathbf{tr}(A(I-R))\right)$. Making use of Lemma 2.2.8, one obtains

$$\Psi_{1,A} \circ \Gamma(R, p) = 2\lambda_{v_i}^{\mathbf{E}(A)} - 2\sin^2(\theta)\Delta(v_i, u_p), \tag{A.23}$$

where $\Delta(v_i, u_p) = v_i^\top \big(\mathbf{E}(A) + [u_p]_\times \mathbf{E}(A)[u_p]_\times\big)v_i$. Note that, since $u_1 = -u_2 = u$, it follows that $\Delta(v_i, u_p) = \Delta(v_i, u_q) = \Delta(v_i, u)$. Consequently, since $\Psi_{1,A} \circ \Gamma(R, q) = \Psi_{1,A}(\mathbf{R}_a(\pi, v_i)) = 2\lambda_{v_i}^{\mathbf{E}(A)}$, one has

$$\Psi_{1,A} \circ \Gamma(R, q) - \Psi_{1,A} \circ \Gamma(R, p) = 2\sin^2(\theta)\Delta(v_i, u). \tag{A.24}$$

Therefore, for the synergism condition (3.40) to hold one must have $\Delta(v_i, u) > 0$ and $\sin(\theta) \neq 0$. Now, let us show that if $\Delta(v_i, u) > 0$ then $\theta \in ]0, \pi[$ and therefore $\sin(\theta) \neq 0$. In view of (A.22) and using the result of Lemma 2.2.8 one obtains

$$\begin{aligned}\mathbf{tr}(A(I-R)) &= \mathbf{tr}(A(I - \mathbf{R}_a(\pi, v_i)\mathbf{R}_a(-\theta, u_q))) &\text{(A.25)}\\ &= 4\lambda_{v_i}^{\mathbf{E}(A)} - 4\sin^2(\theta/2)\Delta(v_i, u). &\text{(A.26)}\end{aligned}$$

On the other hand, one has $\sin(\theta/2) = k\mathbf{tr}(A(I-R))$ which leads to

$$\frac{1}{k}\sin(\theta/2) = 4\lambda_{v_i}^{\mathbf{E}(A)} - 4\sin^2(\theta/2)\Delta(v_i, u). \tag{A.27}$$

Solving the above quadratic equation in $\sin(\theta/2)$ yields

$$\sin(\theta/2) = \frac{-1 + \sqrt{1 + 64k^2\Delta(v_i, u)\lambda_{v_i}^{\mathbf{E}(A)}}}{8k\Delta(v_i, u)} > 0. \tag{A.28}$$

Consequently, the above results lead, in view of Definition 3.3.6, to the conclusion that $\Psi_{1,A} \circ \Gamma$ is synergistic if and only if $\Delta(v_i, u) > 0$ for all $i \in \{1, 2, 3\}$.

## A.11 Proof of Lemma 3.3.14

The condition of Lemma 3.3.13 can be written as

$$\Delta(v_i, u) = v_i^\top \left(\mathbf{E}(A) + [u]_\times \mathbf{E}(A)[u]_\times\right) v_i > 0, \tag{A.29}$$

where $\mathcal{V} = \{v_1, v_2, v_3\}$ is an orthonormal basis of eigenvectors of $A$. Using the cross product identity (2.1) and the fact $u = [u^\top v_1, u^\top v_2, u^\top v_3]_{\mathcal{V}}^\top$ one has

$$v_i \times u = \sum_{j,k} \varepsilon_{ijk} (u^\top v_j) v_k, \tag{A.30}$$

where $\varepsilon_{ijk}$ is the Levi-Cevita symbol (2.2). This leads to

$$\begin{aligned}
\Delta(v_i, u) &= v_i^\top \left(\mathbf{E}(A) + [u]_\times \mathbf{E}(A)[u]_\times\right) v_i && \text{(A.31)}\\
&= \lambda_{v_i}^{\mathbf{E}(A)} - \big(\sum_{j,k} \varepsilon_{ijk} (u^\top v_j) v_k\big)^\top \mathbf{E}(A) \big(\sum_{j,k} \varepsilon_{ijk} (u^\top v_j) v_k\big) && \text{(A.32)}\\
&= \lambda_{v_i}^{\mathbf{E}(A)} - \sum_{j,k} \varepsilon_{ijk}^2 (u^\top v_j)^2 \lambda_{v_k}^{\mathbf{E}(A)}. && \text{(A.33)}
\end{aligned}$$

Using (2.2), it is straightforward to verify that $\Delta(v_i, u)$ can explicitly be written as

$$\begin{aligned}
\Delta(v_1, u) &= \lambda_{v_1}^{\mathbf{E}(A)} - (u^\top v_2)^2 \lambda_{v_3}^{\mathbf{E}(A)} - (u^\top v_3)^2 \lambda_{v_2}^{\mathbf{E}(A)},\\
\Delta(v_2, u) &= \lambda_{v_2}^{\mathbf{E}(A)} - (u^\top v_1)^2 \lambda_{v_3}^{\mathbf{E}(A)} - (u^\top v_3)^2 \lambda_{v_1}^{\mathbf{E}(A)},\\
\Delta(v_3, u) &= \lambda_{v_3}^{\mathbf{E}(A)} - (u^\top v_2)^2 \lambda_{v_1}^{\mathbf{E}(A)} - (u^\top v_1)^2 \lambda_{v_2}^{\mathbf{E}(A)}.
\end{aligned} \tag{A.34}$$

Since $u$ is a unit vector it verifies the unit constraint $(u^\top v_3)^2 = 1 - (u^\top v_1)^2 - (u^\top v_2)^2$. Thus, equations (A.34) are rewritten as

$$\begin{aligned}
\Delta(v_1, u) &= (\lambda_{v_1}^{\mathbf{E}(A)} - \lambda_{v_2}^{\mathbf{E}(A)}) + (u^\top v_2)^2 (\lambda_{v_2}^{\mathbf{E}(A)} - \lambda_{v_3}^{\mathbf{E}(A)}) + (u^\top v_1)^2 \lambda_{v_2}^{\mathbf{E}(A)}\\
\Delta(v_2, u) &= (\lambda_{v_1}^{\mathbf{E}(A)} - \lambda_{v_3}^{\mathbf{E}(A)})(u^\top v_1)^2 + \lambda_{v_1}^{\mathbf{E}(A)} (u^\top v_2)^2 - (\lambda_{v_1}^{\mathbf{E}(A)} - \lambda_{v_2}^{\mathbf{E}(A)})\\
\Delta(v_3, u) &= -\lambda_{v_2}^{\mathbf{E}(A)} (u^\top v_1)^2 - \lambda_{v_1}^{\mathbf{E}(A)} (u^\top v_2)^2 + \lambda_{v_3}^{\mathbf{E}(A)}.
\end{aligned}$$

Also, since $v_i$ is the eigenvector associated to $\lambda_i^A$, one has the following facts

$$\begin{aligned}
\lambda_{v_1}^{\mathbf{E}(A)} &= \frac{1}{2}(\mathbf{tr}(A) - \lambda_1^A) = \frac{\lambda_2^A + \lambda_3^A}{2} \\
\lambda_{v_2}^{\mathbf{E}(A)} &= \frac{1}{2}(\mathbf{tr}(A) - \lambda_2^A) = \frac{\lambda_1^A + \lambda_3^A}{2} \\
\lambda_{v_3}^{\mathbf{E}(A)} &= \frac{1}{2}(\mathbf{tr}(A) - \lambda_3^A) = \frac{\lambda_1^A + \lambda_2^A}{2}.
\end{aligned}$$

Moreover, $0 < \lambda_1^A < \lambda_2^A < \lambda_3^A$ which implies that $\lambda_{v_1}^{\mathbf{E}(A)} > \lambda_{v_2}^{\mathbf{E}(A)} > \lambda_{v_3}^{\mathbf{E}(A)} > 0$ and hence $\Delta(v_1, u) > 0$. The conditions $\Delta(v_2, u), \Delta(v_3, u) > 0$ are equivalent to $\underline{\chi}(u^\top v_1) < (u^\top v_2)^2 < \bar{\chi}(u^\top v_1)$ where

$$\begin{aligned}
\underline{\chi}(u^\top v_1) &= -\frac{(\lambda_{v_1}^{\mathbf{E}(A)} - \lambda_{v_3}^{\mathbf{E}(A)})}{\lambda_{v_1}^{\mathbf{E}(A)}}(u^\top v_1)^2 + \frac{(\lambda_{v_1}^{\mathbf{E}(A)} - \lambda_{v_2}^{\mathbf{E}(A)})}{\lambda_{v_1}^{\mathbf{E}(A)}} \\
\bar{\chi}(u^\top v_1) &= -\frac{\lambda_{v_2}^{\mathbf{E}(A)}}{\lambda_{v_1}^{\mathbf{E}(A)}}(u^\top v_1)^2 + \frac{\lambda_{v_3}^{\mathbf{E}(A)}}{\lambda_{v_1}^{\mathbf{E}(A)}}.
\end{aligned}$$

Replacing $\lambda_i^{\mathbf{E}(A)}$ by its expression function of $\lambda_i^A$ in the above inequality leads to the result of Lemma 3.3.14.

# Appendix B

# Proofs of Propositions

## B.1 Proof of Proposition 3.2.1

First, it should be noted that in view of condition (3.20) and the fact that $\max_{\mathbb{S}^1} \Phi_E(x) = 2$, one has $|k_q \Phi_E(x)| < \sqrt{3}/2 < 1$ for all $(x, q) \in \mathbb{S}^1 \times \mathcal{Q}$. This implies that the map $\theta(x, q)$ is well defined and differentiable on the whole space. Now, let us compute the gradient $\nabla\theta(x, q)$ and show that (3.18) is not met for all $(x, q) \in \mathbb{S}^1 \times \mathcal{Q}$. Using (3.19) one has

$$\nabla\theta(x,q) = \frac{2k_q \nabla\Phi_E(x)}{\sqrt{1 - k_q^2 \Phi_E(x)^2}} = \frac{2k_q e_1}{\sqrt{1 - k_q^2 \Phi_E(x)^2}}. \tag{B.1}$$

Therefore, one obtains

$$\nabla\theta(x,q)^\top Sx = \frac{2k_q x_2}{\sqrt{1 - k_q^2 (1 - x_1)^2}}. \tag{B.2}$$

Now, in view of the fact that $x_1^2 + x_2^2 = 1$, one has

$$4x_2^2 + (1 - x_1)^2 = 5 - 2x_1 - 3x_1^2 \leq \frac{16}{3}, \tag{B.3}$$

which implies, under the condition (3.20), that $|\nabla\theta(x, q)^\top Sx| < 1$ and, hence, condition (3.18) is not met for all $(x, q) \in \mathbb{S}^1 \times \mathcal{Q}$. Now, let us compute the critical points of the composite potential function $\Phi_E \circ \Gamma(x, q)$ defined by (3.17). Consider $(x, q) \in \mathbb{S}^1 \times \mathcal{Q}$

such that $\Gamma(x,q) = e_1$. Then, one has

$$x = R(-\theta(x,q))e_1 = \begin{bmatrix} \cos(\theta(x,q)) \\ -\sin(\theta(x,q)) \end{bmatrix}, \tag{B.4}$$

which leads to

$$\Phi_E(x) = 1 - e_1^\top \begin{bmatrix} \cos(\theta(x,q)) \\ -\sin(\theta(x,q)) \end{bmatrix} = 1 - \cos(\theta(x,q)) = 2\sin^2(\theta(x,q)/2) = 2k_q^2\Phi_E(x)^2. \tag{B.5}$$

Therefore $\Phi_E(x)(1 - 2k_q^2\Phi_E(x)) = 0$ which leads to $\Phi_E(x) = 0$ (thus $x = e_1$) since $2k_q^2\Phi_E(x) < 6\Phi_E(x)/16 \leq 12/16 < 1$ and thus the quantity $1 - 2k_q^2\Phi_E(x)$ cannot vanish. Now, let us consider $(x,q) \in \mathbb{S}^1 \times \mathcal{Q}$ such that $\Gamma(x,q) = -e_1$. Then, in view of (3.11) and (3.19), one obtains

$$x = -R(-\theta(x,q))e_1 = \begin{bmatrix} -\cos(\theta(x,q)) \\ \sin(\theta(x,q)) \end{bmatrix}, \tag{B.6}$$

which leads to the following fact

$$\Phi_E(x) = 1 - e_1^\top \begin{bmatrix} -\cos(\theta(x,q)) \\ \sin(\theta(x,q)) \end{bmatrix} = 1 + \cos(\theta(x,q)) = 2(1 - \sin^2(\theta(x,q)/2)) \tag{B.7}$$

$$= 2(1 - k_q^2\Phi_E(x)^2). \tag{B.8}$$

The above quadratic equation in $\Phi_E(x)$ can be solved to determine the unique value of $\Phi_E(x) \geq 0$ as follows

$$\Phi_E(x) = \frac{-1 + \sqrt{1 + 16k_q^2}}{4k_q^2}. \tag{B.9}$$

Once the value of $\Phi_E(x)$ is computed, the solution $x$ to (B.6) is readily obtained

$$x = \begin{bmatrix} 2\sin^2(\theta(x,q)/2) - 1 \\ 2\sin(\theta(x,q)/2)\cos(\theta(x,q)/2) \end{bmatrix} = \begin{bmatrix} 2k_q^2\Phi_E(x)^2 - 1 \\ 2k_q\Phi_E(x)\sqrt{1 - k_q^2\Phi_E(x)^2} \end{bmatrix} = c_q. \tag{B.10}$$

## B.2 Proof of Proposition 3.2.2

Let $(x, q) \in \mathbb{S}^1 \times \mathcal{Q}$ be an undesired critical point of $\Phi_E(\Gamma(x, q))$ which means that $\Gamma(x, q) = -e_1$. Now, for any $p \in \mathcal{Q} \setminus \{q\}$, one has

$$\Gamma(x,p) = R(\theta(x,p))x = -R(\theta(x,p))R(-\theta(x,q))e_1 \tag{B.11}$$
$$= -R(\theta(x,p) - \theta(x,q))e_1 \tag{B.12}$$
$$= \begin{bmatrix} -\cos(\theta(x,p) - \theta(x,q)) \\ \sin(\theta(x,p) - \theta(x,q)) \end{bmatrix}. \tag{B.13}$$

Therefore, one obtains

$$\Phi_E \circ \Gamma(x,p) = 1 + \cos(\theta(x,p) - \theta(x,q)) = 2(1 - \sin^2(\theta(x,p)/2 - \theta(x,q)/2)), \tag{B.14}$$

which leads to

$$\begin{aligned}
&\Phi_E \circ \Gamma(x,q) - \Phi_E \circ \Gamma(x,p) \\
&= 2\sin^2(\theta(x,p)/2 - \theta(x,q)/2) \\
&= 2\sin^2(\arcsin(k_p\Phi_E(x)) - \arcsin(k_q\Phi_E(x))) \\
&= 2\sin^2\left(\arcsin\left(k_p\Phi_E(x)\sqrt{1 - k_q^2\Phi_E(x)^2} - k_q\Phi_E(x)\sqrt{1 - k_p^2\Phi_E(x)^2}\right)\right) \\
&= 2\left(k_p\Phi_E(x)\sqrt{1 - k_q^2\Phi_E(x)^2} - k_q\Phi_E(x)\sqrt{1 - k_p^2\Phi_E(x)^2}\right)^2.
\end{aligned}$$

Taking $k_p = -k_q = k$ and in view of (B.9) and the above equation, one obtains

$$\Phi_E \circ \Gamma(x,q) - \Phi_E \circ \Gamma(x,p) = 8k^2\Phi_E(x)^2(1 - k^2\Phi_E(x)^2) = \frac{\left(-1 + \sqrt{16\,k^2 + 1}\right)^3}{16k^4}.$$

## B.3 Proof of Proposition 3.3.10

First, let us show that $\Psi_1 \circ \Gamma$ is exp-synergistic with gap exceeding some $\delta_1 > 0$. Define the parameters set $\mathcal{T}_1 = \{\Psi_1 \circ \Gamma, \mathcal{Q}, \delta_1\}$. Let us verify that $\Psi_1 \circ \Gamma$ is a valid potential function. To do so, one needs to show that the transformation $\Gamma$ proposed in Proposition 3.3.10 satisfies item 3) of Lemma 3.3.9 so that the composite function $\Psi_1 \circ \Gamma \in \mathcal{P}_{\mathbb{SO}(3)\times\mathcal{Q}}$. It should be mentioned that $\theta(R) = 2\arcsin(k|R|_I^2)$ is well defined thanks to the facts $k < 1/\sqrt{2}$ and $|R|_I \leq 1$. Moreover since the arcsin is differentiable on $(-1, 1)$ and $k|R|_I^2 < 1$ it follows that the function $\theta(R)$ is differentiable on the whole manifold $\mathbb{SO}(3)$.

The gradient of the function $\theta(R)$ satisfies

$$\nabla\theta(R) = \frac{2k\nabla|R|_I^2}{\sqrt{1-k^2|R|_I^4}} = \frac{k\nabla\mathbf{tr}(I-R)}{2\sqrt{1-k^2|R|_I^4}} = \frac{kR\mathbf{P}_{\mathfrak{so}(3)}(R)}{2\sqrt{1-k^2|R|_I^4}},$$

where (2.71) has been used. Therefore, for this choice of $\Gamma$ the function $\Theta(R,q)$ which appears in Lemma 3.3.9 is written as

$$\Theta(R,q) = \mathbf{R}_a(\theta(R),u_q)^\top + 2u_q\psi(R^\top\nabla\theta(R))^\top = \mathbf{R}_a(\theta(R),u_q)^\top + \frac{ku_q\psi(R)^\top}{\sqrt{1-k^2|R|_I^4}},$$

which leads, using the facts $\mathbf{R}_a(\theta(R),u_q)^\top u_q = u_q$ and $\mathbf{det}(\mathbf{R}_a(\theta(R),u_q)^\top) = 1$, to

$$\begin{aligned}\mathbf{det}(\Theta(R,q)) &= \mathbf{det}\left(\mathbf{R}_a(\theta(R),u_q)^\top\left(I + \frac{ku_q\psi(R)^\top}{\sqrt{1-k^2|R|_I^4}}\right)\right)\\ &= \mathbf{det}\left(I + \frac{ku_q\psi(R)^\top}{\sqrt{1-k^2|R|_I^4}}\right) = 1 + \frac{ku_q^\top\psi(R)}{\sqrt{1-k^2|R|_I^4}},\end{aligned}$$

where (2.46)-(2.47) have been used. Now, in view of (2.84), one has $\|\psi(R)\| \leq 1$ which implies

$$\frac{k|u_q^\top\psi(R)|}{\sqrt{1-k^2|R|_I^4}} \leq \frac{k\|\psi(R)\|}{\sqrt{1-k^2|R|_I^4}} \leq \frac{k}{\sqrt{1-k^2}} < 1, \tag{B.15}$$

thanks to the fact that $k < 1/\sqrt{2}$. Finally, one concludes that $\mathbf{det}(\Theta(R,q)) \neq 0$ for all $(R,q) \in \mathbb{SO}(3)$. Let $(R,q) \in \mathbb{SO}(3)\times\mathcal{Q}$ such that $\Gamma(R,q) = I$ which implies that $R = \mathbf{R}_a(\theta(R),u_q)^\top = \mathbf{R}_u(\sqrt{1-k^2|R|_I^2}, -k|R|_I^2u_q)$. Using (2.75), one obtains

$$|R|_I^2 = \mathbf{tr}(I-R)/4 = k^2|R|_I^4, \tag{B.16}$$

which admits the unique solution $R = I$ since $k < 1/\sqrt{2}$. Therefore, one has $\Gamma^{-1}(\{I\}) = \{I\}\times\mathcal{Q} = \mathcal{A}$. Hence, by Lemma 3.3.9, the composite function $\Psi_1\circ\Gamma \in \mathcal{P}_{\Gamma^{-1}(\mathbb{SO}(3))}$. Now, let us show that the exp-synergism conditions in Definition 3.3.7 hold.

Let $(\eta,\epsilon)$ and $(\eta_q,\epsilon_q)$ be the quaternion representations of the attitude matrices $R$ and $\Gamma(R,q)$, respectively. The unit quaternion associated to $\mathbf{R}_a(2\arcsin(k|R|_I^2),u_q)$ is given by $(\sqrt{1-k^2|R|_I^4}, k|R|_I^2u_q)$. Note that, in view of (2.75), one has $|R|_I^2 = \mathbf{tr}(I-R)/4 = \|\epsilon\|^2$ and $|\Gamma(R,q)|_I^2 = \mathbf{tr}(I-\Gamma(R,q))/4 = \|\epsilon_q\|^2$. Therefore, in view of (3.58) and using the

quaternion multiplication rule (2.28), one obtains

$$\eta_q = \eta\sqrt{1-k^2\|\epsilon\|^4} - k\|\epsilon\|^2\epsilon^\top u_q, \tag{B.17}$$

$$\epsilon_q = k\eta\|\epsilon\|^2 u_q + \sqrt{1-k^2\|\epsilon\|^4}\epsilon + k\|\epsilon\|^2\epsilon \times u_q. \tag{B.18}$$

This leads to

$$\|\epsilon_q\|^2 = \|\epsilon\|^2 + k^2\|\epsilon\|^4\eta^2 - \cos^2(\varphi_q)k^2\|\epsilon\|^6 + 2k\eta\|\epsilon\|^3\sqrt{1-k^2\|\epsilon\|^4}\cos(\varphi_q)$$

where $\varphi_q$ is the angle between $\epsilon$ and $u_q$. Using the fact that $|\eta|\cdot\|\epsilon\| \leq \frac{1}{2}$, it follows that

$$\|\epsilon_q\|^2 \leq \|\epsilon\|^2[1+k+k^2/4] = [1+k+k^2/4]|R|_I^2.$$

Moreover, since $k < \frac{1}{\sqrt{2}}$ it is possible to show that

$$\begin{aligned}\|\epsilon_q\|^2 &\geq \|\epsilon\|^2\sqrt{1-k^2\|\epsilon\|^4}\left[\sqrt{1-k^2\|\epsilon\|^4} - 2k|\eta|\cdot\|\epsilon\|\right] \geq \|\epsilon\|^2\sqrt{1-k^2\|\epsilon\|^4}\left[\sqrt{1-k^2} - k\right] \\ &\geq \|\epsilon\|^2\left[1-k^2-k\sqrt{1-k^2}\right] = \left[1-k^2-k\sqrt{1-k^2}\right]|R|_I^2.\end{aligned}$$

On the other hand, one has

$$\Psi_1 \circ \Gamma(R,q) = \frac{1}{2}\mathbf{tr}(I-\Gamma(R,q)) = 2|\Gamma(R,q)|_I^2 = 2\|\epsilon_q\|^2.$$

This shows that $\alpha_1|R|_I^2 \leq \Psi_1\circ\Gamma(R,q) \leq \alpha_2|R|_I^2$ with $\alpha_1 = 2[1-k^2-k\sqrt{1-k^2}]$ and $\alpha_2 = [1+k+k^2/4]$. It is easy to check that $\alpha_1$ and $\alpha_2$ are strictly positive for all $0 \leq k < 1/\sqrt{2}$. Now, let us show the following fact: $\Gamma(R,q) \in \Pi_{\mathbb{SO}(3)}$ for all $(R,q) \in \mathcal{F}_{\mathcal{T}_1}$, which implies that the rotation $\Gamma(R,q)$ cannot be of $180^\circ$ angle whenever $(R,q) \in \mathcal{F}_{\mathcal{T}_1}$. Let us prove this by contradiction. Assume that $\Gamma(R,q) \notin \Pi_{\mathbb{SO}(3)}$. Let $Q = (\eta,\epsilon)$, $Q_q = (\eta_q,\epsilon_q)$ and $Q_m = (\eta_m,\epsilon_m)$ be the quaternion representation of the attitude $R$, $\Gamma(R,q)$ and $\Gamma(R,m)$, respectively. Since $\Gamma(R,q) \notin \Pi_{\mathbb{SO}(3)}$ it follows that $Q_q \notin \Pi_{\mathbb{Q}}$ or, equivalently, $\eta_q = 0$. Therefore, in view of (B.17) one obtains $\eta_m - \eta_q = \eta_m = k\|\epsilon\|^2\epsilon^\top(u_q - u_m)$. Moreover, since $u_{m+3} = -u_m, m \in \{1,2,3\}$ there exist always three indices $m_i \in \mathcal{Q}, i \in \{1,2,3\}$, such that $u_{m_i}$ is orthonormal to $u_{m_j}$, for $i \neq j$ and $\epsilon^\top u_{m_i}$ and $\epsilon^\top u_q$ have opposite signs. Therefore, one has

$$\max_{m\in\mathcal{Q}}|\eta_m| = k\|\epsilon\|^2\max_{m\in\mathcal{Q}}|\epsilon^\top(u_q-u_m)| \geq k\|\epsilon\|^2\max_{m_i\in\{1,2,3\}}|\epsilon^\top u_{m_i}| \geq k\|\epsilon\|^3/\sqrt{3}.$$

Furthermore if $\eta_q = 0$ then equation (B.17) implies that

$$\sqrt{1-\|\epsilon\|^2}\sqrt{1-k^2\|\epsilon\|^4} = |k|\|\epsilon\|^3|\cos(\varphi_q)|.$$

The above equation reads $f(\|\epsilon\|^2) = 0$ where $f(x) := g(x) + \sin^2(\varphi_q)k^2x^3$, and $g(x) := 1 - x - k^2x^2$. It is easy to verify that $f(x)$ and $g(x)$ are decreasing on the interval $[0,1]$ for all $\varphi_q \in \mathbb{R}$. Therefore, since $f(x) \geq g(x)$, the solution $x_f \in [0,1]$ to equation $f(x_f) = 0$ is greater than or equals to $x_g \in [0,1]$, with $g(x_g) = 0$. Thus, it is clear that $f(\|\epsilon\|^2) = 0$ implies that $\|\epsilon\|^2 \geq (-1+\sqrt{1+4k^2})/2k^2$. Consequently, $\max\limits_{m\in\mathcal{Q}} |\eta_m| \geq [-1+\sqrt{1+4k^2}]^{\frac{3}{2}}/2\sqrt{6}k^2$. Now, using the quaternion norm constraint, one obtains

$$\begin{aligned}\Psi_1 \circ \Gamma(R,q) - \min_{m\in\mathcal{Q}} \Psi_1 \circ \Gamma(R,m) &= 2\|\epsilon_q\|^2 - 2\min_{m\in\mathcal{Q}}\|\epsilon_m\|^2 = 2\max_{m\in\mathcal{Q}}|\eta_m|^2 \\ &\geq \frac{[-1+\sqrt{1+4k^2}]^3}{12k^4} = \bar{\delta}_1 > \delta_1. \end{aligned} \tag{B.19}$$

Therefore $(R,q) \notin \mathcal{F}_{\mathcal{T}_1}$ which confirms that $\Gamma(R,q) \in \Pi_{\mathbb{SO}(3)}$ for all $(R,q) \in \mathcal{F}_{\mathcal{T}_1}$. In view of (A.14) and (2.71), the gradient of $\Psi_1 \circ \Gamma$ is given by

$$\nabla(\Psi_1 \circ \Gamma)(R,q) = \frac{1}{2}R\left[\Theta(R,q)^\top \psi\left(\Gamma(R,q)\right)\right]_\times.$$

Now, in view of (2.80)-(2.82), one has $\mathbf{tr}(I-X) = 4|X|_I^2$ and $\alpha(I,X) = 1-|X|_I^2$ for all $X \in \mathbb{SO}(3)$, from which one can write

$$\|\psi(X)\|^2 = 4|X|_I^2(1-|X|_I^2) = (1+\mathbf{tr}(X))|X|_I^2 \tag{B.20}$$

Therefore $\|\psi(\Gamma(R,q))\|^2 = |\Gamma(R,q)|_I^2(1+\mathbf{tr}(\Gamma(R,q)))$ which implies that, for all $(R,q) \in \mathcal{F}_{\mathcal{T}_1}$, there exists $\underline{\alpha} > 0$ such that $\underline{\alpha}|\Gamma(R,q)|_I^2 \leq \|\psi(\Gamma(R,q)\|^2 \leq 4|\Gamma(R,q)|_I^2$ since $\Gamma(R,q) \in \Pi_{\mathbb{SO}(3)}$. Moreover since $\mathbf{det}(\Theta(R,q)) \neq 0$ for all $(R,q) \in \mathbb{SO}(3)\times\mathcal{Q}$ the matrix $\Theta(R,q)\Theta(R,q)^\top$ is full rank and positive definite for all $(R,q) \in \mathbb{SO}(3)\times\mathcal{Q}$. Therefore it is not difficult to find positive constants $\alpha_3$ and $\alpha_4$ such that the gradient $\|\nabla(\Psi_1\circ\Gamma)(R,q)\|_F^2$ satisfies (3.43). Finally, $\Psi_1 \circ \Gamma$ does not have any singular point and therefore the condition $\mathcal{F}_{\mathcal{T}_1} \subseteq \mathcal{D} = \mathbb{SO}(3)\times\mathcal{Q}$ holds. It follows that $\Psi_1 \circ \Gamma$ is an exp-synergistic potential function with gap exceeding $\delta_1$.

Next, let us show that $\Psi_2 \circ \Gamma$ is exp-synergistic. Define the parameters set $\mathcal{T}_2 = \{\Psi_2 \circ \Gamma, \mathcal{Q}, \delta_2\}$. A similar argument as above can be conducted to show that $\Psi_2 \circ \Gamma \in \mathcal{P}_{\mathcal{D}}$ where $\mathcal{D} = \Gamma^{-1}(\Pi_{\mathbb{SO}(3)}) = \{(R,q) \in \mathbb{SO}(3)\times\mathcal{Q} \mid \mathbf{tr}(\Gamma(R,q)) \neq -1\}$. Moreover, since $\Psi_1 \circ \Gamma$ is quadratic in $|R|_I$ and by noticing that $\frac{1}{2}\Psi_1(\cdot) \leq \Psi_2(\cdot) \leq \Psi_1(\cdot)$ it follows

that $\Psi_2 \circ \Gamma$ satisfies (3.42). Recall from (B.19) that for all $(R,q) \notin \mathcal{D}$ or, equivalently, $\Gamma(R,q) \notin \Pi_{\mathbb{SO}(3)}$ one has $\Psi_1 \circ \Gamma(R,q) - \min_{m \in \mathcal{Q}} \Psi_1 \circ \Gamma(R,m) \geq \bar{\delta}_1$ which implies that $\Psi_2 \circ \Gamma(R,q) - \min_{m \in \mathcal{Q}} \Psi_2 \circ \Gamma(R,m) = \sqrt{2}[\Psi_1 \circ \Gamma(R,q) - \min_{m \in \mathcal{Q}} \Psi_1 \circ \Gamma(R,m)]^{\frac{1}{2}} \geq \sqrt{2\bar{\delta}_1} = \bar{\delta}_2 > \delta_2$. Consequently, the condition $\mathcal{F}_{\mathcal{T}_2} \subseteq \mathcal{D}$ holds which means that all the singular points of $\Psi_2 \circ \Gamma$ do not belong to the set $\mathcal{F}_{\mathcal{T}_2}$. Furthermore, the gradient of $\Psi_2 \circ \Gamma$ on the set $\mathcal{F}_{\mathcal{T}_2}$ is given by

$$\nabla(\Psi_2 \circ \Gamma)(R,q) = \frac{\nabla(\Psi_1 \circ \Gamma)(R,q)}{\sqrt{1 + \mathbf{tr}(\Gamma(R,q))}} = \frac{R\left[\Theta(R,q)^\top \psi\left(\Gamma(R,q)\right)\right]_\times}{2\sqrt{1 + \mathbf{tr}(\Gamma(R,q))}}.$$

which implies that

$$\frac{\underline{\lambda}^*_\Theta}{8} \frac{\|\psi(\Gamma(R,q))\|^2}{1 - |\Gamma(R,q)|_I^2} \leq \|\nabla(\Psi_2 \circ \Gamma)(R,q)\|_F^2 \leq \frac{\bar{\lambda}^*_\Theta}{8} \frac{\|\psi(\Gamma(R,q))\|^2}{1 - |\Gamma(R,q)|_I^2}.$$

Using (B.20) it follows that

$$\frac{\underline{\lambda}^*_\Theta}{2} |\Gamma(R,q)|_I^2 \leq \|\nabla(\Psi_2 \circ \Gamma)(R,q)\|^2 \leq \frac{\bar{\lambda}^*_\Theta}{2} |\Gamma(R,q)|_I^2.$$

Finally, one concludes that there exist positive scalars $\alpha_3$ and $\alpha_4$ such that the potential function $\Psi_2 \circ \Gamma$ satisfies condition (3.43). The proof is complete.

## B.4 Proof of Proposition 3.3.15

In view of (A.33), the optimization problem (3.67) is equivalent to the following standard linear programming problem:

$$\begin{array}{lrl}
\text{maximize} & x_4 & \\
\text{subject to} & x_4 + x_2\lambda_3^{\mathbf{E}(A)} + x_3\lambda_2^{\mathbf{E}(A)} - \lambda_1^{\mathbf{E}(A)} & \leq 0, \\
& x_4 + x_3\lambda_1^{\mathbf{E}(A)} + x_1\lambda_3^{\mathbf{E}(A)} - \lambda_2^{\mathbf{E}(A)} & \leq 0, \\
& x_4 + x_1\lambda_2^{\mathbf{E}(A)} + x_2\lambda_1^{\mathbf{E}(A)} - \lambda_3^{\mathbf{E}(A)} & \leq 0, \\
& x_1 + x_2 + x_3 & = 1, \\
& x_1, x_2, x_3 & \geq 0, \\
& x_4 & > 0.
\end{array}$$

where the variables $x_j = (u^\top v_j)^2$, for $j \in \{1,2,3\}$, are defined. Consequently, one can use the simplex algorithm [Vanderbei, 1996] to solve this optimization problem, leading

to the following result: If the condition

$$\lambda_2^A \geq \frac{\lambda_1^A \lambda_3^A}{\lambda_3^A - \lambda_1^A} \tag{B.21}$$

is satisfied, then the optimal solution to (3.67) is given by

$$(u^\top v_1)^2 = 0, \quad (u^\top v_2)^2 = \frac{\lambda_2^A}{\lambda_2^A + \lambda_3^A}, \quad (u^\top v_3)^2 = \frac{\lambda_3^A}{\lambda_2^A + \lambda_3^A}$$

and the maximum is $\max\limits_{u \in \mathbb{S}^2} \min_i \Delta(v_i, u) = \lambda_1^A$. Otherwise, the optimal solution is

$$(u^\top v_i)^2 = 1 - 4\frac{\prod_{j \neq i} \lambda_j^A}{\sum_{j \neq k} \lambda_j^A \lambda_k^A}, \quad i \in \{1, 2, 3\}$$

with the maximum being $\max\limits_{u \in \mathbb{S}^2} \min_i \Delta(v_i, u) = 4\frac{\prod_{j=1}^3 \lambda_j^A}{\sum_{j \neq k} \lambda_j^A \lambda_k^A}$.

## B.5 Proof of Proposition 3.3.16

First, let us show that $\Phi = \Psi_{1,A} \circ \Gamma$ is exp-synergistic. In view of Lemma 3.3.9 and Lemma 3.3.12, it is clear that the composite function $\Psi_{1,A} \circ \Gamma \in \mathcal{P}_{\mathbb{SO}(3) \times \mathcal{Q}}$. Let $(\eta, \epsilon)$ and $(\eta_q, \epsilon_q)$ be, respectively, the unit quaternion representation of $R$ and $\Gamma(R, q)$. In view of (3.63) and the fact that $\mathbf{R}_a(2\arcsin(k\mathbf{tr}(A(I-R)), u_q)$ corresponds to the unit quaternion $([1 - k^2\mathbf{tr}(A(I-R))^2)]^{\frac{1}{2}}, k\mathbf{tr}(A(I-R))u_q)$, and using the quaternion multiplication rule (2.28), one can deduce that

$$\epsilon_q = k\eta\mathbf{tr}(A(I-R))u_q + [1 - k^2\mathbf{tr}(A(I-R))^2]^{\frac{1}{2}}\epsilon + k\mathbf{tr}(A(I-R))[\epsilon]_\times u_q.$$

Taking the norm square of $\epsilon_q$ yields

$$\begin{aligned}\|\epsilon_q\|^2 =& (1 - k^2\mathbf{tr}(A(I-R))^2)\|\epsilon\|^2 + k^2\mathbf{tr}(A(I-R))^2\|\epsilon\|^2 \sin^2(\varphi_q) + \\ & k^2\eta^2\mathbf{tr}(A(I-R))^2 + 2k\eta\|\epsilon\|\mathbf{tr}(A(I-R))[1 - k^2\mathbf{tr}(A(I-R))^2]^{\frac{1}{2}} \cos(\varphi_q),\end{aligned}$$

where $\varphi_q$ is the angle between $\epsilon$ and $u_q$. Using the facts that $|R|_I^2 = \|\epsilon\|^2$ and $|\eta| \cdot \|\epsilon\| = \|\epsilon\|\sqrt{1 - \|\epsilon\|^2} \leq 1/2$, and in view of (2.80), it follows that

$$\|\epsilon_q\|^2 \leq \|\epsilon\|^2[1 + 4k\lambda_{\max}^{\mathbf{E}(A)} + 4(k\lambda_{\max}^{\mathbf{E}(A)})^2]. \tag{B.22}$$

Moreover, in view of (3.64) one has $4k\lambda_{\max}^{\mathbf{E}(A)} < 1/\sqrt{2}$ and hence the following lower bound can be derived

$$\begin{aligned}\|\epsilon_q\|^2 &\geq \|\epsilon\|^2[1 - k^2\mathbf{tr}(A(I-R))^2 - 4k\lambda_{\max}^{\mathbf{E}(A)}\sqrt{1 - k^2\mathbf{tr}(A(I-R))^2}] \\ &\geq \|\epsilon\|^2[1 - (4k\lambda_{\max}^{\mathbf{E}(A)})^2 - 4k\lambda_{\max}^{\mathbf{E}(A)}\sqrt{1 - (4k\lambda_{\max}^{\mathbf{E}(A)})^2}]. \end{aligned} \tag{B.23}$$

On the other hand, making use of (2.80), one has $4\lambda_{\min}^{\mathbf{E}(A)}\|\epsilon_q\|^2 \leq \Psi_{1,A} \circ \Gamma(R,q) \leq 4\lambda_{\max}^{\mathbf{E}(A)}\|\epsilon_q\|^2$ and, hence, there exist $\alpha_1, \alpha_2$ such that $\Psi_{1,A} \circ \Gamma(R,q)$ satisfies (3.42).

In view of (A.14) and (2.71), the gradient of $\Psi_{1,A} \circ \Gamma$ is given by

$$\nabla(\Psi_{1,A} \circ \Gamma)(R,q) = \frac{1}{2}R[\Theta(R,q)^\top \psi(A\Gamma(R,q))]_\times. \tag{B.24}$$

Now, for $(R,q) \in \mathbb{SO}(3) \times \mathcal{Q}$, let $\lambda_{\min}^{\Theta}(R,q)$ and $\lambda_{\max}^{\Theta}(R,q)$ denote, respectively, the smallest and largest eigenvalue of $\Theta(R,q)\Theta(R,q)^\top$, and let the constants $\underline{\lambda} = \min_{\mathbb{SO}(3)\times\mathcal{Q}}(\lambda_{\min}^{\Theta}(R,q))$ and $\overline{\lambda} = \max_{\mathbb{SO}(3)\times\mathcal{Q}}(\lambda_{\max}^{\Theta}(R,q))$. It is clear that $\underline{\lambda}$, $\overline{\lambda} > 0$ by the fact that $\Theta(R,q)$ is full rank. Then, from (B.24) and using (2.80)-(2.82), one can show that

$$\begin{aligned}\|\nabla(\Psi_{1,A} \circ \Gamma)(R,q)\|_F^2 = \frac{1}{2}\left\|\Theta(R,q)^\top \psi(A\Gamma(R,q))\right\|^2 &\leq \frac{1}{2}\overline{\lambda}\left\|\psi(A\Gamma(R,q))\right\|^2 \\ &\leq 2\overline{\lambda}(\lambda_{\max}^{\mathbf{E}(A)})^2\alpha(A,\Gamma(R,q))|\Gamma(R,q)|_I^2\end{aligned}$$

and

$$\begin{aligned}\|\nabla(\Psi_{1,A} \circ \Gamma)(R,q)\|_F^2 = \frac{1}{2}\left\|\Theta(R,q)^\top \psi(A\Gamma(R,q))\right\|^2 &\geq \frac{1}{2}\underline{\lambda}\left\|\psi(A\Gamma(R,q))\right\|^2 \\ &\geq 2\underline{\lambda}(\lambda_{\min}^{\mathbf{E}(A)})^2\alpha(A,\Gamma(R,q))|\Gamma(R,q)|_I^2\end{aligned}$$

where $\alpha(A,\Gamma(R,q))$ is given by

$$\alpha(A,\Gamma(R,q)) = 1 - |\Gamma(R,q)|_I^2\cos^2(u, \mathbf{E}(A)u) \tag{B.25}$$

such that $u$ is the axis of rotation of $\Gamma(R,q)$. Define the set of parameters $\mathcal{T}_1 = (\Psi_{1,A} \circ \Gamma, \mathcal{Q}, \delta_1)$. Now, let us show that $\alpha(A,\Gamma(R,q)) > 0$ for all $(R,q) \in \mathcal{F}_{\mathcal{T}_1}$. First, using the results from the proof of Lemma 3.3.13 provided in Appendix A.10, more precisely equations (A.23) and (A.28) one obtains for all undesired critical points $(R,q) \in$

$\Gamma^{-1}(\mathbf{R}_a(\pi, \mathcal{E}_v^{\mathbb{R}}(A)))$

$$\Psi_{1,A} \circ \Gamma(R,q) - \min_{p \in \mathcal{Q}} \Psi_{1,A} \circ \Gamma(R,p) \\ = 8\sin^2(\theta/2)(1-\sin^2(\theta/2))\Delta(v,u) = \sigma(k, \lambda_v^{\mathbf{E}(A)}, \Delta(v,u)),$$

where $v$ is some eigenvector of $A$ and the function $\sigma(\cdot,\cdot,\cdot)$ is defined as follows

$$\sigma(k,\lambda,\Delta) = 8k^2\bar{V}(k,\lambda,\Delta)^2(1-k^2\bar{V}(k,\lambda,\Delta)^2)\Delta, \tag{B.26}$$

$$\bar{V}(k,\lambda,\Delta) = \frac{-1+\sqrt{1+64k^2\Delta\lambda}}{8k^2\Delta}. \tag{B.27}$$

Moreover, by direct differentiation of the function $\sigma(k,\lambda,\Delta)$ with respect to its arguments, it is not difficult to show that the partial derivatives are positive and, therefore, one obtains

$$\sigma(k, \lambda_v^{\mathbf{E}(A)}, \Delta(v,u)) \geq \sigma(k, \lambda_{\min}^{\mathbf{E}(A)}, \underline{\Delta}(u)) > 0, \tag{B.28}$$

where $\underline{\Delta}(u) = \min_{i\in\{1,2,3\}} \Delta(v_i, u)$. Therefore, one concludes that

$$\forall (R,q) \in \mathcal{F}_{\mathcal{T}_1}, \quad \Gamma(R,q) \notin \mathbf{R}_a(\pi, \mathcal{E}_v^{\mathbb{R}}(A)). \tag{B.29}$$

This is equivalent to say that for all $(R,q) \in \mathcal{F}_{\mathcal{T}_1}$ one has $|\Gamma(R,q)| < 1$ if $\cos^2(u, \mathbf{E}(A)u) < 1$. Therefore, $\alpha(A, \Gamma(R,q)) > 0$ for all $(R,q) \in \mathcal{F}_{\mathcal{T}_1}$. Finally, one concludes that $\Psi_{1,A} \circ \Gamma$ satisfies (3.43). The last condition (3.44) is naturally satisfied since $\mathcal{D} = \mathbb{SO}(3) \times \mathcal{Q}$. The proof of exp-synergism for $\Psi_{1,A} \circ \Gamma$ is complete. Following similar steps as above, the proof of exp-synergism for $\Psi_{2,A} \circ \Gamma$ can be conducted.

## B.6 Proof of Proposition 3.4.3

In view of (3.75) and (3.84), the angular velocity error $\tilde{\omega}$ satisfies

$$I_B\dot{\tilde{\omega}} = I_B\omega \times \omega + u_\tau - I_B\dot{\omega}_d \tag{B.30}$$

$$= I_B\omega \times \tilde{\omega} + I_B\tilde{\omega} \times \omega_d + I_B\omega_d \times \omega_d + u_\tau - J\dot{\omega}_d \tag{B.31}$$

$$= [I_B\omega]_\times\tilde{\omega} - (K_2 + [\omega_d]_\times I_B)\tilde{\omega} - R_d^\top\psi(K_1\tilde{R}). \tag{B.32}$$

Note that the term $[I_B\omega]_\times\tilde{\omega}$ in the last equation is passive with respect to $\tilde{\omega}$. Consider the following Lyapunov function candidate

$$\mathbf{V}(\tilde{R},\tilde{\omega}) = \frac{1}{2}\mathbf{tr}(K_1(I-\tilde{R})) + \frac{1}{2}\tilde{\omega}^\top I_B\tilde{\omega}. \tag{B.33}$$

Using (2.72), (3.79), (B.32) and Assumption 3.4.2 one obtains

$$\dot{\mathbf{V}} = -\tilde{\omega}^\top(K_2 + [\omega_d]_\times I_B)\tilde{\omega} \leq -(\lambda_{\min}^{K_2} - \lambda_{\max}^{I_B}c_{\omega_d})\|\tilde{\omega}\|^2 \leq -\lambda\|\tilde{\omega}\|^2 \leq 0, \tag{B.34}$$

where $\lambda$ is a positive constant satisfying $\lambda_{\min}^{K_2} - \lambda_{\max}^{I_B}c_{\omega_d} \geq \lambda > 0$ which exists thanks to condition (3.85). Therefore, one concludes that the equilibrium point $(\tilde{R},\tilde{\omega}) = (I,0)$ is stable and that the angular velocity error $\tilde{\omega}$ is bounded (note that $\tilde{R}$ is naturally bounded since $\mathbb{SO}(3)$ is compact). Since, by assumption, the desired angular velocity is bounded it follows that the angular velocity $\omega = \tilde{\omega} + \omega_d$ is also bounded. Let us denote by $c_\omega$ and $c_{\tilde{\omega}}$ the upper bound on the norm of $\omega$ and $\tilde{\omega}$, respectively. This implies that $\dot{\tilde{\omega}}$ is also bounded and therefore one can easily show that $\ddot{\mathbf{V}}$ is bounded. By invoking Barbalat's Lemma it follows that $\dot{\mathbf{V}}$ must converge to zero and therefore $\tilde{\omega} \to 0$ as well. Moreover, one can show that $\ddot{\tilde{\omega}}$ is bounded and using again Barbalat's Lemma one has $\dot{\tilde{\omega}} \to 0$ which leads to conclude that $\psi(K_1\tilde{R})$ tends to zero in view of (B.32). Therefore the attitude error must converge either to the desired equilibrium $(\tilde{R},\tilde{\omega}) = (I,0)$ or to one of the undesired equilibria $\tilde{R} \in \mathbf{R}_a(\pi, \mathcal{E}_v^{\mathbb{R}^3}(A))$. Now, let us show that the desired equilibrium is exponentially stable. The set $\mathcal{S} = \{(\tilde{R},\tilde{\omega}) : \mathbf{V}(\tilde{R},\tilde{\omega}) \leq \mathbf{V}(\tilde{R}(0),\tilde{\omega}(0))\}$ is an invariant set for the closed-loop system. However, in view of (2.80), one has

$$2\lambda_{\min}^{\mathbf{E}(K_1)}|\tilde{R}|_I^2 \leq \frac{1}{2}\mathbf{tr}(K_1(I-\tilde{R})) \leq \mathbf{V}(\tilde{R},\tilde{\omega}) \leq \mathbf{V}(\tilde{R}(0),\tilde{\omega}(0)) < 2\lambda_{\min}^{\mathbf{E}(K_1)}, \tag{B.35}$$

which leads to conclude that $|\tilde{R}(t)|_I^2 < 1$ for all $t \geq 0$. Now, consider the cross term $\mathfrak{X} = \psi(K_1\tilde{R})^\top R_d I_B\tilde{\omega}$. The time derivative of $\mathfrak{X}$ along the trajectories of (3.79) and (B.32) satisfies

$$\begin{aligned}\dot{\mathfrak{X}} = \psi(K_1\tilde{R})^\top R_d\big([I_B\omega]_\times\tilde{\omega} - (K_2 + [\omega_d]_\times I_B)\tilde{\omega} - R_d^\top\psi(K_1\tilde{R})\big) + \\ \tilde{\omega}^\top J R_d^\top\mathbf{E}(K_1\tilde{R})R_d\tilde{\omega} + \psi(K_1\tilde{R})^\top R_d[\omega_d]_\times I_B\tilde{\omega},\end{aligned} \tag{B.36}$$

where (2.73) has been used. Moreover using (2.70) one has $\|\mathbf{E}(K_1\tilde{R})\|_F \leq \|\mathbf{E}(K_1)\|_F := c_E$ and using (2.80)-(2.84) one has $\|\psi(K_1\tilde{R})\| \leq 2\lambda_{\max}^{\mathbf{E}(K_1)}|\tilde{R}|_I$ which implies that

$$\dot{\mathfrak{X}} \leq -\|\psi(K_1\tilde{R})\|^2 + 2\lambda_{\max}^{\mathbf{E}(K_1)}|\tilde{R}|_I\|\tilde{\omega}\|\big(c_\omega\lambda_{\max}^{I_B} + \lambda_{\max}^{K_2}\big) + c_E\lambda_{\max}^{I_B}\|\tilde{\omega}\|^2. \tag{B.37}$$

On the other hand, since $|\tilde{R}|_I < 1$ for all times, it follows that there exists $\varepsilon > 0$ such that $1 - |\tilde{R}|_I^2 \geq \varepsilon$ and hence by using (2.80)-(2.82) one obtains that $\|\psi(K_1\tilde{R})\|^2 \geq 4\varepsilon(\lambda_{\min}^{\mathbf{E}(K_1)})^2|\tilde{R}|_I^2$. This leads to conclude that there exist $\varsigma_1, \varsigma_2, \varsigma_3 > 0$ such that

$$\dot{\mathfrak{X}} \leq -\varsigma_1|\tilde{R}|_I^2 + \varsigma_2\|\tilde{\omega}\|^2 + 2\varsigma_3|\tilde{R}|_I\|\tilde{\omega}\|. \tag{B.38}$$

Now, consider the following complete Lyapunov function candidate

$$\mathbf{W} = \mathbf{V}(\tilde{R}, \tilde{\omega}) + \mu\mathfrak{X}, \quad \mu > 0. \tag{B.39}$$

Again, using (2.80) and the fact that $\|\psi(K_1\tilde{R})\| \leq 2\lambda_{\max}^{\mathbf{E}(K_1)}|\tilde{R}|_I$, one can show that

$$\frac{1}{2}[|\tilde{R}|_I \ \|\tilde{\omega}\|]M_2[|\tilde{R}|_I \ \|\tilde{\omega}\|]^\top \leq \mathbf{W} \leq \frac{1}{2}[|\tilde{R}|_I \ \|\tilde{\omega}\|]M_2[|\tilde{R}|_I \ \|\tilde{\omega}\|]^\top \tag{B.40}$$

where the matrices $M_1$ and $M_2$ are given by

$$M_1 = \begin{bmatrix} 4\lambda_{\min}^{\mathbf{E}(K_1)} & -\mu\lambda_{\max}^{\mathbf{E}(K_1)}\lambda_{\max}^{J} \\ -\mu\lambda_{\max}^{\mathbf{E}(K_1)}\lambda_{\max}^{J} & \lambda_{\min}^{J} \end{bmatrix}, \quad M_2 = \begin{bmatrix} 4\lambda_{\max}^{\mathbf{E}(K_1)} & \mu\lambda_{\max}^{\mathbf{E}(K_1)}\lambda_{\max}^{J} \\ \mu\lambda_{\max}^{\mathbf{E}(K_1)}\lambda_{\max}^{J} & \lambda_{\max}^{J} \end{bmatrix}. \tag{B.41}$$

The time derivative of $\mathbf{W}$, in view of (B.34) and (B.38), satisfies

$$\dot{\mathbf{W}} \leq -[|\tilde{R}|_I \ \|\tilde{\omega}\|] \underbrace{\begin{bmatrix} \mu\varsigma_1 & -\mu\varsigma_3 \\ -\mu\varsigma_3 & \lambda - \mu \end{bmatrix}}_{M_3} [|\tilde{R}|_I \ \|\tilde{\omega}\|]^\top. \tag{B.42}$$

The matrices $M_1, M_2$ and $M_3$ are all positive definite provided that the scalar $\mu$ satisfies

$$0 < \mu < \left\{ \frac{2\sqrt{\lambda_{\min}^{\mathbf{E}(K_1)}\lambda_{\min}^{J}}}{\lambda_{\max}^{\mathbf{E}(K_1)}\lambda_{\max}^{J}}, \frac{\varsigma_1\lambda}{\varsigma_1\varsigma_2 + \varsigma_3^2} \right\}.$$

Note that the scalar $\mu$ is only used for analysis purposes and does not have an effect on the applied control. Finally, in view of (B.40)-(B.42), one has $\dot{\mathbf{W}} \leq -2(\lambda_{\min}^{M_3}/\lambda_{\max}^{M_3})\mathbf{W}$ and, therefore, the vector $[|\tilde{R}|_I, \|\tilde{\omega}\|]^\top$ is exponentially converging to zero which shows that the equilibrium $(\tilde{R}, \tilde{\omega}) = (I, 0)$ is exponentially stable.

## B.7 Proof of Proposition 4.2.6

Consider the trace function $\Psi_{1,A}$ defined in (3.28) for some $A$ such that $\mathbf{E}(A) > 0$ and let $\Phi = \Xi = \Psi_{1,A}$. Clearly in view of (2.80) the potential function $\Psi_{1,A}$ satisfies the first condition of Theorem 4.2.4. Moreover, the potential function $\Psi_{1,A}$ is smooth and does not have any singular points which implies that the third condition of Theorem 4.2.4 is also satisfied. It remains to show the second condition of Theorem 4.2.4. This condition implies that the gradient of $\Phi$ does not vanish except at the identity rotation $\tilde{R} = I$ during the flows of $\hat{\mathcal{F}}$. Therefore, it is necessary to guarantee that all the undesired critical points of $\Psi_{1,A}$ are inside the jump set $\hat{\mathcal{J}}$. Let $\tilde{R} = \mathbf{R}_a(\pi, v)$ where $v \in \mathcal{E}_v^{\mathbb{R}}(A)$ which represents an undesired critical point for $\Psi_{1,A}$, see (3.32). Therefore, using (2.74), one has $\Psi_{1,A}(\tilde{R}) = 2v^\top \mathbf{E}(A)v = 2\lambda_v^{\mathbf{E}(A)}$. Moreover, in view of Lemma 2.2.8, one has

$$\Psi_{1,A}(\tilde{R}\mathbf{R}_a(\theta, u)) = 2\lambda_v^{\mathbf{E}(A)} - 2\sin^2(\theta/2)\Delta(v, u). \tag{B.43}$$

Hence, it follows that

$$\Psi_{1,A}(\tilde{R}) - \min_{q\in\mathcal{Q}} \Psi_{1,A}(\tilde{R}\mathbf{R}_a(\theta, u_q)) = 2\sin^2(\theta/2) \max_{q\in\mathcal{Q}} \Delta(v, u_q), \tag{B.44}$$

where $\Delta(v, u) = v^\top(\mathbf{E}(A) + [u]_\times \mathbf{E}(A)[u]_\times)v = \lambda_v^{\mathbf{E}(A)} - (u \times v)^\top \mathbf{E}(A)(u \times v)$. Three different cases presents:

- $A$ has the same positive eigenvalues $\lambda_1^A = \lambda_2^A = \lambda_3^A = \lambda > 0$. In this case $\mathcal{E}_v^{\mathbb{R}}(A) = \mathbb{S}^2$ and therefore $\Delta(v, u_q) = \lambda(1 - \|u_q \times v\|^2) = \lambda\cos^2\angle(u_q, v)$. It follows that $\sum_{q=1}^3 \Delta(v, u_q) = \lambda\sum_{q=1}^3 \cos^2\angle(u_q, v) = \lambda$ since $\{u_q\}_{q\in\{1,2,3\}}$ forms an orthonormal basis. Hence $\max_{q\in\mathcal{Q}} \Delta(v, u_q) \geq \frac{1}{3}\sum_{q=1}^3 \Delta(v, u_q) = \lambda/3$ for all $v \in \mathbb{S}^2$.

- $A$ has two distinct eigenvalues $\lambda_1^A = \lambda_2^A$ and $\lambda_3^A > 0$. In this case $\mathcal{E}_v^{\mathbb{R}}(A) = (\text{span}\{u_1, u_2\} \cap \mathbb{S}^2) \cup \{u_3\}$. Let $v \in \text{span}\{u_1, u_2\} \cap \mathbb{S}^2$ such that $v = \alpha_1 u_1 + \alpha_2 u_2$. This implies that $u_1 \times v = \alpha_2 u_3$, $u_2 \times v = -\alpha_1 u_3$ and $u_3 \times v = -\alpha_2 u_1 + \alpha_1 u_2$. Hence, $\Delta(v, u_1) = \lambda_{u_1}^{\mathbf{E}(A)} - \alpha_2^2\lambda_{u_3}^{\mathbf{E}(A)}$, $\Delta(v, u_2) = \lambda_{u_1}^{\mathbf{E}(A)} - \alpha_1^2\lambda_{u_3}^{\mathbf{E}(A)}$ and $\Delta(v, u_3) = 0$. It follows that $\max_{q\in\mathcal{Q}} \Delta(v, u_q) \geq \frac{1}{3}\sum_{q=1}^3 \Delta(v, u_q) = \frac{1}{3}(2\lambda_{u_1}^{\mathbf{E}(A)} - \lambda_{u_3}^{\mathbf{E}(A)}) = \lambda_3^A/3$. In the case where $v = u_3$, then it is clear that $\max_{q\in\mathcal{Q}} \Delta(v, u_q) = \Delta(v, u_3) = \lambda_{u_3}^{\mathbf{E}(A)} = \frac{1}{2}(\lambda_1^A + \lambda_2^A) = \lambda_1^A$.

- $A$ has three distinct eigenvalues $0 \leq \lambda_1^A < \lambda_2^A < \lambda_3^A$. In this case $\mathcal{E}_v^{\mathbb{R}}(A) = \{u_1, u_2, u_3\}$. Let $v = u_p$ for some $p \in \mathcal{Q}$. Consequently $\max_{q\in\mathcal{Q}} \Delta(v, u_q) = \Delta(u_p, u_p) = \lambda_{u_p}^{\mathbf{E}(A)} \geq \lambda_{\min}^{\mathbf{E}(A)} = \frac{1}{2}(\lambda_1^A + \lambda_2^A)$.

By choosing $0 < \delta < \max_{q\in\mathcal{Q}} \Delta(v, u_q)$, across all the possible values of $v \in \mathcal{E}_v^{\mathbb{R}}(A)$, it follows that all the undesired critical points of $\Psi_{1,A}$ are inside the jump set $\hat{\mathcal{J}}$ defined in (4.17). Now, in view of (2.71) and (2.80)-(2.82) one has

$$\|\nabla\Psi_{1,A}(\tilde{R})\|_F^2 = \frac{1}{4}\|\mathbf{P}_{\mathfrak{so}(3)}(A\tilde{R})\|_F^2 = \frac{1}{2}\|\psi(A\tilde{R})\|^2 \leq 4(\lambda_{\max}^{\mathbf{E}(A)})|\tilde{R}|_I^2 \tag{B.45}$$

$$\geq 4(\lambda_{\min}^{\mathbf{E}(A)})\alpha(A,\tilde{R})|\tilde{R}|_I^2 \tag{B.46}$$

where $\alpha(A,\tilde{R}) = 1 - |\tilde{R}|_I^2\cos^2(v, \mathbf{E}(A)v)$ where $v$ is the rotation axis of $\tilde{R}$. However, $\alpha(A,\tilde{R}) = 0$ implies that $|\tilde{R}|_I^2 = 1$ and $v \in \mathcal{E}_v(A)$. In this case $\tilde{R} = \mathbf{R}_a(\pi, v)$ which is a critical point of $\Psi_{1,A}$. It follows that $\alpha(A,\tilde{R}) = 0$ implies $\tilde{R} \in \hat{\mathcal{J}}$. Therefore, for all $\tilde{R} \in \hat{\mathcal{F}}$ one has $\alpha(A,\tilde{R}) > 0$. Consequently, there exist $\alpha_3, \alpha_4 > 0$ such that

$$\alpha_4|\tilde{R}|_I^2 \leq \|\nabla\Psi_{1,A}(\tilde{R})\|_F^2 \leq \alpha_4|\tilde{R}|_I^2. \tag{B.47}$$

Therefore all the conditions of Theorem 4.2.4 are satisfied with $\Phi = \Xi = \Psi_{1,A}$.

## B.8 Proof of Proposition 4.2.7

Since $\Phi(\tilde{R}) = \Psi_1(\tilde{R}) = \frac{1}{2}\mathbf{tr}(I - \tilde{R}) = 2|\tilde{R}|_I^2$ then it is clear that item *i)* of Theorem 4.2.4 is satisfied. Moreover, in view of (2.71), one has

$$\begin{aligned}
\langle\langle\nabla\Phi(\tilde{R}), \nabla\Xi(\tilde{R})\rangle\rangle &= \langle\langle\nabla\Psi_1(\tilde{R}), \nabla\Psi_{1,A}(\tilde{R})\rangle\rangle \\
&= \langle\langle R\mathbf{P}_{\mathfrak{so}(3)}(\tilde{R}), R\mathbf{P}_{\mathfrak{so}(3)}(A\tilde{R})\rangle\rangle && \text{(by (2.71))} \\
&= \langle\langle\mathbf{P}_{\mathfrak{so}(3)}(\tilde{R}), \mathbf{P}_{\mathfrak{so}(3)}(A\tilde{R})\rangle\rangle \\
&= 2\psi(\tilde{R})^\top\psi(A\tilde{R}) && \text{(by (2.56))} \\
&= 2\psi(\tilde{R})^\top\mathbf{E}(A)\psi(\tilde{R}) && \text{(by (2.83))} \\
&\leq 2\lambda_{\max}^{\mathbf{E}(A)}\|\psi(\tilde{R})\|^2 \leq 8\lambda_{\max}^{\mathbf{E}(A)}|\tilde{R}|_I^2 && \text{(by (B.20))} \\
&\geq 2\lambda_{\min}^{\mathbf{E}(A)}\|\psi(\tilde{R})\|^2 = 8\lambda_{\min}^{\mathbf{E}(A)}|\tilde{R}|_I^2(1 - |\tilde{R}|_I^2) && \text{(by (B.20)).}
\end{aligned}$$

However, it is shown in the proof of Proposition 4.2.6 that for all $\tilde{R} \in \mathbf{R}_a(\pi, \mathbb{S}^2)$ (case where $A = I$) one has $\tilde{R} \in \hat{\mathcal{J}}$ if $\delta$ is chosen such that $0 < \delta < \bar{\delta} = 2\sin^2(\theta/2)/3$. It follows that for all $\tilde{R} \in \hat{\mathcal{F}}$ one has $\mathbf{tr}(\tilde{R}) > -1$ or, equivalently, $1 - |\tilde{R}|_I^2 > 0$ which implies that item *ii)* of Theorem 4.2.4 is also satisfied. Item *iii)* is naturally verified since $\Xi = \Psi_{1,A}$ is smooth and does not have any singular points. The last item also can be checked by noticing that $\|\nabla\Psi_{1,A}(\tilde{R})\|_F = \|\mathbf{P}_{\mathfrak{so}(3)}(A\tilde{R})\|_F = \sqrt{2}\|\psi(A\tilde{R})\| \leq 2\sqrt{2}\lambda_{\max}^{\mathbf{E}(A)}|\tilde{R}|_I$

where (2.80)-(2.82) have been used. Therefore, all conditions of Theorem 4.2.4 are met.

# Appendix C

# Proofs of Theorems

## C.1 Proof of Theorem 2.3.3

- The proof of item *i)* follows directly from Theorem 2.3.2 since all the conditions of the theorem are satisfied.

- Let us show item *ii)*. Assume that $\lambda_2 \leq 0$, $\lambda_1 > -\lambda_2\gamma$ and $j \leq \gamma t + J$ for some $\gamma \geq 0$ and $J \in \mathbb{N}$. Define the set

$$\Omega = \{x \in \mathcal{M} : \ \mathbf{V}(x) < \underline{\alpha}\mu^p\}. \tag{C.1}$$

  Then, in view of (2.99), for all $x \in \Omega$ one has $|x|_{\mathcal{A}}^p \leq \frac{1}{\underline{\alpha}}\mathbf{V}(x) < \mu^p$ which implies that $|x|_{\mathcal{A}} < \mu$ and, thus, $\Omega \subseteq (\mathcal{A} + \mu\mathbb{B})$. Consider the evolution of a solution $x$ satisfying

$$|x(0,0)|_{\mathcal{A}} < \exp((\lambda_2(J+1) - \lambda J)/p)(\underline{\alpha}/\bar{\alpha})^{\frac{1}{p}}\mu \tag{C.2}$$

  where $\lambda = (\lambda_1 + \lambda_2\gamma)/(1+\gamma) > 0$. Note that $|x(0,0)|_{\mathcal{A}} < \mu$ since the factor $\exp((\lambda_2(J+1)-\lambda J)/p)(\underline{\alpha}/\bar{\alpha})^{\frac{1}{p}}$ in (C.2) is less than 1. Let us show that $|x(t,j)|_{\mathcal{A}} < \mu$ for all $(t,j) \in \text{dom } x$. Assume that the solution $x$ of (2.89) stays inside the set $(\mathcal{A} + \mu\mathbb{B})$ up to $(t,j) \succeq (0,0)$. It is sufficient to show that, for all $\delta \geq 0$ such that $(t+\delta, j+1) \in \text{dom } x$, one has $x(t+\delta, j+1) \in (\mathcal{A} + \mu\mathbb{B})$ as well. It follows from arguments similar to the comparison lemma [Cai and Teel, 2009, Lemma C.1] and from (2.100)-(2.101) that

$$\mathbf{V}(x(t,j)) \leq \exp(-(\lambda_1 t + \lambda_2 j))\mathbf{V}(x(0,0)). \tag{C.3}$$

However, using $j \leq \gamma t + J$, $\lambda_2 \leq 0$ and $\lambda_1 + \gamma\lambda_2 > 0$, one obtains

$$-(\lambda_1 t + \lambda_2 j) \leq -(\lambda_1 + \lambda_2\gamma)t - \lambda_2 J \tag{C.4}$$

$$\leq -\frac{(\lambda_1 + \lambda_2\gamma)}{1+\gamma}t - \frac{(\lambda_1 + \lambda_2\gamma)}{1+\gamma}\gamma t - \lambda_2 J \tag{C.5}$$

$$\leq -\frac{(\lambda_1 + \lambda_2\gamma)}{1+\gamma}t - \frac{(\lambda_1 + \lambda_2\gamma)}{1+\gamma}(j - J) - \lambda_2 J \tag{C.6}$$

$$= -\lambda(t + j) + (\lambda - \lambda_2)J. \tag{C.7}$$

It follows from (C.3) that

$$\mathbf{V}(x(t,j)) \leq \exp((\lambda - \lambda_2)J)\exp(-\lambda(t+j))\mathbf{V}(x(0,0)). \tag{C.8}$$

Therefore, in view of (C.8), (2.99) and (C.2), one has $\mathbf{V}(x(t,j)) < \underline{\alpha}\exp(\lambda_2)\mu^p \leq \underline{\alpha}\mu^p$. Let $t_{j+1}$ be the instant of time where the $(j+1)$-th jump happens, *i.e.* $(t_{j+1}, j), (t_{j+1}, j+1) \in \operatorname{dom} x$. Thus, it is clear that $(t,j) \preceq (t_{j+1}, j) \preceq (t_{j+1}, j+1) \preceq (t+\delta, j+1)$. Since $\mathbf{V}$ is nonincreasing during the flows, by (2.100), it is clear that $\mathbf{V}(x(t_{j+1}, j)) \leq \mathbf{V}(x(t,j)) < \underline{\alpha}\exp(\lambda_2)\mu^p < \underline{\alpha}\mu^p$. Thus $x(t_{j+1}, j) \in \Omega$ which implies that $x(t_{j+1}, j) \in (\mathcal{A} + \mu\mathbb{B})$. Therefore, in view of (2.101), one obtains

$$\mathbf{V}(x(t_{j+1}, j+1)) \leq \exp(-\lambda_2)\mathbf{V}(x(t_{j+1}, j)) < \underline{\alpha}\mu^p. \tag{C.9}$$

This again implies that $x(t_{j+1}, j+1) \in (\mathcal{A} + \mu\mathbb{B})$. Repeating the above argument, it is easy to show that $x$ cannot leave the set $(\mathcal{A} + \mu\mathbb{B})$ by flowing between the two hybrid times $(t_{j+1}, j+1)$ and $(t+\delta, j+1)$. Therefore $x(t+\delta, j+1) \in (\mathcal{A} + \mu\mathbb{B})$. We have just shown that, starting from an initial condition satisfying (C.2), one has $x(t,j) \in (\mathcal{A} + \mu\mathbb{B})$ for all $(t,j) \in \operatorname{dom} x$ which implies that the bound (C.8) holds for all $(t,j) \in \operatorname{dom} x$ as well. Finally, in view of (2.99) and (C.8), it follows that if $x(0,0)$ satisfies (C.2), $x(t,j)$ satisfies the following exponential bound

$$|x(t,j)|_{\mathcal{A}} \leq \left[\frac{\bar{\alpha}\exp((\lambda - \lambda_2)J)}{\underline{\alpha}}\right]^{\frac{1}{p}} \exp(-\lambda p^{-1}(t+j))|x(0,0)|_{\mathcal{A}}. \tag{C.10}$$

- Let us show item *iii)*. Assume that $\lambda_1 \leq 0$, $\lambda_2 > -\lambda_1\gamma$ and $t \leq \gamma j + T$ for some $\gamma, T \geq 0$. Consider the evolution of a solution $x$ satisfying

$$|x(0,0)|_{\mathcal{A}} < \exp((\lambda_1(T+\varepsilon) - \lambda T)/p)(\underline{\alpha}/\bar{\alpha})^{\frac{1}{p}}\mu \tag{C.11}$$

where $\lambda = (\lambda_2 + \lambda_1\gamma)/(1+\gamma) > 0$ and $\varepsilon > 0$ is any strictly positive constant. Let us show that $|x(t,j)|_{\mathcal{A}} < \mu$ for all $(t,j) \in \text{dom } x$. First, in view of (2.99) and (C.11), one has $\mathbf{V}(x(0,0)) < \underline{\alpha}\mu^p$ which implies that $x(0,0) \in \Omega$ with $\Omega$ defined in (C.1). Since $\lambda_2 > 0$, $\mathbf{V}$ is decreasing during the jumps, one concludes that $x$ cannot leave $\Omega$ by jumping. Let us verify that $x$ cannot leave $\Omega$ by flowing as well. Let $j \in \mathbb{N}$ such that $t_{j+1} - t_j > 0$ and $(t_j, j), (t_{j+1}, j) \in \text{dom } x$. That's to say, the time interval $[t_j, t_{j+1}]$, associated to the $j$-th jump, is not empty. If the solution $x$ is purely discrete then this $j$ does not exist. However, in this case of discrete solutions, exponential convergence is trivial since one has exponential decrease of $\mathbf{V}(x)$ at every jump and no flow occurs. Assume, moreover, that $x(t',j') \in (\mathcal{A}+\mu\mathbb{B})$ for all $(t',j') \preceq (t,j) \prec (t_{j+1}, j)$ where $(t,j) \in \text{dom } x$ is a hybrid time between the two hybrid times $(t_j, j)$ and $(t_{j+1}, j)$ . Then, from (2.100)-(2.101), one has

$$\mathbf{V}(x(t,j)) \leq \exp(-(\lambda_1 t + \lambda_2 j))\mathbf{V}(x(0,0)). \tag{C.12}$$

However, using $t \leq \gamma j + T$, $\lambda_1 \leq 0$ and $\lambda_2 + \gamma\lambda_1 > 0$, one obtains

$$\begin{aligned} -(\lambda_1 t + \lambda_2 j) &\leq -(\lambda_2 + \lambda_1\gamma)j - \lambda_1 T && \text{(C.13)}\\ &\leq -\frac{(\lambda_2 + \lambda_1\gamma)}{1+\gamma} j - \frac{(\lambda_2 + \lambda_1\gamma)}{1+\gamma}\gamma j - \lambda_1 T && \text{(C.14)}\\ &\leq -\frac{(\lambda_2 + \lambda_1\gamma)}{1+\gamma} j - \frac{(\lambda_2 + \lambda_1\gamma)}{1+\gamma}(t - T) - \lambda_1 T && \text{(C.15)}\\ &= -\lambda(t+j) + (\lambda - \lambda_1)T. && \text{(C.16)} \end{aligned}$$

It follows that

$$\mathbf{V}(x(t,j)) \leq \exp((\lambda - \lambda_1)T)\exp(-\lambda(t+j))\mathbf{V}(x(0,0)). \tag{C.17}$$

It is clear that $x(t,j)$ is still inside the set $\Omega$. Now, let $(t+\varepsilon', j) \in \text{dom } x$, with $0 < \varepsilon' < \varepsilon$, be a hybrid time after a small enough flow has occurred. Assume, moreover, that $\mathbf{V}(x(t+\varepsilon', j)) = \underline{\alpha}\mu^p$ which corresponds to the boundary of the open set $\Omega$. Now, by integrating (2.100) between $(t,j)$ and $(t+\varepsilon', j)$, one has

$$\mathbf{V}(x(t+\varepsilon', j)) \leq \exp(-\lambda_1\varepsilon')\mathbf{V}(x(t,j)). \tag{C.18}$$

Therefore, combining (C.11), (C.17) and (C.18), one obtains

$$\mathbf{V}(x(t+\varepsilon', j)) < \exp(\lambda_1(\epsilon - \varepsilon'))\underline{\alpha}\mu^p \leq \underline{\alpha}\mu^p \tag{C.19}$$

which contradicts the assumption that $\mathbf{V}(x(t+\varepsilon', j)) = \underline{\alpha}\mu^p$. Therefore, $x$ cannot leave $\Omega$ by flowing. Hence, it is true that $x(t,j) \in \Omega \subseteq (\mathcal{A} + \mu\mathbb{B})$ for all $(t,j) \in \operatorname{dom} x$. This implies that the bound (C.17) holds as well for all times and jumps. Consequently, using again (2.99), one deduces that

$$|x(t,j)|_{\mathcal{A}} \leq \left[\frac{\bar{\alpha}\exp((\lambda - \lambda_1)T)}{\underline{\alpha}}\right]^{\frac{1}{p}} \exp(-\lambda p^{-1}(t+j))|x(0,0)|_{\mathcal{A}}. \tag{C.20}$$

## C.2 Proof of Theorem 3.3.1

Assume that $R(0) \in \Pi_{\mathbb{SO}(3)}$ which implies, in view of the fact that $\mathbf{R}_a(\pi, \mathbb{S}^2)$ is a repeller, that $R(t) \in \Pi_{\mathbb{SO}(3)}$ for all $t \geq 0$. Therefore, the inverse map $\mathbf{Z}(R)$, defined in (2.32), exists for all $t \geq 0$ such that $\mathbf{R}_r(\mathbf{Z}(R(t))) = R(t)$. Consequently, in view of (2.35), (2.79) and (3.31), one obtains

$$\begin{aligned}
\frac{d}{dt}\mathbf{Z}(R) &= \frac{1}{2}\big(I + [\mathbf{Z}(R)]_\times + \mathbf{Z}(R)\mathbf{Z}(R)^\top\big)\omega = -k\big(I + [\mathbf{Z}(R)]_\times + \mathbf{Z}(R)\mathbf{Z}(R)^\top\big)\psi(AR) \\
&= -k\big(I + [\mathbf{Z}(R)]_\times + \mathbf{Z}(R)\mathbf{Z}(R)^\top\big)\frac{(I - [\mathbf{Z}(R)]_\times)}{1 + \|\mathbf{Z}(R)\|^2}\mathbf{E}(A)\mathbf{Z}(R) \\
&= -k\frac{\big(I - [\mathbf{Z}(R)]_\times^2 + \mathbf{Z}(R)\mathbf{Z}(R)^\top\big)}{(1 + \|\mathbf{Z}(R)\|^2)}\mathbf{E}(A)\mathbf{Z}(R) = -k\mathbf{E}(A)\mathbf{Z}(R),
\end{aligned} \tag{C.21}$$

where $[\mathbf{Z}(R)]_\times^2 = -\|\mathbf{Z}(R)\|^2 I + \mathbf{Z}(R)\mathbf{Z}(R)^\top$ is used to obtain the last equality. By simple integration of (C.21), it follows that $\mathbf{Z}(R(t)) = e^{-k\mathbf{E}(A)t}\mathbf{Z}(R(0))$, for all $t \geq 0$, which yields (3.34).

## C.3 Proof of Theorem 3.3.8

Let $\Phi \in \mathcal{P}_{\mathcal{D}}$, where $\mathcal{D} \subseteq \mathbb{SO}(3) \times \mathcal{Q}$, be an exp-synergistic potential function with gap exceeding $\delta$. Define the state $X = (R, q) \in \mathbb{SO}(3) \times \mathcal{Q}$. The closed-loop system (3.27)

with (3.49) is written as

$$\dot{X} = \mathbf{F}(X) = \begin{bmatrix} -\nabla\Phi(R,q) \\ 0 \end{bmatrix} \qquad X \in \mathcal{F}_{\mathcal{T}}, \tag{C.22}$$

$$X^+ \in \mathbf{J}(X) = \begin{bmatrix} R \\ \arg\min_{m\in\mathcal{Q}} \Phi(R,m) \end{bmatrix} \qquad X \in \mathcal{J}_{\mathcal{T}}. \tag{C.23}$$

Then, for all $(R,q) \in \mathcal{F}_{\mathcal{T}}$, the time derivative of $\Phi$ along (C.22) satisfies

$$\dot{\Phi}(R,q) = \langle \nabla\Phi(R,q), \dot{R}\rangle_R = -\|\nabla\Phi(R,q)\|_F^2 \leq -\alpha_3 |R|_I^2 \leq -\frac{\alpha_3}{\alpha_2}\Phi(R,q)$$

where (2.13) and (3.42)-(3.43) are used. Moreover, for all $(R,q) \in \mathcal{J}_{\mathcal{T}}$, one has

$$\Phi(R^+,q^+) = \min_{m\in\mathcal{Q}} \Phi(R,m) \leq \Phi(R,q) - \delta < \Phi(R,q).$$

The closed-loop system satisfies the following:

- The basic hybrid assumptions (C1)-(C3) (provided in Section 2.3). In fact, the sets $\mathcal{F}_{\mathcal{T}}$ and $\mathcal{J}_{\mathcal{T}}$ are closed. The flow map $\mathbf{F}$ is continuous and single-valued and, therefore, locally bounded, outer semicontinuous, and the set $\mathbf{F}(X)$ is nonempty and convex. The jump map $\mathbf{J}$ is outer semicontinuous, locally bounded, and nonempty.

- Every solution is precompact (complete and bounded). In fact, the configuration manifold $\mathbb{SO}(3) \times \mathcal{Q}$ is compact and therefore all solutions are bounded preventing finite escape time. Moreover, the space $\mathbb{SO}(3)\times\mathcal{Q}$ is viable under the flow (*i.e.* there exists a nontrivial solution from any initial condition in $\mathcal{F}_{\mathcal{T}}$) and $\mathbf{J}(\mathcal{J}_{\mathcal{T}}) \subset \mathcal{F}_{\mathcal{T}} \cup \mathcal{J}_{\mathcal{T}}$. It follows from [Goebel and Teel, 2006, Proposition 2.4] that every solution is complete.

- $\mathcal{J}_{\mathcal{T}} \cap \mathbf{J}(\mathcal{J}_{\mathcal{T}}) = \emptyset$ since every jump maps the state $(R,q)$ to the flow set $\mathcal{F}_{\mathcal{T}}$.

Therefore, using [Sanfelice *et al.*, 2007, Lemma 2.7], one concludes that there exists $\bar{\gamma} > 0$ such that $t_{j+1} - t_j \geq \bar{\gamma}$ for all $j \geq 1$ and $(t_j, j), (t_{j+1}, j) \in \mathrm{dom}(R,q)$. This means that there is a minimum elapsed time between every two possible jumps. This leads to the fact that $t \geq \bar{\gamma}(j-1)$ for all $(t,j) \in \mathrm{dom}\, x$. Consequently, all the conditions of item *ii)* of Theorem 2.3.3 are met, with $\lambda_1 = \alpha_3/\alpha_2, \lambda_2 = 0, \gamma = 1/\bar{\gamma}, J = 1$, and one concludes that the set $\mathcal{A}_1$ is globally exponentially stable.

## C.4 Proof of Theorem 3.4.4

Define the state $X = (\tilde{R}, q, I_B\tilde{\omega}, R_d, \omega_d) \in \mathbb{SO}(3) \times \mathcal{Q} \times \mathbb{R}^3 \times \mathbb{SO}(3) \times \mathbb{R}^3$. Note that $R_d$ and $\omega_d$ are included in the state $X$ so that one can write the closed-loop system as an autonomous hybrid system. One can show that $X$ follows the dynamics of an autonomous hybrid system written in the general form (2.89) with the following data

$$\mathbf{F}(X) = \begin{bmatrix} \tilde{R}[R_d\tilde{\omega}]_\times \\ 0 \\ I_B\tilde{\omega} \times \tilde{\omega} + I_B\omega_d \times \tilde{\omega} - K_2\tilde{\omega} - R_d^\top \psi(\tilde{R}^\top \nabla\Phi(\tilde{R}, q)) \\ R_d[\omega_d]_\times \\ c_{\dot{\omega}_d}\mathbb{B} \end{bmatrix}, \tag{C.24}$$

$$\mathbf{J}(X) = \begin{bmatrix} \tilde{R}^\top & \mathbf{J}_{\mathcal{T}}(\tilde{R}) & (I_B\tilde{\omega})^\top & R_d^\top & \omega_d^\top \end{bmatrix}^\top, \tag{C.25}$$

$$\mathcal{F} = \mathcal{F}_{\mathcal{T}} \times \mathbb{R}^3 \times \mathbb{SO}(3) \times \mathbb{R}^3, \tag{C.26}$$

$$\mathcal{J} = \mathcal{J}_{\mathcal{T}} \times \mathbb{R}^3 \times \mathbb{SO}(3) \times \mathbb{R}^3. \tag{C.27}$$

Consider the following Lyapunov function candidate

$$\mathbf{V}(X) = \frac{1}{2}\Phi(\tilde{R}, q) + \frac{1}{2}\tilde{\omega}^\top I_B\tilde{\omega}. \tag{C.28}$$

The time derivative of the function $\mathbf{V}$ along the flows of $\mathcal{F}$ satisfies

$$\dot{\mathbf{V}}(X) = -\tilde{\omega}^\top K_2\tilde{\omega} \leq 0. \tag{C.29}$$

Moreover, for all $X \in \mathcal{J}$ and $G \in \mathbf{J}(X)$, one has

$$\mathbf{V}(G) - \mathbf{V}(X) = \frac{1}{2}(\min_{m \in \mathcal{Q}} \Phi(\tilde{R}, m) - \Phi(\tilde{R}, q)) \leq -\frac{\delta}{2} < 0. \tag{C.30}$$

It follows that $\mathbf{V}$ is nonincreasing during both the flows and jumps. Thus, the angular velocity error $\tilde{\omega}$ is uniformly bounded. Also, since $\omega_d$ is bounded by assumption, it follows that $\omega = \tilde{\omega} + \omega_d$ is bounded. Let us denote by $c_\omega, c_{\tilde{\omega}}$ the upper bound on the angular velocity and the angular velocity error, respectively. To show exponential stability, consider the following Lyapunov function candidate

$$\mathbf{W}(X) = \frac{1}{2}\Phi(\tilde{R}, q) + \frac{1}{2}\tilde{\omega}^\top I_B\tilde{\omega} + \mu\tilde{\omega}^\top J R_d^\top \psi(\tilde{R}^\top \nabla\Phi(\tilde{R}, q)), \tag{C.31}$$

for some positive constant $\mu$. In view of (3.42)-(3.43), one can show that $\mathbf{W}$ satisfies

$$\frac{1}{2}\begin{bmatrix}|\tilde{R}|_I\\ \|\tilde{\omega}\|\end{bmatrix}^\top \underbrace{\begin{bmatrix}\alpha_1 & -\mu\lambda_{\max}^{I_B}\sqrt{\frac{\alpha_4}{2}}\\ \star & \lambda_{\min}^{I_B}\end{bmatrix}}_{M_1}\begin{bmatrix}|\tilde{R}|_I\\ \|\tilde{\omega}\|\end{bmatrix} \leq \mathbf{W}(X) \leq \frac{1}{2}\begin{bmatrix}|\tilde{R}|_I\\ \|\tilde{\omega}\|\end{bmatrix}^\top \underbrace{\begin{bmatrix}\alpha_2 & \mu\lambda_{\max}^{I_B}\sqrt{\frac{\alpha_4}{2}}\\ \star & \lambda_{\max}^{I_B}\end{bmatrix}}_{M_2}\begin{bmatrix}|\tilde{R}|_I\\ \|\tilde{\omega}\|\end{bmatrix}. \tag{C.32}$$

For all $X \in \mathcal{F}$, the time derivative of $\mathbf{W}(X)$ along (C.24)-(C.27) is given by

$$\begin{aligned}\dot{\mathbf{W}}(X) &= \dot{\mathbf{V}}(X) + \mu(I_B\omega\times\tilde{\omega} - K_2\tilde{\omega} - R_d^\top\psi(\tilde{R}^\top\nabla\Phi(\tilde{R},q)))^\top R_d^\top\psi(\tilde{R}^\top\nabla\Phi(\tilde{R},q))\\ &\quad - \mu\tilde{\omega}^\top J[\omega_d]_\times R_d^\top\psi(\tilde{R}^\top\nabla\Phi(\tilde{R},q)) + \mu\tilde{\omega}^\top JR_d^\top D(\tilde{R},q)R_d\tilde{\omega}\\ &\leq -\mu\|\psi(\tilde{R}^\top\nabla\Phi(\tilde{R},q))\|^2 - \tilde{\omega}^\top K_2\tilde{\omega} + \mu\lambda_{\max}^{I_B}c_D\|\tilde{\omega}\|^2\\ &\quad + \left(\lambda_{\max}^{K_2} + \lambda_{\max}^{I_B}(c_\omega + c_{\omega_d})\right)\|\psi(\tilde{R}^\top\nabla\Phi(\tilde{R},q))\|\|\tilde{\omega}\|\\ &\leq -\frac{\mu\alpha_3}{2}|\tilde{R}|_I^2 - (\lambda_{\min}^{K_2} - \mu\lambda_{\max}^{I_B}c_D)\|\tilde{\omega}\|^2 + \mu(\lambda_{\max}^{I_B}(c_\omega + c_{\omega_d}) + \lambda_{\max}^{K_2})\sqrt{\frac{\alpha_4}{2}}|\tilde{R}|_I\|\tilde{\omega}\|\end{aligned}$$

where the fact that

$$\dot{\psi}(\tilde{R}^\top\nabla\Phi(\tilde{R},q)) = D(\tilde{R},q)R_d\tilde{\omega}, \tag{C.33}$$

for some matrix $D(\tilde{R},q) \in \mathbb{R}^{3\times 3}$, has been used. The matrix $D(\cdot,\cdot)$ has a bounded norm, by some $c_D > 0$, thanks to the compactness of $\mathbb{SO}(3)$. As a result, and in view of (3.43), one deduces that

$$\dot{\mathbf{W}}(X) \leq -\frac{1}{2}\begin{bmatrix}|\tilde{R}|_I\\ \|\tilde{\omega}\|\end{bmatrix}^\top \underbrace{\begin{bmatrix}\mu\alpha_3 & -\mu(\lambda_{\max}^{I_B}(c_\omega + c_{\omega_d}) + \lambda_{\max}^{K_2})\sqrt{\frac{\alpha_4}{2}}\\ \star & 2(\lambda_{\min}^{K_2} - \mu c_D)\end{bmatrix}}_{M_3}\begin{bmatrix}|\tilde{R}|_I\\ \|\tilde{\omega}\|\end{bmatrix}. \tag{C.34}$$

It can be verified that there exists $\bar{\mu} > 0$ such that matrices $M_1, M_2$ and $M_3$ are positive definite for any $0 < \mu < \bar{\mu}$. Therefore, from (C.32)-(C.34) one has $\dot{\mathbf{W}}(X) \leq -\lambda_1\mathbf{W}(X)$, for all $X \in \mathcal{F}$, where $\lambda_1 = \lambda_{\min}^{M_3}/\lambda_{\max}^{M_2}$. Moreover, for all $X \in \mathcal{J}$, if the constant $\mu$ is chosen sufficiently small such that $\mu < \frac{\delta}{8c_{\tilde{\omega}}\lambda_{\max}^{I_B}\sqrt{\alpha_4/2}}$, one obtains

$$\begin{aligned}\mathbf{W}(X^+) - \mathbf{W}(X) &= \frac{1}{2}\left(\Phi(\tilde{R},q^+) - \Phi(\tilde{R},q)\right) + \mu\tilde{\omega}^\top JR_d^\top\psi(\tilde{R}^\top\nabla\Phi(\tilde{R},q))|_q^{q^+}\\ &\leq -\frac{1}{2}\delta + 2\mu c_{\tilde{\omega}}\lambda_{\max}^{I_B}\sqrt{\alpha_4/2} < -\frac{1}{4}\delta < 0.\end{aligned}$$

Finally, using similar argument as in the proof of Theorem 3.3.8, one can show the existence of $\bar{\gamma} > 0$ satisfying $t \geq \bar{\gamma}(j-1)$ for all $(t,j) \in \text{dom}X$. Therefore, using item *ii)* from Theorem 2.3.3 with $\lambda_1 = \lambda_{\min}^{M_3}/\lambda_{\max}^{M_2}, \lambda_2 = 0, \gamma = 1/\bar{\gamma}$ and $J = 1$, one can conclude that the set $\mathcal{A}_2$ is globally exponentially stable.

## C.5 Proof of Theorem 3.4.5

Define $\tilde{x} = x - \psi(\tilde{R}^\top \nabla\Phi(\tilde{R}, q))$ and let $X = (\tilde{R}, q, I_B\tilde{\omega}, \tilde{x}, R_d, \omega_d) \in \mathbb{SO}(3) \times \mathcal{Q} \times \mathbb{R}^3 \times \mathbb{R}^3 \times \mathbb{SO}(3) \times \mathbb{R}^3$. Then, using (3.74)-(3.75), (3.77), (3.87)-(3.88) and (C.33), one can show that $X$ follows the dynamics of an autonomous hybrid system written in the general form (2.89) with the following data

$$\mathbf{F}(X) = \begin{bmatrix} \tilde{R}[R_d\tilde{\omega}]_\times \\ 0 \\ I_B\tilde{\omega} \times \tilde{\omega} + I_B\omega_d \times \tilde{\omega} - K_2\tilde{\omega} - R_d^\top \tilde{x} - R_d^\top \psi(\tilde{R}^\top \nabla\Phi(\tilde{R}, q)) \\ -K_3\tilde{x} - D(\tilde{R}, q)R_d\tilde{\omega} \\ R_d[\omega_d]_\times \\ c_{\dot{\omega}_d}\mathbb{B} \end{bmatrix}, \tag{C.35}$$

$$\mathbf{J}(X) = \begin{bmatrix} \tilde{R} \\ \mathbf{J}_{\mathcal{T}}(\tilde{R}) \\ I_B\tilde{\omega} \\ \tilde{x} + \psi(\tilde{R}^\top \nabla\Phi(\tilde{R}, q)) - \psi(\tilde{R}^\top \nabla\Phi(\tilde{R}, \mathbf{J}_{\mathcal{T}}(\tilde{R}))) \\ R_d \\ \omega_d \end{bmatrix}, \tag{C.36}$$

$$\mathcal{F} = \mathcal{F}_{\mathcal{T}} \times \mathbb{R}^3 \times \mathbb{R}^3 \times \mathbb{SO}(3) \times \mathbb{R}^3, \tag{C.37}$$

$$\mathcal{J} = \mathcal{J}_{\mathcal{T}} \times \mathbb{R}^3 \times \mathbb{R}^3 \times \mathbb{SO}(3) \times \mathbb{R}^3. \tag{C.38}$$

First, since $\Phi$ is exp-synergistic then, in view of (3.43), one has $\|\psi(\tilde{R}^\top \nabla\Phi(\tilde{R}, q))\| \leq \sqrt{\alpha_4/2}$. If follows from (3.88) and the boundedness of $\psi(\tilde{R}^\top \nabla\Phi(\tilde{R}, q))$ that that for all $(t,j) \in \text{dom}X$

$$\|x(t,j)\| \leq e^{-\lambda_{\min}^{K_3} t}\|x(0,0)\| + \frac{\lambda_{\max}^{K_3}}{\lambda_{\min}^{K_3}}\sqrt{\frac{\alpha_4}{2}} \leq c_x + \frac{\lambda_{\max}^{K_3}}{\lambda_{\min}^{K_3}}\sqrt{\frac{\alpha_4}{2}}. \tag{C.39}$$

Therefore, $\tilde{x}$ is also bounded such that for all $(t, j) \in \text{dom}X$

$$\|\tilde{x}(t,j)\| \leq c_{\tilde{x}} := c_x + \left(\frac{\lambda_{\max}^{K_3}}{\lambda_{\min}^{K_3}} + 1\right)\sqrt{\frac{\alpha_4}{2}}. \tag{C.40}$$

Let $\mu_2 > 0$ be a positive scalar satisfying

$$\mu_2 \leq \frac{\delta}{4c_{\tilde{x}}^2}, \tag{C.41}$$

$$\frac{(1+\mu_2 c_D)^2}{\mu_2 \lambda_{\min}^{K_2}} < \lambda_{\min}^{K_3}. \tag{C.42}$$

Consider the following Lyapunov function candidate

$$\mathbf{V}(X) = \frac{1}{2}\Phi(\tilde{R}, q) + \frac{1}{2}\tilde{\omega}^\top I_B \tilde{\omega} + \frac{1}{2}\mu_2 \|\tilde{x}\|^2. \tag{C.43}$$

The time derivative of the function $\mathbf{V}$ along the flows of $\mathcal{F}$ satisfies

$$\dot{\mathbf{V}}(X) = -\tilde{\omega}^\top K_2 \tilde{\omega} - \mu_2 \tilde{x}^\top K_3 \tilde{x} + (1+\mu_2 c_D)\|\tilde{\omega}\|\|\tilde{x}\| \tag{C.44}$$

$$= -\begin{bmatrix}\|\tilde{\omega}\| \\ \|\tilde{x}\|\end{bmatrix}^\top \begin{bmatrix}\lambda_{\min}^{K_2} & -(1+\mu_2 c_D)/2 \\ \star & \mu_2 \lambda_{\min}^{K_3}\end{bmatrix}\begin{bmatrix}\|\tilde{\omega}\| \\ \|\tilde{x}\|\end{bmatrix} \tag{C.45}$$

which, under the gain condition (C.41)-(C.42), is negative semidefinite such that $\dot{\mathbf{V}}(X) \leq 0$. Moreover, for all $X \in \mathcal{J}$ one has

$$\mathbf{V}(X^+) - \mathbf{V}(X) = \frac{1}{2}(\min_{m \in \mathcal{Q}} \Phi(\tilde{R}, m) - \Phi(\tilde{R}, q)) + \frac{1}{2}\mu_2 \|\tilde{x}\|^2 |_q^{q+} \tag{C.46}$$

$$\leq -\frac{\delta}{2} + \mu_2 c_{\tilde{x}}^2 \leq -\frac{\delta}{4} < 0. \tag{C.47}$$

It follows that $\mathbf{V}$ is nonincreasing during both the flows and jumps. Thus all signals are bounded, including $\tilde{\omega}, \omega$ and $\tilde{x}$. Let us denote by $c_\omega$ and $c_{\tilde{\omega}}$ the upper bounds on the norm of the angular velocity $\omega$ and the angular velocity error $\tilde{\omega}$. Let $\mu_1 > 0$ be a scalar satisfying

$$\mu_1 < \min\left\{\frac{[2\alpha_1 \lambda_{\min}^{I_B}]^{\frac{1}{2}}}{\lambda_{\max}^{I_B}\sqrt{\alpha_4}}, \frac{\delta/8\sqrt{2}}{c_{\tilde{\omega}}\lambda_{\max}^{I_B}\sqrt{\alpha_4}}, \frac{\mu_2 \alpha_3 \lambda_{\min}^{K_3}}{\alpha_4}, \frac{\alpha_3 \lambda_{\min}^{K_2}}{\alpha_4(\lambda_{\max}^{I_B}(c_\omega + c_{\omega_d}) + \lambda_{\max}^{K_2}) + 2\alpha_3 c_D}\right\}. \tag{C.48}$$

Now, consider the complete Lyapunov function candidate

$$\mathbf{W}(X) = \frac{1}{2}\Phi(\tilde{R}, q) + \frac{1}{2}\tilde{\omega}^\top I_B \tilde{\omega} + \mu_1 \tilde{\omega}^\top J R_d^\top \psi(\tilde{R}^\top \nabla\Phi(\tilde{R}, q)) + \frac{1}{2}\mu_2 \|\tilde{x}\|^2. \tag{C.49}$$

Note that the first three terms of $\mathbf{W}(X)$ are similar to the Lyapunov function defined (C.31) which satisfies (C.32). Therefore, under the condition (C.48) on the scalar $\mu_1$, one guarantees that $\mathbf{W}(X)$ is positive definite with respect to $\mathcal{A}_3$. Moreover, it is not difficult to show that the time derivative of $\mathbf{W}$ satisfies, during the flows of $\mathcal{F}$, the bound

$$\dot{\mathbf{W}} \leq -\frac{1}{2} z_1^\top M_1 z_1 - \frac{1}{2} z_2^\top M_2 z_2 - \frac{1}{2} z_3^\top M_3 z_3, \tag{C.50}$$

where

$$M_1 = \begin{bmatrix} \mu_1 \frac{\alpha_3}{2} & -\mu_1(\lambda_{\max}^{I_B}(c_\omega + c_{\omega_d}) + \lambda_{\max}^{K_2})\sqrt{\frac{\alpha_4}{2}} \\ \star & \lambda_{\min}^{K_2} - 2\mu_1 c_D \end{bmatrix},$$
$$M_2 = \begin{bmatrix} \mu_1 \frac{\alpha_3}{2} & -\mu_1\sqrt{\frac{\alpha_4}{2}} \\ \star & \mu_2 \lambda_{\min}^{K_3} \end{bmatrix},$$
$$M_3 = \begin{bmatrix} \lambda_{\min}^{K_2} & -(1 + \mu_2 c_D) \\ \star & \mu_2 \lambda_{\min}^{K_3} \end{bmatrix},$$

and $z_1 = [|\tilde{R}|_I,\ \|\tilde{\omega}\|]^\top$, $z_2 = [|\tilde{R}|_I,\ \|\tilde{x}\|]^\top$ and $z_3 = [\|\tilde{\omega}\|,\ \|\tilde{x}\|]^\top$. Condition (C.48) on $\mu_1$ ensures that the matrices $M_1$ and $M_2$ are positive definite. Moreover, under the gain condition (C.41)-(C.42) one ensures that $M_3$ is positive definite as well. In this case there exists $\lambda_1$ such that $\dot{\mathbf{W}}(X) \leq -\lambda_1 \mathbf{W}(X)$ for all $X \in \mathcal{F}$. Between jumps, one has, for all $X \in \mathcal{J}$,

$$\begin{aligned}\mathbf{W}(X^+) - \mathbf{W}(X) &= -\frac{1}{2}(\Phi(\tilde{R}, q^+) - \Phi(\tilde{R}, q)) + \mu_1 \tilde{\omega}^\top J R_d^\top \psi(\tilde{R}^\top \nabla\Phi(\tilde{R}, q))|_q^{q^+} + \frac{\mu_2}{2}\|\tilde{x}\|^2|_q^{q^+} \\ &\leq -\frac{\delta}{2} + 2\mu_1 c_{\tilde{\omega}} \lambda_{\max}^{I_B}\sqrt{\alpha_4/2} + \mu_2 c_{\tilde{x}} \leq -\frac{\delta}{8}\end{aligned}$$

where, again, the conditions (C.48) and (C.41) have been used. Finally, using similar argument as in the proof of Theorem 3.3.8, one can show the existence of $\bar{\gamma} > 0$ satisfying $t \geq \bar{\gamma}(j-1)$ for all $(t, j) \in \mathrm{dom} X$. Therefore, using item *ii)* from Theorem 2.3.3 with $\lambda_1 > 0, \lambda_2 = 0, \gamma = 1/\bar{\gamma}$ and $J = 1$, one concludes that the set $\mathcal{A}_3$ is globally exponentially stable.

## C.6 Proof of Theorem 4.2.3

In view of (4.1), (4.2) and (4.7), one obtains

$$\begin{aligned}\dot{\tilde{R}} = \dot{R}\hat{R}^\top - R\dot{\hat{R}}^\top &= R[\omega]_\times \hat{R}^\top - R\big[\omega_y - \hat{b}_\omega + K_1\hat{R}^\top \mathbf{w}(\tilde{R}, q)\big]_\times \hat{R}^\top \\ &= \tilde{R}\big[ - \hat{R}\tilde{b}_\omega - \hat{R}K_1\hat{R}^\top \mathbf{w}(\tilde{R}, q)\big]_\times,\end{aligned}$$

where identity (2.61) has been used to obtain the last equality. Define the state $X = (\tilde{R}, q, \tilde{b}_\omega, \hat{R}, \omega) \in \mathbb{SO}(3) \times \mathcal{Q} \times \mathbb{R}^3 \times \mathbb{SO}(3) \times \mathbb{R}^3$. Then, one can show that $X$ follows the dynamics of an autonomous hybrid system written in the general form (2.89) with the following data

$$\mathbf{F}(X) = \begin{bmatrix} \tilde{R}[-\hat{R}\tilde{b}_\omega - \hat{R}K_1\hat{R}^\top \mathbf{w}(\tilde{R}, q)]_\times \\ 0 \\ k_2\hat{R}^\top \mathbf{w}(\tilde{R}, q) \\ \hat{R}[\omega + \tilde{b}_\omega + K_1\hat{R}^\top \mathbf{w}(\tilde{R}, q)]_\times \\ c_{\dot{\omega}}\mathbb{B} \end{bmatrix}, \tag{C.51}$$

$$\mathbf{J}(X) = \begin{bmatrix} \tilde{R}^\top & \mathbf{J}_{\mathcal{T}}(\tilde{R}) & \tilde{b}_\omega^\top & \hat{R}^\top & \omega^\top \end{bmatrix}^\top, \tag{C.52}$$

$$\mathcal{F} = \mathcal{F}_{\mathcal{T}} \times \mathbb{R}^3 \times \mathbb{SO}(3) \times \mathbb{R}^3, \tag{C.53}$$

$$\mathcal{J} = \mathcal{J}_{\mathcal{T}} \times \mathbb{R}^3 \times \mathbb{SO}(3) \times \mathbb{R}^3. \tag{C.54}$$

Consider the following Lyapunov function candidate

$$\mathbf{V}(X) = \frac{1}{2}\Phi(\tilde{R}, q) + \frac{1}{2k_2}\|\tilde{b}_\omega\|^2 \tag{C.55}$$

The time derivative of $\mathbf{V}$ along the flows of (C.51) satisfies

$$\dot{\mathbf{V}}(X) = \psi(\tilde{R}^\top \nabla\Phi(\tilde{R}, q))^\top(-\hat{R}\tilde{b}_\omega - \hat{R}K_1\hat{R}^\top \mathbf{w}(\tilde{R}, q)) + \tilde{b}_\omega^\top \hat{R}^\top \mathbf{w}(\tilde{R}, q) \tag{C.56}$$

$$\leq -\lambda_{\min}^{K_1}\|\mathbf{w}(\tilde{R}, q)\|^2 \leq -\frac{1}{2}\lambda_{\min}^{K_1}\alpha_3|\tilde{R}|^2 \leq 0 \tag{C.57}$$

where (3.44) has been used. Moreover, for all $X \in \mathcal{J}$ and $G \in \mathbf{J}(X)$, one has

$$\mathbf{V}(G) - \mathbf{V}(X) = \frac{1}{2}(\Phi(\tilde{R}, q^+) - \Phi(\tilde{R}, q)) \leq -\frac{\delta}{2} < 0. \tag{C.58}$$

It follows that $\mathbf{V}$ is nonincreasing during both the flows and jumps. Thus all signals are bounded, including $\tilde{b}_\omega$. Denote by $\bar{c}_b > 0$ the bound on the norm of $\tilde{b}_\omega$. Define the cross

term $\mathfrak{X}(X) = \tilde{b}_\omega^\top \hat{R}^\top \psi(\tilde{R})$. In view of (C.51), the time derivative of $\mathfrak{X}$ during the flows of $\mathcal{F}$ is

$$\dot{\mathfrak{X}}(X) = \tilde{b}_\omega^\top \hat{R}^\top \mathbf{E}(\tilde{R}) \left(-\hat{R}\tilde{b}_\omega - \hat{R}K_1\hat{R}^\top \mathbf{w}(\tilde{R}, q))\right) - \tilde{b}_\omega^\top [\omega + \tilde{b}_\omega + K_1\hat{R}^\top \mathbf{w}(\tilde{R}, q)]_\times \hat{R}^\top \psi(\tilde{R}) + k_2 \hat{R}^\top \mathbf{w}(\tilde{R}, q)^\top \hat{R}^\top \psi(\tilde{R}).$$

In addition, one has the following bound

$$\begin{aligned} -\tilde{b}_\omega^\top \hat{R}^\top \mathbf{E}(\tilde{R}) \hat{R}\tilde{b}_\omega &= -\|\tilde{b}_\omega\|^2 + \tilde{b}_\omega^\top \hat{R}^\top (I - \mathbf{E}(\tilde{R}))\hat{R}\tilde{b}_\omega \\ &\leq -\|\tilde{b}_\omega\|^2 + \frac{1}{2}\mathbf{tr}(I - \tilde{R})\|\tilde{b}_\omega\|^2 \qquad \text{(by (2.67))} \\ &\leq -\|\tilde{b}_\omega\|^2 + 2\bar{c}_b^2 |\tilde{R}|_I^2 \qquad \text{(by (2.38))} \end{aligned}$$

Moreover, since $\Phi$ is exp-synergistic it satisfies (3.44) which implies that $\|\mathbf{w}(\tilde{R}, q)\| \leq \sqrt{\alpha_4/2}|\tilde{R}|_I$. It follows that

$$\begin{aligned} -\tilde{b}_\omega^\top \hat{R}^\top \mathbf{E}(\tilde{R}) \hat{R} K_1 \hat{R}^\top \mathbf{w}(\tilde{R}, q) &\leq \sqrt{3}\lambda_{\max}^{K_1}\sqrt{\alpha_4/2}|\tilde{R}|_I \|\tilde{b}_\omega\| \\ -\tilde{b}_\omega^\top [\omega + \tilde{b}_\omega + K_1\hat{R}^\top \mathbf{w}(\tilde{R}, q)]_\times \hat{R}^\top \psi(\tilde{R}) &= -\tilde{b}_\omega^\top [\omega + K_1\hat{R}^\top \mathbf{w}(\tilde{R}, q)]_\times \hat{R}^\top \psi(\tilde{R}) \\ &\leq c_\omega \|\tilde{b}_\omega\| \|\psi(\tilde{R})\| + \lambda_{\max}^{K_1} \|\tilde{b}_\omega\| \|\psi(\tilde{R})\| \|\mathbf{w}(\tilde{R}, q)\| \\ &\leq 2c_\omega \|\tilde{b}_\omega\| |\tilde{R}|_I + 2\lambda_{\max}^{K_1} \bar{c}_b \sqrt{\alpha_4/2} |\tilde{R}|_I^2, \quad \text{(by (B.20))}. \end{aligned}$$

Consequently, one deduces that there exist $\varsigma_1, \varsigma_2 > 0$ such that

$$\dot{\mathfrak{X}}(X) \leq -\|\tilde{b}_\omega\|^2 + \varsigma_1 |\tilde{R}|_I^2 + \varsigma_2 \|\tilde{b}_\omega\| |\tilde{R}|_I, \quad X \in \mathcal{F}. \tag{C.59}$$

Now, consider the following Lyapunov function candidate

$$\mathbf{W}(X) = \mathbf{V}(X) + \mu \mathfrak{X}(X), \quad \mu > 0. \tag{C.60}$$

Since $\Phi$ satisfies (3.42) and in view of (B.20) one obtains the following lower and upper bounds on $\mathbf{W}(X)$

$$\frac{1}{2}[|\tilde{R}|_I \ \|\tilde{b}_\omega\|]^\top \begin{bmatrix} \alpha_1 & -2\mu \\ \star & k_2^{-1} \end{bmatrix} \begin{bmatrix} |\tilde{R}|_I \\ \|\tilde{b}_\omega\| \end{bmatrix} \leq \mathbf{W}(X) \leq \frac{1}{2}[|\tilde{R}|_I \ \|\tilde{b}_\omega\|]^\top \begin{bmatrix} \alpha_2 & 2\mu \\ \star & k_2^{-1} \end{bmatrix} \begin{bmatrix} |\tilde{R}|_I \\ \|\tilde{b}_\omega\| \end{bmatrix}$$

Define the distance $|X|_{\mathcal{A}}^2 = |\tilde{R}|_I^2 + \|\tilde{b}_\omega\|^2$ from the set $\mathcal{A}$ to any point $X$ on the manifold. If $\mu$ is selected such that $\mu < \sqrt{\alpha_1 k_2^{-1}}/2$ then it is clear from the above bound on $\mathbf{W}$ that $\mathbf{W}(X)$ satisfies condition (2.99) of Theorem (2.3.3) with $p = 2$. Moreover, in view

of (C.59) and (C.57) one deduces that

$$\dot{\mathbf{W}}(X) = -\frac{1}{2}[|\tilde{R}|_I \ \|\tilde{b}_\omega\|]^\top \begin{bmatrix} \lambda_{\min}^{K_1}\alpha_3 - 2\mu\varsigma_1 & -\mu\varsigma_2 \\ \star & 2\mu \end{bmatrix} \begin{bmatrix} |\tilde{R}|_I \\ \|\tilde{b}_\omega\| \end{bmatrix}, \quad X \in \mathcal{F}.$$

Assume that $0 < \mu < 2\lambda_{\min}^{K_1}\alpha_3/(4\varsigma_1 + \varsigma_2^2)$. Then, there exists $\lambda_1 > 0$ such that $\dot{\mathbf{W}}(X) \leq -\lambda_1 \mathbf{W}(X)$ for all $X \in \mathcal{F}$. Besides, for all $X \in \mathcal{J}$ and $G \in \mathbf{J}(X)$, one has

$$\mathbf{W}(G) - \mathbf{W}(X) = \mathbf{V}(G) - \mathbf{V}(X) = \frac{1}{2}(\Phi(\tilde{R}, q^+) - \Phi(\tilde{R}, q)) \leq -\frac{\delta}{2}. \tag{C.61}$$

Therefore, one has $\mathbf{W}(X(t,j)) \leq \mathbf{W}(X(0,0)) - \frac{\delta}{2}j$ which implies that $j \leq 2\mathbf{W}(X(0,0))/\delta$. Hence, the number of jumps is bounded (finite) for all initial conditions. Moreover, following steps as in the last part of the proof of Theorem 3.3.8, one can show the existence of $\bar{\gamma} > 0$ satisfying $t \geq \bar{\gamma}(j-1)$ for all $(t,j) \in \text{dom}X$. Therefore, using item *ii)* from Theorem 2.3.3 with $\lambda_1 > 0, \lambda_2 = 0, \gamma = 1/\bar{\gamma}$ and $J = 1$, one concludes that the set $\mathcal{A}$ is globally exponentially stable.

## C.7 Proof of Theorem 4.2.4

In order to write the closed-loop system as an autonomous system, let us define the state $X = (\tilde{R}, \tilde{b}_\omega, \hat{R}, \hat{b}_\omega, \omega, t) \in \mathbb{SO}(3) \times \mathbb{R}^3 \times \mathbb{SO}(3) \times \mathbb{R}^3 \times \mathbb{R}^3 \times \mathbb{R}_{\geq 0}$. Note that the time $t$ is included as a state variable which has the trivial hybrid dynamics $\dot{t} = 1$ and $t^+ = t$. Then, in view of (4.1) and (4.14)-(4.17), one can show that $X$ follows the dynamics of an autonomous hybrid system written in the general form (2.89) with the following data

$$\mathbf{F}(X) = \begin{bmatrix} \tilde{R}[-\hat{R}\tilde{b}_\omega - k_1\mathbf{w}(t,\tilde{R})]_\times \\ \mathbf{P}_{c_b}(\hat{b}_\omega, k_2\hat{R}^\top\mathbf{w}(t,\tilde{R})) \\ \hat{R}[\omega + \tilde{b}_\omega + k_1\hat{R}^\top\mathbf{w}(t,\tilde{R})]_\times \\ -\mathbf{P}_{c_b}(\hat{b}_\omega, k_2\hat{R}^\top\mathbf{w}(t,\tilde{R})) \\ c_{\dot{\omega}}\mathbb{B} \\ 1 \end{bmatrix}, \tag{C.62}$$

$$\mathbf{J}(X) = \begin{bmatrix} \mathbf{R}_a(\theta,u_q)^\top\tilde{R}^\top & \tilde{b}_\omega^\top & \hat{R}^\top\mathbf{R}_a(\theta,u_q) & \hat{b}_\omega^\top & \omega^\top & t \end{bmatrix}^\top, \tag{C.63}$$

$$\mathcal{F} = \hat{\mathcal{F}} \times \mathbb{R}^3 \times \mathbb{SO}(3) \times \mathbb{R}^3 \times \mathbb{R}^3 \times \mathbb{R}_{\geq 0}, \tag{C.64}$$

$$\mathcal{J} = \hat{\mathcal{J}} \times \mathbb{R}^3 \times \mathbb{SO}(3) \times \mathbb{R}^3 \times \mathbb{R}^3 \times \mathbb{R}_{\geq 0}. \tag{C.65}$$

The objective is to establish global exponential stability of the "closed", but unbounded, set $\mathcal{A}$ defined in Theorem 4.2.4. First note that item *iii)* of Theorem 4.2.4 is necessary for the implementation of the correction term $\mathbf{w}(t, \tilde{R})$ since we do not want to encounter, during the flows of $\mathcal{F}$, a singularity in the gradient of the potential function $\Xi(t, \tilde{R})$. The bias estimation error $\tilde{b}_\omega = b_\omega - \hat{b}_\omega$ is *a priori* bounded, such that

$$\|\tilde{b}_\omega\| \leq \|b_\omega\| + \|\hat{b}_\omega\| \leq 2c_b + \varepsilon := \bar{c}_b \tag{C.66}$$

thanks to the fact that $b_\omega$ is bounded by assumption and $\hat{b}_\omega$ is also bounded as per property (2.4) of the projection operator $\mathbf{P}_{c_b}(\cdot)$. Define the cross term function $\mathfrak{X}(X) = \tilde{b}_\omega^\top \hat{R}^\top \psi(\tilde{R})$. In view of (C.62) one has

$$\begin{aligned}\dot{\mathfrak{X}}(X) = \tilde{b}_\omega^\top \hat{R}^\top \mathbf{E}(\tilde{R}) \left(-\hat{R}\tilde{b}_\omega - k_1 \mathbf{w}(t, \tilde{R})\right) - \tilde{b}_\omega^\top [\omega + \tilde{b}_\omega + k_1 \hat{R}^\top \mathbf{w}(t, \tilde{R})]_\times \hat{R}^\top \psi(\tilde{R}) + \\ \mathbf{P}_{c_b}(\hat{b}_\omega, k_2 \hat{R}^\top \mathbf{w}(t, \tilde{R}))^\top \hat{R}^\top \psi(\tilde{R}), \qquad X \in \mathcal{F}.\end{aligned}$$

In addition, one has the following bound

$$\begin{aligned}-\tilde{b}_\omega^\top \hat{R}^\top \mathbf{E}(\tilde{R}) \hat{R} \tilde{b}_\omega &= -\|\tilde{b}_\omega\|^2 + \tilde{b}_\omega^\top \hat{R}^\top (I - \mathbf{E}(\tilde{R})) \hat{R} \tilde{b}_\omega \\ &\leq -\|\tilde{b}_\omega\|^2 + \frac{1}{2}\mathbf{tr}(I - \tilde{R})\|\tilde{b}_\omega\|^2 && \text{(by (2.67))} \\ &\leq -\|\tilde{b}_\omega\|^2 + 2\bar{c}_b^2 |\tilde{R}|_I^2 && \text{(by (2.38) and (C.66))}\end{aligned}$$

Moreover, by item *iv)* of Theorem 4.2.4 the norm of the innovation term is bounded as $\|\mathbf{w}(t, \tilde{R})\| = \|\nabla \Xi(t, \tilde{R})\|_F / \sqrt{2} \leq (\alpha_5 / \sqrt{2}) |\tilde{R}|_I$. It follows that

$$\begin{aligned}&- k_1 \tilde{b}_\omega^\top \hat{R}^\top \mathbf{E}(\tilde{R}) \mathbf{w}(t, \tilde{R}) \\ &= -k_1 \tilde{b}_\omega^\top \hat{R}^\top \mathbf{w}(t, \tilde{R}) + k_1 \tilde{b}_\omega^\top \hat{R}^\top (I - \mathbf{E}(\tilde{R})) \mathbf{w}(t, \tilde{R}) \\ &\leq -k_1 \tilde{b}_\omega^\top \hat{R}^\top \mathbf{w}(t, \tilde{R}) + \frac{k_1}{2}\mathbf{tr}(I - \tilde{R}) \tilde{b}_\omega^\top \hat{R}^\top \mathbf{w}(t, \tilde{R}) + \frac{k_1}{2}\|I - \tilde{R}\|_F \|\tilde{b}_\omega\| \|\mathbf{w}(t, \tilde{R})\|, \text{(by (2.68))} \\ &\leq -k_1 \tilde{b}_\omega^\top \hat{R}^\top \mathbf{w}(t, \tilde{R}) + k_1 \bar{c}_b \alpha_5 (\sqrt{2} + 1) |\tilde{R}|_I^2, \ \text{(by (2.38) and (C.66))}\end{aligned}$$

The following bounds can also be derived using (B.20) and (C.66)

$$\begin{aligned}-\tilde{b}_\omega^\top [\omega + \tilde{b}_\omega + k_1 \hat{R}^\top \mathbf{w}(t, \tilde{R})]_\times \hat{R}^\top \psi(\tilde{R}) &= -\tilde{b}_\omega^\top [\omega + k_1 \hat{R}^\top \mathbf{w}(t, \tilde{R})]_\times \hat{R}^\top \psi(\tilde{R}) \\ &\leq c_\omega \|\tilde{b}_\omega\| \|\psi(\tilde{R})\| + k_1 \|\tilde{b}_\omega\| \|\psi(\tilde{R})\| \|\mathbf{w}(t, \tilde{R})\| \\ &\leq 2c_\omega \|\tilde{b}_\omega\| |\tilde{R}|_I + \sqrt{2} k_1 \bar{c}_b \alpha_5 |\tilde{R}|_I^2.\end{aligned}$$

$$\mathbf{P}_{c_b}(\hat{b}_\omega, k_2\hat{R}^\top\mathbf{w}(t,\tilde{R}))^\top\hat{R}^\top\psi(\tilde{R}) \leq$$
$$k_2\|\mathbf{w}(t,\tilde{R})\|\|\psi(\tilde{R})\| \leq \sqrt{2}k_2\alpha_5|\tilde{R}|_I^2, \quad \text{(by (2.6) and (B.20))}.$$

Consequently, one deduces that the cross term $\mathfrak{X}$ satisfies the following

$$\dot{\mathfrak{X}}(X) \leq -\|\tilde{b}_\omega\|^2 - k_1\tilde{b}_\omega^\top\hat{R}^\top\mathbf{w}(t,\tilde{R}) + (\varsigma_1 + k_1\varsigma_2)|\tilde{R}|_I^2 + 2c_\omega\|\tilde{b}_\omega\||\tilde{R}|_I, \quad X \in \mathcal{F} \tag{C.67}$$

where $\varsigma_1 = 2\bar{c}_b^2 + \sqrt{2}k_2\alpha_5$ and $\varsigma_2 = \bar{c}_b\alpha_5(2\sqrt{2}+1)$. Now, consider the following Lyapunov function candidate

$$\mathbf{V} = \Phi(\tilde{R}) + \frac{\mu k_1}{2k_2}\|\tilde{b}_\omega\|^2 + \mu\mathfrak{X}, \quad \mu > 0. \tag{C.68}$$

Using (B.20) it can be verified that $\mathbf{V}$ satisfies

$$\frac{1}{2}[|\tilde{R}|_I, \|\tilde{b}_\omega\|]M_1[|\tilde{R}|_I, \|\tilde{b}_\omega\|]^\top \leq \mathbf{V} \leq \frac{1}{2}[|\tilde{R}|_I, \|\tilde{b}_\omega\|]M_2[|\tilde{R}|_I, \|\tilde{b}_\omega\|]^\top \tag{C.69}$$

where matrices $M_1$ and $M_2$ are defined as follows

$$M_1 = \begin{bmatrix} 2\alpha_1 & -\mu \\ -\mu & \frac{\mu k_1}{k_2} \end{bmatrix}, \quad M_2 = \begin{bmatrix} 2\alpha_2 & \mu \\ \mu & \frac{\mu k_1}{k_2} \end{bmatrix} \tag{C.70}$$

The time derivative of $\mathbf{V}$ along the flows of (C.62) satisfies

$$\begin{aligned}
\dot{\mathbf{V}} &= \langle\langle\nabla\Phi(\tilde{R}), \tilde{R}[-\hat{R}\tilde{b}_\omega]_\times\rangle\rangle - k_1\langle\langle\nabla\Phi(\tilde{R}), \nabla\Xi(t,\tilde{R})\rangle\rangle + \\
&\quad \frac{\mu k_1}{k_2}\tilde{b}_\omega^\top\mathbf{P}_{c_b}(\hat{b}_\omega, k_2\hat{R}^\top\mathbf{w}(t,\tilde{R})) + \mu\dot{\mathfrak{X}} \\
&\leq \sqrt{2}\alpha_6\|\tilde{b}_\omega\||\tilde{R}|_I - k_1\alpha_3|\tilde{R}|_I^2 + \\
&\quad \frac{\mu k_1}{k_2}\tilde{b}_\omega^\top\mathbf{P}_{c_b}(\hat{b}_\omega, k_2\hat{R}^\top\mathbf{w}(t,\tilde{R})) + \mu\dot{\mathfrak{X}}, \quad \text{(by item ii) and vi) of Theorem 4.2.4)} \\
&\leq \sqrt{2}\alpha_6\|\tilde{b}_\omega\||\tilde{R}|_I - k_1\alpha_3|\tilde{R}|_I^2 + \mu k_1\tilde{b}_\omega^\top\hat{R}^\top\mathbf{w}(t,\tilde{R}) + \mu\dot{\mathfrak{X}}, \quad \text{(by (2.5))} \\
&\leq \sqrt{2}\alpha_6\|\tilde{b}_\omega\||\tilde{R}|_I - k_1\alpha_3|\tilde{R}|_I^2 - \mu\|\tilde{b}_\omega\|^2 + \mu(\varsigma_1 + k_1\varsigma_2)|\tilde{R}|_I^2 + 2\mu c_\omega\|\tilde{b}_\omega\||\tilde{R}|_I, \quad \text{(by (C.67))} \\
&\leq -[|\tilde{R}|_I, \|\tilde{b}_\omega\|]M_3[|\tilde{R}|_I, \|\tilde{b}_\omega\|]^\top,
\end{aligned}$$

where the matrix $M_3$ is defined by

$$M_3 = \begin{bmatrix} k_1(\alpha_3 - \mu\varsigma_2) - \mu\varsigma_1 & \star \\ -(\alpha_6/\sqrt{2} + \mu c_\omega) & \mu \end{bmatrix}.$$

Therefore, it is sufficient to pick $0 < \mu < \min\{2\alpha_1 k_1/k_2, \alpha_3/\varsigma_2\}$ and $k_1$ satisfying

$$k_1 > \left\{ \frac{\mu^2\varsigma_1 + (\alpha_6/\sqrt{2} + \mu c_\omega)^2}{\mu(\alpha_3 - \mu\varsigma_2)} \right\}$$

to guarantee that all the matrices $M_1, M_2$ and $M_3$ are positive definite. Therefore, there exists $\lambda_1 > 0$ such that $\dot{\mathbf{V}}(X) \leq -\lambda_1 \mathbf{V}(X)$ for all $X \in \mathcal{F}$. Moreover for all $X \in \mathcal{J}$ and $G \in \mathbf{J}(X)$ one has

$$\begin{aligned}
\mathbf{V}(G) - \mathbf{V}(X) &= \Phi(\tilde{R}\mathbf{R}_a(\theta, u_q)) - \Phi(\tilde{R}) + \mu\tilde{b}_\omega \hat{R}^\top(\psi(\tilde{R}\mathbf{R}_a(\theta, u_q)) - \psi(\tilde{R})) \\
&\leq -\delta + 2\bar{c}_b\mu, \quad \text{(by (2.84) and (C.66))} \\
&< -\frac{\delta}{2}, \qquad \text{(C.71)}
\end{aligned}$$

provided that $\mu$ is chosen such that $\mu < \delta/4\bar{c}_b$. Therefore, one has $\mathbf{V}(X(t,j)) \leq \mathbf{V}(X(0,0)) - \frac{\delta}{2}j$ which implies that $j \leq 2\mathbf{V}(X(0,0))/\delta$. Hence, for all initial conditions, the number of jumps is bounded (finite). Now, in contrast to the synergistic-based approach, the reset-based observer do not guarantee that the elapsed time between two consecutive jumps is bounded since the jumps do not (in general) map the state $X$ to the flow set. Let us show that the number of consecutive jumps (jumps that occur in a row without flowing) is bounded. Let $(t,j), (t,j') \in \text{dom}X$ such that $j' > j$. Then, in view of (4.15) and (4.17) one has

$$\Phi(\tilde{R}(t,j)) - \Phi(\tilde{R}(t,j+1)) \geq \delta \qquad \text{(C.72)}$$

$$\vdots \qquad \text{(C.73)}$$

$$\Phi(\tilde{R}(t,j'-1)) - \Phi(\tilde{R}(t,j')) \geq \delta \qquad \text{(C.74)}$$

which implies that

$$\Phi(\tilde{R}(t,j)) - \Phi(\tilde{R}(t,j')) \geq (j'-j)\delta. \qquad \text{(C.75)}$$

However, in view of item *i)* of Theorem 4.2.4 one has $0 \leq \Phi(\tilde{R}) \leq \alpha_2|\tilde{R}|_I^2 \leq \alpha_2$ for all $\tilde{R} \in \mathbb{SO}(3)$. Therefore, one obtains the bound $(j'-j) \leq \alpha_2/\delta$ which shows that it is not possible to have more than $\bar{J} := \max\{j \in \mathbb{N} : j \leq \alpha_2/\delta\}$ number of jumps at the same instant of time. Note that in view of Remark 4.2.5 one has necessarily $\alpha_2 \geq \delta$ under the

conditions of Theorem 4.2.4. It follows that there exists $\bar{\gamma} > 0$ such that

$$t_{j'} - t_j \geq \bar{\gamma}, \ \forall (t_{j'}, j'), (t_j, j) \in \text{dom}X \text{ s.th. } j' > j + \bar{J}. \tag{C.76}$$

Let $(t, j) \in \text{dom}X$ which implies, by the structure of the hybrid time domain dom$X$, that $t \in [t_j, t_{j+1}]$. Let $n \in \mathbb{N}$ such that the jump index $j$ satisfies

$$n(\bar{J} + 1) \leq j < (n + 1)(\bar{J} + 1). \tag{C.77}$$

Note that $n$ always exists for all $j \in \mathbb{N}$. Then, one has

$$\begin{aligned} t_j - t_{j-n(\bar{J}+1)} &= t_j - t_{j-(\bar{J}+1)} + t_{j-(\bar{J}+1)} - t_{j-2(\bar{J}+1)} + \cdots + t_{j-(n-1)(\bar{J}+1)} - t_{j-n(\bar{J}+1)} \\ &= \sum_{k=1}^{n} \left( t_{j-(k-1)(\bar{J}+1)} - t_{j-k(\bar{J}+1)} \right) \\ &\geq n\bar{\gamma} \end{aligned} \tag{C.78}$$

where (C.76) is used with the fact that $j - (k-1)(\bar{J}+1) > j - k(\bar{J}+1) + \bar{J}$ for all $k \in \{1, \cdots, n\}$. Therefore, in view of (C.77) and (C.78) one obtains

$$t \geq t_j \geq n\bar{\gamma} + t_{j-n(\bar{J}+1)} \geq n\bar{\gamma} > \left( \frac{j}{\bar{J}+1} - 1 \right) \bar{\gamma}. \tag{C.79}$$

Therefore, all conditions of item *ii)* of Theorem 2.3.3 are met, with $\lambda_1 > 0, \lambda_2 = 0, \gamma = (\bar{J}+1)/\bar{\gamma}$ and $J = \bar{J} + 1$. It follows that the set $\mathcal{A}$ is globally exponentially stable.

## C.8 Proof of Theorem 4.3.1

The quaternion representation of the attitude error $\tilde{R}$ is used to proceed with the proof. Let $Q = (\eta, \epsilon) \in \mathbb{Q}$ be the quaternion representation of the attitude error $\tilde{R} \in \mathbb{SO}(3)$. The quaternion $\mathbf{Q}(\sigma) := ([1 + \|\sigma\|^2]^{-\frac{1}{2}}, \sigma[1 + \|\sigma\|^2]^{-\frac{1}{2}})$ is a quaternion associated to the rotation matrix $\mathbf{R}_r(\sigma)$. It can be verified that the equivalent closed-loop hybrid system for (4.36)-(4.37), using the quaternion representation, is written as follows

$$\begin{cases} \dot{Q} = 0 \\ \dot{\tau} = 1 \end{cases} \qquad (Q, \tau) \in \mathcal{F}_q, \tag{C.80}$$

$$\begin{cases} Q^+ = Q \odot \mathbf{Q}(\sigma)^{-1} \\ \tau^+ = 0 \end{cases} \qquad (Q, \tau) \in \mathcal{J}_q, \tag{C.81}$$

where the flow set $\mathcal{F}_q$ and jump set $\mathcal{J}_q$ are defined as

$$\mathcal{F}_q = \big\{(Q,\tau) \in \mathbb{Q} \times \mathbb{R}_{\geq 0} : \ \tau \in [0, T_2]\big\}, \tag{C.82}$$

$$\mathcal{J}_q = \big\{(Q,\tau) \in \mathbb{Q} \times \mathbb{R}_{\geq 0} : \ \tau \in [T_1, T_2]\big\}. \tag{C.83}$$

Consider the following Lyapunov function candidate

$$\mathbf{V}(\eta, \epsilon, \tau) = \|\epsilon\|^2. \tag{C.84}$$

During the flows of $\mathcal{F}_q$ one has $\dot{Q} = 0$ which implies that $\dot{\epsilon} = 0$ and therefore $\dot{\mathbf{V}}(\eta, \epsilon, \tau) = 0$ for all $(\eta, \epsilon, \tau) \in \mathcal{F}_q$. To evaluate the change in $\mathbf{V}$ during the jumps of $\mathcal{J}_q$, notice from (2.86) and (2.78) that

$$\sigma = \sum_{i=1}^{n} \rho_i [\hat{R} b_i]_\times a_i = 2\psi(A\tilde{R}) = 4(\eta I - [\epsilon]_\times)\mathbf{E}(A)\epsilon \tag{C.85}$$

where $\mathbf{E}(A) = \frac{1}{2}(\mathbf{tr}(A)I - A)$ and $A = \sum_{i=1}^{n} \rho_i a_i a_i^\top$. During the jumps of $\mathcal{J}_q$ one has $Q^+ = Q \odot \mathbf{Q}(\sigma)^{-1}$ which implies, using the quaternion multiplication rule (2.27), that

$$\begin{aligned}
\epsilon^+ &= \frac{-\eta\sigma + \epsilon - [\epsilon]_\times \sigma}{\sqrt{1 + \|\sigma\|^2}} \\
&= \frac{-4\eta(\eta I - [\epsilon]_\times)\mathbf{E}(A)\epsilon + \epsilon - 4[\epsilon]_\times(\eta I - [\epsilon]_\times)\mathbf{E}(A)\epsilon}{\sqrt{1 + \|\sigma\|^2}} \\
&= \frac{\epsilon + 4\epsilon\epsilon^\top \mathbf{E}(A)\epsilon - 4\mathbf{E}(A)\epsilon}{\sqrt{1 + \|\sigma\|^2}} \\
&= \frac{I + 4(\epsilon^\top \mathbf{E}(A)\epsilon)I - 4\mathbf{E}(A)}{(1 + 16\epsilon^\top \mathbf{E}(A)(I - \epsilon\epsilon^\top)\mathbf{E}(A)\epsilon)^{\frac{1}{2}}}\epsilon \\
&:= M(\epsilon)\epsilon.
\end{aligned} \tag{C.86}$$

Now, let us compute the norm square of the quaternion vector part $\epsilon^+$. In view of (C.86) and using the fact that $\|\sigma\|^2 = 16\epsilon^\top \mathbf{E}(A)(I - \epsilon\epsilon^\top)\mathbf{E}(A)\epsilon$, one has

$$\begin{aligned}
\|\epsilon^+\|^2 &= \epsilon^\top M(\epsilon)^2\epsilon \\
&= \frac{\epsilon^\top(I + 4(\epsilon^\top\mathbf{E}(A)\epsilon)I - 4\mathbf{E}(A))(I + 4(\epsilon^\top\mathbf{E}(A)\epsilon)I - 4\mathbf{E}(A))\epsilon}{1 + \|\sigma\|^2} \\
&= \frac{\epsilon^\top((1 + 4\epsilon^\top\mathbf{E}(A)\epsilon)^2 I - 8(1 + 4\epsilon^\top\mathbf{E}(A)\epsilon)\mathbf{E}(A) + 16\mathbf{E}(A)^2)\epsilon}{1 + \|\sigma\|^2} \\
&= \frac{(1 + 4\epsilon^\top\mathbf{E}(A)\epsilon)^2\|\epsilon\|^2 - 8(1 + 4\epsilon^\top\mathbf{E}(A)\epsilon)\epsilon^\top\mathbf{E}(A)\epsilon + 16\epsilon^\top\mathbf{E}(A)^2\epsilon}{1 + \|\sigma\|^2} \\
&= \frac{(1 + 4\epsilon^\top\mathbf{E}(A)\epsilon)^2(\|\epsilon\|^2 - 1) + 1 - 16(\epsilon^\top\mathbf{E}(A)\epsilon)^2 + 16\epsilon^\top\mathbf{E}(A)^2\epsilon}{1 + \|\sigma\|^2} \\
&= \frac{(1 + 4\epsilon^\top\mathbf{E}(A)\epsilon)^2(\|\epsilon\|^2 - 1) + 1 + 16\epsilon^\top\mathbf{E}(A)(I - \epsilon\epsilon^\top)\mathbf{E}(A)\epsilon}{1 + \|\sigma\|^2} \\
&= \frac{(1 + 4\epsilon^\top\mathbf{E}(A)\epsilon)^2(\|\epsilon\|^2 - 1) + 1 + \|\sigma\|^2}{1 + \|\sigma\|^2} \\
&= \|\epsilon\|^2 + (1 - \|\epsilon\|^2)\frac{1 + \|\sigma\|^2 - (1 + 4\epsilon^\top\mathbf{E}(A)\epsilon)^2}{1 + \|\sigma\|^2} \\
&= \|\epsilon\|^2 + (1 - \|\epsilon\|^2)\frac{8\epsilon^\top(2\mathbf{E}(A)^2 - \mathbf{E}(A))\epsilon - 32(\epsilon^\top\mathbf{E}(A)\epsilon)^2}{1 + 16\epsilon^\top\mathbf{E}(A)(I - \epsilon\epsilon^\top)\mathbf{E}(A)\epsilon} \\
&= \|\epsilon\|^2 - (1 - \|\epsilon\|^2)f(\epsilon, \mathbf{E}(A)),
\end{aligned} \tag{C.87}$$

where the function $f(\epsilon, \mathbf{E}(A))$ is defined as follows:

$$f(\epsilon, \mathbf{E}(A)) := \frac{8\epsilon^\top(\mathbf{E}(A) - 2\mathbf{E}(A)^2)\epsilon + 32(\epsilon^\top\mathbf{E}(A)\epsilon)^2}{1 + 16\epsilon^\top\mathbf{E}(A)(I - \epsilon\epsilon^\top)\mathbf{E}(A)\epsilon}. \tag{C.88}$$

Note that the following inequality holds:

$$f(\epsilon, \mathbf{E}(A)) \geq 8\epsilon^\top(\mathbf{E}(A) - 2\mathbf{E}(A)^2)\epsilon, \quad \forall\|\epsilon\| \in [0, 1]. \tag{C.89}$$

It follows that for all $(\eta, \epsilon, \tau) \in \mathcal{J}_q$, one has

$$\begin{aligned}
\mathbf{V}(\eta^+, \epsilon^+, \tau^+) - \mathbf{V}(\eta, \epsilon, \tau) &= \|\epsilon^+\|^2 - \|\epsilon\|^2 \\
&= -(1 - \|\epsilon\|^2)f(\epsilon, \mathbf{E}(A)).
\end{aligned} \tag{C.90}$$

However, in view of (4.41), one has $0 < \lambda_{\max}^{\mathbf{E}(A)} < \frac{1}{2}$ which implies that the matrix $B = 8(\mathbf{E}(A) - 2\mathbf{E}(A)^2)$ is symmetric positive definite and all the eigenvalues of $B$ satisfy $0 < \lambda^B < 1$. Hence, $f(\epsilon, \mathbf{E}(A))$ is lower by a positive definite quadratic function.

Consequently for all $\|\epsilon\| \in (0,1)$ the above difference is strictly negative which implies that $\mathbf{V}$ is strictly decreasing during the jumps of the closed-loop hybrid system provided that the initial condition satisfies $\|\epsilon(0,0)\| \in (0,1)$. This rules out all attitude errors of angle $180^\circ$ which are characterized by $\|\epsilon\|^2 = 1$ or equivalently $\mathbf{tr}(\tilde{R}) = -1$. In this case one has $\mathbf{V}(\eta^+, \epsilon^+, \tau^+) = \mathbf{V}(\eta, \epsilon, \tau) = \|\epsilon\|^2 = 1$ which implies that the undesired manifold where $\mathbf{tr}(\tilde{R}) = -1$ is forward invariant. The case of $\|\epsilon(0,0)\|^2 = 0$ corresponds to the desired equilibrium where $\tilde{R} = I$. Assume that $\|\epsilon\|^2 < 1$, then there exists $\delta > 0$ such that $\|\epsilon\|^2 \leq \delta < 1$. Therefore, one has

$$\mathbf{V}(\eta^+, \epsilon^+, \tau^+) = \|\epsilon\|^2 - \lambda^B_{\min}(1-\delta)\|\epsilon\|^2 \leq \exp(-\lambda_2)\mathbf{V}(\eta, \epsilon, \tau) \tag{C.91}$$

with $\lambda_2 = -\ln(1 - \lambda^B_{\min}(1-\delta)) > 0$. On the other hand, in view of (4.29), the time between two consecutive jumps is upper bounded by $T_2$, therefore the following holds

$$t \leq T_2(j+1),$$

for each $(t,j) \in \mathrm{dom}(\eta, \epsilon, \tau)$. Consequently, by using item *iii*) of Theorem 2.3.3 with $\lambda_1 = 0, \lambda_2 > 0, \gamma = T_2$ and $T = T_2$, one deduces that the set $\mathcal{A}_s$ is almost globally exponentially stable.

## C.9 Proof of Theorem 4.3.2

Let $Q = (\eta, \epsilon) \in \mathbb{Q}$ be the quaternion representation of the attitude error $\tilde{R} \in \mathbb{SO}(3)$. To proceed with the proof, the hybrid closed-loop system (4.42)-(4.43) is lifted to the space of quaternion $\mathbb{Q} \times \mathbb{R}^n_{\geq 0}$. Defining the state $\bar{X} = (Q, \tau_1, \cdots, \tau_n) \in \mathbb{Q} \times \mathbb{R}^n_{\geq 0}$, one has

$$\dot{\bar{X}} = \bar{\mathbf{F}}(\bar{X}), \qquad \bar{X} \in \bar{\mathcal{F}}, \tag{C.92}$$

$$\bar{X}^+ \in \bar{\mathbf{J}}(\bar{X}), \qquad \bar{X} \in \bar{\mathcal{J}}. \tag{C.93}$$

where the data of the hybrid system are defined as $\bar{\mathbf{F}}(\bar{X}) = (0_{1\times 4}, 1, \cdots, 1)$, $\bar{\mathbf{J}}(\bar{X}) = \{\bar{\mathbf{J}}_i(\bar{X}), \bar{X} \in \bar{\mathcal{J}}_i\}$, $\bar{\mathbf{J}}_i(\bar{X}) = (Q \odot \mathbf{Q}(-\sigma_i), \tau_1, \cdots, \tau_{i-1}, 0, \tau_{i+1}, \cdots, \tau_n)$ and $\bar{\mathcal{J}}_i = \{\bar{X} \in \mathbb{Q}\times\mathbb{R}^n_{\geq 0} : \tau_i \in [T_1^i, T_2^i]\}$, $\bar{\mathcal{F}} = \mathbb{Q}\times[0, T_2^1]\times\cdots\times[0, T_2^n]$ and $\bar{\mathcal{J}} = \bar{\mathcal{J}}_1 \cup \cdots \cup \bar{\mathcal{J}}_n$. The objective is therefore to show asymptotic stability of the set $\bar{\mathcal{A}}_a = \{(\pm 1, 0)\} \times [0, T_2^1] \times \cdots \times [0, T_2^n]$. Consider the following Lyapunov function candidate

$$\mathbf{V}(\bar{X}) = \|\epsilon\|^2. \tag{C.94}$$

Clearly, one has $\dot{\mathbf{V}}(\bar{X}) = 0$ for all $\bar{X} \in \bar{\mathcal{F}}$. To evaluate the "discrete" change in $\mathbf{V}$, consider the following function [Sanfelice *et al.*, 2007]

$$u_D(\bar{X}) = \begin{cases} \max_{\xi \in \bar{\mathbf{J}}(\bar{X})} \{\mathbf{V}(\xi) - \mathbf{V}(\bar{X})\}, & \bar{X} \in \bar{\mathcal{J}}, \\ -\infty, & \text{otherwise.} \end{cases}$$

Now, let $\bar{X} \in \bar{\mathcal{J}}$ and define $\mathcal{I}(\bar{X}) = \{i : \bar{X} \in \bar{\mathcal{J}}_i\}$. In view of the definition of the jump map $\bar{\mathbf{J}}(\bar{X})$, the function $u_D(\bar{X})$ can be written as

$$u_D(\bar{X}) = \begin{cases} \max_{i \in \mathcal{I}(\bar{X})} \{\mathbf{V}(\bar{\mathbf{J}}_i(\bar{X})) - \mathbf{V}(\bar{X})\}, & \bar{X} \in \bar{\mathcal{J}}, \\ -\infty, & \text{otherwise.} \end{cases}$$

On the other hand one has $\sigma_i = 4(\eta I - [\epsilon]_\times)\mathbf{E}(A_i)\epsilon$ where $\mathbf{E}(A_i) = \frac{1}{2}(\mathbf{tr}(A_i)I - A_i)$ with $A_i = \rho_i a_i a_i^\top$. Using this result and the quaternion multiplication rule (similar step as (C.86)), one can show that

$$Q \odot \mathbf{Q}(-\sigma_i) = (\alpha_i(\epsilon)\eta, M_i(\epsilon)\epsilon) \tag{C.95}$$

where

$$\alpha_i = \frac{1 + 4\epsilon^\top \mathbf{E}(A_i)\epsilon}{(1 + 16\epsilon^\top \mathbf{E}(A_i)(I - \epsilon\epsilon^\top)\mathbf{E}(A_i)\epsilon)^{\frac{1}{2}}}, \tag{C.96}$$

$$M_i(\epsilon) = \frac{I + 4(\epsilon^\top \mathbf{E}(A_i)\epsilon)I - 4\mathbf{E}(A_i)}{(1 + 16\epsilon^\top \mathbf{E}(A_i)(I - \epsilon\epsilon^\top)\mathbf{E}(A_i)\epsilon)^{\frac{1}{2}}}. \tag{C.97}$$

Now, letting $\bar{X} \in \bar{\mathcal{J}}$, it follows that

$$u_D(\bar{X}) = \max_{i \in \mathcal{I}(\bar{X})} \{\mathbf{V}(\bar{\mathbf{J}}_i(\bar{X})) - \mathbf{V}(\bar{X})\} \tag{C.98}$$

$$= \max_{i \in \mathcal{I}(\bar{X})} \|M_i(\epsilon)\epsilon\|^2 - \|\epsilon\|^2 \tag{C.99}$$

$$= -(1 - \|\epsilon\|^2) \max_{i \in \mathcal{I}(\bar{X})} f(\epsilon, \mathbf{E}(A_i)) \tag{C.100}$$

$$\leq 8(1 - \|\epsilon\|^2) \max_{i \in \mathcal{I}(\bar{X})} \epsilon^\top (2\mathbf{E}(A_i)^2 - \mathbf{E}(A_i))\epsilon. \tag{C.101}$$

The matrix $\mathbf{E}(A_i)$ is explicitly given by $\mathbf{E}(A_i) = -\frac{\rho_i}{2}[a_i]_\times^2$ which is positive semi-definite. The eigenvalues of $\mathbf{E}(A_i)$ are $\{0, \frac{\rho_i\|a_i\|^2}{2}, \frac{\rho_i\|a_i\|^2}{2}\}$. The zero eigenvalue $\lambda_1^{\mathbf{E}(A_i)} = 0$ of $\mathbf{E}(A_i)$ corresponds to the eigenvector $a_i/\|a_i\|$ and leads to a zero eigenvalue of $2\mathbf{E}(A_i)^2 - \mathbf{E}(A_i)$. The two other eigenvalues of $\mathbf{E}(A_i)$ are strictly positive and, under the condition of Theorem 4.3.2, satisfy $0 < \lambda_{2,3}^{\mathbf{E}(A_i)} < \frac{1}{2}$. In this case, the corresponding eigenvalues of

$2\mathbf{E}(A_i)^2 - \mathbf{E}(A_i)$ are strictly negative. Consequently, one has

$$u_D(\bar{X}) \leq 0, \quad \forall \|\epsilon\| \in [0,1). \tag{C.102}$$

Therefore, by virtue of [Sanfelice *et al.*, 2007, Theorem 7.6, Theorem 4.7], one concludes that the compact set $\bar{\mathcal{A}}_a$ is stable, and $\bar{X}$ must approach the largest weakly invariant set in

$$\mathbf{V}^{-1}(r) \cap u_D^{-1}(0) \cap \bar{\mathbf{J}}(u_D^{-1}(0)) \tag{C.103}$$

for some $r \in [0,1)$. Let us show that the only weakly invariant subset of $\mathbf{V}^{-1}(r)$ with $r > 0$ is the empty set. Assume that $\bar{X}(0,0) \in \mathbf{V}^{-1}(r)$ which implies that $\|\epsilon(0,0)\|^2 = r$. Since $\dot{\mathbf{V}}(\bar{X}) = 0$ one must have $\|\epsilon(t_1,0)\|^2 = \|\epsilon(0,0)\|^2 = r$ where $t_1$ is the time corresponding to the first jump which is explicitly given by $t_1 = \min_{i\in\{1,\cdots,n\}} t_0^i$. After the first jump one has $\|\epsilon(t_1,1)\|^2 = \|M_i(\epsilon(t_1,0))\epsilon(t_1,0)\|^2 \leq \|\epsilon(t_1,0)\|^2 = r$ for some $i \in \arg\min_{i\in\{1,\cdots,n\}} t_0^i$. If $\|\epsilon(t_1,1)\|^2 < r$, it means that $\bar{X}(t_1,1)$ has left the level set $\mathbf{V}^{-1}(r)$. If on the other hand $\|\epsilon(t_1,1)\|^2 = \|M_i(\epsilon(t_1,0))\epsilon(t_1,0)\|^2 = r$ then this means that $\epsilon(t_1,0)$ is an eigenvector of $M_i(\epsilon(t_1,0))$ corresponding to the eigenvalue 1 which leads to the fact that $\epsilon(t_1,0)$ is an eigenvector of $\mathbf{E}(A_i)$ corresponding to the eigenvalue 0. Therefore $\epsilon(t_1,0)$ must be parallel to $a_i$, the inertial vector corresponding to the sensor measurement $b_i$. Now, let us define the time $t = \min_{l,k}\{t_k^l : t_k^l \geq t_1, a_l \times a_i \neq 0\}$ which corresponds to the first instant of time after $t_1$ such that a sensor measurement $b_l$ has been received with a corresponding inertial vector $a_l$ not parallel to $a_l$. The existence of this time is guaranteed by Assumption 4.2.1. Since the projection of the hybrid time domain on $\mathbb{R}_{\geq 0}$ is unbounded and the fact that $t$ corresponds to a measurement instant (thus there is a jump at time $t$) then there exists $j$ such that $(t,j),(t,j+1) \in \text{dom}\bar{X}$. Therefore one has $\epsilon(t,j) = \epsilon(t_1,0) = \epsilon(0,0)$ and $\|\epsilon(t,j+1)\|^2 = \|M_l(\epsilon(0,0))\epsilon(0,0)\|^2 < \|\epsilon(0,0)\|^2 = r$. One concludes that $\bar{X}$ must leave the set $\mathbf{V}^{-1}(r)$ for all $r > 0$. Then $r$ in (C.103) must be zero. However $\mathbf{V}^{-1}(r) = \bar{\mathcal{A}}_a$ which implies that all trajectories must converge to a subset of $\bar{\mathcal{A}}_a$ and hence $\bar{\mathcal{A}}_a$ is attractive. This proves that the set $\bar{\mathcal{A}}_a$ is asymptotically stable.

## C.10 Proof of Theorem 4.3.3

Now, using (4.55)-(4.57) and (4.58), the attitude estimation error $\tilde{R} = R\hat{R}^\top$ can be shown to satisfy

$$\begin{aligned} \tilde{R}(s_{m+1}) &= \tilde{R}(s_m)\mathbf{R}(-\sigma(s_m)), && s_m = t_k,\ k \in \mathbb{N}, \\ \tilde{R}(s_{m+1}) &= \tilde{R}(s_m), && s_m \neq t_k,\ k \in \mathbb{N}. \end{aligned}$$

During the instants of time $s_m$ such that $s_m \neq t_k$, the attitude estimation error is constant. This leads to the following fact

$$\tilde{R}(t_{k+1}) = \tilde{R}(t_k)\mathbf{R}(-\sigma(t_k)), \quad \forall k \in \mathbb{N}.$$

Following similar steps as in (C.85)-(C.89), it can be shown that the quaternion vector part of the attitude estimation error satisfies

$$\epsilon(t_{k+1}) = M(\epsilon(t_k))\epsilon(t_k), \quad \forall k \in \mathbb{N},$$

and in particular one has

$$\|\epsilon(t_{k+1})\|^2 - \|\epsilon(t_k)\|^2 \leq 8(1 - \|\epsilon(t_k)\|^2)\epsilon(t_k)^\top(2\mathbf{E}(A)^2 - \mathbf{E}(A))\epsilon(t_k), \forall k \in \mathbb{N}.$$

Now, since the initial attitude error satisfies $\mathbf{tr}(\tilde{R}(0)) \neq -1$, then $\|\epsilon(0)\| = \|\epsilon(t_1)\| < 1$. The attitude matrix $2\mathbf{E}(A)^2 - \mathbf{E}(A)$ is negative definite under the condition of Theorem 4.3.1. Therefore, it is clear that $\|\epsilon(t_{k+1})\|^2 \leq \|\epsilon(t_k)\|^2 \leq \cdots \leq \|\epsilon(t_1)\|^2 < 1$ for all $k \in \mathbb{N}$. It follows that $\|\epsilon(t_{k+1})\|^2 = \|\epsilon(t_k)\|^2$ only when $\epsilon(t_k) = 0$ which implies that $\lim_{k\to\infty} \epsilon(t_k) = 0$. This limit obviously corresponds to the attitude error $\tilde{R} = I$. Therefore, the discrete version (4.55)-(4.57) of the proposed event-triggered attitude estimation scheme (4.30)-(4.31) guarantees asymptotic stability as well when connected with the discrete approximation (4.58) of the attitude kinematic system (4.27).

## C.11 Proof of Theorem 4.3.4

Let us linearize the closed-loop system (4.74)-(4.75) around the equilibrium set where $\tilde{R} = I$ and $\tilde{b}_\omega = 0$. For small rotations near $I$, one has $\tilde{R} \approx I + [z_1]_\times$ for some $z_1 \in \mathbb{R}^3$. Define $z_2 = -\hat{R}\tilde{b}_\omega$ then in view of (4.74) one has $[\dot{z}_1]_\times = (I + [z_1]_\times)[z_2]_\times \approx [z_2]_\times$. It follows that, during the flows of (4.74), the linear dynamics for the variables $z_1$ and $z_2$

are given by

$$\dot{z}_1 = z_2, \tag{C.104}$$
$$\dot{z}_2 = [\hat{R}\omega]_\times z_2. \tag{C.105}$$

On the other hand, the innovation term $\sigma$ satisfies

$$\begin{aligned}\sigma = \sum_{i=1}^{n} \rho_i [\hat{R} b_i]_\times a_i = \sum_{i=1}^{n} \rho_i [\tilde{R}^\top a_i]_\times a_i \approx \sum_{i=1}^{n} \rho_i [(I - [z_1]_\times) a_i]_\times a_i \\ = -\sum_{i=1}^{n} \rho_i [[z_1]_\times a_i]_\times a_i = -\sum_{i=1}^{n} \rho_i [a_i]_\times^2 z_1 = 2\mathbf{E}(A) z_1\end{aligned}$$

where $A = \sum_{i=1}^{n} \rho_i a_i a_i^\top$. For small rotation errors and in view of (2.31), one has $\mathbf{R}_r(-\sigma) \approx I - 2[\sigma]_\times$. Therefore, during the jumps of (4.75) and neglecting high order terms for $z_1$, one has

$$I + [z_1^+]_\times \approx (I + [z_1]_\times)(I - 2[\sigma]_\times) \approx I + [z_1]_\times - 4[\mathbf{E}(A) z_1]_\times = I + [(I - 4\mathbf{E}(A)) z_1]_\times.$$

Moreover, in view of (4.73) and (4.75), one has

$$z_2^+ = -\hat{R}^+ \tilde{b}_\omega^+ = -\mathbf{R}_r(\sigma)\hat{R}(\tilde{b}_\omega + \gamma_b T^{-1} \hat{R}^\top \sigma) = \mathbf{R}_r(\sigma) z_2 - \gamma_b T^{-1} \mathbf{R}_r(\sigma)\sigma \approx z_2 - \gamma_b T^{-1}\sigma$$

where the facts that $\mathbf{R}_r(\sigma)\sigma = \sigma$ and $\mathbf{R}(\sigma) z_2 \approx (I - 2[\sigma]_\times) z_2 = z_2 - 4[\mathbf{E}(A) z_1]_\times z_2 \approx z_2$ have been used. It follows that the linear dynamics, during the jumps of (4.75), satisfy

$$z_1^+ = (I - 4\mathbf{E}(A)) z_1, \tag{C.106}$$
$$z_2^+ = z_2 - 2\gamma_b T^{-1} \mathbf{E}(A) z_1. \tag{C.107}$$

Consider the following change of variables

$$\begin{aligned} x_1 &= z_1 - \tau z_2, \\ x_2 &= T z_2. \end{aligned}$$

Defining $x = [x_1^\top, x_2^\top]^\top$, then in view of (4.74)-(4.75), (C.104)-(C.105) and (C.106)-(C.107), one can show that

$$\left.\begin{array}{rcl} \dot{x} &=& A_c(\hat{R}\omega,\tau)x \\ \dot{\tau} &=& 1 \\ \dot{\hat{R}} &=& \hat{R}[\omega - \hat{R}^\top x_2/T]_\times \\ \dot{\omega} &\in& c_{\dot{\omega}}\mathbb{B} \end{array}\right\} \quad (x,\tau,\hat{R},\omega) \in \mathbb{R}^6 \times [0,T] \times \mathbb{SO}(3) \times \mathbb{R}^3, \tag{C.108}$$

$$\left.\begin{array}{rcl} x^+ &=& A_d x \\ \tau^+ &=& 0 \\ \hat{R}^+ &=& \mathbf{R}_r(\sigma)\hat{R} \\ \omega^+ &=& \omega \end{array}\right\} \quad (x,\tau,\hat{R},\omega) \in \mathbb{R}^6 \times \{T\} \times \mathbb{SO}(3) \times \mathbb{R}^3, \tag{C.109}$$

where the matrices $A_c(\hat{R}\omega,\tau)$ and $A_d$ are given by

$$A_c(\hat{R}\omega,\tau) = \begin{bmatrix} 0 & -(\tau/T)[\hat{R}\omega]_\times \\ 0 & [\hat{R}\omega]_\times \end{bmatrix},$$
$$A_d = \begin{bmatrix} I - 4\mathbf{E}(A) & I - 4\mathbf{E}(A) \\ -2\gamma_b\mathbf{E}(A) & I - 2\gamma_b\mathbf{E}(A) \end{bmatrix}.$$

Let us show that the norm of the matrix $A_c(\hat{R}\omega,\tau)$ is uniformly bounded. Note that

$$A_c(\hat{R}\omega,\tau)A_c(\hat{R}\omega,\tau)^\top = \begin{bmatrix} -(\tau/T)^2[\hat{R}\omega]_\times^2 & -(\tau/T)[\hat{R}\omega]_\times^2 \\ -(\tau/T)[\hat{R}\omega]_\times^2 & -[\hat{R}\omega]_\times^2 \end{bmatrix}. \tag{C.110}$$

Therefore, one has $\|A_c(\hat{R}\omega,\tau)\|_F^2 = \mathbf{tr}(A_c(\hat{R}\omega\tau)A_c(\hat{R}\omega\tau)^\top) = 2((\tau/T)^2+1)\|\omega(t)\|^2 \leq 4c_\omega^2$ thanks to the assumption that $\omega(t)$ is uniformly bounded. Now, let us establish the necessary and sufficient condition for the matrix $A_d$ to be *Schur* stable. Let $\lambda$ be an eigenvalue of $A_d$. Then

$$\begin{aligned} &\mathbf{det}(\lambda I - A_d) \\ &\quad = \mathbf{det}\begin{bmatrix} (\lambda-1)I + 4\mathbf{E}(A) & -(I - 4\mathbf{E}(A)) \\ 2\gamma_b\mathbf{E}(A) & (\lambda-1)I + 2\gamma_b\mathbf{E}(A) \end{bmatrix} \\ &\quad = \mathbf{det}((\lambda-1)^2 I + ((2\gamma_b+4)(\lambda-1) + 2\gamma_b)\mathbf{E}(A)) \\ &\quad = 0. \end{aligned}$$

This implies that 0 is the unique eigenvalue of the matrix $(\lambda-1)^2 I + ((2\gamma_b+4)(\lambda-1)+2\gamma_b)\mathbf{E}(A)$ and thus one obtains the equation

$$P(\lambda) = (\lambda-1)^2 + ((2\gamma_b+4)(\lambda-1)+2\gamma_b)\lambda^{\mathbf{E}(A)} = 0 \tag{C.111}$$

where $\lambda^{\mathbf{E}(A)}$ is an eigenvalue of $\mathbf{E}(A)$. It follows that each eigenvalue of $\mathbf{E}(A)$ (total 3 eigenvalues) gives rise to 2 eigenvalues of $A_d$ (total of 6 eigenvalues). The matrix $A_d$ is Schur stable if an only if all its eigenvalues are inside the unit circle. Consider the bilinear transformation $\lambda \mapsto (1+w)/(1-w)$ which maps the left half-plane to the open unit disc. Hence, $P(\lambda)$ is Schur stable if and only if the polynomial $Q(w) = (1-w)^2 P((1+w)/(1-w))$ is Hurwitz stable (poles in the left half-plane) and $P(1) \neq 0$. After some algebra one obtains

$$Q(w) = (4 - 8\lambda^{\mathbf{E}(A)} - 2\gamma_b\lambda^{\mathbf{E}(A)})w^2 + 8\lambda^{\mathbf{E}(A)}w + 2\gamma_b\lambda^{\mathbf{E}(A)} = 0.$$

Using Routh-Hurwitz criterion, one derives the following necessary and sufficient condition for the poles of $Q(w)$ to lie in the left half-plane

$$2(1-2\lambda^{\mathbf{E}(A)}) - \gamma_b\lambda^{\mathbf{E}(A)} > 0. \tag{C.112}$$

Note that in view of condition (4.41), one has $0 < \lambda^{\mathbf{E}(A)} < \frac{1}{2}$, and thus a sufficient condition for $A_d$ to be stable is

$$0 < \gamma_b < \frac{2(1-2\lambda_{\max}^{\mathbf{E}(A)})}{\lambda_{\max}^{\mathbf{E}(A)}}. \tag{C.113}$$

Assume that condition (C.113) is met, which implies that $A_d$ is stable. Then, for any symmetric positive semidefinite matrix $L$, there exists a unique positive definite matrix $P$ solution of the following discrete Lyapunov equation

$$A_d^\top P A_d - P = -L.$$

Consider the following Lyapunov function candidate $\mathbf{V} = x^\top P x$ where $P$ is solution of the discrete Lyapunov equation for some positive semidefinite matrix $L$. Then, during

the flows of the closed-loop system (C.108)-(C.109), one has

$$\begin{aligned}\dot{\mathbf{V}}(x) = x^\top(PA_c + A_c^\top P)x \leq 2\|A_c\|_F\|P\|\|x\|^2 &\leq 2\|A_c\|_F(\lambda^P_{\max}/\lambda^P_{\min})\mathbf{V}(x)\\ &\leq 4c_\omega(\lambda^P_{\max}/\lambda^P_{\min})\mathbf{V}(x)\\ &:= -\lambda_1\mathbf{V}(x).\end{aligned}$$

Moreover, during the jumps, one has

$$\mathbf{V}(x^+) - \mathbf{V}(x) = x^\top(A_d^\top PA_d - P)x = -x^\top Lx \leq -\frac{\lambda^L_{\min}}{\lambda^P_{\max}}\mathbf{V}(x).$$

Therefore, one can write

$$\mathbf{V}(x^+) \leq \exp(-\lambda_2)\mathbf{V}(x), \tag{C.114}$$

where $\lambda_2 = -\ln(1 - \lambda^L_{\min}/\lambda^P_{\max}) > 0$ which is well defined thanks to $\lambda^L_{\min}/\lambda^P_{\max} \leq 1$ as explained in the following. In fact, in view of [Yasuda and Hirai, 1979, Corollary 2], one can obtain a lower bound on the maximum eigenvalue of $P$ as follows

$$\lambda^P_{\max} \geq \lambda^L_{\min}/(1 - \max_i |\lambda_i^{A_d}|^2). \tag{C.115}$$

Note that, since $A_d$ is Schur stable, one has $\max_i |\lambda_i^{A_d}|^2 < 1$. This implies that $\lambda^L_{\min}/\lambda^P_{\max} \leq 1 - \max_i |\lambda_i^{A_d}|^2 \leq 1$. Moreover, since the time between two consecutive jumps is equal to $T$ one has $t \leq T(j+1)$. Therefore, using item *iii)* of Theorem 2.3.3, a sufficient condition for exponential stability of the set $\mathcal{A}$ is $\lambda_2 > -T\lambda_1$ which leads to

$$T < \frac{-\ln(1 - \lambda^L_{\min}/\lambda^P_{\max})}{4c_\omega(\lambda^P_{\max}/\lambda^P_{\min})}.$$

# Curriculum Vitae

| | |
|---|---|
| **Name:** | Soulaimane Berkane |
| **Post-Secondary Education and Degrees:** | 2017 Ph.D.<br>Robotics and Control<br>University of Western Ontario<br>London, Ontario, Canada<br><br>2013 M.Sc. & Engineer Diploma<br>Automatic Control<br>Ecole Nationale Polytechnique<br>Algiers, Algeria |
| **Honours and Awards:** | Graduate Student Award for Excellence in Research<br>University of Western Ontario<br>London, Ontario, Canada, 2017<br><br>Award for Outstanding Presentation in Research Symposium<br>University of Western Ontario<br>London, Ontario, Canada, 2017<br><br>Best Student Paper Award Finalist<br>American Control Conference<br>Boston, MA, USA, 2016 |
| **Related Work Experience:** | Teaching Assistant<br>The University of Western Ontario<br>London, Ontario, Canada<br>2014 - 2017 |

**Selected Publications:**

- **S. Berkane**, A. Abdessameud and A. Tayebi, "*Hybrid Global Exponential Stabi-*

*lization on $SO(3)$*", Automatica, Vol. 81, pp. 279–285, 2017.

- **S. Berkane** and A. Tayebi, "*Construction of Synergistic Potential Functions on $SO(3)$ with Application to Velocity-Free Hybrid Attitude Stabilization*", IEEE Transactions on Automatic Control, Vol. 62, No. 1, pp. 495–501, 2017.

- **S. Berkane**, A. Abdessameud and A. Tayebi, "*Hybrid Attitude and Gyro-bias Observer on $SO(3)$*", IEEE Transactions on Automatic Control, Vol. 62, No. 11, pp. 6044 - 6050, 2017.

- **S. Berkane** and A. Tayebi, "*On the Design of Attitude Complementary Filters on $SO(3)$*", IEEE Transactions on Automatic Control, 2017, to appear.